Dissertation
submitted to the
Combined Faculty of Natural Sciences and Mathematics
of the Ruperto Carola University Heidelberg, Germany
for the degree of
Doctor of Natural Sciences

Presented by

M.Sc. Priyata Kalra
born in: Dehradun, India
Oral examination: 13.11.2018

Integration of pharmacokinetic and intracellular models of interferon administration and induced responses

Referees: Prof. Dr. Ursula Kummer
Dr. Frederik Graw

Abstract

Doctor of Natural Sciences

Integration of pharmacokinetic and intracellular models of interferon administration and the induced responses

by Priyata KALRA

A thorough understanding of drug-target relationships is essential in preclinical and clinical translation studies. However, there is a gap of knowledge in the quantitative understanding of dose-response relationships at the target site. To fill that gap, a particularly promising approach is quantitative systems pharmacology (QSP) where, mechanistic and hence comprehensive models of dose-effect relationships are used to guide the design of clinical and translational studies.

In this thesis, I present for the first time a QSP approach for a therapeutic protein, interferon alpha (IFN-α), by coupling physiologically based pharmacokinetic (PBPK) models at the whole-body level with intracellular models of signal transduction in the liver. Whole-body distribution models of an injected dose of IFN-α calibrated to quantitative measurements of the plasma concentration are established for humans and mice. They are then coupled to mechanistic intracellular models of the triggered JAK/STAT signalling cascade that describes the dynamic response in the expression of the antiviral mRNAc of IRF9 for humans and antiviral protein Mx2 for mice on the cellular scale. By doing so, I am able to establish the quantitative dose-effect relationship of the injected IFN-α dose to the responding interferon stimulated genes (ISGs) triggered at the target site, the liver.

The established multi-scale physiologically based pharmacokinetic/pharmacodynamic (PBPK/PD) model of human predict a reduced response of IRF9 mRNAc to IFN-α under physiological *in vivo* conditions as compared to *in vitro*. The QSP model also elicits the large impact of the IFN-receptors on the clearance of IFN-α in the liver, thus, not only providing mechanistic insights into the pharmacodynamic (PD) response but also elucidating the influence of receptor variability on the response.

Although IFN-α is specifically used in humans, in preclinical studies, it is also tested in mice for understanding the medical impact of IFN-α for other diseases. Therefore, I elaborate an analogous QSP model for the IFN-α response in mice to illustrate possibilities of model-based cross species translation. Like the human model, a whole body PBPK/PD mouse model was also established to follow the response of antiviral protein Mx2. The model clarified the differences between the pharmacokinetics of human and murine IFN-α injection in mice and will support quantitative cross-species extrapolation in the future.

Finally, as heterogeneity in ISGs reflects inter-cell variability in response to IFN-α, I study the impact of sources of this heterogeneity by implementing the mechanistic stochastic model of the JAK/STAT signalling pathway. The model was developed on the basis of time-resolved flow cytometry data of two ISGs, MxA and IFIT1, in Huh7.5 cells. The model analysed intrinsic variability in the concentration of the molecules of the pathway and generated a graded response of MxA and IFIT1 instead of an all-or-none response. Ultimately, the model concludes that the stochasticity in the initiation of the signalling pathway, i.e., at the receptor level, can be buffered by the system and a more robust response of ISGs, MxA and IFIT1 is induced.

Zusammenfassung

Vernetzung von pharmakokinetischen und intrazellulären Modellen der Interferonverabreichung und der darauffolgenden induzierten Antwort

by Priyata KALRA

Ein umfassendes Verständnis der Wechselwirkung zwischen einem Arzneimittel und seinem Zielmolekül bildet die Grundlage präklinischer Studien im Rahmen der Translationsmedizin. Aufgrund der Systemdynamik des menschlichen Körpers ist eine quantitative Beschreibung zwischen verabreichter Dosis und Wirkung jedoch erschwert. Die quantitative Systempharmakologie (QSP) setzt an diesem Punkt an und beschreibt die Verteilung eines Arzneimittels im Körper sowie seine Wirkweise am Zielort mithilfe komplexer mechanistischer Modelle.

In der vorliegenden Arbeit wird zum ersten Mal ein QSP-Ansatz für ein therapeutisches Protein - IFN-α - entwickelt. Hierfür wird ein Physiologie-basiertes pharmakokinetisches Modell (PBPK-Modelle) der Ganzkörperverteilung von IFN-α mit einem intrazellulären Modell der Signaltransduktion in der Leber gekoppelt. Das Modell der Ganzkörperverteilung wird für Mensch und Maus getrennt erstellt und mit quantitativen Messungen der Plasmakonzentration von IFNa nach Injektion kalibriert. Anschließend wird das Ganzkörpermodell an ein intrazelluläres Modell des JAK/STAT-Signalwegs gekoppelt, das die dynamische Antwort einer antiviralen RNA - IRF9 im Mensch und Mx2 in der Maus – auf zellulärer Ebene beschreibt. Somit lässt sich die Expression Interferon-stimulierter Gene (ISGs) am Zielort der Leber in Abhängigkeit der verabreichten IFN-α-Dosis quantitativ beschreiben.

Modellsimulationen des menschlichen QSP-Modells sagen vorher, dass physiologische Bedingungen die Antwort der IRF9 mRNAc auf IFN-α-Stimulation im Vergleich zu *in vitro*-Bedingungen reduzieren. Weitere Analysen des Modells legen außerdem einen hohen Einfluss der IFN-Rezeptordichte auf die Clearance in der Leber dar. Dementsprechend ermöglicht das QSP-Modell nicht nur mechanistische Einsichten in die pharmakodynamische Antwort, sondern zeigt auch den Einfluss der Rezeptorvariabilität auf die physiologische Antwort auf.

Wenngleich IFN-α in erster Linie als Arzneimittel für den Menschen dient, wird sein Potential zur Behandlung weiterer Krankheiten in präklinischen Studien an Mäusen untersucht. Um Forschungsergebnisse, die an Mäusen erhoben wurden, auf den Menschen zu übertragen, wird im zweiten Teil der vorliegenden Arbeit ein QSP-Modell für die Maus erarbeitet. Dem murinen QSP-Modell unterliegt im Wesentlichen die Struktur des humanen Modells; allerdings dient im murinen Modell die Expression des antiviralen Proteins Mx2 als Surrogat für die IFN-α-Antwort. Mithilfe des murinen QSP-Modells lassen sich Unterschiede zwischen der Pharmakokinetik in Mensch und Maus aufklären und somit quantitative Studien an Mäusen auf den Menschen übertragen.

Heterogene Expression von ISGs spiegelt die interzelluläre Variabilität der IFN-α-Antwort wider. Der dritte Teil der vorliegenden Arbeit untersucht die Ursache dieser Heterogenität anhand eines stochastischen Modells des JAK/STAT-Signalwegs. Das Modell beruht auf zeitaufgelösten Daten zweier ISGs, MxA und IFIT1, die mit Durchflusszytometrie in Huh7.5 Zellen erhoben wurden. Aufgrund der intrinsischen Variabilität in der Konzentration der Signalwegmoleküle legt das Modell statt einer Alles-oder-nichts-Reaktion eine graduelle Antwort von MxA und IFIT1 auf IFN-α-Stimulierung nahe. Im Gegensatz dazu kann das System die Stochastizität auf Rezeptorebene, die zu Fluktuationen in der Signalwegaktivierung führt, puffern und ermöglicht somit eine robuste Antwort der ISGs MxA und IFIT1.

Contents

List of Figures

List of Tables

List of Abbreviations

ADME	**A**bsorption **D**istribution **M**etabolism and **E**limination
AGS	**A**icardi-**G**outieres **S**yndrome
BAC	**B**acterial **A**rtificial **C**hromosome
CRF	**C**ell **R**estriction **F**actors
$\mathbf{C_{max}}$	**C**oncentration **max**imum
COPD	**C**hronic **O**bstructive **P**ulmonary **D**isease
DAA	**D**irect **A**cting **A**ntiviral
DC	**D**endritic **C**ells
FDA	**F**ood and **D**rug **A**dministration
G-CSF	**G**ranulocyte- **C**olony **S**timulating **F**actor
GFP	**G**reen **F**luorescent **P**rotein
GI	**G**astro **I**ntestinal
HCV	**H**epatitis **C** **V**irus
HIV	**H**uman **I**mmunodeficiency **V**irus
HSC	**H**epatic **S**tellate **C**ell
IFN	**I**nterferon
IFIT1	**IF**nterferon-**I**nduced protein with **T**tetratricopeptide repeats 1
IL	**I**nterleukins
IMID	**I**mmune-**M**ediated **I**nflammatory **D**isease
IRF9	**I**nterferon **R**egulatory **F**actor 9
ISG	**I**nterferon **S**timulated **G**enes
ISGF3	**I**nterferon-**S**timulated **G**ene **F**actor 3
ISRE	**I**FN-**S**timulated **R**esponse **E**lements
IV	**I**ntra **V**enous
JAK	**J**anus **k**inase
KC	**K**upffer **C**ells
KS	**K**olmogorov **S**mirnov
LSEC	**L**iver **S**inusoidal **E**ndothelial **C**ells
MS	**M**ultiple **S**clerosis
MX	**M**yxovirus resistance protein
NK	**N**atural **K**iller cells
ODE	**O**rdinary **D**ifferential **E**quations
PBPK	**P**hysiologically **B**ased **P**harmaco **K**inetic
PBS	**P**hosphate **B**uffered **S**aline
PD	**P**harmaco **D**ynamic
PK	**P**harmaco **K**inetic
PK/PD	**P**harmaco **K**inetic **P**harmaco **D**ynamic
PIAS	**P**rotein **I**nhibitors of **A**ctivated **S**TATs
PTP	**P**hospho**t**yrosine **P**hosphatases
RBV	**R**ibavirin

RMSE	**R**oot **M**ean **S**quare **E**rror
SB	**S**ystems **B**iology
SC	**S**ub**C**utenuous
STAT	**S**ignal **T**ransducers and **A**ctivators of **T**ranscription
SH2	**S**rc **H**omology domain
SSA	**S**tochastic **S**imuations **A**lgorithm
SOCS	**S**uppressor **o**f **C**ytokine **S**ignalling
TFBS	**T**ranscription **F**actor **B**inding **S**ites
$\mathbf{T_{max}}$	**T**ime taken to reach the **max**imum concentration
TMDD	**T**arget **M**ediated **D**rug **D**isposition
TNF	**T**umor **N**ecrosis **F**actor
QSP	**Q**uantitative **S**ystems **P**harmacology

तत् त्वम् असि

tat tvam asi

You are that

You exist in everything and the universe exists in you.

- Chandogya Upanisad

Chapter 1

Introduction

1.1 Chapter Summary

The work in this thesis describes the study of Interferon-α (IFN-α) as a therapeutic protein using a combination of modelling, experimental approaches and the growing domain of quantitative systems pharmacology. The work explores not only IFN-α drug distribution in the body, but also the effects on the downstream JAK/STAT signalling pathway and the intricacies of the response at the target site. From a methodological point of view, the thesis tackles the integration of theoretical and modelling frameworks from two different domains: Systems pharmacology and systems biology. In summary, this thesis describes the establishment of molecular pathway models at the cellular level and physiology-based pharmacokinetic (PBPK) models at organism scale by using experimental data from both scales. These models are later combined to quantify the available therapeutic dose at the liver and the triggered cellular response for the same.

In this chapter, I provide a brief introduction to various biological aspects of IFN-α as a therapeutic, as well as an introduction to the methods, focusing on the modelling approaches. This chapter covers the elementary background that will inform the discussions throughout the thesis.

1.2 General introduction to cytokines

Cytokines
(noun)
Etymology: κύτος meaning *cavity or cell* and κίνησις meaning *movement*.
Proposed by Cohen et al. in 1974 [1]

1. The cytokine protein super-family encompasses immunological proteins that regulate a wide range of biological functions, including immunity, hematopoiesis, inflammation & proliferation and repair. They are primarily large molecules (around 80 kDa in size).

In the last decades, much light has been thrown on the role of various cytokines in our body. They are thereby aptly called immunomodulators, due to their ability regulate the defence mechanisms in our body. In the current times, cytokine research is being actively developed by biotechnology and pharmaceutical companies to aid in the treatment and prevention of various diseases.

1.3 Medical relevance of cytokines

Cytokines are secreted by a large variety of cells and function in both paracrine and autocrine fashion. They have been successfully utilised to treat immune-mediated inflammatory diseases (IMID), chronic obstructive pulmonary disease (COPD), asthma, cancer, multiple sclerosis (MS), and various viral infections (HCV, HIV, Influenza, etc.) [2]. Some examples of well-studied cytokines include interleukins (IL1-10), tumor necrosis factors (TNF-α, TNF-β), granulocyte-colony stimulating factor (G-CSF) and interferons (IFN-α, IFN-β, IFN-λ). For atleast two decades, these molecules have been probed as potential therapeutics for various infections or immunomodulatory diseases, leading to a number of successful clinical therapies involving cytokine modulation. For example, TNF-α blocking agents are used in rheumatic diseases and asthma [3]–[5], IFNs are used as antivirals, ILs are extremely efficient in few cancer therapies [6] and IFN-β is used for MS therapy [7].

To be able to use immunomodulators to target diseases showing inadequate immune response is an exciting possibility. Nevertheless, their full potential against diseases is an ongoing investigation. Hence, many endeavours are pursued on understanding efficacy, specificity and toxicity of cytokines. These have led to two very different strategies towards using cytokines as therapeutics. In several treatment strategies, the purified recombinant cytokine is administered, e.g., interferon in viral diseases. Alternatively, therapeutic approaches can also target endogenously up-regulated cytokines as in the case of cancer.

Due to the large size of cytokines and their ability to be therapeutic proteins, they are classified as drugs and are commonly addressed as *biologics* or *biopharmaceuticals* in the pharmaceutical industry. These can be produced via protein engineering (e.g. recombinant technology) and are optimised copies of the endogenous proteins e.g., pegylated-interferon alpha 2b (peg-IFN-α). Cytokines usually bind to a very specific receptor, especially when applied in cancer therapy and therefore, have lesser side effects compared to chemotherapy. In the next section, I shall discuss in detail, the type I interferons- a large subclass of cytokines.

1.4 The biology of type I interferons

IFNs are are polypeptides that influence the development of humoral and cell-based immune responses. They were discovered in 1957, as proteins which *interfere* viral replication [8]. They are known to exhibit multiple biological properties such as antiviral, anti-proliferative and immunomodulatory effects [9], [10]. Once produced, they bind to IFN-α/β receptors, which induce the cell's intrinsic antimicrobial state leading to controlled transcription of various interferon stimulated genes (ISGs).

Type-I IFNs constitutes the largest class of IFNs. In humans, this class comprises IFN-α, IFN-β, IFN-ω, IFN-κ, IFN-ϵ, IFN-ζ and IFN-δ whose genes are located on chromosome 9 [11], [12]. All of these genes, except for IFN-ϵ, are transcribed towards the direction of the telomere in the chromosome (in plus direction). Type I IFNs exhibit high homology in their sequence and protein structure (75-99%) [13]. Also, all of them bind to the ubiquitously expressed IFN-α receptors (IFNAR) but have distinct biological activities.

IFN-α has multiple subtypes which are expressed by 14 genes, two of which are pseudogenes. The remaining 12 subtypes share a homology of ¿ 75% . *In vitro* studies have shown that the antiviral potential (measured in U/mg of protein) amongst IFN-α subtypes can vary upto 100 fold while the anti-proliferative response varies around 20 fold, hence, establishing no correlations among the activities [14]–[16].

Although various subspecies of IFN-α are produced for therapeutic interventions, IFN-α2 (subspecies 2a and 2b) is predominantly used [17], [18]. However, varied levels of responsiveness to IFN-α2 have been observed in different cell lines, e.g., $\sim$ difference of antiviral potency of IFN-α2 on human fibrosarcoma cell lines to human hepatoma cell lines [19]–[21]. Another study by Wolber et al. [22] elaborates upon the strong variance of response to IFN-α2 treatment in different human hepatic cell lines [22]. Because of this difference, which is presumably associated with receptor recognition and kinetics, IFN-α2 has been subject to pre-clinical and clinical studies.

Having briefly introduced the class of type I interferons, I will now focus on IFN-α, the *biologic* (i.e., the biological compound) of this thesis.

1.5 IFN-α as immunotherapeutic protein

Over the years, proteins have been gaining a lot of attention as a therapeutic to treat various diseases. All three classes of IFNs (α, β, λ) have therapeutic scopes as antivirals or anti-proliferatives and/or immunomodulators. Since 20 years, particularly IFN-α has been approved by the FDA to be clinically effective as an antiviral and antineoplastic therapeutic protein. However therapeutic proteins are traditionally administered intravenously, which proves to be both inconvenient and expensive for the patients. This shortcoming has led to evolving the chemical structure of the drug compound from being a native protein (eg. IFN-α, IFN-β) to a biotherapeutic version, e.g., using conjugates of polyehtylene glycol (PEG) (PEG-IFN-α, RBV-IFN-α) or albumin (albIFN) to increase the half-life of the compound in the blood plasma. These changes in the chemical structure of the proteins as drugs have introduced new challenges in the understanding of their metabolism and elimination from the body. Due to their vast applications in diseases, there are newly engineered variants of IFN-α that are often being introduced in the pharmaceutical market.

To design effective dosing schedules (toxicology studies, best efficacy and safety formulations of the drug), an understanding of the pharmacokinetics is of paramount

importance. Hence, in the next section, I shall discuss the present-day knowledge of the pharmacology and pharmacokinetics of IFN-α.

1.5.1 Pharmacology of IFN-α

Studies have shown that IFN-α is secreted by fibroblasts, T cells, macrophages, plasmacytoid monocytes, natural killer cells (NK) and dendritic cells (DCs) [23]–[25]. The current working hypothesis is that the *"professional"* IFN-α secreting cells are the CD4+CD11c-type 2 precursors (pDC2s) [26], [27]. DCs are important producers of IFN-α, and since DCs are the part of the local immune responses, this implies indirect involvement of IFN-α in the regulation of local immune responses [28]. This highlights an important aspect of IFN biology: The IFN-α therapy dose and administration schedule determine the regulation of patients innate and adaptive immunity, consequently, the systemic administration of IFN-α at low-doses leads to priming of the immune response and governs the induction of interferon stimulated genes (ISGs) [29]–[31]. It has observed that a low-dose IFN-α treatment in patients resembles the endogenous response of IFN-α [32]. High doses, on the other hand, are poorly tolerated by the patients [33]. Additionally, undesirable side effects have been seen in patients injected with pure IFN-α, some of which are nausea, anorexia, psychomotor slowing, bone marrow depression, hair loss and fatigue.

The choice of dosage and regimes are devised and optimised by pharmacokinetic (PK) studies where the *movement* of the *drug through* the *body* is evaluated. Once approved, the doses are tested with clinical trials. To gain insights into the *effect of the body on the drug*, the drugs' *absorption, distribution, metabolism, and elimination* (ADME) properties are required. The ADME parameters are quantified descriptors of the drug. They provide information on the *(A)bsorption* of the drug in organs and tissues from the plasma, the *(D)istribution* at the site of action of the drug and the mechanism of *metabolism* and *elimination* (ME) or clearance (such as by urine) with systemic distribution of the drug.

In the 1970s - 1980s, several fundamental pharmacokinetic studies were performed for IFN-α. In the following subsection, I review the studies that led to a coherent understanding of the IFN-α PK.

Fundamental PK of IFN-α

Several pharmacokinetic and tissue distribution studies with different doses of IFN-α have been performed on rats [34]–[37], mice [38]–[42], rabbits [41], [43], [44] and monkeys [36], [41], [45]. Additionally, some pharmacokinetic studies have also been carried out on humans. However, no work has been reported on the investigation of the tissue distribution of recombinant (r)IFN-α in humans. Currently, (r)IFN-α-2a and -2b are manufactured by recombinant DNA technology using a genetically engineered *Escherichia coli* bacterium (approximate molecular weight (MW): 20,000 daltons).

1. **Absorption**
   As stated previously, oral doses of IFN-α were found to be poorly absorbed in the gastro-intestinal tract (GI) due to its natural proteolytic digestion . Thus, other administration sites were explored and measures for IFN-α, such as, intravenous (i.v.), subcutaneous (s.c.), and intramuscular (i.m.) absorption of IFN-α was measured [46]. i.v., i.m. and s.c. doses for rIFN-α were accessed in various studies [47]–[52] and the systemic absorption for all other sites were remarkably good. In the case of IFN-α dose administered IV, the maximum

plasma concentrations (C_{max}) of IFN-α occur around 0.6-1 hour (T_{max}) after administration, while for IM and SC the T_{max} is 7-10 hours, along with relatively low detectable rIFN-α in the plasma [47], [50]–[52]. Type I interferons are poorly absorbed by gastrointestinal tracts and hence work best as parenteral (a dose which bypasses the GI tract, such as an injection) dose. The general routes of IFN-α administration are: intravenous infusion and subcutaneous injections. Usually the therapies have a schedule and range from a period of 6 months to 2 years.

2. **Distribution and metabolism**
   Different dosage regimes and frequencies have been tested for rIFN-α, ranging from daily to intermittent administration. It is noted that the plasma concentration rapidly declines in a bi-exponential manner after IV administration [47]–[52]. rIFN-α plasma concentrations can be measured for 24 hours after the injection to follow the bi-exponential behaviour. The volume of distribution ranges from 12 to 40L in different studies stated above.

3. **Elimination**
   Terminal elimination half-life of rIFN-α range from 4 to 16 hours depending on the routes of administration, the fastest being IV administration. There has been no work reported on the catabolism of rIFN-α in humans. The work performed thus far on animal models suggests that major clearance/catabolism takes place in the kidney and the liver [39], [40], [42].

In a review by Bocci [42], IFN-α half-life values have a considerable variability. This can be partially explained because of the strength of various doses, i.e., a larger dose has a longer half-life than a smaller one. Moreover, past work [53], [54] has shown that repetitive daily doses tend not to differ in effect, which suggests that saturation and down-regulation of cell receptors play a role in this phenomenon.

There is a strong relationship between the pharmacokinetics-pharmacodynamics (PK/PD) and ADME processes of IFN-α, where the ADME properties influence the observed PK. Properties like molecular mass, charge, glycosylation and protein modification, size and target-mediated binding can heavily influence the ADME profile of IFN-α. One particularly important example in this regard is that target binding (at the receptors) has a profound effect on IFN-α ADME. This phenomenon is known as target-mediated drug disposition (TMDD) and has been successfully modelled to account for various IFN-α PK distributions [55]–[57]. The TMDD is simultaneously linked to the IFN-α signal transaction, as the activation of the receptors in turn activates various genes that are a nexus for the innate-to-adaptive transition of immune response.

1.5.2 Mechanism of action: IFN-α signalling

As shown in the following Figure 1.1, the ligand binding induces the JAK/STAT signalling pathway. Upon ligand binding, the receptors move to closer proximity and lead to auto/trans phosphorylation of Janus kinase (JAK). The phosphorylated form of JAK is the activated form and it induces the activation of the downstream signalling pathway. Once JAKs are activated, they phosphorylate the members of signal transducers and activators of transcription (STAT) family [58], [59]. The STAT1 and STAT2 bind to the src homology domain (SH2) of the receptors where they are activated individually and dimerise, either independently or with each other. The activated dimer either independently translocates to the nucleus or interacts with

Interferon regulatory factor 9 (IRF9) to form the interferon-stimulated gene factor 3 (ISGF3) complex and translocates in the nucleus [60]. In the nucleus, ISGF3 binds to various palindromic sequences called IFN-stimulated response elements (ISREs) which lead to expression of several hundred IFN-stimulated genes (ISGs). Of these, some ISGs are now used as gold-standard genomic biomarkers for example, IFIT1 (a.k.a. ISG56) for glioblastoma [61], ISG15 for tumor detection [62], [63] and Aicardi-Goutières syndrome (AGS) [64], [65]. As the response ISGs, IFIT1 (ISG56) and MxA are commonly used biomarker to follow IFN treatment response along with understanding the antiviral activity of IFN against various viruses like Paramyxoviridae, Orthomyxoviridae and many others [66]–[72]. Many of the ISGs activated as the response to IFN are classified as cell restriction factors (CRF), responsible for the establishment of an antiviral state [73].

At every step, the JAK/STAT pathway is fine-tuned by many regulatory mechanisms to restrain the amplitude and duration of the signal. These negative regulators control the cytokine effects and suppress the activity associated with disease state. There are three key regulatory modules, two of which act on the level of receptors and one on the level of gene transcription. On the receptor level there are many phosphotyrosine phosphatases (PTPs) which dephosphorylate the JAKs [74]. The second module on the receptor level is the suppressor of cytokine signalling (SOCS) [75] proteins, which in turn act as negative regulators in the circuit. The third module involves the protein inhibitors of activated STATs (PIAS) which conceal STAT-driven gene transcription by various mechanisms in the nucleus.

Presumably, because IFN-α regulates the transcription of numerous genes, the effect of IFN-α treatment is described as pleomorphic. In addition, the regulation of various cytokines adds to the complexity in identifying the IFN-α-specific response. Furthermore, the JAK/STAT pathway is used by many other signalling molecules and these complexities add to variability in inter-cell response of a population of cells.

A part of heterogeneity of IFN-α pleomorphic response difference in inter-cell of a population can be explained by i) cell-extrinsic factors (like the different viral infections) or ii) cell-intrinsic noise, which can be understood by exploring the cell to cell response variability to the IFN-α treatment.

1.5.3 The noise in the interferon signalling pathway

At the single cell level, the IFN response system is dedicated to processing and transducing information about the environment provided by the extracellular immune stimuli (e.g., viruses). The task of relaying this information into the cell becomes challenging when the normal cellular molecular processes also add to the determination of the response. These processes include diffusion, chemical reaction (like association, dissociation and conversion of molecules), range of molecular numbers of involved molecules (the infrequency of molecular events because of small numbers of molecules) and gene expression (variation due to mutations, from cell-cycle progression or random environmental differences). We use the term *"noise"* to refer to inter-cellular response variation to IFN-α stimulus regardless of source, within a supposedly identical cell population [76]. *Noise* can be divided into two components: *intrinsic noise* and *extrinsic noise*. *Intrinsic noise* is a result of randomness in the molecular processes, e.g., in the process of gene expression, the promoter binding to translation of mRNA to the protein synthesis and degradation will manifest the intrinsic noise [77]. *Extrinsic noise*, on the other hand, is caused by cell to cell variation or by variations in the cell components, e.g., differences due to the local

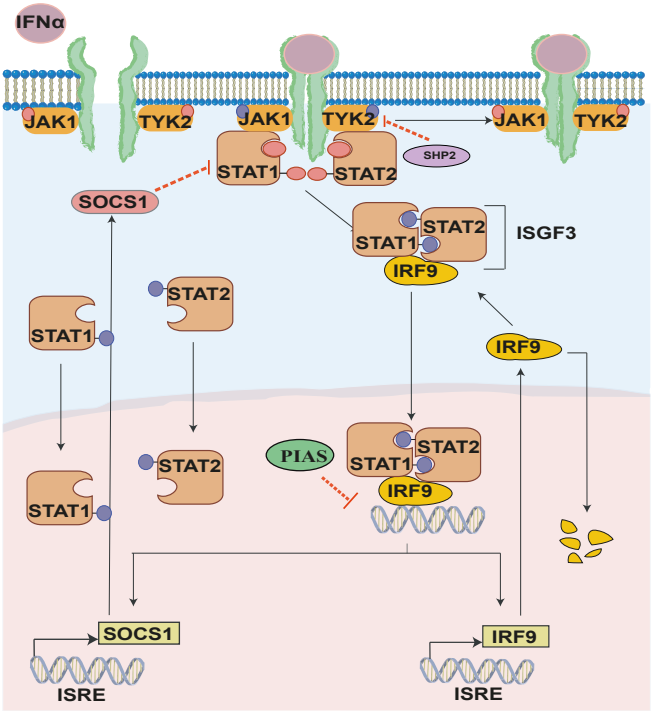

FIGURE 1.1: IFN binds to the heterodimeric complex of the IFNAR1 and IFNAR2 to activate the signal transduction from the JAK/STAT pathway. STAT1 and STAT2 are phosphorylated in the cytoplasm where they form a heterodimer (dimer STAT). This dimer interacts with IRF9 to form the ISGF3 complex which translocates in the nucleus and binds to the ISREs to transcribe various ISGs. This leads to the production of IRF9 as positive feedback and SOCS1 as negative feedback. PTPs act on the receptor level and dephosphorylate the JAKs to lead to another negative feedback, which are called SHPs (SH2 domain-containing protein tyrosine phosphatase). The nuclear negative feedback is exerted by PIAS [58], [59], [73].

environment in the cells of the population or differences in the concentration or activity of any of the molecules that effect the gene expression [78]. Recently, it has been shown that the information transduced in cellular signalling pathways is affected by noise [79], but little is known about its effect on the signalling response [80]. Noise in cellular signalling pathways is conceptually different from the noise resulting from stochastic fluctuations of low-abundance genetic regulators. In cellular signalling pathways, noise can consist of low levels of enzyme activity through random transient interactions of receptors, binding of ligands to receptors in non-functional complexes, and background interactions along the pathway [80].

Noise plays an important role in IFN responses. It has been observed in populations of nearly identical cells, that not all cells that are infected by a virus or that not all cells stimulated by IFN express ISGs [81]–[84]. In all these cases, the suggested mechanisms behind this heterogeneity have been related to stochastic events along the JAK/STAT signalling pathway.

However, since the initiation of IFN-α signalling is initiated by highly specific ligand-receptor interaction, part of the heterogeneity can be unwound by understanding the interaction between IFN-α and IFNARs. The stochastic induction of inter-cellular IFN-α response leads to large heterogeneity in the response at onset

of the infection, consequentially leading to variability in the bound receptors which transmit this variability further in the induced JAK/STAT pathway. By understanding what happens at the level of the interaction of IFN-α with IFNARs, we can get insights on the impact of heterogeneity on autocrine and paracrine signalling of IFN-α in a collection of cell populations [85].

1.5.4 IFN-α receptors

A substantial deal of non-redundancy in the JAK/STAT pathway activation is driven by the IFNARs which have functional plasticity for all type I IFN ligands. Thus, signal activation is refined by the subtle interplay of the affinity of the receptors to the different ligands, the stability of the ternary complex and the number of receptors presented on the cell's surface [86]–[88]. The receptors have two subunits which come together to form a heterodimer: IFNAR1 and IFNAR2, which belong to the family of class II helical cytokine receptors [89]. When IFNAR1 and IFNAR2 interact with the ligand they form a ternary complex. The two receptors differ substantially in their binding affinities towards different IFNs. IFNAR1 is a low affinity receptor with binding affinity in micromolar range whereas IFNAR2 is a high affinity receptor with binding affinity in nanomolar range [90], [91]. Activation of both receptors is necessary to activate the downstream signalling. The current hypothesis on ligand receptor binding is that IFN-α binds to IFNAR2 which then interacts with IFNAR1 to form the heterodimeric complex. The stability of this complex is determined by the affinity of the receptors to the ligand. The receptor distribution and abundancy per cell also varies depending on the cell-type. For example, there are 3300 binding sites/cell for AU937 (human monocytoid cells) or approximately 2500 binding sites/cell for MBDK bovine cells and 12700 binding sites/cell for Daudi lymphoblastoids [92], [93].

Near a cell population, the secreted IFN-α diffuses and binds to the IFNARs which activate the signalling. Therefore, this step is one major component that induces the *noise* in the signalling pathway in individual cells. The noise can propagate or deplete depending on the threshold fraction of bound and unbound receptors per cell, their affinity to the temporally fluctuating presence of IFN-α near the cell surface area and their spatial distribution on the cell surface.

Once IFN-α activates the JAK/STAT pathway, the effects are very heterogenous, even within cell-type. For example, in liver, the JAK/STAT pathway can promote liver damage or provide hepato-protection. The next section discusses the immunobiology of IFN-α in the liver and the hepatocytes.

1.6 The role of liver and hepatocytes in interferon signalling

The liver serves as a buffer between the gut and systemic circulation: 80% of the hepatic blood is delivered from the gut via the portal vein [94]. The venous blood in the hepatic environment mixes with oxygen-laden blood of the artery at the hepatic sinusoids, through plates of hepatocytes. The sinusoids have three non-paranchymal resident populations: Specialised liver sinusoidal endothelial cells (LSEC) that line the sinusoids, the liver resident macrophages (known as Kupffer cells (KC)) in the sinusoids, and hepatic stellate cells (HSCs) found in the space of Disse in the liver microanatomy [95], as seen in Figure 1.2. It is the richest source of of the gamma/delta T cell subpopulation [96].

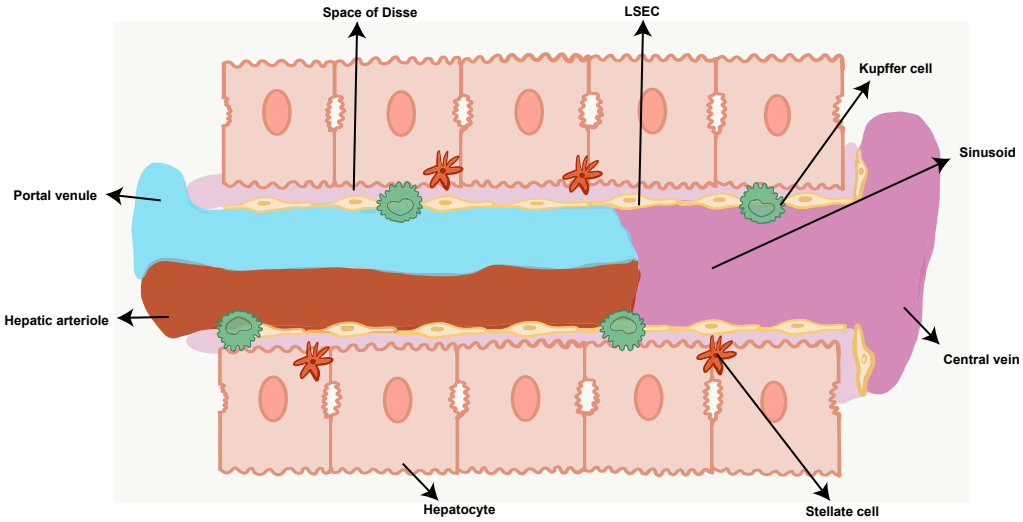

FIGURE 1.2: **Liver anatomy:** The hepatic arteriole and the portal venule circulate blood into the liver sinusiodal space, which is carried away by the central vein. The liver sinusoidal space is lined with non-parenchymal cells: Kupffer cells (liver macrophage), LSEC (endothelial cells) and Stellate cells (source of extracellular matrix proteins). The plasma components from the blood seep through the LSECs and the space of Disse (the interstitial space between the LSECs and hepatocytes) towards hepatocytes. The hepatocytes are organised in the form of plates.

The hepatic micro-environment is also influenced by dietary fats and carbohydrates in the hepatic blood supply. The carbohydrates are taken up by the hepatocytes. Hepatocytes make up 70-85% of the liver volume [97]. They are pivotal for metabolism, protein synthesis, and detoxification. Hepatocytes take up carbohydrates from the hepatic micro-environment, which are provided by the blood supply. Additionally, hepatocytes also receive pathogenic and inflammatory signals, and respond by releasing acute phase proteins in the blood [98]. They also contribute to T cell activation [99]. Hepatocytes are well studied for their innate immune response via the expression of a variety of pattern recognition receptors for major pathogens, such as, HCV [100]. Therefore, hepatocytes have a vital role in producing innate immunity proteins and controlling bacterial infection and chronic liver disease, especially cirrhosis. As mentioned in subsection 1.5.1, the liver is the predominant site for elimination of IFN-α. Consequently, hepatocytes are a key element of study for translational experiments, to understand the interaction of immunity with bacterial infections and how theses are combated with the production of ISGs.

In the above sections I have covered the biological aspects of IFN-α as a protein therapeutic and the importance of the liver and hepatocytes in the generation of immune response via JAK/STAT pathway. In the following sections, I will introduce the concepts of mathematical modelling applied in this work in order to understand the mechanistic details of the JAK/STAT pathway activated by IFN-α.

1.7 Mathematical models in biology

At the turn of 21st century, modelling was vastly accepted as a tool for analysing and explaining biological systems and has since become an integral part of drug discovery pipelines. However, the reliability and the explanatory power of the models depends on the chosen modelling approaches and level of details that are included in the model. With respect to quantitative biology and pharmacology, modelling helps to validate hypotheses which are supported by experimental data. In addition, it has lent its hand to experimental predictions and contributing positively towards good experimental/ clinical study-design. Over time, impressive cases of models have been published which have provided fresh perspective towards biological/clinical studies due to the holistic approach of such models.

Existing modelling techniques employed in biology can be grouped in various classes. In the following sections, I will cover two approaches commonly used in this work: Deterministic modelling applied in systems biology and physiologically-based pharmacokinetic (PBPK) modelling utilised in systems pharmacology.

1.7.1 Quantitative models for signalling dynamics

On one hand, with the advent of high-throughput technology and the associated cost reduction (microarrays and flow cytometry etc.), has led to the literature filled with what it's known as a "data iceberg". On the other, the signalling pathways are complex and the effect of single players is not easy to understand without the surrounding context. Computational modelling allows the integration of various datasets (the "data iceberg") to help understand the big picture. This kind of systems thinking is of increasing importance in biology, because of the high inter-connectivity and high interdependence of of molecules, at cell-level, following to tissue and finally to body level. Computational modelling is a tool through which we can make sense of such quantitative data. On the cellular scale, one can have simple ordinary differential equations (ODEs) models, stochastic (SDEs) models and spatial models. The ODEs and SDE represent change of species over time ($\frac{\partial[Species]}{\partial t}$), while the partial differential equations (PDE) represent the change of species in geometric state space ($\frac{\partial[Species]}{\partial x}$).

ODE-based models are generally used to describe population dynamics and are often termed as deterministic models. In deterministic systems, no randomness is involved in calculating the interaction of existing molecules with future molecules, thus, when simulated multiple times, such models always produce the same result when triggered [101]–[104]. Experimentally, such dynamics can be measured by techniques like western immuno-blots, PCR or microarray to detect concentration changes over time for the particular protein or mRNAc, and the model is therefore based on these quantitative experimental datasets. In reality, the repeated measurements of such experiments result to time-course dynamics which look similar but have slight variations in them. These variations are largely driven by stochastic processes which are subject to random external perturbations, hence in every repeat of the experimental procedure, it is impossible to yield the exact same result. These random effects occur at the microscopic scale where the stochastic motion of the molecules are characterised by two properties: i) their random occurrence in time and ii) no correlation between successive interaction. The consequences of such random processes can be investigated and analysed by the development of SDE-based models [101], [105], [106].

In the case of dynamical deterministic modelling of cellular signal transduction, systems biology has made considerable advances [107]–[109]. For the JAK/STAT pathway activated by IFN-α, the quantitative mechanistic models predict the behaviour of the system over time and track the dynamical changes for a set of proteins in the pathway, helping explain the complexity, dynamics and specificity of the activated response. The first computational model to describe the JAK/STAT pathway via Epo signalling was established in the work of Swameye et al. [110] where the model revealed that the pathway is non-linear and that the nucleus plays a major role in regulating STAT5. This model has been used as the base model for further works and has been expanded by the inclusion of more complex molecular events of cytoplasmic shuttling, along with time series data [111]–[113]. In parallel, the first ODE-based model of activation of the JAK/STAT pathway by IFN-γ was developed by Yamada et al. [114], where they analysed the control ofthe feedback by the SOCS1 molecule on the pathway. Other dynamic mathematical modelling describing the pathway in the context of interferon were done by Smeija et al. [115] and Maiwald et al. [116]. Finally, Rybiński et al. [117] have analysed various models of the JAK/STAT receptor activation and laid emphasis on model selection methods for the same, when the model is evaluated and analysed without sufficient data. In the studies by Sharma et al., Papin et al. and Heinrich et al. [118]–[120] large scale JAK/STAT signalling models including the feedback on the pathway were reconstructed and analysed for descriptive insight on the fundamental system properties of the pathway.

Nevertheless, all the deterministic efforts lack an exhaustive and systematic analysis of the influence of the randomness introduced by stochastic fluctuations in the molecular reactions among the molecules involved in the pathway. Experimentally, the individual mechanisms behind the heterogeneity in isogenic cell populations have been related to stochastic events in the JAK/STAT pathway responsible for eliciting the antiviral response have been well documented [81], [82], [84], [87], [121]. Development of stochastic counterparts of these using modelling still remains an open topic [122]. However, there have been some endeavours for stochastic models for JAK/STAT pathway, where the pathway is activated by different IFN types. For example, Auguilera et al. [123] studied the stochastic model of JAK/STAT pathway response to IFN-β and analysed the control of positive and negative feedback on the bistable response of IRF7. Zhang et al. [124] developed a small model of the IFN-β induced activation of IRF7 and ISG56 response to the virus and analysed the control of the negative feedback of ISG56 in the stochastic expression of IFN-β. Finally, a recent study by Czerkies et al. [125] has analysed the stochastic effect of IFN-β pre-stimulation on responses to poly(I:C) which replicates the viral stimulation.

In conclusion, such systems biology models of the activated JAK/STAT pathway by IFN-α can offer insights into complex decisions made by this pathway for immunity. In order to understand the cellular processes that contribute to drug development, it is crucial to model the signalling system which includes the sufficient details of the complexity: The feedback and -forward loops. In the past few years, systems biology has served as a complementary tool to the preclinical and clinical drug development pipeline and is slowly finding its way into clinical pharmacology modelling approaches.

1.7.2 Pharmacokinetic/Pharmacodynamic modelling

In the drug development pipeline, computational models are implemented in the form of pharmacokinetic and pharmacodynamic (PK/PD) models. These models

describe the relationship between the body and the drug in complementary ways: PK *how the body processes and clears the drug*, whereas the PD describes *how the drug makes the body respond* [126]. Only with a PK/PD model is it possible to assess the clinical significance of differences in PK under various circumstances. With the growing importance of preclinical understanding of drug discovery processes, empirical PK models and mechanistic PK/PD models [127], [128] can provide strong insights into clinical outcomes. In many cases, these models are "minimal" where two or three-compartment (where the compartments mimic the physiological organs of the body) models are used to describe the distribution profile of the drug into the organs of the body by using zero, first or second order rates as absorption rates between the different organs.

In the past, the virus effects on the animals and later humans were measured for the effect of the virus on the IFN-α PK [129]–[132]. Mathematical models were developed to analyse IFN-α PK and understand the effects of HCV RNA decay and to access the effectiveness of the therapy [133]–[135]. On the other hand, classical one-compartment PK models were developed to describe IFN-α distribution of different routes of administration, e.g., in a study by Chatelut et al. [136], effect of a subcutaneous dose on IFN-α PK was analysed. Similarly, a simple model of absorption and elimination could describe the pharmacokinetics for subcutaneous doses of pegIFN-α and ribavarin in HCV-HIV co-infected patients, published by Powers et al. [137]. Jeon et al. [138] developed a one-compartment model with first order elimination and turnover and a transit compartment to model PKPD of a sustained release of IFN-α PK and neopterin PD in healthy human volunteers. There have been models to understand the toxicology and dosing regime of IFN-α on animals because such studies and their validation serve an important role in pre-clinical assessment [139]–[141]. For example, a minimal two-compartment PKPD model of IFN-α distribution in mice was developed in the study by Benson et al. [134]. A two-compartment receptor-mediated pharmacokinetic model for IFN-β in monkeys was developed by Mager et al. [55] and by Abraham et al. [142]. Additionally, some models were developed to describe interspecies scaling of IFN-α doses. Furthermore, it is necessary to rely on PBPK *in vitro in vivo* extrapolation (IVIVE) or scaling of animal data to humans in regards to prediction of absorption and clearance of IFN-α doses [143], [144]. To scale from animal data to humans, the earliest model was developed by Lave et al. [145] where they used published PK data of IFN-α in animals and observed underestimation by allometric scaling on the prediction of parameters in man. Kagan et al. [146] developed two-compartment PKPD models for IFN-α and IFN-β where they described interspecies scaling of target-mediated drug disposition (TMDD) of pharmacokinetics for rodents, monkeys and humans. They were able to conclude that classical allometric scaling performed well in case of type-I interferons and described the TMDD at the liver.

1.7.3 PBPK methodology

As mentioned in the previous section, PK/PD models do not represent human physiology in detail. PBPK modelling aims for a detailed representation of human or animal physiology at the whole-body level in which prior information available on the biological system and on the drug are combined together to predict a priori the expected pharmacokinetics. These models mimic the physiology of an organism. The anatomical compartments of the PBPK model are coupled to each other via ODEs. The organs (anatomical compartments) are linked by the circulatory system. These

compartments replicate the most important organs of the body that contribute to the drug ADME profile [147]–[149].

Parameters in PBPK models are, on the one hand, based on large-scale collections of physiological parameters such as organ volumes or blood flows which build up the physiological database or organism properties for different species such as mouse, rat, dog or human. On the other hand, physicochemical properties of the drug such as lipophilicity and molecular weight are used to parametrise the distribution model describing the steady state tissue concentrations as well as the corresponding permeation rates. Hence, even though PBPK models may comprise several hundreds of ordinary differential equations, the number of independent model parameters is usually small (less than 5 per compound in most cases), due to the large degree of prior physiological information contained in the models. Each organ in a PBPK model is characterised by an associated blood flow rate, organ volume, permeability and tissue partition coefficient linked together by arterial and venous blood compartments (see Figure 1.3). These parameters are obtained from the literature.

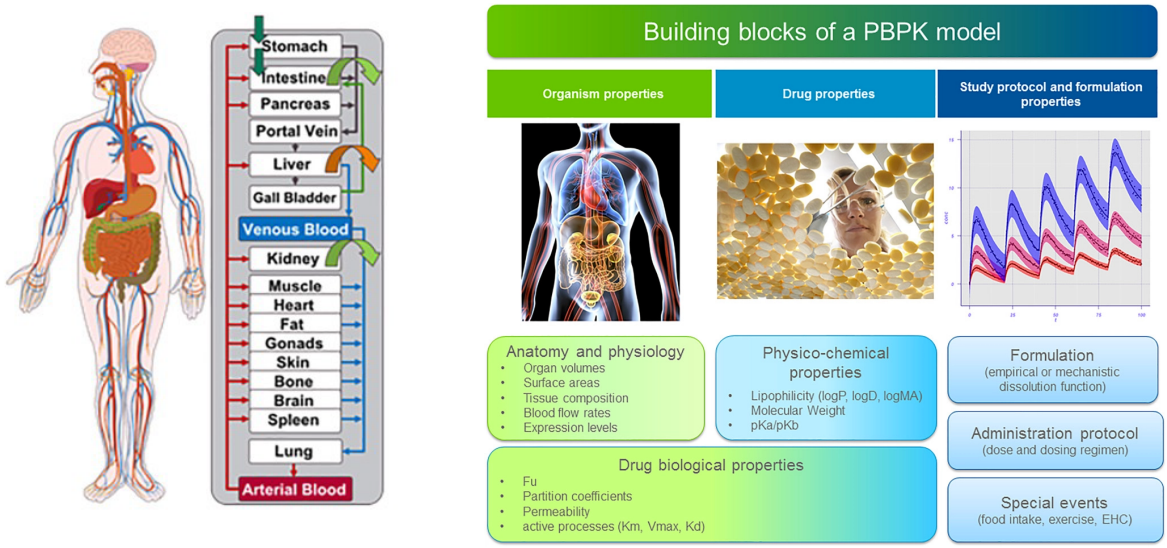

FIGURE 1.3: **Figure adapted from Kuepfer et al. 2016 [144].** The representation of a whole body PBPK model containing all the important organs required to simulate the ADME of a compound. The organs are linked to the arterial and venous blood compartment with partition coefficients, permeability, blood-flow rates and volumes. The PBPK models typically consists of building blocks which are either organism properties or drug compound properties and both of them can be combined to simulate different drug-dose scenarios.

1.8 Quantitative Systems Pharmacology (QSP)

More recently, QSP has evolved from systems pharmacology where the integration of two levels of complexity is achieved. On the whole body level, the drug distribution (in the form of ADME profile) is modelled and on the intracellular level, the biochemical/signalling cascade are included from approaches of systems biology. Thus, this field aims to have a perspective on the system as a whole, as reviewed

in the literature [150]–[152]. Hence, multi-scale physiologically based pharmacokinetic and pharmacodynamic (PBPK/PD) modelling [144], [153], [154] is advocated for its holistic approach of modelling towards clinical decision making of a pharmaceutical molecule. Furthermore, these models are integrated in animal and human physiology along with *in vitro* experiments and allow translation of experimental results from pre-clinical research to clinical development and contribute to an efficient design of cost-effective animal studies too.

For the design of QSP models, one has to cautiously consider the *granularity* of the model. Granularity is the detail level to which the molecular and pharmacological processes are represented and associated such that the model has higher predictive power and flexibility to follow more than one molecule. But inclusion of such details comes with a penalty, which is the difficulty of building, running, integrating and maintaining a model with a vast number of molecular species and parameters. This can be summarised as complexity in the approach of QSP. The *sine qua non* for detailed PBPK/PD models is quantitative data on each scale, i.e., molecular, cellular and organ level (as detailed in the Figure 1.4).

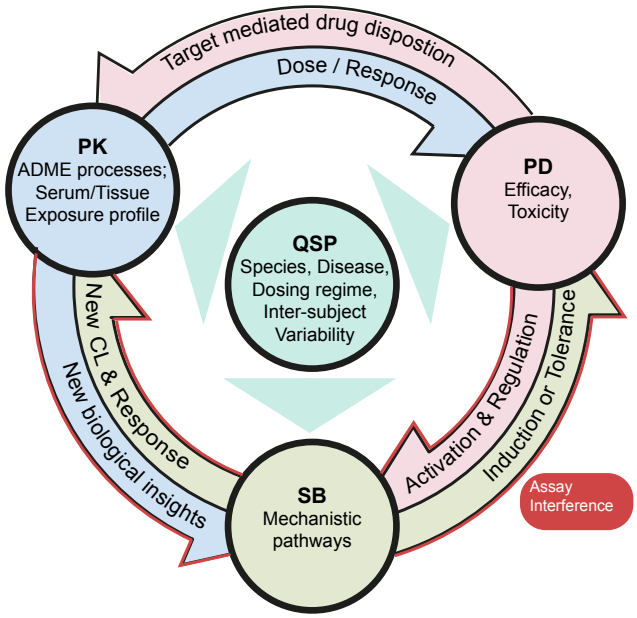

FIGURE 1.4: The relationship between Pharmacokinetic (PK) ADME and the immune response to the treatment of a therapeutic protein can be modelled by combining the mechanistically detailed pathway described by systems biology (SB) approach with PK modelling, giving the opportunity to explore the cross-species extrapolation, individual inter-variability and dosing regimes through quantitative systems pharmacology (QSP). Exposure profiles of the PK and the biological activity induced by it as dose-response relationship describe the balance between the induced response and the tolerance of the biological system to a certain biologic. Inter-dependencies on the impact of the biological activity on the PK can lend better insights on TMDD and ADME profiles. To help infer the inter-dependencies, assays can be used to check and infer the established model at various stages resulting into an iterative cycle for data interpretation and establishing a clear PK-PD relationship.

PBPK/PD models help understand translation. As stated earlier, pharmacological aspect is focused on human application. The wealth of information that lies in the data on a molecular scale and in animals is important to give insights into the early-stage drug discovery, biological implications and *in vitro* assay design. Such models help to bridge the understanding of biological, metabolic and physiological differences on a molecular and animal scales such as cell culture vs *in vivo* animal models vs *in vivo* human conditions. Thus, they characterise the longitudinal and physiologically varied effects of drug intervention. Hence, building such models requires integration of the scientific network (wet-lab biologists, systems biology modellers) and drug discovery experts. Such strong collaborations imply standardised modelling language and quantitative validation sets for model verification.

In the case of biologics, PBPK/PD models are of increasing importance as they not only help to decide whether the dose regimen should be adjusted accordingly, but give clear understanding into the biomarker of choice for therapies of immuno-oncology interest.

1.9 This thesis in context

This thesis is an endeavour to implement the state-of-art quantitative systems pharmacology (QSP) approach to determine a quantitative understanding of the action of injected dose of the therapeutic protein, IFN-α. This work combines whole-body physiologically-based pharmacokinetic models (PBPK) with mechanistic intracellular signalling models (PD) for humans and mice. The resulting PBPK/PD aids to analyse the liver response to IFN-α injection.

In chapter 2, I will introduce the data and software used to establish the PBPK/PD model. I will also elaborate on the single-cell data which laid the basis for the side project on cell to cell variability with respect to IFN-α response in the hepatic cell culture. In particular, I will detail the methodology of preparing cellular and PBPK models for IFN-α in humans and mice. Moreover, I will discuss the current understanding and availability of experimental and PK data in the context of IFN-α drug action and cellular response, respectively. During the course of this dissertation, the establishment of such models led to collaborative effort on this topic, which will be discussed in this chapter. I contributed to the experimental design of the experiments produced by our collaborators.

In chapter 3, I will elaborate upon the PBPK/PD model for IFN-α in human where I describe the establishment and analysis of the model. In this chapter, I further examine the multi-scale target-mediated drug disposition (TMDD) as the primary clearance process of IFN-α from blood plasma. Finally, I characterise the quantifiable differences between *in vitro-in vivo* situations of IFN-α responses. I simultaneously investigate the differences in temporal dose-response relationship between IFN-α and antiviral response of IRF9 mRNAc. I also consider the strength of PBPK models where large number of compartments (depicting organs) describe the physiology of the organism and predict the the tissue concentration–time profiles of IFN-α distribution following i.v. administration.

In chapter 4, I will focus on preclinical translation. Mice have been extensively used in preclinical research as their genes are closely related to that of humans (reviewed in Emes et al. [155]). Animal studies serve as intermediate step between *in vitro* and

in vivo studies. The development of computational models for animals help contextualise the research on them. Thereby, in this chapter, I will elaborate on the set-up of the whole-body PBPK/PD model for the mouse to simulate the effect of the injected murine IFN-α. I will explore the difference in the plasma concentration profile (ADME distribution) of murine IFN-α and human IFN-α in mice and its implication in species-specific response to the aforementioned IFN-α subtypes. Further, as most tissue distribution studies are conducted on animals, I will compare the simulated PBPK tissue concentration–time profiles of murine IFN-α distribution following i.v. administration in mice with the available experimental data.

Chapter 5 is a side-project for this dissertation. The work in this chapter is motivated from the variability in the JAK/STAT pathway response to IFN-α which has been reported in the literature [85]. The molecules of the signalling pathway have inherent variability in their endogenous abundance which determines the fate and strength of the response to the stimuli. Therefore, the work of this chapter describes the cell to cell variablity in response of the JAK/STAT pathway to the trigger of IFN-α in human hepatic cell lines (Huh7.5). The chapter encompasses the development of a mechanistically detailed stochastic model of the JAK/STAT pathway using flow cytometry data provided by our collaborators as the basis of the model analysis to aid in understanding the impact of biochemical noise (intrinsic and extrinsic) on the pathway. The stochastic model described in this chapter is by far the most detailed stochastic model for the activation of JAK/STAT pathway in response to IFN-α.

As a final note, despite over 70 years of research, relevant new findings are still being uncovered about surprisingly fundamental aspects of the immune response when triggered with IFN-α. In general, as a therapeutic protein, IFN-α is outdated with regards to protection against the global burden of HCV, but it is still an important therapeutic for other viral infections and for different cancer treatments. Besides, in the past years, great attention is being brought on the aspect of humane animal testing in clinical drug discovery pipelines. In the light of this topic, many attempts are drawn towards the principles of *3R*s (reduction, refinement and replacement) (reviewed in Ranganatha et al. [156]). In this regards, the computational simulations can be a method to replace the animal experiments in the future. In the last decades, mathematical models have expanded to be potential support in biomedical research. Therefore, it is of increasing importance to implement translational mathematical models to be able to explore the relationship of drug action to the induced response of IFN-α in a model organism by implementing QSP approaches.

Chapter 2

The building blocks of PBPK/PD modelling: Data and software

2.1 Chapter summary

In the fields of systems biology and pharmacology, an iterative process is now established where experimental data is used as a knowledge base to created computational models. The scope of this work is to deal with models for two species, namely, human and mice. To be able to establish and analyse multi-scale PBPK/PD models, quantitative experiments are a must. In this chapter, I will detail the extensive experimental research which was the basis of the PBPK model development and prediction for humans and mice. For the QSP approach, system biology models serve complementary to PBPK models. Therefore, I will detail on experimental data used to establish the two models respectively. I will elaborate the data used to establish PBPK models where the injected i.v. IFN-α dose in humans and mice were used and also on the data used to establish systems biology models of JAK/STAT pathway. The systems biology models are based on data of various molecules in the signal trasduction pathway obtained in primary human and mouse hepatocytes. Most importantly, I will describe on the experimental data that was a result of collaborations established during the course of this work and to a great extent drive the fruitfulness and analysis of this work. This chapter also contains the details of single cell experiments that were performed to implement and validate the mechanistic stochastic model which is used to analyse the cellular response variability to IFN-α treatment on human hepatic cell-line.

Furthermore, this chapter covers the software and methods used to establish whole body models as well as the cellular scale for the respective species. The methodology which focused on the integration of the two scales is also discussed such that in the later chapters a clear understanding of the methodology of the establishment of the models and their results is achieved.

2.2 Experimental data

This work focuses on the models of humans and mice. For the models developed on humans, a large amount of experimental data has been procured from the literature. In the case of the mouse model, the experimental data used was taken from the literature and data obtained in collaboratory effort. In the following subsections, I describe the different datasets used for the PBPK/PD model and for the inter-cellular stochastic model of the JAK/STAT pathway.

2.2.1 Pharmacokinetic blood plasma measurement of IFN-α for humans

Four datasets of IFN-α plasma concentrations were obtained from three publications for the PBPK modelling. These data were divided into two sets: One dataset was used for parameter estimation to establish the model and the rest were the basis of the validation of the established model. The data from the publication Wills et al. (1984) [50] was used for the model prediction and the remaining two datasets from Shah et al.(1984) [48] and Radwanski et al(1987) [49] were available for model validation.

The first pharmacokinetic profile of recombinant leukocyte IFN-α (rIFN-α) was extracted from Wills et al. (1984) [50]. In this work, a dose of 36×10^6 U rIFN-α was administered as an intravenous infusion to a group of 6 human subjects for 40 mins. rIFN-α is a water soluble protein with a molecular weight of 19500Da. The activity of rIFN-α is commonly expressed in terms of units (U) where 1 mg of rIFN-α protein corresponded to 1.7×10^8 U. The publication multiplied the dose with a factor of 6 to convert it into picograms (pg). This information was used to calculate the dose in milligrams (mg). The blood plasma concentrations were measured over a period of 24 hours in this study. This data was retrieved, digitised and converted into concentrations using a global unit for specific activity of rIFN-α specified in the publication. This concentration data was used for fitting the human PBPK model.

Two plasma pharmacokinetic profiles of rIFN-α-2 were extracted from Shah et al. (1984) [48]. A group of seven patients were administered intravenous rIFN-α-2 doses of 30×10^6 U and 60×10^6 U over a period of 30 mins. The specific activity of rIFN-α-2 was taken from the NIH standard. Although the plasma concentration samples were collected for 48 hours, the samples for a period of 8 hours were available in the research paper.

The final plasma profile of rIFN-α-2b was taken from Radwanski et al. (1987) [49]. In this study, a group of four healthy volunteers was administered an intravenous dose of 5×10^6 U/m^2 body surface area rIFN-α-2b over 30 mins. The reported interferon specific cativity was 2.2×10^8 U/mg. The serum concentration was plotted for a period of 6 hours in this study.

The doses were calculated in *mg* for all the publications using the formula depicted in 2.1

$$Dose\ in\ mg\ = \frac{Dose\ in\ IU}{Specific\ Activity\ in\ \frac{IU}{mg}} \tag{2.1}$$

The pharmacokinetic data from all the literature were digitised and the concentrations were calculated as in 2.2.

$$Concentration\ in\ \frac{\mu mol}{l}\ = \frac{Concentration\ in\ \frac{IU}{ml}}{Molecular\ Weight\ \times Specific\ Activity} \tag{2.2}$$

This concentration data was used to validate the model.

2.2.2 Pharmacokinetic blood plasma measurement of IFN-α for mice

To model the mouse pharmacokinetics, three plasma concentrations of murine IFN-α (mu-IFN-α) were used in total, out of which two datasets were used for validation. The first was taken from Bohoslawec [39] where the mice were injected with a bolus intravenous injection of mu-IFN-α (subtype unknown). The dose was 8.7×10^5U. For each measurement time point, 3 mice were killed to yield the average of the data. mu-IFN-α concentrations were quantified by an antiviral assay and this concentration data was used in the parameter estimation of the PBPK model.

The second dataset was provided by our collaborator Dr. Mario Köster[1]. This dataset was published in 2010 by Pulverer et al. (2010) [157]. C57BL/6 Mx2-Luc transgenic mice were injected with an intravenous bolus dose of 5000U mu-IFN-α-4. Before sacrificing the mice were injected with luciferin so that the Mx2-Luciferace activity in the liver could be measured. They were then sacrificed and Mx2-Luciferase activity was measured by light emission from the organs of the mouse body. Details can be found in the publication [157]. The residual plasma mu-IFN-α-4 in the serum was measured for 20 mins and the sample concentration was determined by ELISA. The specific activity of mu-IFN-α-4 was 1.410^8 U/mg; the conversion of the IU to concentrations are described in the aforementioned equations 2.1 and 2.2. This dataset was used in preliminary analysis as it was for a short-time scale of 20 minutes. It has to be noted that Pulverer et al. [157] measured a fraction of less than 10 % of the injected mu-IFN-α 4 dose in the serum and this was scaled to 100% in the publication.

The third dataset was digitised from Rosztoczy et al. (1986) [158] where an i.v. bolus dose of 2000 IU/g of mu-IFN-α was injected into male CFP mice with weight 20 ± 1 gram. The specific activity of mu-IFN-α used in this publication was 1.2×10^7 U/mg. Data (an average of a set of six mice) was collected over a time period of 12 hours post injection.

For validation, the first dataset was extracted and digitised from the publication Kiuchi et al. (1983) [159]. In this work, mu-IFN-α was injected in male CDF1 mice as i.v. dose of 1×10^5 IU/mouse. Plasma volume was estimated as one tenth of the body weight and serum volume as 50 % of the plasma volume. The specific activity of the mu-IFN-α used was 3×10^{7} IU/mg. Each data-point was a measurement of pooled sera of three mice and the measurements were taken for 3 hours.

The second dataset was extracted from Koyanagi et al. (1997) [160]. In this study an i.v. dose of 10 MIU/kg human IFN-α (hu-IFN-α) was injected in mice. Here, two measurements were reported: From the light and dark cycles (one measurement done after the injection at 5 a.m. and the other after the injection at 5 p.m.). The serum samples were collected at the time points: 0.167, 0.5, 1.0, 2.0, 3.0, and 4.0 hr post injection, and each data-point represented a mean of six mice.

Further calculations of all the datasets into proper dose of mg/kg and the plasma concentrations of nmol/ml are described in the Appendix A in Table A.2 and Appendix C, Table C.1 .

[1]Department of Gene Regulation and Differentiation, HZI – Helmholtz Centre for Infection Research, Inhoffenstr. 7, 38124, Braunschweig, Germany.

2.2.3 Human hepatocyte data

The intracellular measurements of the JAK/STAT pathway were used to parameterise the intracellular signalling model. The time course data for molecules after IFN-α stimuli on Huh7.5 were taken from Maiwald et al. (2010) [116] for 0, 1, 2, 3, 4 and 6 hours. Huh7.5 and primary human hepatocytes (PHH) were treated with 500 U/ml of human leukocyte IFN-α and the abundance of the induced intracellular molecules was measured. These datasets encompass the measurements of pJAK, pSTAT1, pSTAT2, SOCS and IRF9. The proteins were monitored using quantitative immunoblotting. The publication also had measurements of wildtype Huh 7.5 cells and IRF9 over-expressing Huh7.5 for IRF9 mRNAc expression using quantitative PCR and microarray analysis. Furthermore, dose-response measurements of pJAK, pSTAT1 and pSTAT2 for the doses 500 U/ml and 1000 U/ml leukocyte IFN-α were performed on primary human hepatocytes. The specific activity of human leukocyte IFN-α was 1×10^6 U/mg which was then converted to the model units as used by Maiwald et al. [116], further explained in Appendix A, section A.1.

The second validation dataset was obtained from Bolen et al. (2014) [161], kindly provided by Christopher R. Bolen , Michael D. Robek and Steven H. Kleinstein from Yale University. The dataset represented long-term (24 hours) time course data to support the model prediction A.3. In this work, the measurements were performed on human Huh 7 and PHH. The cells were treated with 500 U/ml of IFN-α and data was collected at time points 0.5, 1, 2, 4, 6, 12 and 24 hours post-treatment. Total RNA was collected and analysed by microarray and quantitative PCR. Huh 7 cells were treated with 10 U/ml, 100 U/ml, 500 U/ml and 2500 U/ml IFN-α and IRF9 mRNAc was analysed using RT-qPCR at time points 1, 4, 6, 12 and 24 hours after stimulation.

The third validation dataset was digitised from Jilg et al. (2014) [162]. In this publication, the Huh7.5 cells and PHH from three donors were used. PHH recieved the stimulus of 0.21 ng/ml pegylated IFN-α (peg-IFN-α) (equivalent to 6.91×10^{-6} nmol/ml or 15 U/ml). Huh7.5 were stimulated with 0.43 ng/ml (1.38×10^{-5} nmol/ml or 30 U/ml) $(IFN-\alpha)$. They identified differential effects of $(IFN-\alpha)$ and IL28B on hepatocytes using transcriptomic microarray and followed the temporal dynamics of IRF9 gene expression at 4,8 and 24 hour respectively by isolating the RNA. Gene induction was determined by expression microarrays.

2.2.4 Mice hepatocyte data

Primary mouse hepatocytes (PMH) isolated from transgenic mice were treated with different doses of mu-IFN-α-4 by our collaboration partner, Dr. Mario Köster. He quantified the luciferase activity by measurement of the emitted light intensity of the luciferin-luciferase reactions for the reporter gene expression (Mx2) [157]. The response of Mx2-Luc light intensity was measured for mu-IFN-α-4 doses of 1 U/ml, 10 U/ml, 100 U/ml, 500 U/ml, and 2500 U/ml at 18 hours or 24 hours. Two repeats for doses 5 U/ml and 500 U/ml mu-IFN-α-4 were performed at time points 0, 4, 8, 12, 19, 23, 27, and 34.5 hours. The specific activity of mu-IFN-α-4 was 1.4×10^8 U/mg.

2.2.5 Flow cytometry data for stochastic modelling

For the establishment of intracellular stochastic model, the datasets were provided by our collaborator, Dr. Marco Binder[2]. The experiments were kindly performed

[2]Research Group "Dynamics of early viral infection and the innate antiviral response", Division Virus-associated carcinogenesis, German Cancer Research Center (DKFZ), Heidelberg, Germany.

by Pascal Mutz and Christopher Daechert. Human IFN-α-2a with a specific activity of 3.91 $\times$ 10 ^{8} U/mg was used in this study. Human Huh7.5 cells harboured a bacterial artificial chromosome (BAC) containing destabilised enhanced fused green fluorescent protein (GFP) mxa and ifit1. 1.5 $\times$ 10^5 cells were seeded per well and were treated with IFN-α doses 10 U, 100 U, 500 U and 1000 U, 24 hours after seeding. The time course measurements were taken at 8, 12, 16, 20 and 32 hours after treatment with IFN-α doses and the cells were harvested at the above mentioned measured time points. Further protein expression was inhibited by treating the cells with 2 % paraformaldehyde. The cells were then washed with phosphate-buffered saline (PBS) and measurements were performed with flow cytometry.

2.2.6 Databases accessed for parameter values

The assumptions and reasons for using certain values for kinetic parameters, initial concentration of the molecules present in the cell/body for modelling are based on the data from various databases. In particular, I used information from the BioNumbers database [163] to find the molecular numbers of the proteins present in the cell and compute the initial concentrations for the same. BLAST [164] was used for evaluating the differences in protein structure identities and homology between mouse and human molecules (e.g. receptors, JAKs, STATs etc.), See Appendix C, Table C.7. Drugbank [165] was accessed to find the values of the lipophilicitiy, molecular weight and other compound-specific information needed for the PK model of IFN-α (see Appendix A.2, Table A.4). Information on the transcription factor binding sites was obtained from ENCODE [166].

2.3 The modelling resources

In this section, I cover the software used to achieve the multi-scale integration of experimental data to *"learn"* and *"predict"* the behaviour of the system, to answer the questions asked in this work. The whole-body plasma distribution models were developed in the software, PK-Sim and the intracellular models were developed in the software, COPASI. The integration of the models was executed in MoBi. This step-wise procedure helped in effectively integrating the experimental data at multi-scale level into the PBPK/PD model which aids in predictions.

2.3.1 Physiologically-based pharmacokinetic model

Model setup

Open Systems Pharmacology Suite (OSPsuite) was used to estbish the PBPK/PD model of IFN-α drug action. The OSPsuite includes two software tools: PK-Sim and MoBi which were formerly commercially available [167], [168]. Since January 2017, it is a freeware under the license GPLv2. The software suite is publicly available at Github[3].

PK-Sim is a software for physiologically based pharmacokinetic modelling. The software has database of relevant expression information of the protein binding partners for human and common animal models. The software has a user-friendly interface and allows for integrating information on the organism, the compound and the administration protocol with the formulation of the compound. Independently,

[3] https://github.com/Open-Systems-Pharmacology

PK-Sim enables the simulation of pharmacokinetics (drug distribution ADME processes) resulting from single or multiple dosing regimes through all routes of administration. It enables the modelling of small (size < 900 daltons) via three sub-compartment as well as large molecules (size > 900 daltons) via four sub-compartment (large molecules) per organ. The mentioned three sub-compartmental structures differentiate the separation between plasma/interstitial space, thus defining instantaneous permeation (without interstitial compartment; for small molecules). The four compartment model represents high permeation barrier between plasma and interstitium thus describing non-instantaneous equilibrium between plasma/interstitium concentrations (with interstitial compartment; for large molecules that are highly bound to plasma). Once set-up, the models from PK-Sim can be linked to the intracellular pharmacodynamics in MoBi. Furthermore, the software tool MoBi is available for multi-scale physiological modelling and allows the user to access, manipulate and extend the models developed in PK-Sim. MoBi can also be used to develop systems pharmacology models from scratch. It is a tool for developing mechanistic dynamical models of biological processes and is complementary to PK-Sim. In this work, all models were created with PK-Sim, exported to MoBi and extended with pharmacodynamic interactions in MoBi.

The PK-Sim (Version 7.0; OSPsuite) software tool was used to model the PK IFN-α-2 in humans and mu-IFN-α-4 in mice (PK-Sim Version 7.2; OSPsuite) using the PBPK approach. The organism details of healthy human and mouse were integrated with physico-chemical information of IFN-α to parameterise the IFN-α PBPK model.

In PK-Sim, the biometrics of the average individual species were described. The software has building blocks which can be later compiled into a simulation. Please note, in the upcoming explanation, the words which are *italicised* are the components of the software PK-Sim where the model components are set up. In a nutshell, the *compound* building block carried the information on physico-chemical properties of IFN-α. Since IFN-α is a therapeutic protein, it is depicted as a large molecule in the *compound* building block. The information of *renal clearance* from the kidney along with the specific binding values (K_{off}, K_D) of the *protein binding partners* was established in the *ADME* subsection of the *compound*. The gene expression of receptors were queried in the internal database. The database described the expression values of the receptors in all organs collected from micro-array experiments. The health-state of the individual was chosen as normal hence the expression is not governed by a diseased state. In the *Administration Protocol* building block, the intravenous dose given for human and mouse was inputted respectively for each model. In the *Observed Data* building block, the data for fitting and validation were loaded and assigned to the venous plasma concentration of IFN-α such that they could be used in the simulation later on. Finally, all building blocks were combined to simulate the PBPK model for the respective species. In the model settings, *model for large proteins and molecules* was chosen.

MoBi The simulation was exported from PK-Sim to MoBi as *pkml* format. Here, the drug-receptor binding reactions were restructured to mimic the physiological conditions. The IFN-α PBPK model was coupled with the IFN-α intracellular model in MoBi (version 7.2; OSPsuite).

Reactions and rate laws Most reactions were modelled as mass action kinetics (2.3).

$$v_i = k_i \times [Substrate1] \times [Substrate2] - \frac{1}{keq_i} \times [Product] \tag{2.3}$$

Here, the velocity of the reaction is determined by the k_i and keq_i and the transition concentration of *Substrate1*, *Substrate2*, and the *Product*.

Parameter estimation

Model parameterisation and identification was done in MoBi and MoBi Toolbox for MATLAB (product of Matworks Inc., USA; version R2014b). The toolbox function '*generateMatlabCodeForXML*' was used to export the XML from MoBi to MATLAB and custom scripts were created for plotting. Parameter scans for various parameters were executed in MoBi and MATLAB.

The IFN-α models for human and mouse were fitted in MoBi. The human IFN-α model fitting was performed using the Levenberg-Marquadt algorithm (Maximum number of iterations 200; Initial step-bound factor 100; multiple optimisation runs of 500). The Monte Carlo method was time-consuming and did not perform as well as Levenberg-Marquadt. The mouse IFN-α model fitting was performed using two algorithms: Levenberg-Marquadt algorithm (Maximum number of iterations 200; initial step bound factor 100; multiple optimisation runs of 500) and Monte Carlo method (Break condition for error improvement: 0.001; alpha: 30; multiple optimisation runs of 50). Both the algorithms rendered similar solutions. Since there were more iterations performed with Levenberg-Marquadt, the values from the fit were used for further analysis. Further simulations and analysis of the models were executed using MATLAB.

time course, sensitivities and parameter scan

The time course was simulated in MoBi using ODERHS function written in MATLAB. The MATLAB code for differential equations can be accessed by exporting the simulation.

The sensitivity analysis was performed in MoBi using the sensitivity analysis section. For advanced sensitivity analysis, the simulation was exported as *xml* into MATLAB and custom scripts were written for the same.

The model was exported as xml and the parameter scan was performed using custom scripts written in MATLAB.

2.3.2 Hepatocyte model

Model setup

The JAK/STAT pathway model (referred in the text as hepatocyte model/petridish model/pharmacodynamic model) was modelled using **CO**mplex **PA**thway **SI**mulator [169] (COPASI). COPASI is open source software for mathematical modelling of biological processes. The software can be found at COPASI website[4] and is maintained by international collaborators from University of Manchester, UK; Virginia Bioinformatics Institute, USA and University of Heidelberg, Germany. The software allows simulations for stochastic as well as deterministic kinetics on time course or steady state data. The simulations can be evaluated using the feature of parameter scan for parameter sampling and by creating multiple simulations simultaneously. Furthermore, it provides various features for analysing the developed models such as

[4] http://copasi.org/

metabolic flux analysis, time scale separation, optimisation to name a few. COPASI allows for SBML export/import which supports inter-operability of the model files in different modelling environments.

The human hepatocyte model developed by Tim Maiwald [116] was altered in COPASI version 4.16.104. Over the course of time the COPASI version 4.22 Build 170 was used to do the analysis. The human hepatocyte model was extended to include the reactions for Mx2 transcription, translation and degradation to establish the mouse model. The mouse hepatocyte model was established in COPASI version 4.22 Build 170.

Reactions and rate laws The hepatocyte models consists of 2 compartments. The substrates and the product of each reaction are indicated in COPASI. The reversible, irreversible and multi-compartment reactions are indicated in COPASI as = , $\rightarrow/\leftarrow$ and ☑ Multi Compartment, respectively. Most of the reactions are described using mass action kinetics (2.4 and 2.5) [170], [171].

$$v_i = k_i \times [Substrate] \tag{2.4}$$

$$v_i = k_i \times [Substrate] - \frac{1}{keq} \times [Product] \tag{2.5}$$

Here, v_i is the velocity of the reaction which is defined by k_i or keq and the transient concentration of the *substrate* or *product*.

Parameter estimation

Due to the large size of the model, all the parameters could not be determined experimentally. The human hepatocyte model was fitted and validated with the published data detailed in Section 2.2.3. The mouse model was fitted and validated using the data detailed in Section 2.2.4. The model fits for both the models were performed on the cluster using command line interface COPASI SE 4.19.140.

The models were optimised using Particle Swarm which is a global method on the cluster. The obtained top models were further optimised on the local machine using local algorithm, hooke and jeeves. The resulting models were analysed to find the top 20 models using a script written in MATLAB.

Time course, sensitivities and parameter scan

The time courses of the models were simulated using the LSODA algorithm [172].

For both models, the scaled sensitivities were calculated using the the subtask *Time Series* in COPASI and the option *Single Object* was chosen in COPASI to determine the control of the single parameter on the system. The scaled sensitivities were used because they are normalised and hence allow for comparability of parameters within the model.

Parameter scan was applied to aid in the further analysis of the models. The parameter scans were performed using the task *Time Course* and object *Initial Concentration/Kinetic Value Of Species* in COPASI.

The data visualisation was performed by extracting the report files as text files from COPASI and were plotted in MATLAB by custom-made scripts.

2.4 Integrated PBPK/PD model

The PK models for hu-IFN-α and mu-IFN-α were set up using PK-Sim. They were then exported, fitted and validated in MoBi. The hepatocyte models using human and mouse cell culture data were set up, fitted and validated in COPASI. Up to this point, the models existed separately in the two different software. After that the integration was executed in MoBi as described in chapter 3 section 3.5. Further analysis was done in MATLAB by using custom-made scripts.

2.5 Stochastic intracellular model

The stochastic model of the JAK/STAT signalling pathway was set up using COPASI. A special version of COPASI was provided by Dr. Frank Bergmann. This version allowed to export the model to MATLAB where the algorithm developed by Aguilera et al. [123] was used to fit the model to the single cell data. The Intrinsic noise was introduced by solving the model using Gillespie algorithm in COPASI 4.21. Extrinsic noise was simulated as suggested by Shahrezaei et al. [173] where the extrinsic noise is introduced on the SSA as a time varying parameter and can simultaneously execute on many parameters of the model. This work focuses on introduction of extrinsic noise only on the molecular count of the molecules in the pathway where the noise is normally distributed over the following three values of three values of σ: 0, 0.3, 0.6.

Chapter 3

Multi-scale PBPK/PD model of IFN-α dose in humans

3.1 Chapter summary

The work in this chapter is motivated from the key issue that there is no intra-cellular *in vivo* data for biological processes available on humans except that of the PK for IFN-α. Ultimately, we need to be able to scale the animal *in vivo* or human *in vitro* data to human *in vivo* scenarios. Thus, to make the most of pre-clinical to clinical translation of IFN-α we must rely on either animal *in vivo* data or human *in vitro* data. To achieve this with the present knowledge on IFN-α, the use pf PBPK/PD approach is a powerful strategy.

In this chapter, I elaborate the establishment of such PBPK/PD model, describing the role of IFN-α dose on human body using the methodology described in chapter 2.

This chapter will cover establishment of the cellular model using time course experimental data for the JAK/STAT pathway obtained in PHH and Huh7 cell lines. I will detail the model structure, the parameter identification and the resulting intracellular model containing the cytoplasm and the nuclear compartment of a hepatocyte. I will further discuss how the model is calibrated with dose-response data. Then, I will cover the establishment of the pharmacokinetic model for the IFN-α intravenous injection on humans along with validation of the fit. Finally, the chapter will focus on the establishment and the analysis of a multi-scale PBPK/PD model in human body. Here, I use the mRNAc of IRF9 as a biomarker to compare the IFN-α response *in vivo* vs. *in vitro*. The results highlight the quantitative differences of *in vitro-in vivo* response of the biomarker IRF9 mRNAc for this study.

The text of some subsections and discussion is taken from Kalra et al. 2018 (in preparation) [174] and has been originally written by myself. Most Figures used in this chapter are adapted from Kalra et al. [174] and were originally produced by myself. The experimental data used in this chapter is described in chapter 2, section 2.2; subsections 2.2.1 and 2.2.3 respectively.

3.2 Motivation and open questions

Pharmacokinetics (PK) and pharmacodynamics (PD) play an important role in understanding the relationship between the temporal changes of induced signalling cascades in the cell and the drug distribution in the body [175]. Thus, unfurling the PK-PD relationship contributes to the pre-clinical to clinical translation of doses of the drug. Although IFN-α was first used as antiviral, there is growing evidence for broader clinical applications of IFN-α. IFN-α is extremely potent. It interacts with specific receptors and drives the expression of ~ 300 genes whose products mediate antiviral or anti-proliferative responses. Even though, there is clear understanding on the pharmacokinetics (ADME profile) of IFN-α [44], [50], [176], there is a gap of knowledge towards understanding the dynamics of the response of IFN-α with its receptor at the target site (in this case, the liver) [177]. In addition, the association between the association between gene expression of a variety of genes to the clinical response have not been clearly established [178], [179]. The efficacy of IFN-α *in vitro* remains enigmatic as the work on understanding the antiviral response of IFN-α at the cellular level is ongoing [180], [181].

Classical pharmacokinetic modelling has been employed for decades to understand the distribution of pharmaceuticals in the body [147]. Of late, mechanistic PBPK models have been successfully used as tools for predicting dose recommendations and selecting drug candidates [182]. However, these approaches are limited to the description of the fate of biologics in the blood and do not consider any biochemical consequences [183]. However, in the recent years, kinetic models have been used to understand the biochemical processes in detail [114], [116]. So far, the two modelling techniques exist in isolation. To achieve a systems level understanding of a drug's effect, an integration of both modelling techniques is necessary [144].

The coupling of the PBPK model with the intracellular model will help to analyse IFN-α drug effects in a holistic way - advocating effective treatment methods as different proteins and molecules can be simulated simultaneously. Predominantly, such a PBPK/PD model allows for studying processes that are not accessible by experimental procedures and analysing the IFN-α drug-response interaction at the target site (namely, the liver) in a time resolved manner. Hence, the motivation behind the work described in this chapter is to have a better understanding of the temporal dose-effect relationship at the target site.

In this chapter, I detail on the development a human whole body distribution model of IFN-α and its integration with adjusted detailed intracellular model of the JAK/STAT signalling cascade localised in the liver. Finally, I infer effective concentrations of IFNα arriving in the liver after intravenous injection. This approach opens the opportunity to study the impact of *in-vivo* drug dose on the signalling behaviour in the liver, taking into account the effective dose at the target site..

3.3 IFN-α PBPK model

To represent the distribution of IFN-α at the whole body level and to quantify the exposure on the liver, a protein PBPK model of IFN-α was established. The corresponding model comprises more than one hundred ODEs. However, the a posteriori physiological knowledge constrains the number of independent parameters in the PBPK model which need to be identified. The clear separation of physiological and drug-specific parameters also allow for the separated inference of the parameters on the ADME profile.

For the human PBPK model of IFN-α, the weight, height and BMI of an average European individual were selected as individual biometrics (Appendix A B.1). Physico-chemical information of IFN-α was obtained from the literature (Appendix A, Table A.4).

There are two ways IFN-α gets eliminated from the plasma: By binding to the receptors present in the liver (TMDD) and by pand via excretion through the kidneys. These modes of clearance were included in the PBPK model. The TMDD was accounted by relative tissue-specific distribution of IFANR1/2 that was taken from the gene expression database within PK-Sim [184]. This allows for the estimation of *in vivo* receptor abundancies in the liver and other organs. The clearance parameter was inserted from [50], where the elimination of IFN-α by the GFR were described. The receptor kinetics and binding values were implemented in the model according to the established kinetic mechanisms described in previous studies [185]–[187].

3.3.1 Human PBPK model overview

The following text is taken from the publication Kalra et al. [174] and has been written by myself.

"The clinical profile of IFN-α was modelled as zero order input rate and first order elimination rate. All the parameters for the pharmacokinetic modelling are listed in Table 3.2. For modelling purposes, the liver was simplified as one big cell with keeping the hepato-cellularity number to calculate the cell content and concentrations of the receptors [188], [189]. The liver was divided into three compartments: the interstitial, the cytoplasm and the nucleus. The defined volumes of each compartment are described in Appendix B, Table B.3. As seen in Figure 3.1 the IFN receptor dynamics were modelled in the interstitial compartment and consist of a detailed representation of the receptor binding and turnover. Here, the IFN-α arriving to interstitial compartment binds to IFNAR2 to form a dimeric ligand-receptor complex (IFNA-IFNAR2 Complex) (**M1**). The ligand-receptor complex (IFNA-IFNAR2 Complex) binds to IFNAR1 to form the hetero-trimeric ligand receptor complex (Activated Receptor Complex) (**M2**). The hetero-trimeric ligand receptor complex was internalised and degraded (**M5**). Finally, IFNAR1 and IFNAR2 undergo a turnover process under basal conditions (**M3 and M4**). "

The parameterisation of the PBPK model was derived on the basis of the observed plasma concentration after intravenous application of recombinant leukocyte-A of 0.22 mg on human subjects as reported by Wills et al. (1984) [50]. These data served as a basis to estimate parameters like receptor abundancy, binding affinity and internalisation (details in Appendix B, Table B.2).

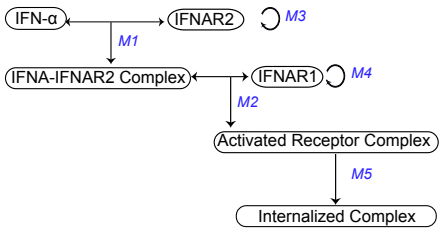

FIGURE 3.1: The structure of the kinetic model of the IFNα drug interaction in the liver of the whole-body model. For the model an i.v.injected dose of 0.22 mg (36 U) was assumed. The clearance was modelled by taking into account renal (GFR; not depicted in this Figure) and hepatic clearance (Receptor binding partners). The basal receptor (IFNAR1 and IFNAR2) turnover in the absence of the drug is included in the whole-body model. The dose arriving in the liver binds to the receptors which are activated, followed by internalisation and degradation of the drug-receptor complex.

The range of biologically valid concentration values for IFNAR2 and IFNAR1 as used in parameter estimation was calculated as in subsection 3.3.2. Remaining downstream reactions were compartmentalised as presented in the cellular signalling model section 3.4, model overview 3.4.1.

Reactions and rate laws used for the PBPK model IFN-α first binds to the IFNAR2 subunit and then recruits the IFNAR1 subunit on the membrane surface to form a heterodimeric complex [90], [91], [185]–[187]. Most model reactions are described by mass action kinetics. This reaction is depicted by the following equation 3.1.

$$v_{\mathrm{i}} = k_{\mathrm{i}} \times [Substrate1] \times [Substrate2] - \frac{1}{keq_{\mathrm{i}}} \times [Product] \tag{3.1}$$

Here, the velocity of the reaction is determined by the k_i and keq_i which are the kinetic constants and the transient concentration of the *Substrate1*, *Substrate2* and the *Product*.

The basal receptor turnover of IFNAR1 and IFNAR2 were modelled as:

$$v_{\mathrm{i}} = rel\_norm\_exp \times [S\_reference\_conc] \times K\_turnover - [S\_conc] \times K\_turnover \tag{3.2}$$

Here, the velocity of the turnover was determined by the parameter *K_turnover*, the reference concentration of the receptors (*[S_reference_ conc]*), the normalised relative expression of each receptor in different organs (*rel_norm_exp*) along with the transition concentration of the receptors in the liver *[S_conc]*.

3.3.2 Calculations for the PBPK model

Calculation of receptor concentration A mean receptor density was taken as approximately 0.55 molecules/μm^2 based on [190], which corresponds to 500-1000 binding sites per cell [191]–[193]. The number of hepatocytes per gram of human liver has been estimated as 139×10^6 cells/g liver [188]. The average liver volume was previously determined to be 1.6 L [194]. With this information, the total receptor (including IFNAR1 and IFNAR2) concentration in liver was calculated:

$$Number\ of\ cells\ in\ liver = (Liver\ weight \times (\frac{Cells}{g\ liver})) = 2.085 \times 10^{11} \tag{3.3}$$

$$\begin{aligned} Receptors\ per\ liver &= number\ of\ cells \times receptors\ per\ cell \\ &= 2.085 \times 10^{11} \times 1000\ receptors\ per\ cell \\ &= 2.085 \times 10^{15}\ receptors \end{aligned} \tag{3.4}$$

$$Rec_{Amount}\ Liver = (\frac{number\ of\ receptors}{avogadro\ constant}) = (\frac{2.085 \times 10^{15}}{6.02 \times 10^{23}}) = 3.46 \times 10^{-9} mol \tag{3.5}$$

$$Receptor\ amount = 3.88 \times 10^{-4} \mu mol \tag{3.6}$$

From this amount, the total receptor concentration (IFNAR1 and IFNAR2) in the liver was calculated as:

$$\begin{aligned} Receptor\ Concentration\ Liver = Receptor\ density\ per\ cell \times \\ Human\ hepatocellularity\ number \times liver\ density \end{aligned} \tag{3.7}$$

$$Rec_{exp}(\frac{Receptor}{ml}) = 1000(\frac{Receptor}{cell}) \times 139 \times 10^6 (\frac{Cells}{g\ liver}) \times 1.05(\frac{g\ liver}{ml}) \tag{3.8}$$

$$Rec_{conc}(\frac{mol}{ml}) = \frac{14595 \times 10^7 (\frac{Receptor}{ml})}{6.02 \times 10^{23}} = 2.424 \times 10^{-13} (\frac{mol}{ml}) \tag{3.9}$$

$$Rec_{conc} Liver = 0.242 nmol/l \tag{3.10}$$

3.3.3 Parameter estimation strategy for the human PBPK model

The simulated venous blood plasma concentrations of human IFN-α were fitted to the observed average venous blood plasma concentration of 20 volunteers (data from Wills et al. [50]). The parameters used for the estimation were:

- Reference concentrations of the individual receptors
- Individual receptor binding kinetic constants (K_{off} and K_D)
- Receptor complex binding kinetic constants
- Endocytosis of the receptor complex into the cells
- Glomerular filteration of IFN-α from the kidneys

150 randomised parameter-sets of the established human PBPK model were obtained by using the Levenberg-Marquardt algorithm. The above mentioned parameters were randomised in parameter identification for the PBPK model. The renal clearance is a very well defined parameter (0.0002 - 0.0003 ml/min/kg). The reference concentrations of IFN-α receptors were in 20% range from the reported receptor values in the literature [90]. The mean squared error (measure of the differences between values predicted by the PBPK model and the values observed in the dataset) for the top 5 fits was 0.7. Most parameters estimation results spanned 2 orders in magnitude as seen in Table B.4. It can be seen in Figure B.1 that the top models exhibit a similar fit and the parameter-sets of these fits have similar values. For all top 5 fits, the correlation of the plasma clearance is high with the receptor k_{eq} of the receptors. The basal turnover of each receptor is highly correlated to the concentrations of the individual receptors. This was an indication that the different PBPK model paramterisations do not differ with regards to the IFN-α venous plasma concentrations, hence, fit 1 (seen in Figure 3.2, a.k.a Fit 1 in Table B.4 and Figure B.1. The fitted values of the parameters are found in Table B.2) was a good representation of the pharmacokinetics of IFN-α venous plasma concentrations and was chosen for further evaluation. The chosen simulation is able to describe the biphasic IFN-α plasma ADME. It exhibits the rapid distribution phase IFN-α from the venous plasma in the starting 4-6 hours after the injection and the shallower elimination phase for the later hours. The simulated IFN-α half life was 5.5 hours, which is consistent with the measured range of 3.7 - 8.5 hours (mean $t_{1/2}$: 5.1 hours). The simulation represents the total body clearance of 3.14 ml/min/kg which lies in the range of the reported total body clearance (2.14 - 3.62 ml/min/kg) [50]. The IFN-α pharmacokinetics of the chosen simulation is consistent with the published data.

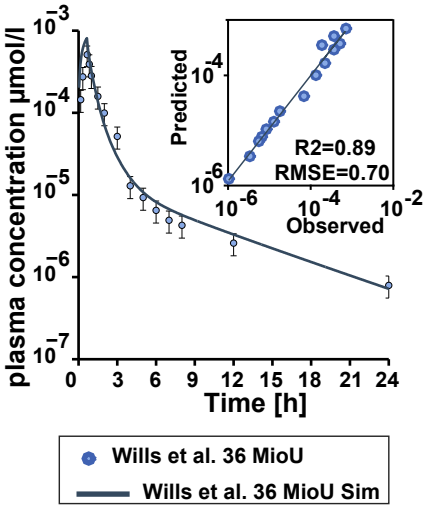

FIGURE 3.2: The Physiologically based pharmacokinetic (PBPK) model simulation (line) and experimental blood plasma profile of Wills et al. [50] (circles) of IFN-α in humans is plotted in the above plot. The y-axis for the larger semi-logarithmic plot represents the venous blood plasma concentration of IFN-α and the x-axis represents a time course of 24 hours. The goodness of fit is plotted on the upper right (small plot). In this plot the mean squared error (RMSE) and the R_2 values are depicted. For the goodness of fit plotted in the smaller box, the y-axis represent the Predicted values at the time-pints corresponding to the observed values in the dataset by Wills et al. [50] which are represented on the x-axis.

3.3.4 Validation of the human PBPK model

The above chosen simulation was validated to different doses of intravenous IFN-α profiles for human injection. The validation was performed on published datasets using varying doses of intravenously applied IFN-α (doses of 0.136 mg and 0.27 mg by Shah et al.(1984) [48] and 0.045 mg by Radwanski et al. (1987). [49]) in humans (see Figure 3.3). The chosen parameter-set for the PBPK model of IFN-α venous blood plasma concentration was able to fit the IFN-α plasma concentration for all chosen experimental conditions. The resulting simulation for Radwanski et al. (1987) [49] displays a biphasic decline of IFN-α plasma concentration. The simulation is able to represent the initial rapid distribution phase. However, it is not able to describe the last two measurements during the elimination phase of IFN-α plasma concentration. Nevertheless, the simulation represents similar $t_{1/2}$ values as that in Radwanski et al. (1987) [49]. The simulation depicts the $t_{1/2}$ at 2.3 hours which is in congurence to the terminal $t_{1/2}$ values reported in Shah et al. [48] (1.9 - 2.9 hours). Thus confirming that the same parameterisation can represent different doses of the IFN-α venous blood plasma concentration.

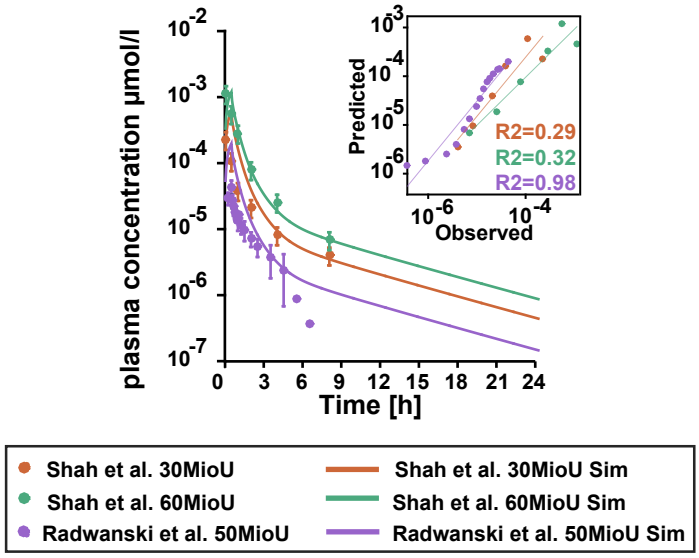

FIGURE 3.3: Validation of the physiologically based pharmacokinetic (PBPK) model to different doses of IFN-α plasma concentrations as reported in the literature. The experimental (circles) blood plasma profiles of IFN-α in humans as reported in Radwanski et al. [49] (purple) and Shah et al. [48] (orange and green) and the corresponding simulations (lines) are plotted. The goodness of fit is plotted on the right (small plot). R_2 values are provided for reference.

3.3.5 Analysis of the human PBPK model

Human PBPK models can help predict the tissue distribution of a drug. After IFN-α injection, understanding its tissue distribution is a key element to predict the efficacy of IFN-α, as the target sites of immune responses are not commonly found in the blood plasma itself [195]. For example, comprehending the pharmacokinetics in plasma alone does not suffice, for example, to understand the antiviral response of IFN-α at the infected site. In literature, tissue distribution profiles of IFN-α in mice and monkeys have been obtained [36], [39]–[41]. These studies indicate that the highest amount of IFN-α can be found in the spleen, liver, kidney and lung. While it has already been possible to obtain useful information about IFN-α pharmacokinetics by studying blood levels in patients, tissue distribution of IFN-α was so far only measured in animal models, as experiments in humans are not ethically feasible. However, the model created in this thesis provides valuable insights into IFN-α pharmakokinetics in humans, which can't yet be obtained experimentally.

From our model, it can be seen (Figure 3.4) that the IFN-α concentration in the highly perfused tissues, such as lung, liver, spleen or kidney is close to the plasma concentration. The low perfused tissue such as the fat or muscle show a lower concentration of IFN-α. Over time the concentration of IFN-α decreases more rapidly in highly perfused tissues than in poorly perfused tissues.

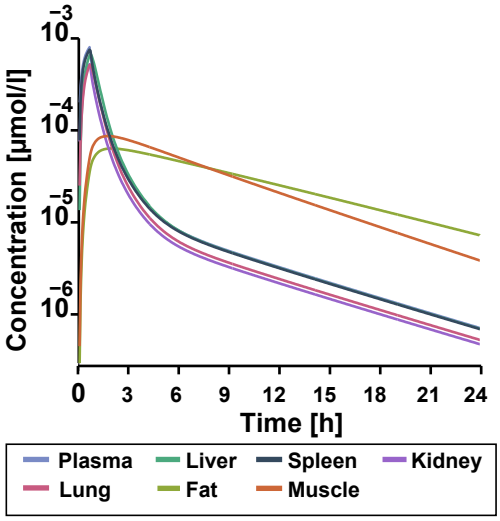

FIGURE 3.4: Simulated tissue distribution profile of IFNα for the dose reported by Wills et al. (1984) [50] for 24 hours. The lines represent the simulated tissue distribution of IFNα in venous blood vs. the different organs. IFNα concentration in the well perfused tissues such as the liver, spleen or the kidney is close to the plasma concentration. Initially, the concentration is high, but it decreases more rapidly as in the poorly perfused tissues.

3.4 IFN-α hepatocyte model

The IFN-α signalling model developed in this work is a reduced model from the one published by Maiwald et al. [116]. The original model can be retrieved at online cellular systems modelling database[1].

In Maiwald et al. [116] , the authors focused on dynamic changes for short time-scales (up to 6 hours) in the JAK/STAT pathway and traced the influence of IRF9 on the pathway activation. In our work, I analysed the response behaviour on longer time-scales (up to 1 day) without an over-expression of IRF9. To this end, I implemented the 24-hour time course and dose-response datasets of the biomarker IRF9 mRNAc to fit and validate the model. Besides reducing the model, I had to reparameterise it in order to adjust the original model [116] to our study. In the process I introduced the following changes in the model:

1. The adapted model replicated the receptor concentration and the kinetics of the surface receptor behaviour predicted by the PBPK model. Furthermore, it included physiological concentrations of the receptors. The new structure of the model at the receptor level is depicted in Figure B.5).

2. The initial expression for the STAT and IRF9 molecules were excluded in the adapted model due to stiffness in the long-time model simulation.

3. The execution of the sensitivity analysis on the adapted model reported less control of two reactions implemented in the Maiwald et al. [116] model:

   (a) Dephosphorylation of the receptors by SHP dephosphatase. This reaction was removed.

[1] http://jjj.biochem.sun.ac.za/database/maiwald/index.html

(b) Feedback of nuclear phosphatase. This rreaction was added as an extra mass balance term to the release of each protein transported to the nucleus (STAT1, STAT2, IRF9 and ISGF3) as an extra mass balance term.

4. The kinetics of SOCS feedback on the receptor is reported as non-competitive kinetics in the literature [196]. In the adapted model the feedback of SOCS was changed from simple mass action to catalytic activation.

5. The model integrated the long time course (24 hours) data data representing the dose-response relationship of IFN-α and IRF9-mRNAc.

6. Finally, the volumes of the cytoplasmic and nuclear compartments of the virtual hepatocyte for human and mouse were calculated from the PK-Sim liver intracellular volume.

There are two prerequisites for intracellular models which allows the meaningful integration and conclusions with PBPK models.

- The hepatocyte model should have identical cell surface receptor behaviour to that of the PK model.
- The hepatocyte model is able to simulate dose-response behaviour for various doses.

In the following section I will provide the in-depth description of the model structure and establishment. In the coming sections this model is addressed as the **Hepatocyte model**.

3.4.1 Intracellular hepatocyte model overview

the deterministic model developed here encompasses the key molecules and feedback mechanisms of the JAK/STAT pathway. The new model comprises 21 molecules and 20 reactions. The reaction kinetics are mainly modelled by mass action kinetics, except for 2 reactions: the transcription of IRF9, which follows the Michaelis Menten kinetics, and the catalytic inhibition described the feedback inhibition of SOCS on the ternary receptor complex. The model consists of two compartments: the cytoplasm and the nucleus. The volume of the cytoplasm corresponds to the volume of the intracellular space of the liver from the PBPK model. The molecule species existing in the two compartments have the suffix *c* when in the cytoplasm and the suffix *n* when in the nucleus (see Figure 3.5 for the structural cartoon of the model). The degradation of IFN$-\alpha$ was modelled (**R1**) as the IFN$-\alpha$ dose is constant and the half life of IFN$-\alpha$ is reported in the range of 4 - 8 hours [197], [198], The IFN$-\alpha$ - receptor binding was described step-wise, where first, the free IFN$-\alpha$ (*IFN_atSite*) binds to IFNAR subunit 2 (*IFNAR2*) forming a ligand receptor complex (*IFNA_R2_Complex*) (**R2**) which then binds to IFNAR subunit 1 (*IFNAR1*) to form a trimeric complex (*Activated Receptor Complex*) (**R3**). The activated trimeric receptor-ligand complex associates to the STAT2 (*STAT2c*) in the cytoplasm to activate the phosphorylated STAT2c (*Rec2*) (**R5**). Then, the union of STAT1c (*STAT1c*) to STAT2c (*STAT2c*) was incorporated to form the heterodimer of STAT1-STAT2 (*Rec 21*) (**R6**). Consequently, binding to IRF9 (*IRF9c*) to form ISGF3 complex in the cytoplasm (*ISGF3c*) (**R7**). Some species were transported independently into the nucleus, namely, STAT1 (*STAT1c/n*) (**R14**), STAT2 (*STAT2c/n*) (**R15**), IRF9 (*IRF9c/n*) (**R16**) and ISGF3 (*ISGF3c/n*) (**R17**). The transcription complex (*ISGF3n*) binds to the promoter sequence on DNA known as ISRE sites (*Open ISGF-3n binding sites*) to transcribe (*Occupied ISGF-3n binding sites*)

(**R18**) the mRNA of IRF9 (*mRNAc*) (**R8**) and SOCS (*mRNAc_SOCS*) (**R10**). The liberation of the DNA-bound transcription factor (*Occupied ISGF-3n binding sites*) by nuclear phosphatase refurbished the individual molecules and freed the ISRE sites (*IRF9n*, *STAT1n*, *STAT2n* and *Open ISGF-3n binding sites*) (**R19**). The mRNAc of IRF9 and SOCS were translated into the respective proteins (*IRF9* and *SOCS1*) which were further degraded (**R12, R13 & R20**). The mRNAc degradation for the IRF9 mRNAc and SOCS1 mRNAc was included (**R9 & R11**). Lastly, the SOCS protein binding is to the heterotrimeric receptor complex and thus, the exertion of the negative feedback resulting in the freed receptor subunit, was incorporated (**R4**). The details of the reactions and their kinetic rate laws are summarised in Table 3.2

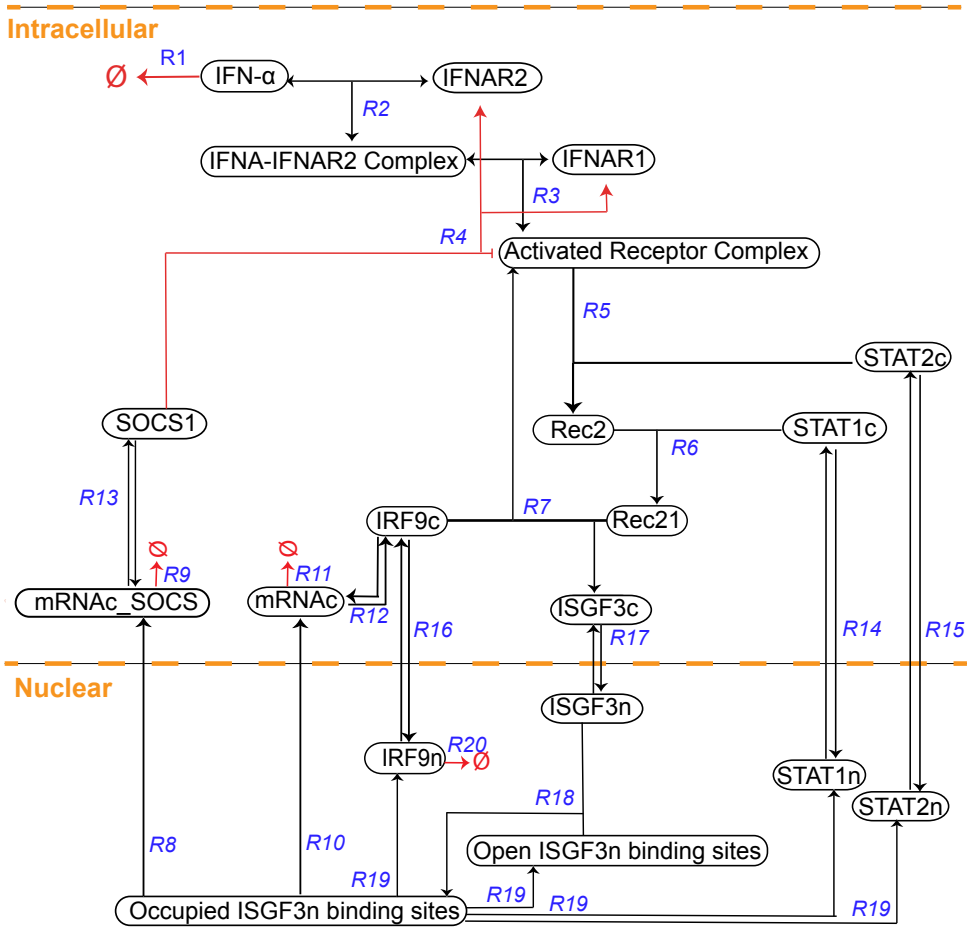

FIGURE 3.5: The structure of kinetic model of the IFN-α signalling pathway in the hepatocyte is drawn here. The JAK/STAT pathway is modelled by simulating a dose of 500 U IFN-α dose (12.96 nmol/l model units) which led to the activation of the receptors in the cytoplasm. The downstream cytoplasmic and nuclear reactions (black solid arrows) and degradation reactions (red arrows with ϕ) are divided into the respective model compartments (yellow dashed line). Finally, the feedback reactions are depicted (red solid lines).

Reactions and rate laws The reaction describing the feedback of SOCS on the receptors is modelled by catalytic activation kinetics. The rest of the reactions are decribed by mass action kinetics. The receptor kinetics were implemented from the PBPK model and these reactions are further explained in the section 3.3.

The feedback inhibition of SOCS on the receptors was modelled as irreversible catalytic activation on the receptors, hence freeing the individual receptors. This reaction kinetics is a simple form to describe the inhibition and the term activator in the below mentioned equation describes the inhibition molecule (SOCS):

$$v_{\mathrm{i}} = \frac{V \times [Substrate] \times [Activator]}{(kms + [Substrate]) \times (Ka + [Activator])} \tag{3.11}$$

Here the velocity of the reaction is determined by *Kms*, *V* and *Ka* and the *Activator* (in this case the inhibitor) is a modifier to the the *Substrate* (the receptor complex).

3.4.2 Calculations for the intracellular hepatocyte model

Converting IFN units: From IU/mL to nmol/l Most parameters of the adapted model were reparameterised by parameter estimation. The kinetic model was fitted to the data reported by Bolen et al. and Maiwald et al. [116], [161]. In the experimental data, various IFN-α stimuli (IFN_{exp}) were applied on the cells to activate the signalling pathway. IFN_{exp} doses ranged from 10 IU/mL to 500 IU/mL (1×10^4 IU/L to 5×10^5 IU/L). The model includes the fold-change ratios between the different IFN-α stimuli, but not the actual protein concentrations. The experimentally applied stimuli of U/ml was assigned to a model value of 12.96 in all subsequent analysis. This was based on the following conversions:

The IFN-α doses (IU/L) were converted to molar concentration (M), that is,

$$IFN_{exp}(M) = \Big(IFN_{exp}(IU/L)/IFN_{sa}(IU/g)\Big)/IFN_w(g/mol), \tag{3.12}$$

where, IFN_{sa} is the IFN specific activity. $IFN_{sa} = 1 \times 10^6$ IU/g (R&D Systems, Minneapolis, MN, USA). IFN_w is the IFN molecular weight. $IFN_w = 19241.0$ (g/mol).

TABLE 3.1: From IFN-α (IU/mL) to nmol/l and to model concentrations.

IFN-α (IU/mL)	M	nmol/l	Model Units
500	2.6×10^{-7}	25.98	12.96
100	5.19×10^{-9}	5.19	2.59
10	5.19×10^{-10}	0.519	0.25

It is worth to mention, that those numbers provide an overall idea of the the final IFN-α concentration at the target cell. However, the numbers can be affected by various factors, including:

- The storage of IFN-α: Concentrations and activity of IFN-α varies widely due to vendor-specific characteristics of the IFN-α sample. The activity is affected by freezing and thawing, which may cause changes to the IFN-α activity over time, even if the same batch is used. Activity may also be different in different solvents or cell culture media. For these reasons, there is a significant potential for variable activity.
- The cells to be studied: It's hard to compare different cell types; cells react very differently to IFN-α and some may not react at all (e.g. they lack the

IFN-α receptor) whereas IFN-α activity varies very much between some cell types (e.g. tumor cell model vs. primary cells). Therefore, additional variance might be added by inconsistent use of cell lines, e.g. use of different cell lines, differences in passage numbers and cell density.

Estimating nuclear binding sites of ISGF3 During re-parameterisation of the model, the TFBS were estimated. Thereby, I confined the range of the TFBS to physiological values. A detailed explanation is presented below:

The human genome consists of 3×10^9 base-pairs, total DNA content of a 2n cell is $2 \times 3 \times 10^9$ base pairs. A transcription factor binding site (TFBS) consists of more than one base-pair. In the study done by Whitfield et al. [199], they predicted a binding site for transcription factor every 5 kb of DNA. Therefore, they calculated the binding sites per nucleus to be 6*10^5. The ENCODE [166] bed file of ChIP seq experiments for STAT1 and STAT2 after IFN-α treatment in the human cell line K562 had 1.36 - 1.74 $\times 10^5$ potential binding sites per nucleus.

In the model published by Maiwald et al. [116] the concentration of the open binding sites was 5312 nmol/l, which translates to 8.55×10^5 binding sites per nucleus (see calculation 3.13). This number is extremely high as compared to the number of base pair in the human genome $\approx 3 \times 10^9$ bp (6×10^9 base-pairs in case of diploid cells).

$$V_{\text{nucleus}} = \frac{4}{3} \times (\textit{nuclear diameter} \times 0.5)^3 \times \pi V_{\text{nucleus}} = 268 \mu m^3 \tag{3.13}$$

$$\textit{Amount TFBS}_{\text{nucleus}} = \textit{Concentration}_{\text{binding sites in the model}} \times V_{\text{nucleus}} \tag{3.14}$$

$$\textit{Amount TFBS}_{\text{nucleus}} = 5312 \frac{nmol}{l} \times 268 \times 10^{-15} l = 1.42 \times 10^{-9} nmol \tag{3.15}$$

$$\textit{Number TFBS}_{\text{nucleus}} = \textit{Amount TFBS}_{\text{nucleus}} \times \textit{Avogadro Constant} \tag{3.16}$$

$$\textit{Number TFBS}_{\text{nucleus}} = 1.42 \times 10^{-18} mol \times 6.022 \times 10^{23} \frac{1}{mol} \tag{3.17}$$

Hence, the initial concentration of the TFBS was fitted to more realistic concentrations as calculated with the help of the above stated calculations.

Up to now, no crystal structure of ISGF3 is available and hence both, the DNA binding contacts and the stoichiometry of ISGF3 DNA complex is unclear [200]. The binding dynamics are are crucial for the model behaviour. The IRF9 promoter contains two putative ISRE binding sites for ISGF3 (as evaluated from sabioscience transcription factor database and ENCODE database (Appendix B, Figure B.3 and Figure B.4)) and has been indicated to have an overlap with the putative IRF7 binding site sequence [200], [201] thus potentially allowing cooperativity in the binding. However, Begitt et al. [202], demonstrated that the cooperative binding of STAT1 is not important for type I interferon responses, as found by using cooperativity-deficient STAT1.

Hence, three different kinetics were defined for the binding of ISGF3 to the nuclear binding sites as follows: mass action kinetics, Michaelis Menten kinetics and Hill cooperativity. Mass action kinetics allows for a graded response to the binding,

while Michaelis Menten allowed saturable response to the binding of ISGF3 to the DNA, whereas Hill cooperativity encoded switch like behaviour of gene expression. It turned out that the model version with mass action kinetics for transcription of IRF9 best described the data during the parameter estimation, The other kinetics were discarded. The model with mass action kinetics was further evaluated. In the further steps, the receptor dephosporylation reaction was removed as it was not included as part of the receptor activation mechanism in the PK model. Besides, the receptor dephosporylation reaction had little to no influence on the model due to the realistic concentrations of the receptors. Furthermore, the nuclear phosphatase feedback was observed to be too fast and and without control over the model parameters, hence this reaction was removed from the model structure. This version of the model (a.k.a. adapted model/ hepatocyte model) was used for investigating the parameter distribution and further evaluations.

3.4.3 Parameter estimation strategy for the intracellular hepatocyte model

Mapping of the model variables to the data For the integration of the hepatocyte model into the PBPK model, I needed to ensure consistency at the receptor kinetics level. Thus, the receptor parameter values and the equation was taken from the PBPK model into the hepatocyte model (the parameter values can be seen in appendix B, Table B.7). The datasets included mRNA abundance profiles followed over time for different IFN-α stimuli. The dataset was split into two parts and one was used for parameter fitting, while the other was used for validation. The doses included in the parameter estimation were 10 U and 100 U from Bolen et al. [161]. As the time points were in arbitrary units, the mRNAc species of the model was mapped to the dataset as follows:

$$IRF9mRNAc^{\dagger}(t_i) = \varphi_1 \times \Big(IRF9mRNAc(t_i)\Big), \tag{3.18}$$

where φ_1 is the scaling factor.

Fitting the deterministic model The model was fitted to short time course (up to 6 hours) experimental data obtained for IFN-α stimuli of 500 U and 1000 U. Various intracellular signalling species (JAK, STAT1, STAT2, IRF9, IRF9 over-expression and SOCS protein) as reported in Maiwald et al. [116] were measured. The ability to predict the dose-response data is crucial for this model. Thus, the model has to be able to estimate the behaviour of IRF9 mRNAc (the key molecule to extrapolate the comparative behaviour *in-vitro* vs.*in-vivo*) when conditioned to low or high doses of IFN-α. IRF9 has been suggested to play a pivotal role in the dynamics of the signalling pathway [116]. Studies on hepatic cell-lines indicated that the transcription of IRF9 mRNA got triggered at a rather low dose of IFN-α, namely between 50U to 100U [21], [22], [161], [162]. Consistently, at doses beyond 500 U IFN-α IRF9 mRNAc response has been reported to be saturating (see Appendix B Figure B.2).

Based on the model structure and available data, many of the parameters of the model were not identifiable. To understand the distribution of possible parameter values for different parameters in the model, a model ensemble of 1000 parameterisations was set up. Each model in this ensemble had identical model structure, but the parameter estimation started with random parameter values. Due to the complex structure of the model, high number of parameters and presence of different

time-scales of the reactions, parameter estimation was a time intensive task. To reduce the computation time, I analysed and removed the reactions which showed structural non-identifiablity. The final parameter estimation was then performed using the implemented particle swarm algorithm in COPASI (iteration Limit: 20000 and swarm size: 60; multiple iterations of 1000 fits; performed on the cluster). All parameters for which experimental data was available were included in the parameter estimation after adding a variance within 20 % of the measured value (see Table B.5). The rest of the parameter values were varied 50-75 % from the values establised in Maiwald et al. [116].

The parameter estimation analysis yielded the result (see Figure 3.6) that most parameters were evidently unidentifiable due to their broad distribution (see Figures B.6 and B.7)).

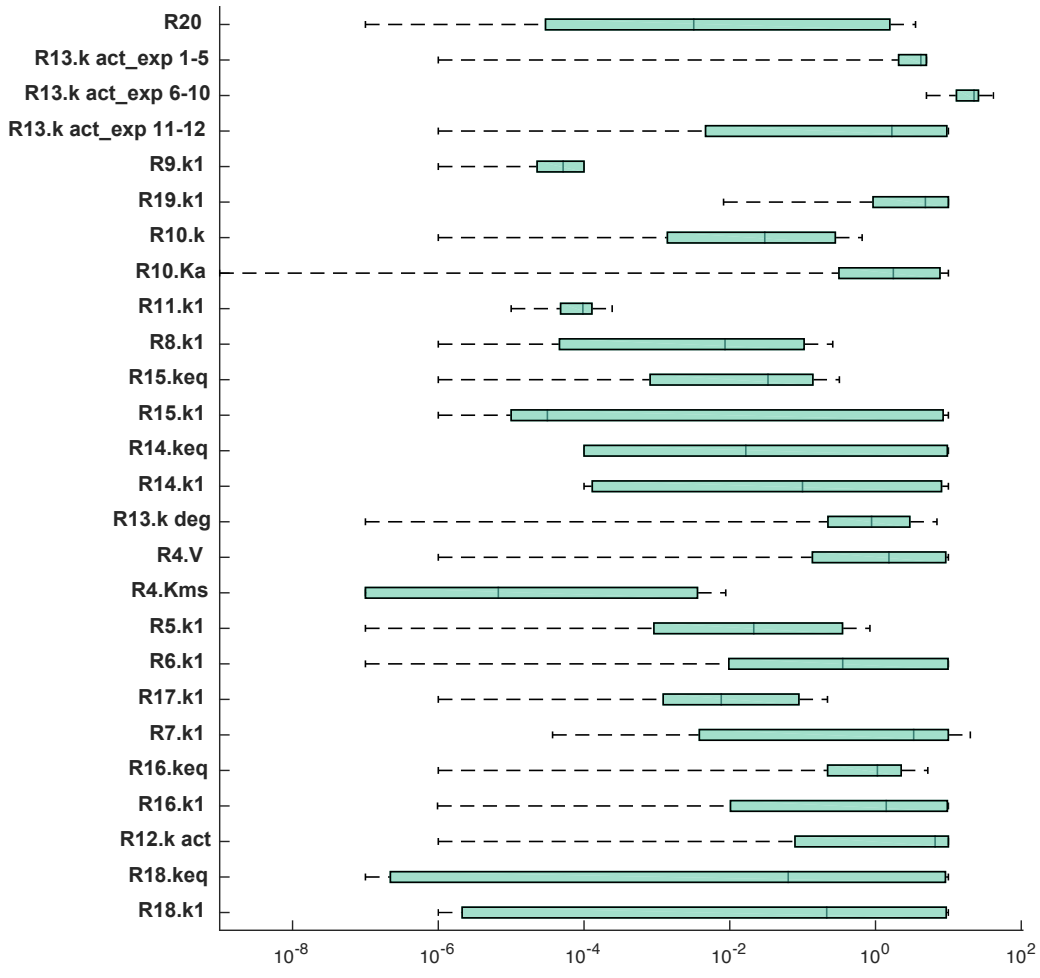

FIGURE 3.6: The parameter values of 1000 fits are represented in the box plot. The 25-75 % quantiles of the fitted parameter is represented by the box (green), the full range of the parameter variation is represented by the dashed line (black) and the median is indicated by a solid line (black).

Information on several parameters modelled was sparse or not measured in human hepatic cell lines. To deal with the model uncertainty and scarcity of the data, further analysis was based on a model ensemble of 10 models [203]. All ten models have identical model topology but different parameter values (see Appendix B, Table B.6) that described the experimental data equally well and cover the full range of possible biologically relevant parameter values. The model ensemble consisted of models that not only fit the experimental data well, but also showed steady state without IFN-α stimulus and described the dose-response behaviour of IRF9 mRNAc well.

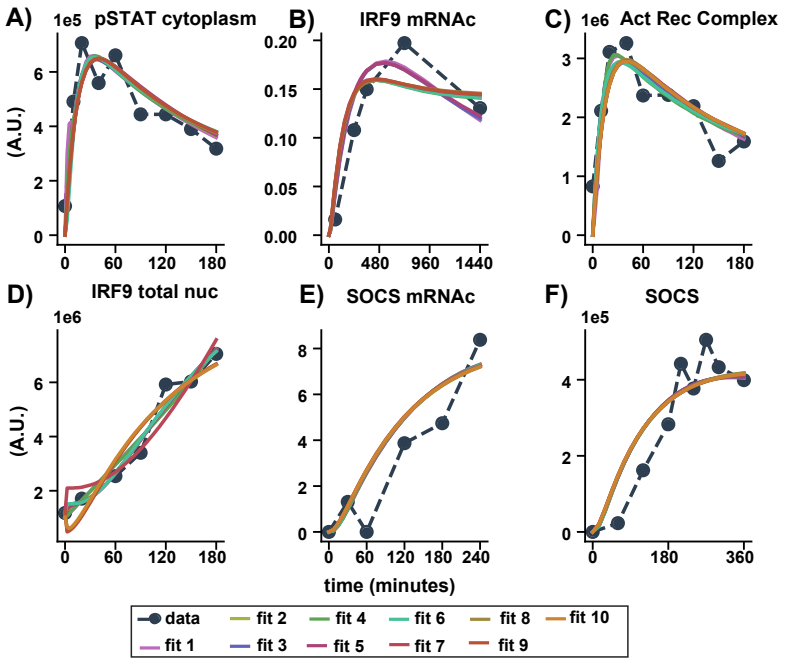

FIGURE 3.7: Parameter estimation results of the top ten models in the ensemble. The experimental time course (dots) and parameter estimation results (solid lines) are plotted. The x-axes of the plots represent the time scale at which the measurements were taken after the applied IFN-α stimulus. The measurements of the protein quantities in arbitrary units are plotted on the y-axes. The protein reaction dynamics was measured and published in Maiwald et al. [116] by quantitative immuno-blotting in Huh 7.5 cells stimulated with 500 U IFN-α for the activation of A) cytoplasmic pSTAT, C) cytoplasmic pJAK (which was mapped to the Act Rec Complex), D) total nuclear IRF9 (IRF9n), E) cytoplasmic SOCS mRNAc and F) cytoplasmic SOCS protein. The dynamic expression of B) IRF9 mRNA was measured and published by Bolen et al. [161] by microarray analysis in Huh 7 cells after the treatment with 10 U IFN-α. Complete fits to all the datasets are shown in appendix B; Figure B.8.

3.4.4 Validation of the intracellular hepatocyte model

For the validation of the parameter estimation result, I used the datasets for IFN-α stimuli of 500 U and 2500 U from Bolen et al. [161] and 15 U and 30 U from Jilg et al. [162]. As the measured biomarker is the same as the one used for model ensemble training (IRF9 mRNAc), the validation data was well suited for testing the validity of the trained model ensemble. The datasets arise from different publications and

are in arbitrary units, they cannot be qualitatively cross compared, although the normalised relative behaviour of IRF9 mRNAc response over time for the different doses can be compared. Hence, as stated previously, the datasets were normalised within the experiments from each publication.

I analysed whether the model ensemble reproduced the temporal dynamics of the validation datasets for the dose-response time profiles (Figure 3.8). In Figure 3.8 A) and B), the model ensemble is able to achieve the peak amplitude of the IRF9 mRNAc response for 500 U and 2500 U at a similar time scale as the dataset, i.e., at nearly 360 mins for 500U and at 245 mins for 2500 U. However, for 2500 U the peak concentrations are under-estimated by the model ensemble (Figure 3.8 B)). In Figure 3.8 C) and D), the model ensemble is simulated against the datasets of 15 U and 30 U from Jilg et al. [162]. The model ensemble simulates the dynamic behaviour quantitatively for 15 U, where the peak amplitude of response IRF9 mRNAc is simulated well, but the model predicts a faster response than the response measured in the dataset. Also, the amplitude of the response of IRF9 mRNAc and the temporal dynamics is under-estimated for 30 U. In Figure 3.8 E) and F) the concentration of IRF9 mRNAc 24 hours after treatment with different concentrations of IFN-α is shown. ¡the model approaches close to saturation in response to 100 U (hollow circles depicting the value was used in the parameter estimation) which is close to the the dose (between 50 U to 100 U) reported in the literature at which the IRF9 mRNAc response saturates (Table B.2).

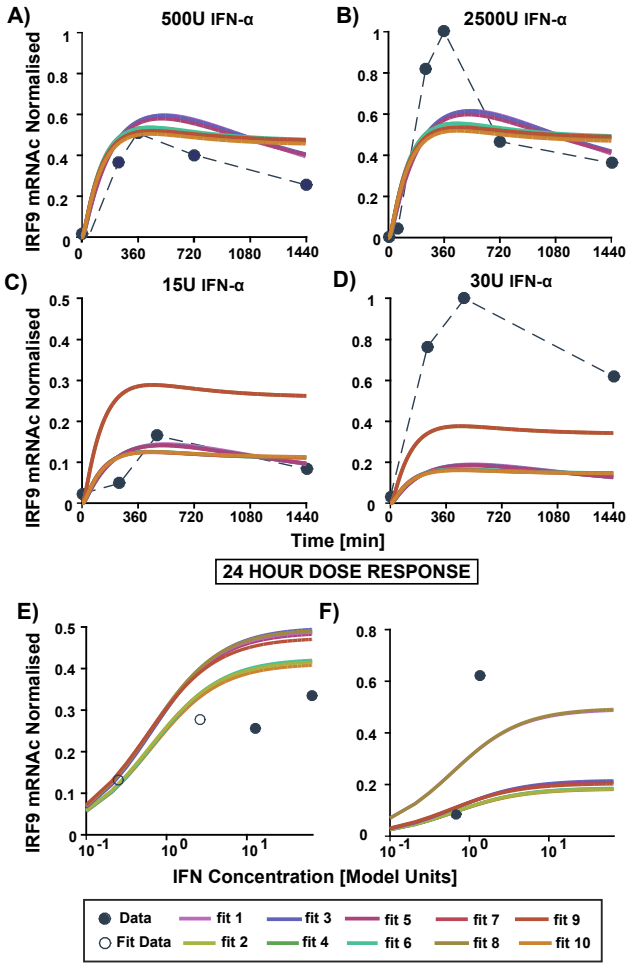

FIGURE 3.8: In the above graph, the model ensemble simulation is plotted (solid) vs. the validation datasets of of IRF9 mRNAc concentrations in response to IFN-α stimuli (circles). In A-D) the dynamical time course behaviour of the datasets and the model ensemble for 24 hours is plotted. The doses are, in A) 500U and B) 2500U of IFN-α dose from the publication Bolen et al. [161]. C) 15U and D) 30U of IFN-α dose from the publication Jilg et al. [162]. In panel E) and F) the 24th hour dose-response curves are shown for E) all datasets from Bolen et al. [161]. The datasets used in the parameter estimation are plotted as hollow circles. F) datasets from Jilg et al. [162].

3.4.5 Analysis of the intracellular hepatocyte model

Simulating the hepatocyte model with constant *in vivo* and *in vitro* doses As the model ensemble was able to simulate the dose-response of IRF9 mRNAc, I used this ensemble for further investigation. The hepatocyte model ensemble was simulated with IFN-α doses applied in two different scenarios to investigate the differences in the signalling dynamics. One was a typical intravenous injection IFN-α stimuli as a constant dose (C_{max} of 0.7 nmol/l in the liver). The second was the constant dose of IFN-α for a typical *in vitro* assay or experiment setup (C_{max} of 13 nmol/l). As all models in the ensemble exhibit identical dynamics, for simplicity, I selected one exemplary model from the model ensemble to represent the analysis. The representative model was simulated with the constant dose of 0.7 nmol/l, which is the typical

in vivo dose of 36 U of IFN-α (but is non-linear in physiological conditions). The representative model was also simulated with a constant dose of 13 nmol/l, which is typical *in vitro* dose of 500 U of IFN-α in the petridish experiments. The important response molecules of the pathway are plotted in Figure 3.9. As the doses were constant (no physiological clearance of IFN-α), the *in vitro* behaviour is evidently sustained for both the doses (36 U and 500 U) for all the models in the ensemble. In addition, clearly, the shape of the temporal response profiles of the molecules is similar for both the doses. However, the fold differences in the C_{max} of the response molecules in the model ensemble were approximately 1.8 fold higher for *in vitro* IFN-α dose (500 U) as compared to the *in vivo* IFN-α dose (36 U) 3.10. The results show that despite the high numerical difference in the doses, i.e., the *in vitro* dose of 500 U being 18 fold higher than the *in vivo* dose of 36 U. The simulation suggested saturation at the IFN-α dose of 36 U. The activated receptor complex reached its peak concentration 2 hours (T_{max}) earlier for *in vivo* dose (36 U) than the *in vitro* dose (500 U). The time scale at which the peak of the SOCS1 concentration is reached for both the doses is similar. Evidently, the moment the feedback protein SOCS1 starts to decline from its C_{max}, the activated receptor starts to slowly build up again until it reaches its saturating C_{max} at 22 hour.

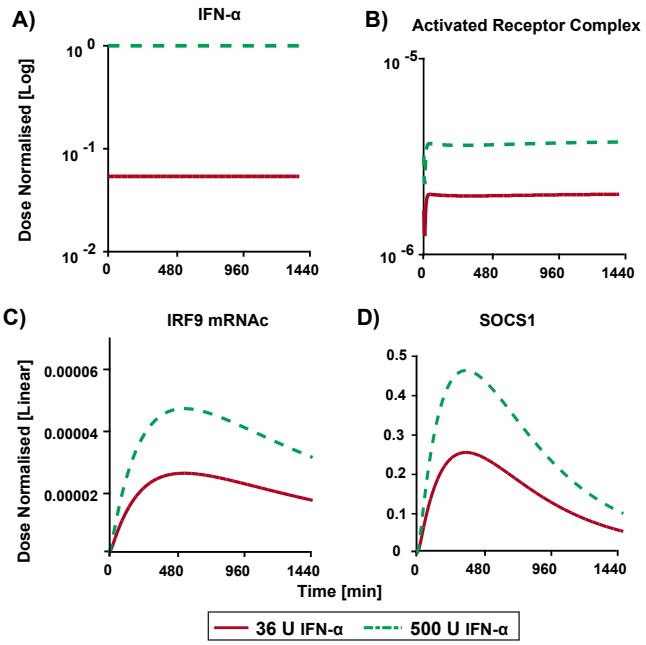

FIGURE 3.9: The hepatocyte model was simulated with a constant low dose (36 U; typically administered dose *in vivo*) vs. the *in vitro* dose (500 U; typically used in experimental setups). The (red lines), hepatocyte culture simulation (green dashed lines). Simulation of concentration time profiles in human and in human cell lines of A) the non-linear IFN-α, B) activated receptor complex C) IRF9 mRNAc and D) SOCS1 activated downstream in the models.

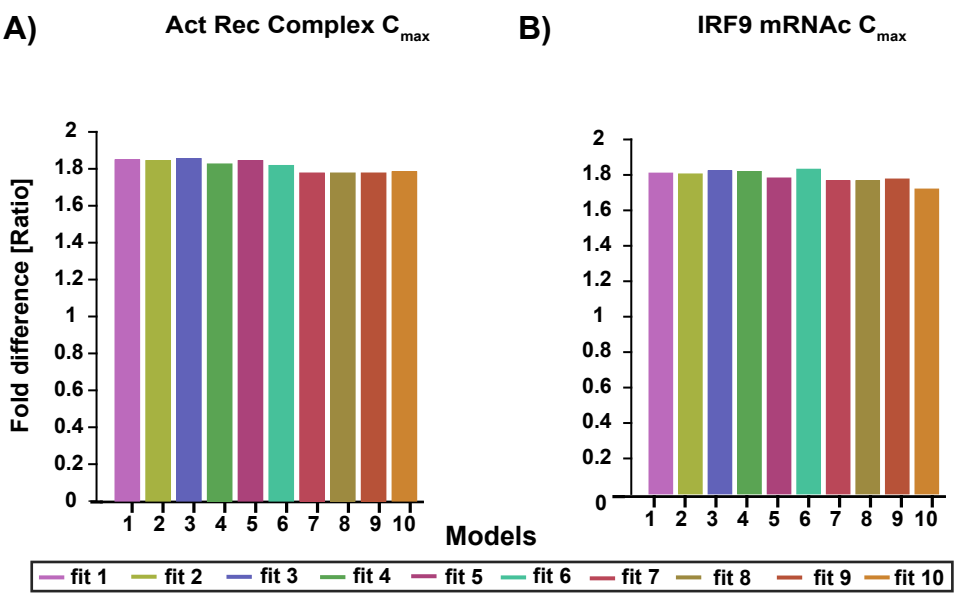

FIGURE 3.10: Relative fold difference of A) activated receptor complex and B) IRF9 mRNAc C_{max} calculated by simulating the typical administered dose of 36 U IFN-α (C_{max} 0.7 nmol/l) and the experimental dose of 500 U (C_{max} 13 nmol/l) for the *in vitro* hepatocyte model. These doses are constant doses for the hepatocyte model.

3.5 IFN-α PBPK/PD model

The PBPK model was coupled to the hepatocyte model in MoBi to establish a whole body PBPK/PD model of IFN-α intravenous injection in humans. The integration of the multi-scale PBPK/PD model was executed as follows:

1. Hepatocyte Model: The model ensemble of the hepatocyte model as set-up in COPASI had to be transferred to MoBi. As there exists no bridging mark up language to exchange models between SBML and PKML format coherently, this was achieved manually. The reactions were carefully compartmentalised replicating the anatomy of the organism and the dimensions. The units used for the kinetic parameters were adjusted.

2. PBPK Model: The reactions connecting the pharmacokinetic model to the hepatocyte model (the receptor dynamics and the feedback inhibition on the receptors by SOCS proteins) were defined in the interstitial compartment of the liver of the organism PBPK model in order to include the complete dynamics of the system.

3.5.1 Establishing the merged PBPK/PD model

The technical details to merge the models in MoBi are described in Appendix B, subsection B.3.1. To replicate the hepatocyte model ensemble in MoBi, the IFN-α drug dose was decoupled from the PBPK model. A constant IFN-α dose was defined in the liver. The concurrency check of the inter-exchanged models was done by comparing the simulation result of COPASI and the liver-restricted PBPK/PD model in MoBi to replicate the *in vitro* condition in the liver of the organism. This was executed using custom scripts written in MATLAB.

During the integration two checks were important to validate the PBPK/PD model. First, the congruence of the simulation of the hepatocyte model and the liver restricted PBPK/PD organism model for identical structure was checked for (the placement of the right molecules in the right compartments). Second, the PBPK/PD model restricted in the liver compartment in MoBi was compared to the hepatocyte model developed in COPASI to confirm that any differences seen solely arise from the pharmacokinetic aspect (See Figure 3.11).

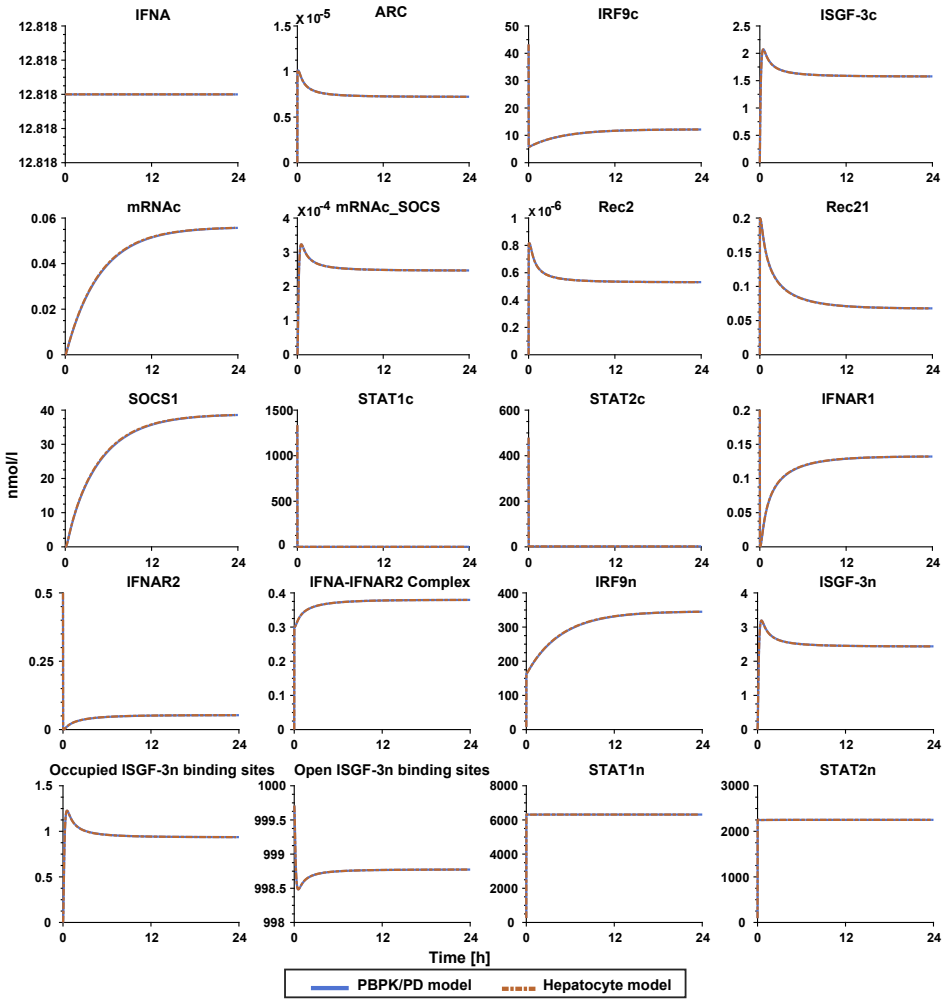

FIGURE 3.11: The congruence between the multi-scale PBPK/PD (blue lines) and hepatocyte model (orange dashed line) was tested by defining the constant influx of IFN-α (experimental dose: 500 U, model units: 13 nmol/l) in PBPK/PD model.

3.5.2 Human PBPK/PD model overview

The hepatocyte model was integrated into the PBPK organism model at the interstitial space of the liver. The receptor binding to IFN-α at the target site is the point of interaction of both models. The receptor concentrations and the kinetics were kept identical to the PBPK organism model simulation after the hepatocyte model integration. The reaction of the receptor binding and the feedback from SOCS on the receptor complex were compartmentalised in the interstitial compartment of the

liver of the PBPK model. The intracellular compartment and structure of the hepatocyte model was preserved from the hepatocyte model in the PBPK/PD model. A detailed description of the individual models is given in the section 3.3.1 and 3.4.1 respectively. The presented whole-body PBPK/PD IFN-α model in humans integrates the whole body distribution model (data from Wills et al. [50]) with activated cellular signalling of IFN-α and represents changes in the signalling behaviour while considering the *in vivo* context. Thereby, it captures the non-linear pharmacokinetic behaviour (absorption, distribution, metabolism and elimination) of IFN-α and is schematically described in Figure 3.12. The details of the kinetic rate laws for the PBPK/PD model are described in Table 3.2 labelled by the reference: *Multi-scale compartment*.

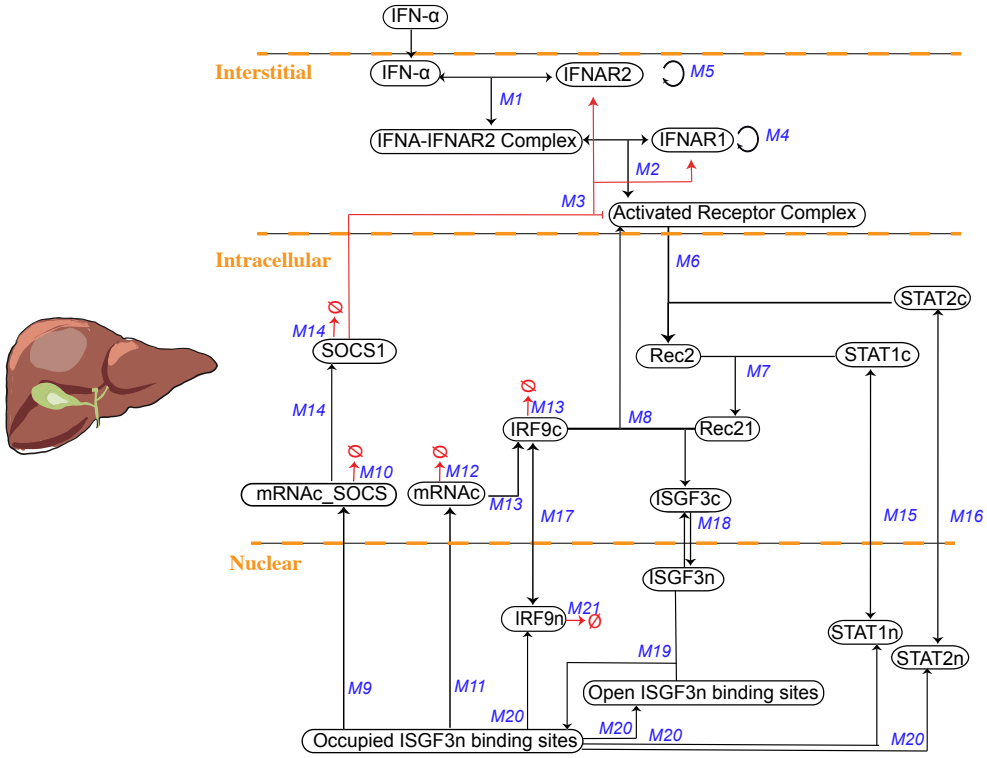

FIGURE 3.12: The schematic representation of the whole-body PBPK/PD model for IFN-α i.v.application in human is shown above. The IFN-α drug dose from the PBPK model arrives in the liver where it interacts with the receptors defined at the interstitium in the PBPK model (reactions M1-M5). The downstream JAK/STAT cascade was introduced at the *Activated receptor complex* from the hepatocyte model and the signalling pathway was implemented in the intracellular and the nuclear compartment in the liver (reactions M6-M14).

TABLE 3.2: **Reaction List:** The individual reactions for both models: the *in vitro* hepatocyte and the *in vivo* PBPK/PD model. The column with R# and Cell Compartment depict the reactions that are present in the *in vitro* hepatocyte model and where. The columns with M# and multi-scale compartment do the same for the *in vivo* PBPK/PD model. The column reactions describe the modelled pathway along with the column kinetic rate law which gives insight on the kinetics used to model each step.

#		Cell Compartment	multi-scale Compartment	Reaction	Kinetic rate law
R1	-	Cell Intracellular	-	IFN $\rightarrow \varnothing$	$k1 \cdot S$
R2	M1	Cell Intracellular	Liver Interstitial	IFNA + IFNAR2 $\rightleftharpoons$ IFNA-IFNAR 2 Complex	$k1 \cdot S1 \cdot S2 - P/keq$
R3	M2	Cell Intracellular	Liver Interstitial	IFNA_R2_Complex + IFNAR1 $\rightleftharpoons$ Activated Receptor Complex	$k1 \cdot S1 \cdot S2 - P/keq$
R4	M3	Cell Intracellular	Liver Interstitial	Activated Receptor Complex $\rightleftharpoons$ SOCS1 IFNAR1 + IFNAR2	$\frac{V \cdot S \cdot A}{(\mathrm{Kms}+S)(\mathrm{Ka}+A)}$
-	M4	-	Liver Interstitial	$\varnothing \longrightarrow$ IFNAR1	$rel\_exp\_out \times AF \times f\_o \times k\_t - S \times k\_t$
-	M5	-	Liver Interstitial	$\varnothing \longrightarrow$ IFNAR2	$rel\_exp\_out \times AF \times f\_o \times k\_t - S \times k\_t$
R5	M6	Cell Intracellular	Liver Intracellular	Activated Receptor Complex + STAT2c $\rightarrow$ Rec2	$k1 \cdot S$
R6	M7	Cell Intracellular	Liver Intracellular	Rec2 + STAT1c $\longrightarrow$ Rec21	$k1 \cdot S$
R7	M8	Cell Intracellular	Liver Intracellular	Rec21 + IRF9c $\longrightarrow$ ISGF−3c + Activated Receptor Complex	$k1 \cdot S$
R8	M9	Cell Intracellular	Liver Intracellular	$\varnothing \xrightleftharpoons[\text{binding sites}]{\text{Occupied ISGF}-3n}$ mRNAc_SOCS	$k1 \cdot M$
R9	M10	Cell Intracellular	Liver Intracellular	mRNAc_SOCS $\longrightarrow \varnothing$	$k1 \cdot S$
R10	M11	Cell Intracellular	Liver Intracellular	$\varnothing \xrightleftharpoons[\text{binding sites}]{\text{Occupied ISGF}-3n}$ mRNAc	$k1 \cdot M$
R11	M12	Cell Intracellular	Liver Intracellular	mRNAc $\longrightarrow \varnothing$	$k1 \cdot S$
R12	M13	Cell Intracellular	Liver Intracellular	$\varnothing \xrightleftharpoons{\text{mRNAc}}$ IRF9c	$(k_{\text{const}} + k_{\text{act}})M - P \cdot IRF9_{\text{deg}}$
R13	M14	Cell Intracellular	Liver Intracellular	$\varnothing \xrightleftharpoons{mRNAc\_SOCS}$ SOCS 1	$k_{\text{act}} \cdot M - K\_deg \cdot P$
R14	M15	Exchange	Exchange	STAT1n $\rightleftharpoons$ STAT1c	$k1 \cdot S - P/keq$
R15	M16	Exchange	Exchange	STAT2n $\rightleftharpoons$ STAT2c	$k1 \cdot S - P/keq$
R16	M17	Exchange	Exchange	IRF9n $\rightleftharpoons$ IRF9c	$k1 \cdot S - P/keq$
R17	M18	Exchange	Exchange	ISGF-3c $\rightleftharpoons$ ISGF-3n	$k1 \cdot S$
R18	M19	Cell Nucleus	Liver Nucleus	Open ISGF-3n binding sites + ISGF-3n $\rightleftharpoons$ Occupied ISGF-3n binding sites	$k1 \cdot S1 \cdot S2 - P/keq$
R19	M20	Cell Nucleus	Liver Nucleus	Occupied ISGF-3n binding sites $\rightarrow$ STAT 1n + STAT 2n + IRF 9n + Open ISGF-3n binding sites	$k1 \cdot S$
R20	M21	Cell Nucleus	Liver Nucleus	IRF9n $\longrightarrow \varnothing$	$k1 \cdot S$

3.5.3 Analysis of the human PBPK/PD model

The pharmacokinetic behaviour of therapeutic proteins after their injection into an organism is often influenced by binding to a specific target, i.e., for example an antigen receptor. Therefore, their PK and PD relationship gives insight into the inter-individual variability in response to a drug [204].

The presented IFN-α model integrated the whole body distribution PBPK model (data from [50]) with cellular signalling of IFN-α (a.k.a. the hepatocyte model). The integrated whole-body PBPK/PD model of IFN-α in humans, allows for the simultaneous description of IFN-α pharmacokinetics at the whole-body level and the resulting pharmacodynamics response in the JAK/STAT signalling cascade. Thus, the simulation of the hepatocyte model within a whole-body context allowed to extrapolate the cellular network to an *in vivo* situation. This is of particular relevance, since the *in vivo* pharmacokinetics is highly dynamic while the *in vitro* assay used for identification of the cellular network considered only stationary concentrations. This was depicted in the analysis of the hepatocyte model. The whole-body PBPK/PD model thus allowed the analysis of the actual amount of IFN-α arriving at the site of action, i.e., the liver and the dynamic profile of the induced intra-cellular response.

***in vitro* - *in vivo* differences of IFN-α drug action** Hereon, for clear understanding the *in vitro* scenario will be referred to as **petridish experiments**.

Similar to the heptaocyte model (which represents the petridish scenario of the JAK/STAT response to IFN-α stimulus), the simulated PBPK/PD model was further analysed to extrapolate the differences of the dynamic behaviour of the responses in the liver when comparing IFN-α doses applied i.v. to an organism or in petridish experiments. To summarise, the *in vivo* dose of 36 U from Wills et al. [50] is non-linear due to clearance processes in the body while the dose given in the petridish experiments is a constant dose of 500 U [116]. One should also keep note, as mentioned in the previous sections that an IFN-α stimulus 500 U is far above saturating levels at least w.r.t. the readout used here, namely the mRNAc of IRF9.

The C_{max} of the *in vivo* dose is 0.7 nmol/l while in the petridish experiments, the dose was constant with a C_{max} of 13 nmol/l. The PBPK/PD model was simulated with the IFN-α dose on petridish experiments and compared to the i.v.-injected *in vivo* dose. The simulation exhibited a 18-fold lower IFN-α amount reaching the liver than was what was pipetted in petridish experiments (Figure 3.14). I further compared the responses of the lower dose (*in vivo*) with the higher dose (petridish). The activated the ternary receptor complex (a.k.a. activated receptor complex) reaches a 1.5 fold lower C_{max} in comparison to petridish experiments (Figure 3.13 A and C). The response of the followed biomarker, i.e., IRF9 mRNAc reached a C_{max} which was 4 fold lower (Figure 3.13 B and D).

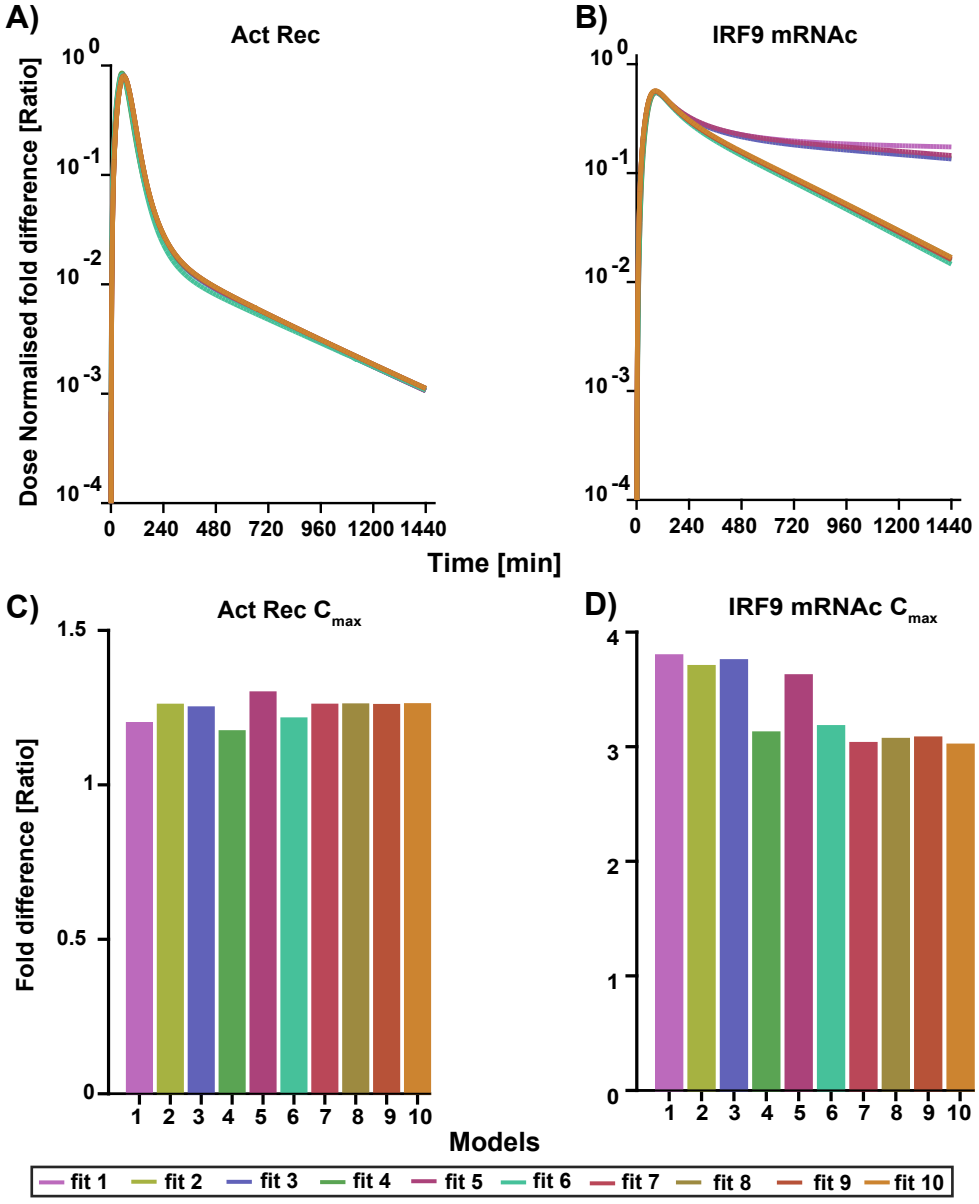

FIGURE 3.13: The difference in intracellular response when considering *in vivo* PBPK/PD model (36 U; injected dose) vs. the *in vitro* model (500 U; constant dose). Fold difference is plotted of A) Activated receptor complex and B) IRF9 mRNAc simulation (solid lines) as a concentration time profile for the top ten models. C) The calculated fold difference C_{max} achieved for activated receptor complex (Act Rec) (bars for each model respectively) and D) fold difference in the C_{max} of IRF9 mRNAc.

Evidently, there are differences in the signalling response's dynamics over time to varying IFN-α doses for *in vivo* and petridish experiments. As the model ensemble simulated identical behaviour of the response to IFN-α stimulus. For clear understanding, I show the best fit of the model ensemble (referred to as **fit 1**) for this analysis. In this model simulation, the differences are clearly seen at the commencement of the signalling where the response in the petridish experiments was faster (peak of the response achieved at 2 hours after IFN-α dose stimulus) than in *in vivo* (Figure 3.14 B, C and D), but, the C_{max} was attained faster in *in vivo* situations. Also,

due to the non-linear dynamics, the *in vivo* response shunts faster than the response in petridish (where the dose was constant, hence the dynamics last more prolonged).

The *in vivo - in vitro* difference was further compared to the analysis done on the hepatocyte model in section 3.4 , subsection 3.4.5, Figure 3.9. In the case of the hepatocyte model, when the *in vitro* model was simulated with the constant dose of 0.7 nmol/l (typical *in vivo* injection dose) and 13 nmol/l (typical *in vitro* petridish experiment dose), the signalling dynamics were sustained and the C_{max} was attained at an identical time scale for most of the molecules. However, Figure 3.10 depicts that although there is a 18 fold difference between the dose pipetted on the petridish experiments to the injected i.v. *in vivo* dose, the C_{max} attained for the activated receptor complex (Figure 3.10 A) and the response biomarker IRF9 mRNAc (Figure 3.10 B) were identical ($\approx$ 1.8 fold). This shows that the intracellular signalling was not only pronounced at a longer time-scale but was also notably higher for the petridish experiments than the drug administration. In addition, saturation in the peak amplitude of the IRF9 mRNAc response was already achieved at the dose of 0.7 nmol/l (36 U; *in vivo*) when it served as a constant stimulus for the petridish experiments. The model ensemble quantitatively exhibited the same behaviour.

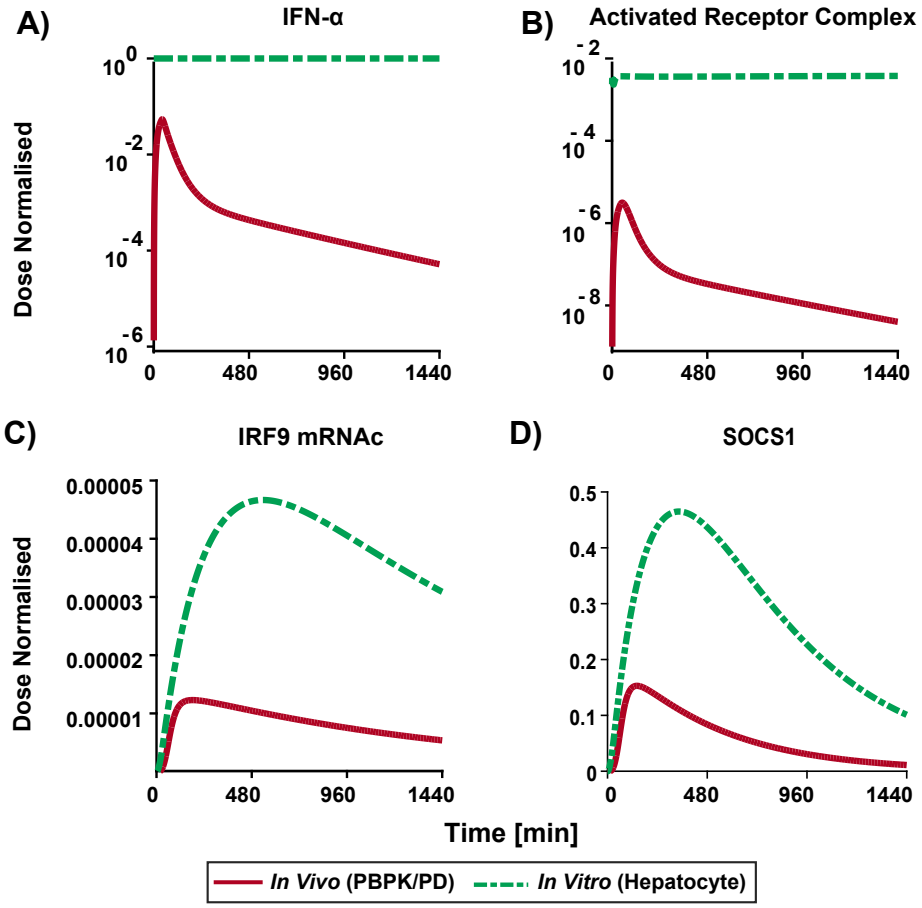

FIGURE 3.14: The difference in signalling patterns in the *in vivo* (PBPK/PD) response vs. the *in vitro* (Hepatocyte) response when dose normalised to the fixed *in vitro* dose (13 nmol/l). The PBPK/PD model are plotted with red lines, the hepatocyte *in vitro* culture simulation are plotted with green lines. Simulation of concentration time profiles in human and in human cell lines of A) the non-linear IFN-α, B) activated receptor complex C) IRF9 mRNAc and D) SOCS1 activated downstream in the models

.

To be able to compare the time-scale of the maximum activation of the intracellular response biomarker (IRF9 mRNAc) to IFN-α stimuli in *in vivo* vs petridish experiments, a simulation with using a dose of 0.7 nmol/l (36 U injection dose) IFN-α for both *in vivo* and petridish experiment was executed. In this simulation, petridish dose was constant (*in vitro*; seen in Figure 3.15 A) due to lack of clearance processes while the *in vivo* dose was a non-linear process due to the clearance of the drug from the body (*in vivo*; seen in Figure 3.15 B). With a similar IFN-α stimulus, as seen in Figure 3.15, the model exhibits identical dynamical behaviour as discussed earlier, i.e., the C_{max} was achieved faster *in vivo* dose as compared to petridish experimental setup. It is noteworthy that at the simulated *in vivo* constant dose, the response was approximately 6 hours (T_{max}) earlier as compared to the response in for the typical petridish experiment dose (B.10). It can also be seen in Appendix B, Figure B.11 that the activation of receptors was 0.6x higher (B.11 A) and the IRF9 mRNAc response was 2x higher (B.11 B) in conditions when the exact same doses were administered in both experiments. This is evidently the case ,because *in vivo*, the IFN-α levels rapidly

decrease after the peak is reached due to clearance processes. The respective impact on the *in vitro* hepatocyte is not witnessed as the dose of IFN-α was constant which led to an add-on response over time. In summary, these results indicate that intracellular signalling is strongly reduced in the context of drug administration compared to the typical lab experiments.

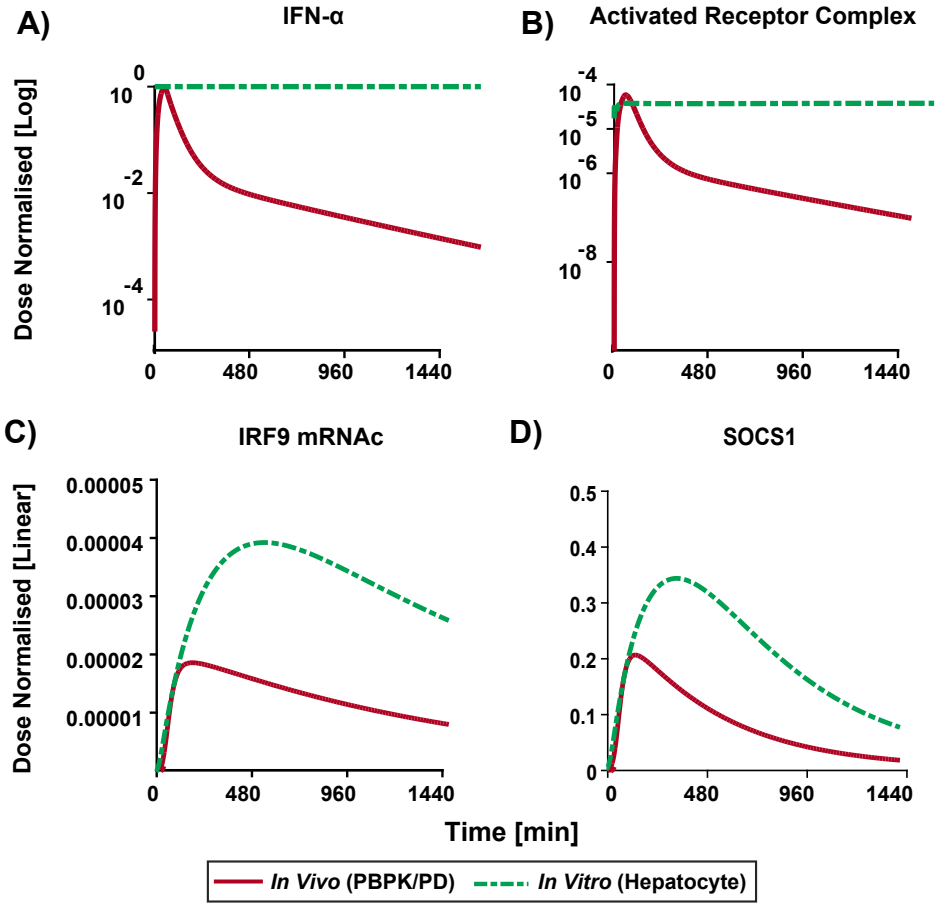

FIGURE 3.15: time course of species for the hepatocyte model and the PBPK/PD model using the same IFN-α dose (that of *in vivo* situations; C_{max} of 0.7 nmol/l) for the hepatocyte model and the PBPK/PD model. Dose normalised temporal dynamics of A) IFN-α B) Activated Receptor Complex C) IRF9 mRNAc D) SOCS calculated by simulating the *in vivo* dose (0.7 nmol/l in the liver from the injected dose of 36 U) of IFN-α for PBPK/PD and *in vitro* model.

Impact of IFNAR2 variability on the IFN-α drug action Finally, as described above, this model used gene expression data from an average healthy European adult to estimate receptor abundance in the liver. Variations herein will strongly influence the results. Variation in physiological parameters also influences the variability in the response profile. This is specially true for receptors. The target-mediated drug disposition (TMDD) is determined by receptor-ligand binding and is one of the essential steps that not only determines the clearance of IFN-α in liver but is also an essential component to account for response in patient variability. The multi-scale PBPK/PD model can help to analyse this influence by varying the concentrations of IFNAR2 (Receptor 2) using parameter scans. To this end, I mimicked differences in both receptor abundanceies as well as receptor binding (since in the model both parameters

were correlated). The parameter scan of different concentrations of IFNAR2 led to slightly different venous plasma distributions (Figure 3.16 A) but relatively different mRNAc profiles (Figure 3.16 B). The difference in plasma profiles highlights the impact of IFN-α binding to the receptor on the clearance of IFN-α in liver as well as the therapeutic outcome of an IFN-α treatment when considering IRF9 mRNAc as a functional endpoint. It is to note that such a model can be further used to investigate the differences in therapeutic responses (patient variability and disease states).

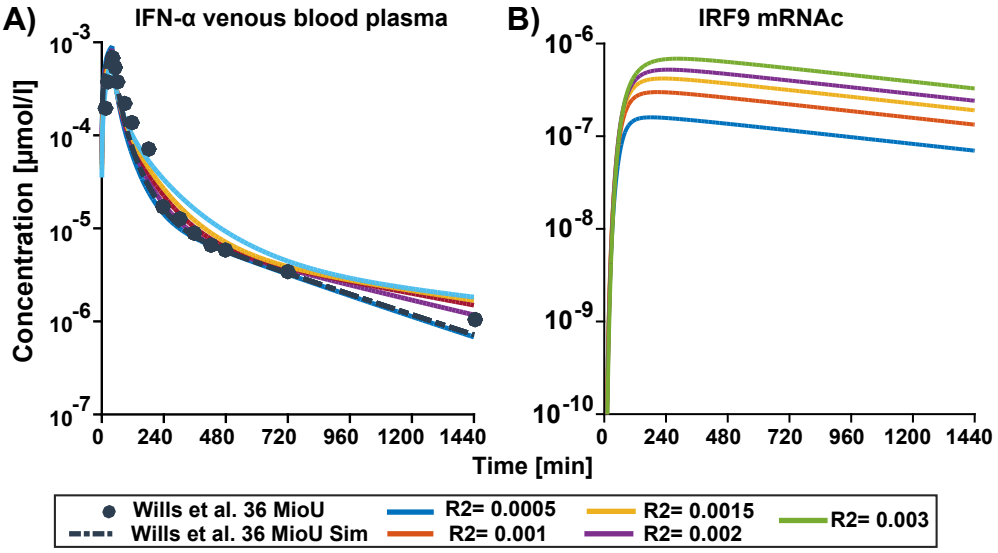

FIGURE 3.16: THe influence of parameter scan of various concentrations of IFNAR2 on the A) IFN-α plasma concentration and B) the corresponding PBPK/PD model response of IRF9 mRNAc in the liver

3.6 Discussion

The presented IFN-α model integrates the hepatocyte model into the whole-body PBPK model and defines the changes in signalling behaviour when considering an *in vivo* context. Thereby, it captures the non-linear pharmacokinetic behaviour (Absorption, Distribution, Metabolism and Elimination) of $IFN-\alpha$. This is a significant step. Establishing the PBPK/PD model to predict $IFN-\alpha$ receptor induced pharmacodynamics during a single $IFN-\alpha$ intravenous administration highlights the importance of ligand receptor binding to be of primary importance for amplification in antiviral $IFN-\alpha$ signalling pathway.

Incontestably, IFN-α is the most extensively used cytokine in clinical medicine. In the form of recombinant or (peg)IFN-α it has been used as an effective therapy against HCV and HCB for the past 20 years. It is compelling that despite being a clinical success, intriguingly little is known about its mode of action and the pharmacodynamic effects. One hindrance for understanding the molecular effects of IFN-α therapy on hepatocytes is that the experimental investigation requires liver biopsies of patients undergoing IFN-α or recombinant/peg- IFN-α therapy. Due to its nature of being clinically cumbersome, it hard to achieve this for a significant amount of patients and for sufficient time-points.

In the past, genome scale network models have been integrated in PBPK models [205], [206]. In addition, PBPK models have been coupled with simplistic or abstract

dynamic cellular network models [168], [207], [208]. Semi-mechanistic PK/PD models were built using monkey, mouse and human data [55], [134], [146], [209]. Additionally, on the macro-scale, analysis of different routes of injections on IFN-α pharmacokinetic were addressed by statistical modelling (a.k.a mixed effect models) [57], [136], [210], [211]. Moreover, two-compartment PK/PD models on patient populations have been reported in the literature [47], [49], [50], [212], [213]. The multi-scale PBPK/PD model established and analysed in this work is a unique example of linking a detailed cellular signalling model to a whole-body PBPK model using the case of therapeutic protein such as IFN-α.

In pre-clinical assessments of the drugs, *in vitro* assays are a routine. In addition, these assays are the basis of research in systems biology and such experiments help understand cellular responses. Thus, most of the knowledge about the biological mechanism of signalling elicited by IFN-α has been obtained through extensive cell culture experiments and animal models [59], [214], [215]. It is clear, that the behaviour of proteins or molecules in isolated primary cell-cultures does not represent the actual behaviour of cells in tissue and *in vivo*. Therefore, one must acknowledge that the actual cellular response *in vivo* is stronger than what is estimated in this study due to, e.g., paracrine signalling in response to IFN-α. Nonetheless, this work elucidates that the intracellular signalling is four-fold reduced in physiological conditions and the temporal dynamics are governed by the *in vivo* drug elimination [216]–[218]. The results of such a PBPK/PD model approach can give insights to improve *in vitro* assay design (this processes is termed as reverse dosimetry) such that in future physiologically relevant doses of IFN-α are used in experiments [219].

This analysis is of relevance because *in vitro* assay concentrations are frequently chosen at high and saturating levels as exhibited in the experimental datasets obtained from the literature for IFN-α where the dose of 500 U is normally used for experiments. Such doses neither reflect natural physiological endogenous concentrations of IFN-α nor doses which are used in clinical applications. As in this study, such a saturating dose is used to establish the intracellular model, we are aware that the model can be challenged and hence the model ensemble was used. It is to note that in the publication of Maiwald et al. [116], there is a strong comparison between Huh 7.5 an primary hepatocytes and depicts that the response behaviour in the cell-line is quantitatively and dynamically comparable to the primary hepatocytes. Clearly, this does not rule out the possibility that the response in isolated primary hepatocytes is not consistent to their behaviour when they are responding in a physiological context. However, in the absence of a methodology that allows to follow IFN-α signalling *in vivo* in a time-dependent manner, the work in this chapter exhibits quantitative differences between *in vivo* and *in vitro* scenarios. Such an approach can contribute to *in vitro-in vivo* extrapolation as integrating pharmacokinetic behaviour with intracellular signalling is profoundly different from calculating the amount of IFN-α in the liver based on pharmacokinetic models followed by separately calculating subsequent intracellular behaviour by administrating the corresponding dose once to the virtual hepatocyte. In the integrated model, both processes occur in parallel and any time-dependent change in the availability of the drug at the site of action immediately influences the cellular behaviour.

Furthermore, PBPK/PD models contribute to the understanding of tissue distribution of drugs using a virtual whole-body model. Such studies in humans are unfeasible. One can use the virtual prediction of tissue distribution in humans and

compare them to the observed tissue distribution in animals, where such studies are possible. Therefore, a PBPK/PD model will help to quantify the differences in response between animal studies and human patients. The model highlighted the impact of target mediated disposition of IFN-α treatments plays a major role in the efficacy of the treatment. Hence such models can be applied to understand inter-individual variability of response in patients.

The hepatocyte model was well established and validated for short-term behaviour with quantitative data. On short-time scale there was a variety of data available in the study of Maiwald et al. [116]. The proteins in this study were quantitatively calibrated. However, the data implemented for the prediction of long-term behaviour of the model was less and therefore the predictive power of the model is also less reliable. However, the most significant intracellular analysis, namely the peak amplitude and speed of activation occurs in a time range for which we have much quantitative experiments and hence a high degree of confidence on it. In addition, for the amounts of IRF9 mRNAc simulated in this work, we did not have qualitative experiments and the data were only described in relative arbitrary units, therefore the model is currently only able to quantify relative changes.

A significant comparison between PBPK/PD approach and classical PKPD approach is how in classical PK models of disease state, one only infers on the dose with simplistic models on the cellular side which are not comparable and do not give away as much insight as the integration of the mechanistic details can. This is truer for compounds like IFN-α as they are produced by most cells of our body and function in both autocrine and paracrine manner. In cases like these, it is more important to have multi-scale modelling approach to understand the efficacy, specificity and toxicity profile of the drug.

Finally, I would like to stress that the workflow presented in this chapter could be applied to other drugs eliciting intracellular responses and is by no means restricted to IFN-α signalling. Patient specific data can be integrated at the level of protein abundancies, e.g. for the receptors. In the end, for an at least semi-automated set-up of such integrated multi-scale models, it would be important to specify a common standard for model exchange between the systems biology and pharmacokinetic models, e.g., accepting SBML as the common standard to exchange cellular models.

Chapter 4

Multi-scale PBPK/PD model of IFN-α dose in mice

4.1 Chapter summary

The use of animal models in drug discovery pipelines is common in preclinical stages. Due to practical and ethical reasons, mice have been an important pillar in biomedical research. They are frequently used to test for toxicity, efficacy and safety of a potential drug or compound. In many instances, mathematical models can reanalyse the data produced by such studies to quantitatively evaluate other aspects of the biological system. In this chapter, we aim to demonstrate a quantitative understanding of IFN-α drug action in mice at both the cellular and whole-organism levels by applying a computational QSP approach.

In this chapter, I focus on the implementation of a virtual mouse model as a potential alternative to gain in-depth understanding of the factors associated with variability of responses to the drug dose in humans. Moreover, as an organism, mouse has been widely used in biomedical research and, thus, establishment of such models is of relevance for cross-species extrapolation of dose predictions.

A mouse PBPK model for i.v. injected murine IFN-α was established. The model simulations analyse the differences in plasma profiles (absorption, distribution, metabolism and elimination (ADME)) of injected human and murine IFN-α. At the cellular level, a signalling pathway model of the JAK/STAT pathway was established to describe the dynamic response of the antiviral protein MX2 following the IFN-α stimulus in mouse hepatocytes. Subsequently, the mouse PBPK/PD model was established by integrating the previous two models. This can be used to facilitate cross-species extrapolation of murine dynamics to humans.

4.2 Motivation and open questions

It is commonly believed that IFN-α stimulates innate immune responses and helps liver cells clear viruses [68], [71]. Yet, a significant fraction of patients does not respond to IFN-α treatment against HCV (reviewed in [220]) and multiple sclerosis [178] and, many experience severe, adverse side effects [33], [221]. This variability in patient response remains a key challenge for effective IFN-α dosage, as noted in chapter 3. In chapter 3, the key obstacles arose from the fact that it is ethically unfeasible to conduct experiments in humans. For example, there are many challenges in obtaining human tissue for biomendical research or in conducting cellular experiments using human tissue (reviewed in [222]). Therefore, after *in vitro* assays, animal models are employed for understanding the response of the human physiology to the drug [223]. Due to their accessibility and resemblance to the human genome (97 %) [155], mice have been regularly used in preclinical research (59% of the animals used). For practical and economic purposes, carrying out tissue distribution and ADME profile studies in mice are not difficult [39], [160], [177]. Before proceeding with *first in human* trials, experiments in mice are absolutely necessary. However, these trials have a low success rate [223]–[226]. Moreover, recently, the study by Seok et al. [227] reported "poor correlation of immune responses between mouse and humans". Consequently, the establishment of PBPK/PD model of mouse can help to understand the reasons to the failure of IFN-α treatments in patients. Such QSP models can also assist in addressing principles of the 3R (reduction, replacement and refinement) for animal studies.

The induction of ISGs such as Mx genes have been correlated to IFN-α's antiviral properties [228]. Myxovirus resistance (Mx) protein is an antiviral ISG that functions like a GTPase and is highly conserved across species. Mouse and humans have 2 forms of Mx proteins:MX1 and MX2 are found in mice, while MXA and MXB proteins are the human homologs. Studies indicated that MX2 is non-functional in most inbred mouse strains but is functional in wildtype strains [229], [230]. In this work, the mouse PBPK/PD model consisting of a mouse PBPK model coupled to an intracellular signaling model was developed. The PBPK model was informed by quantitative data on the i.v. injected IFN-α plasma concentrations measured in mice and the cellular model is parameterised to measurents of antiviral response of Mx2 in JAK/STAT pathway, in primary mouse hepatocytes, respectively.

4.3 Mouse PBPK model

4.3.1 Preliminary analysis for mouse PK data

Some sections of this analysis were performed by Rebekka Fendt in her master thesis. This work was co-supervised by myself.

The datasets from the literature and collaboratory effort measure the murine IFN-α venous plasma concentration for 2 hours [39], 3 hours [158] and for 20 minutes [157] (dataset provided by Dr. Mario Koester[1]). The i.v. injection of murine IFN-α in Bohoslawec et al. [39] was 8.7×10^5 U, Rosztoczy et al. [158] was 1.9×10^7 U whilst, the i.v. injected IFN-α dose published in Pulverer et al. [157] was, 5000 U. Moreover, the conversion factors for the dose units (U) varied significantly in these publications. Hence, the calculations from U to amounts of injected IFN-α resulted to 0.205 nmol, 0.162 nmol and 0.0016 nmol respectively and differed enormously.

[1]Department of Gene Regulation and Differentiation, HZI – Helmholtz Centre for Infection Research, Inhoffenstr. 7, 38124, Braunschweig, Germany.

As the time-scale of the datasets from Pulverer et al. [157] and Bohoslawec et al. [39] range between 20 mins to 2 hours, a compartmental analysis[2] on the two datasets was performed. For an i.v. dose, the pharmacokinetics of a compound can be represented by one-compartment (mono-exponential decay) or multi-compartment (bi or tri-exponential decay) models that are fitted to plasma concentration over time.

In the mono-exponential decay or one-compartment model, the compartment is homogeneous for murine IFN-α and after the i.v. bolus administration, the plasma concentration of murine IFN-α is (also see Figure 4.1 A):

$$C(t) = C_0{}^{K_{el} \times t} \tag{4.1}$$

Where C is the murine IFN-α plasma concentration at time t, K_{el} is the elimination rate constant (represents the total clearance from kidney and liver). The semi logarithmic plot of a mono-exponential decay would be a straight line.

A two-compartmental model (bi-exponential decay) describes the two-phase plasma distribution of murine IFN-α. After i.v. administration, the murine IFN-α is instantaneously distributed to the highly perfused central compartment (which represents the liver and/or kidney) where the elimination of murine IFN-α occurs. This model is represented by bi-exponential decay of murine IFN-α (also see Figure 4.1 B) as follows:

$$C(t) = A \cdot e^{-\alpha \times t} + B \cdot e^{-\beta \times t} \tag{4.2}$$

Where C is the murine IFN-α plasma concentration at time t, A is the distribution phase (slope, α) and B is the elimination phase (slope, β).

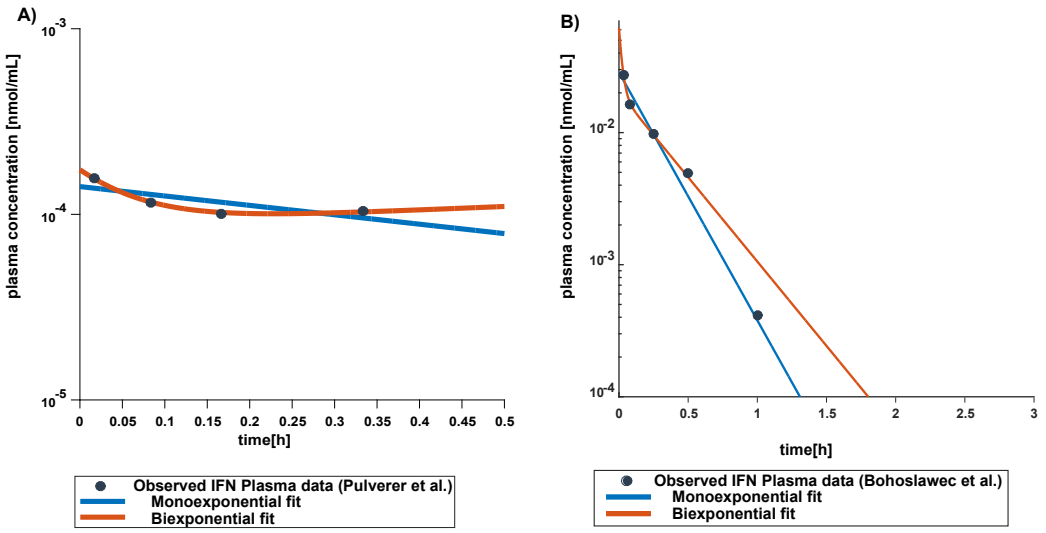

FIGURE 4.1: Fit of exponential models to the observed plasma concentration profile (semi-logarithmic plot). Exponential models were fitted in MATLAB to observed IFN-α plasma concentrations in A) Pulverer et al. [157] B) Bohoslawec et al. [39]. The data are in black solid dots. The mono-exponential fit is represented by a solid blue line and the bi-exponential fit is represented by a solid orange line. ONote the differences in dose and time scale of the datasets.

[2]One or several organs modelled as kinetically homogeneous.

For Bohoslawec et al. [39], $R_{squared}$ was 0.9589 for the mono-exponential fit and 0.9889 for the bi-exponential fit and for Pulverer et al. [157], $R_{squared}$ was 0.5731 for the mono-exponential fit and 0.9970 for the bi-exponential fit indicating that a two compartment model explains the data better. However, fitting Pulverer et al. [157] data is tricky as the last datapoint is 20 mins after the administration, which is potentially the distribution phase for murine IFN-α and there is no information on the terminal phase for this experiment. In addition, the last data point is an outlier as the plasma concentration of murine IFN-α is higher than the second last data point leading to a positive slope for bi-exponential fit. The exclusion of the last data point to fit the model is not possible as the data would be too sparse for the variables fitted (3 data points and 4 variables). Therefore, the fits for Pulverer et al. [157] lack biological explanation. In the data from Bohoslawec et al. [39], the steep decline of murine IFN-α immediately after administration and the resulting good bi-exponential fit is primarily due to rapid distribution of murine IFN-α from plasma to well perfused organs. However, the data are not necessarily indicating the shallower clearance due to insufficient measurements. From the data of Pulverer et al. [157], no conclusion of the PK of murine IFN-α dose-dependent effects can be drawn.

Although a two-compartment model is able to provide a good fit for the plasma concentration of murine IFN-α, a PBPK model was considered to have a detailed physiological understanding in predicting the target site concentrations of murine IFN-α and is able to take mechanistic details into account. Therefore, the PBPK model was solely fitted to the data from Bohoslawec et al. [39] and Roszotoczy et al. [158].

4.4 Mouse IFN-α PBPK model

The goal of this work is to compare quantitative differences between *in vitro- in vivo* scenarios and analyse cross-species extrapolation using QSP approach. For this reason, in the following sections the workflow of the model development and the structure of models (both, PBPK and intracellular model) are identical to that of the human counterpart elaborated in chapter 3. Therefore, in the following sections, wherever the human model approach is retained, I will refer to chapter 3.

A protein PBPK model of murine IFN-α distribution was established in PK-Sim for an average mouse (Appendix C Table C.3), compound specific parameters (Appendix A, Table A.4). The route of administration is intravenous bolus. Mouse IFANR1/2 tissue expressions were defined from the PK-Sim database. The receptors were localised in the mouse liver interstitium. The clearance of murine IFN-α via kidneys was inserted from the literature [39]. i.v. bolus injection of murine IFN-α as reported by Bohoslawec et al. (1984) [39] and Rosztoczy et al. (1986) [158] were used to fit the model.

4.4.1 Mouse PBPK model overview

The ADME profile of murine IFN-α was modelled as zero order input rate and first order elimination rate. All the parameters for the pharmacokinetic modelling are listed in Table 4.1. As stated in chapter 3, the liver was simplified as one big cell and receptor amounts and concentrations were calculated as in the forthcoming subsection 4.4.2, 4.4.2. The liver was divided into 3 compartments: the interstitial, the cytoplasm and the nucleus. The defined volumes of each compartment is described in the Appendix C, Table C.4. Similar to the human PBPK model, the

IFN receptor dynamics were modelled in the interstitial compartment and consists of the detailed receptor ligand interaction and turnover kinetics. Here, the murine IFN-α drug dose arriving in the liver interstitiu binds to IFNAR2 to form a dimeric ligand-receptor complex (IFNA-IFNAR2 Complex) (**M1**). The ligand-receptor complex (IFNA-IFNAR2 Complex) binds to IFNAR1 to form the hetero-trimeric ligand receptor complex (Activated Receptor Complex) (**M2**). The IFNAR2 and IFNAR1 basal turnover in the absence of the drug is modelled (**M3 and M4**). Finally, the hetero-trimeric ligand receptor complex is internalised and degraded (**M5**). Illustration of the interactions can be found in chapter 3, Figure 3.1.

Reactions and rate laws used for the mouse PBPK model The reactions and the rate laws used for the mouse PBPK model are the same as the ones used in the human model. In summary, all the reactions are described by mass action kinetics. For details of the kinetics, please refer to chapter 3, paragraph 3.3.1

4.4.2 Calculations for the PBPK model

Calculation of receptor concentration These calculations were performed by Rebbeka Fendt in her master thesis.

The mean number of receptor IFN-α receptor per animal was assumed to be 1000 receptors per cell (inclusive of receptors: IFNAR1 and IFNAR2) and a cell mass of 10^{-12} kg was measured by others [191]–[193], [231]. The number of hepatocytes per gram of mouse liver has been estimated as 135×10^6 cells/g liver [188] which is close to the human liver hepatocellularity. Different expression profiles of the receptors were not taken into account.

$$Number\ of\ Cells\ per\ animal = \frac{Body\ weight}{cell\ mass} = \frac{0.021\ kg}{10^{-12}\ kg} = 2.1 \times 10^{10}\ cells \tag{4.3}$$

$$\begin{aligned} Receptors\ per\ animal &= number\ of\ cells \times receptors\ per\ cell \\ &= 2.1 \times 10^{10} \times 1000\ receptors\ per\ cell \\ &= 2.1 \times 10^{13}\ receptors \end{aligned} \tag{4.4}$$

$$Rec_{Amount}\ Liver = (\frac{number\ of\ receptors}{avogadro\ constant}) = (\frac{2.1 \times 10^{13}}{6.02 \times 10^{23}}) = 3.5 \times 10^{-11} mol \tag{4.5}$$

$$Receptor\ amount = 35 pmol \tag{4.6}$$

Calculation of the concentration of total receptors in the liver of the mouse

$$\begin{aligned} Receptor\ Concentration\ Liver = Receptor\ density\ per\ cell \times \\ Mouse\ hepatocellularity\ number \times liver\ density \end{aligned} \tag{4.7}$$

$$Rec_{exp}(\frac{Receptor}{ml}) = 1000(\frac{Receptor}{cell}) \times 135 \times 10^6 (\frac{Cells}{gliver}) \times 1.05(\frac{gliver}{ml}) \tag{4.8}$$

$$Rec_{conc}(\frac{mol}{ml}) = \frac{142 \times 10^9(\frac{Receptor}{ml})}{6.02 \times 10^{23}} = 2.35 \times 10^{-13}(\frac{mol}{ml}) \tag{4.9}$$

$$Rec_{conc}Liver = 0.235\frac{pmol}{ml} \tag{4.10}$$

4.4.3 Parameter estimation strategy for the mouse PBPK model

The parameters of the simulated PBPK model were calibrated to plasma concentrations (datasets from Bohoslawec et al. [39] and Roszotoczy et al. [158]). The estimated parameters were- the plasma clearance, the individual receptor (IFNAR1 and IFNAR2) and receptor complex dissociation rates and dissociation constants (K_{off} and K_D), the endocytosis rate of the receptor complex into the cells and the basal turnover rates of the individual receptors (IFNAR1 and IFNAR2). In addition, it was necessary to estimate the clearance as the total body clearance exhibited in the literature was inclusive of the following three clearance rates: renal clearance, hepatic clearance and lung clearance. Furthermore, the total body clearance was given per animal and the animal weight was not specified which makes the normalisation to the body weight required for the input parameter imprecise. However, the clearance rate required for the mouse PBPK model was the renal clearance only as the hepatic clearance rate was estimated for by the mechanistic receptor mediated disposition. The mouse body weight was taken as the average mouse weight due to the reported inconsistent weight.

The parameters of the established PBPK model were estimated by the Levenberg-Marquardt algorithm and 150 parameter sets were obtained describing the venous plasma concentration. The RMSD error (measure of the differences between values predicted by the PBPK model and the values observed in the dataset) of all the fits lay in the range of 1.28-1.30. The top five parameterisations of the simulation exhibited similar plasma profile of murine IFN-α in the plasma, e.g., the similarity of the of the simulations from first two parameter sets of the murine IFN-α plasma profile for the datasets of Bohoslawec et al. [39] and Roszotoczy et al. [158] are shown in Figure 4.2.

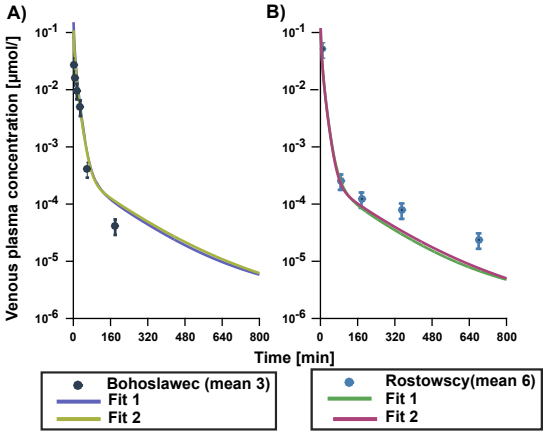

FIGURE 4.2: Semi-logarithmic plot of the simulations of the first two fits of the venous blood plasma profile of murine IFN-α for the datasets of A) Bohoslawec et al. [39] and B) Roszotoczy et al. [158]. The simulations of the fit are plotted in solid line and the datasets are plotted as circles. The y-axis is on a lograthmic scale and describes the venous plasma concentration of murine IFN-α distribution while the x-axis represents the time points in mins.

In some parameterisations, the reference concentrations values of the individual receptors- IFNAR1 and IFNAR2 spanned in large range while presenting similarly good simulation to the observed data, but the ratio of the concentrations of receptors for some fits were not biologically relevant (e.g., the ratio of the concentration of IFNAR1 to IFNAR2 being 30:1, was a 30 order difference in magnitude while the ratio reported in the literature is 2:1 [90]; see Appendix C, Figure C.1). The parameter for clearance rate via kidneys was well defined, but the constants for receptor binding (k_{off}) and the constant for receptor turnover for the individual receptors ranged in a span of 2 orders of magnitude. Since the top five PBPK model parameterisations do not differ with regard to the simulation of murine IFN-α plasma or liver concentrations and are an input to the signalling model which will be integrated, Fit 1 is a good representation of the fit ensemble as it has biologically relevant parameter values (see Figure 4.3). The obtained simulations were not able to describe the terminal points of the dataset. For Bohoslawec et al. [39], the simulation is not able to describe the rapid terminal decline of the murine IFN-α plasma concentration for the last sample measured at 160 mins. A similar difference can be noticed between the PBPK model and the experimental data by Roszotoczy et al. [158], where the last two samples at time points 325 mins and 660 mins show a slow decline in the murine IFN-α plasma concentration.

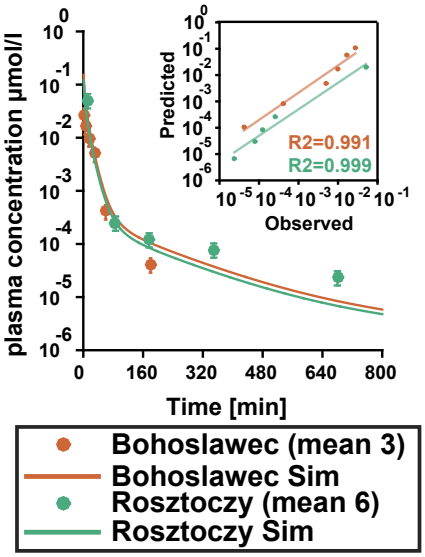

FIGURE 4.3: Physiologically based pharmacokinetic (PBPK) model fit simulation and experimental blood plasma profile for Bohoslawec et al. [39] and Roszotoczy et al. [158] of murine IFN-α in mouse. The goodness of fit is plotted on the right (small plot) where the RMSE and the $R_{squared}$ values are depicted.

4.4.4 Validation of the mouse PBPK model

The PBPK model simulation of murine IFN-α venous blood plasma concentration was validated to the dataset of Kuichi et al. [159] where a 0.154 nmol dose of murine IFN-α was intravenously injected into mice. The validation of the parameter set increases confidence in the prediction of the PBPK model to different murine IFN-α injection doses. Murine IFN-α concentrations in mouse plasma data was successfully simulated for a single i.v. injection (see Figure 4.4) representing the dataset. A striking amount of murine IFN-α is cleared in a mono-exponential fashion, especially in the first 100 mins. (Figure 4.4 and Figure 4.3).

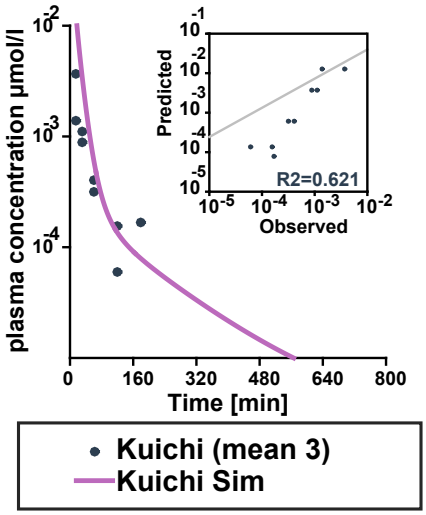

FIGURE 4.4: Physiologically based pharmacokinetic (PBPK) model simulation validated to the experimental blood plasma profile of murine IFN-α from Kuichi et al. [159] in mouse. The goodness of fit is plotted on the right (small plot) where the RMSE and the $R_{squared}$ values are depicted.

The human IFN-α (hu-IFN-α) differs from murine IFN-α w.r.t. its kinetics of its clearance from the plasma. In particular, studies reported inter-species IFNAR binding differences between hu-IFN-α and murine IFN-α for reasons that are not well understood [232]. After injection, murine IFN-α is cleared rapidly from the mice blood (having a half-life of around 4.5 mins) but the clearance of corresponding doses are reported for hu-IFN-α to be slow and with longer half life (15-20 mins) [159]. This behaviour is not understood but hypothesised to result from the strong affinity of murine IFN-α to homologous tissue (mouse tissue) [159]. The other reason is the species-specific antigenicity against heterologous IFN-α (human IFN-α but in mouse tissue) [233]. I tested the two hypotheses with the murine PBPK model. For the first reason, the simulations exhibited no changes (results not shown). For the second hypothesis, I compared model simulations with the measurements by Koyanagi et al. [160] who injected hu-IFN-α in mice. The simulation suggested a more rapid decline than reported of hu-IFN-α from the plasma of mouse. I analysed if the hu-IFN-α plasma concentration could be simulated by changing the binding kinetics of the receptors in the model. This was implemented by scanning the parameter values of the binding kinetics of the receptors but they did not display any significant effect on the clearance of hu-IFN-α in the simulation. I then explored the second reason where, I varied the fraction unbound parameter value of hu-IFN-α to account for varied antigenicity. This variation caused the simulation to slow down the clearance of hu-IFN-α from the plasma (Figure 4.5). Thus, the simulation supported the hypothesis of inter-species differences in the response to different IFN-α types.

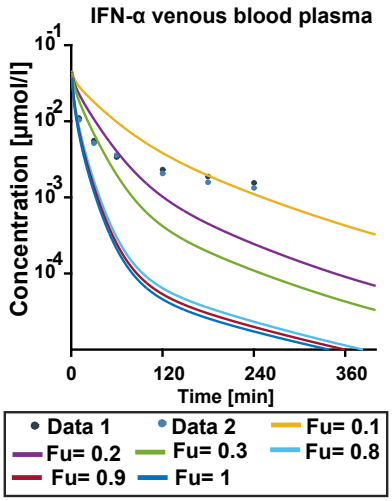

FIGURE 4.5: Physiologically based pharmacokinetic (PBPK) model simulation validated to the experimental blood plasma profile of human IFN-α injected into mice from Koyanagi et al. [160] in mouse.

4.4.5 Analysis of the mouse PBPK model

Tissue distribution of murine IFN-α in mice IFN-α is used as an antiviral drug in humans [6], [41], [234]. Ideally the data on tissue distribution of human interferons should be collected in experiments on humans but, as stated in chapter 3, tissue distribution studies are not feasible in humans. However, its worthy to have data on tissue distribution of IFN-α injection. Therefore, many studies for the same were executed in mouse, rabbits and monkeys [36], [39]–[41], [235], [236]. Johns et al. [40] measured the tissue distribution of murine IFN-α in different tissues of mice 30 mins after the injection of a radioactive single dose of murine IFN-α. They reported the highest amount of murine IFN-α in the liver and the kidneys and small amounts in fat tissue of mice. The whole-body mouse PBPK model gives an opportunity to simulate and analyse the tissue distribution. The results of the simulation indicated that the liver is the organ that contains the highest amount of murine IFN-α at 30 mins. In contrast to the observation by Johns et al. [40], in the simulation the concentration of murine IFN-α in muscle is close to that of kidney, plasma and lungs at 30 mins and is significantly higher than in fat. Thus the model indicates the transfer of murine IFN-α i to the muscle is stronger than *in vivo* experiment. This result should be tested in experimental settings. However, there is congruence between the model and the experiments as initially, the concentration of murine IFN-α in highly perfused organs like kidney, spleen and liver is close to the blood plasma concentration of murine IFN-α but it decreases rapidly over time to be close to the poorly perfused tissues.

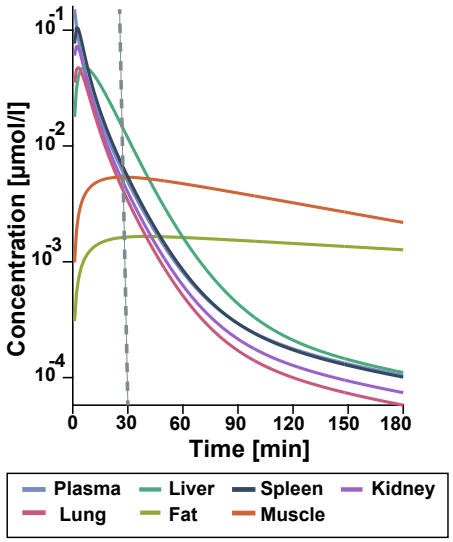

FIGURE 4.6: Simulation of the tissue distribution of murine IFN-α after i.v. administration of a single 2.35 nmol dose in the mouse PBPK model. The vertical dashed line represents time=30 mins. murine IFN-α tissue tissue concentrations in descending order after 30 min: liver, (plasma), kidney, muscle and fat (with kidney and muscle concentrations being almost equal).

4.5 IFN-α mouse hepatocyte model

The hepatocyte model implemented in this study is the extension of the hepatocyte model from in chapter 3. In summary, the model comprised of two compartments: Nuclear and cytoplasmic, 23 species and 23 reactions. The details of the model structure are described in chapter 3, subsection 3.4.1. Due to the lack of data on intermediate pathway, the kinetic parameter values and the initial concentrations of the proteins in the JAK/STAT pathway were kept identical to the human hepatocyte model were kept identical because the molecules depict high homology between human and mouse. Therefore, the existing hepatocyte model of the JAK/STAT pathway was extended by three reactions to include the kinetics of Mx2, which is the followed biomarker of this study. The initial concentrations of the molecules, their kinetic rate law values and the scaling factors of the model were the same as the human hepatocyte model. However, the kinetics of the interaction of the receptors to murine IFN-α, the activation of the ternary complex and the volume of the liver compartment had the physiological parameters describing the mouse plasma concentration from the mouse PBPK model.

4.5.1 Intracellular hepatocyte model overview

For the extension of the human hepatocyte model from chapter 3 I analysed the homology and identity of the molecules for the pathway between the two species (Appendix C, section C.2, TableC.7). The BLAST of the sequences had high homology of the molecules of the JAK/STAT pathway of human and mouse. The details of the upstream JAK/STAT pathway of the human hepatocyte model are found in 3, subsection 3.4.1. The human hepatocyte model of the JAK/STAT pathway was

extended by three reactions. These reactions described the Mx2 mRNAc transcription (**R12**), Mx2 mRNAc degradation (**R13**) and translation of the Mx2 protein (**R16**). For this, the model had 2 different molecules introduced to it: The mRNA of Mx2 (mRNA_Mx2) and the followed protein of interest MX2 (Mx2). The details of the reactions and their kinetic rate laws are summarised in Table 4.1 and in Figure 4.7.

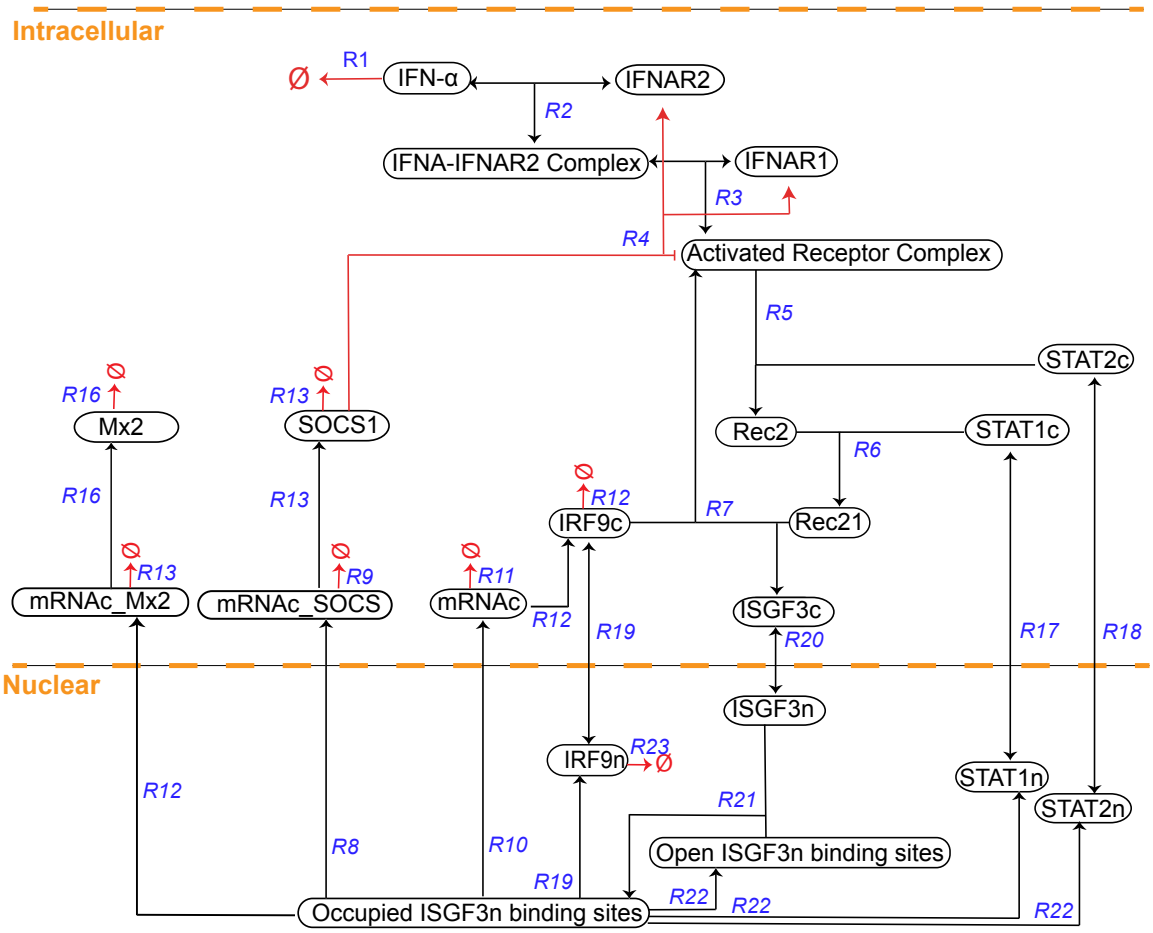

FIGURE 4.7: The structure of the kinetic model of IFN-α signalling pathway from the human hepatocyte model is depicted. It was further extended to include the reaction kinetics of Mx2 transcription, translation and degradation respectively (R12, R13 and R16). The downstream cytoplasmic and nuclear reactions (solid black arrows) and degradation reactions (red arrows with ϕ) are divided into the respective model compartments (dashed yellow line). Finally, the feedback reactions were modelled (solid red line).

Reactions and rate laws Most reactions were modelled as mass action kinetics (4.11).

$$v_i = k_i \times [Substrate1] \times [Substrate2] - \frac{1}{keq_i} \times [Product] \tag{4.11}$$

Here the velocity of the reaction is determined by the k_i and keq_i and the transition concentration of the *[Substrate1]*, *[Substrate2]* and the *[Product]*.

Information on the nuclear binding sites of Mx2 The Mx2 gene has been reported to be non-functional in all laboratory mouse strains due to mutations but expressed in feral mice [237]. Mammals have structurally related nuclear and cytoplasmic Mx proteins (collective of Mx1 and Mx2) [229], [238]. The human MxA promoter site was reported to have three ISRE sites [239]. The mouse Mx2 promoter site was reported to have two putative ISRE binding site and one IRF binding site, thus, allowing for cooperativity [240].

The Mx2-luc expression dose response data on mouse primary hepatocyte in response to mu-IFN-α were generated by Dr. Mario Koester at HZI, Braunschweig. Initially, models with three different transcription rate law for Mx2 gene were evaluated as there is little knowledge on the mechanism of the gene transcription. The models were also evaluated by including nuclear export reaction for Mx2 since the transcription takes place in the nucleus and the protein is expressed in the cytoplasm. The evaluated models that included nuclear transport showed extreme delay in the gene expression and therefore that process was discarded. Thenceforth, the models with different transcription rate law for Mx2 and the cytosolic transcription of Mx2 mRNA were analysed. The rate laws that were tested were Hill kinetics, Michaelis Menten kinetics and mass action. Initial concentrations of the Mx2 protein and Mx2 mRNA were assumed to be zero because there is no constitutive Mx2 expression *in vivo*. The preliminary evaluation of the parameter estimation of the different rate laws showed that mass action kinetics could explain the Mx2 expression data (Figure 4.8).

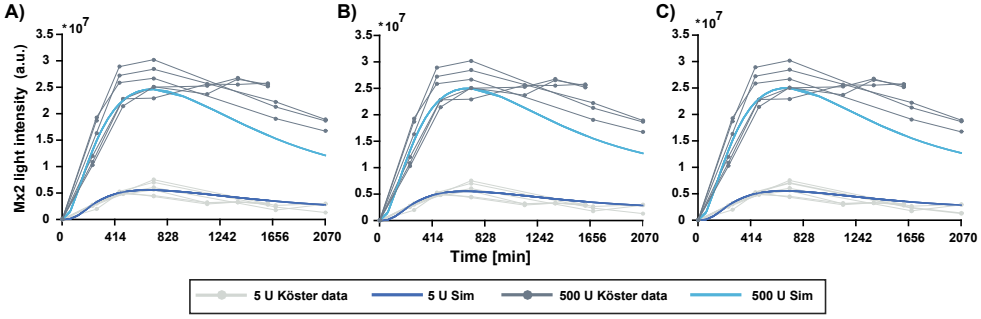

FIGURE 4.8: Parameter estimation of the three rate laws of Mx2 transcription for two doses of mu-IFN-α where the doses are 5 U (light grey, six replicates) and 500 U (dark grey, six replicates) on mouse primary hepatocytes A) Hill kinetics, B) Michaelis Menten kinetics and c) mass action kinetics. The simulations of Mx2 response for the two doses: 500 U (light blue) and 5 U (dark blue) are plotted as solid lines. The y-axis depict the Mx2 luciferase light intensity in arbitrary units and the x-axis define the time in mins (34 hours). Note that mass action kinetics (C) is able to describe the Mx2 expression data.

4.5.2 Parameter estimation strategy for the mouse intracellular hepatocyte model

Mapping of the model variables to the data As detailed in chapter 3, for the integration of the mouse hepatocyte model into the PBPK model, I need to ensure consistencies at the receptor kinetics level. Thus, the receptor parameter values and the equation was taken from the mouse PBPK model into the hepatocyte model (the parameter values can be seen in appendix C, Table C.9). Scaling factors were added

to the model to be able to represent the arbitrary units of the simulated Mx2 concentration observed as light intensity of luciferin-luciferase reaction. The protein Mx2 of the model was mapped (4.12) to the dataset as follows:

$$Mx2^{\dagger}(t_i) = \varphi_1 \times \Big(Mx2(t_i)\Big) \tag{4.12}$$

where φ_1 is the scaling factor.

Fitting the deterministic model Due to the size of the model and the lack of information on the intermediate pathway molecules, the fitting of all the parameters was a hard optimisation problem. Therefore, I extended the human hepatocyte model ensemble of ten models from chapter 3, subsection 3.4.3 with the Mx2 transcription (mass action kinetics), translation and degradation kinetics. The models in the ensemble had identical structure and the parameterisations for the Mx2 reaction kinetics were analysed using the parameter estimation strategy with random start values. 80 different parameterisations of each model in the model ensemble were executed using the Particle Swarm algorithm. Therefore, in total 800 parameterisations were obtained. In the distribution of parameter values of the model ensemble (see Figure 4.9), most parameters were evidently unidentifiable due to their broad distribution. For example, some of the parameters were spread over the range of the parameter variation, such as, the rate constant k1 for the transcription of MX2 mRNA and the activation and degradation constants of the Mx2 protein synthesis, kact and kdeg. Also, there is a correlation in the activation and degradation constants of the Mx2 protein.

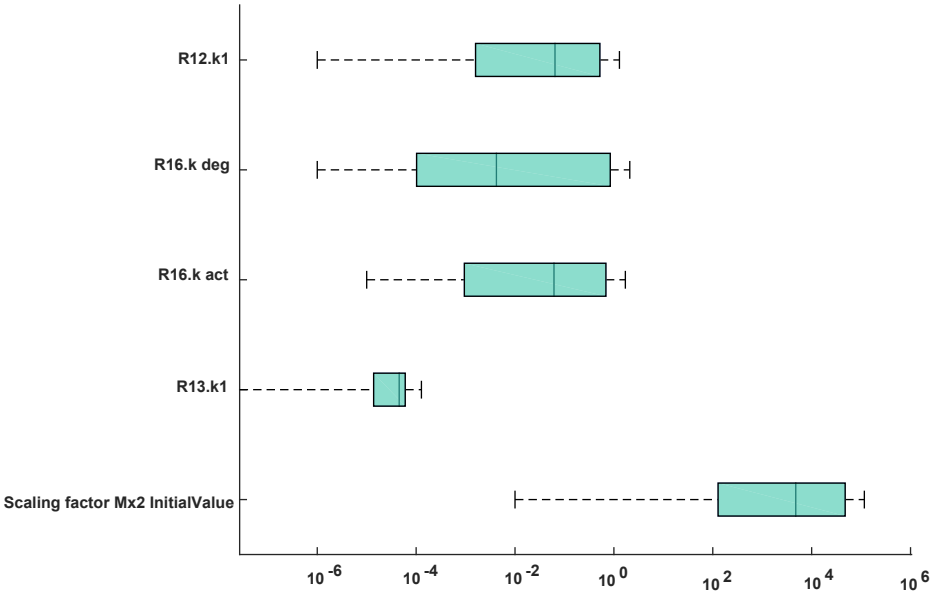

FIGURE 4.9: The parameter values of 800 fits are represented in the box plot. The likely value of the fitted parameter is represented by the box (green), the full range of the parameter variation is represented by the dashed line (black) and the median is indicated by a solid line (black).

As the information on several parameters modelled was sparse, to deal with the model uncertainty and scarcity of the data, further analysis was based on model ensemble of ten models [203]. The ten models have identical model topology but different parameter values (see Appendix C, Table C.8) that described the experimental data equally well and encompass the full range of possible biologically relevant parameter values. Simulations of the top ten models replicate the high and the low murine IFN-α dose of the experimental data.

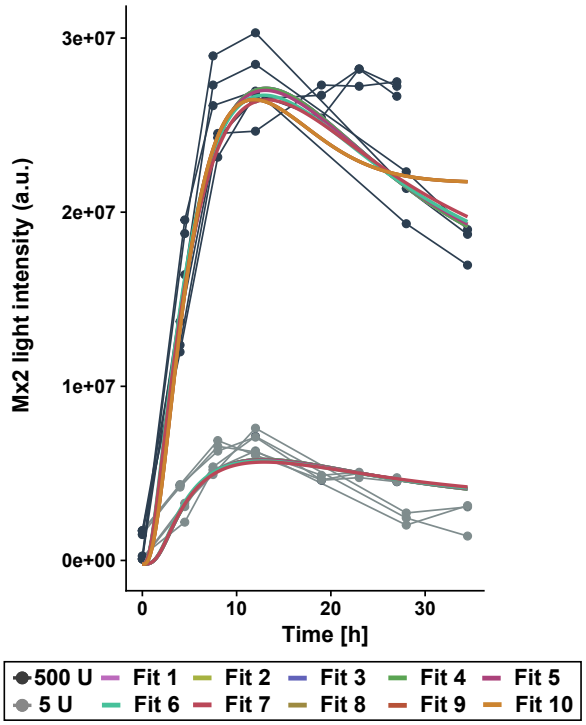

FIGURE 4.10: Here, the parameter estimation results of the top ten models in the model ensemble are shown. The experimental time courses of the response of Mx2 for 500 U (black dots) and for 5 U (grey dots) dose of murine IFN-α on primary mouse hepatocyte are plotted. Corresponding to that the simulations (solid lines) of the model ensemble are plotted. The x-axis of figures represent the time scale at which the measurements were taken after the applied IFN-α stimulus. The measurements of the protein expression are in light intensity and arbitrary units are plotted on y-axis.

4.5.3 Validation of the intracellular mouse hepatocyte model

Further, I analyse the model ensemble against the dose response time points of the dataset provided by Dr. Mario Koester. In the dataset primary mouse hepatocytes were stimulated with murine IFN-α and the Mx2-Luciferase activity was determined 24 hours after stimulation. There are three replicates for each response measurement. The simulations of the model ensemble reproduces the dose response experiments (Figure 4.11). The maximum response of Mx2 was attained at doses between 25 to 100 U. The simulations of the model ensemble were spread between exhibiting sharp peak response of Mx2 after 25 U (Fit 7-10) and exhibiting peak response of Mx2 at 100 U of murine IFN-α stimuli (Fit 1-6).

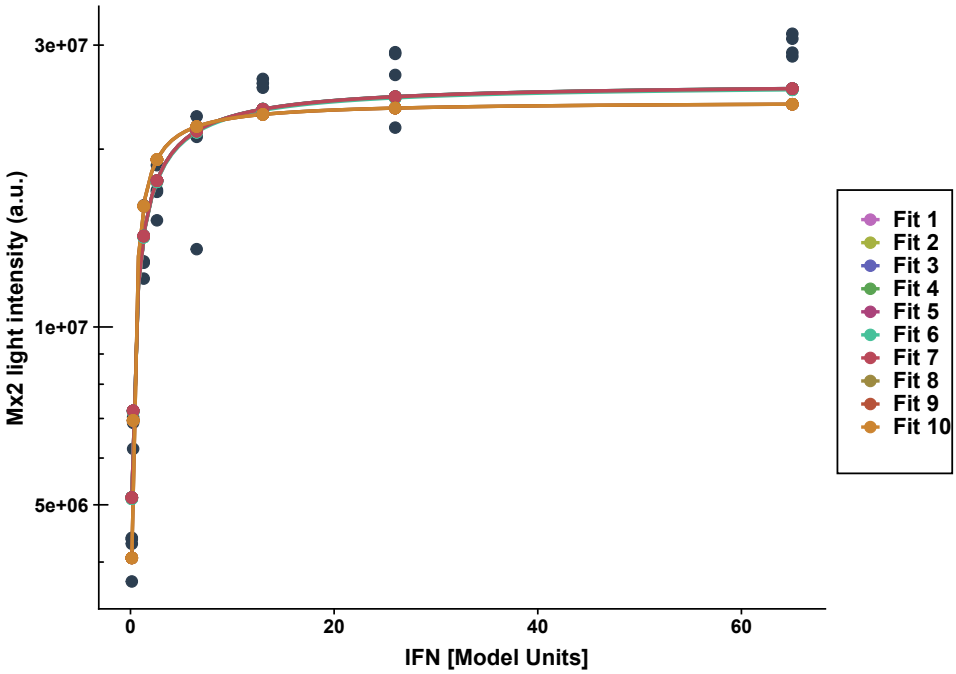

FIGURE 4.11: In the above graph the model ensemble simulations are plotted (solid) against the validation dataset where, the two different doses of murine IFN-α stimuli trigger the response of Mx2 expression (black circles). The 24^{th} hour dose response curve is shown for the datasets. The doses are 1 U, 5 U, 10 U, 25 U, 100 U, 500 U and 2500 U. Semi-logarithmic y-axis represents the Mx2-Luciferase activity in arbitrary units. The x-axis represents the aforementioned (3) interferon doses in model units.

4.5.4 Analysis of the intracellular mouse hepatocyte model

The difference between 5 U and 500 U of murine IFN-α doses on primary mouse hepatocyte response of Mx2 The intracellular mouse hepatocyte models in the ensemble were simulated for the two murine IFN-α doses: 5 U and 500 U. The dynamical behaviour of the ensemble was identical and hence I show the first model from the ensemble as a representative example (Figure 4.12). For the propagation of the signalling cascade, the simulations showed a time delay in reaching the peak concentrations. I.e., from the binding of STAT molecules to the receptors to have their phosphorylated forms (*Receptor + STAT1/2*) to the expression of the proteins (*Mx2 & SOCS1*). Interestingly, the difference in the transcription sites on the DNA that were bound to the transcription factor (occupied sites) differed by a factor of five between the two doses of murine IFN-α while the doses differed by a factor of 100 (5 U and 500 U). This implies the dampening of the signal as it propogates to activate the transcription. Also, the Mx2 expression consistently differed by a factor of four.

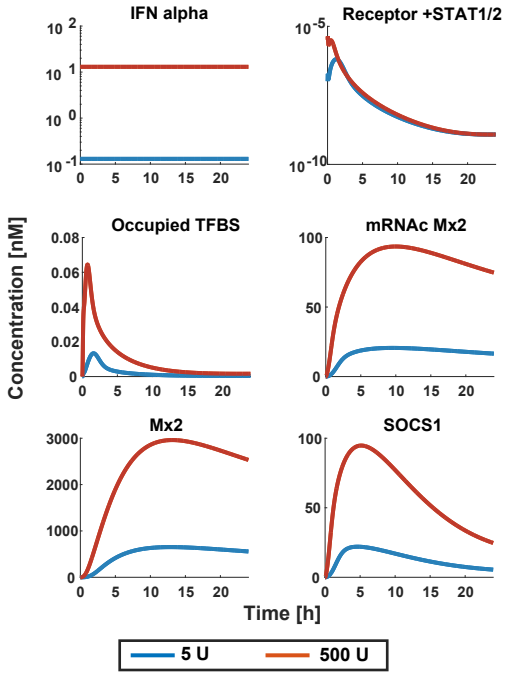

FIGURE 4.12: The simulations of the representative model response to high and low doses of murine IFN-α are shown. The receptor activation dynamics are plotted in the top panel (semi-logarithmic plot). In the middle panel the dynamics of DNA-bound transcription factor and the cytoplasmic mRNA of Mx2 are plotted. In the last panel the dynamics of the proteins Mx2 and SOCS1 are plotted. The y-axis depict the concentration of the molecules and the x-axis depicts the time of the simulation in hours (up to 24 hours). SOCS.

4.6 IFN-α PBPK/PD mouse model

The PBPK model was coupled to the mouse hepatocyte model in MoBi to establish whole body PBPK/PD model of IFN-α intravenous dose in mice. The integration of the multi-scale PBPK/PD model was executed as instructed in chapter 3, Section 3.5.

4.6.1 Mouse PBPK/PD model overview

The hepatocyte model was integrated into the PBPK organism model in the interstitial space of the liver. The point of interaction of both models is the receptor binding of IFN-α at the target site. The receptor concentrations and the kinetics were kept identical to the PBPK organism model simulation after the hepatocyte model integration and the kinetics for the same were present in the interstitium of the liver. The intracellular compartment and structure of the hepatocyte model was preserved from the mouse hepatocyte model in the PBPK/PD model. A detailed description of the individual models are given in the section 4.3 and 4.5 respectively. The presented mouse PBPK/PD IFN-α model integrates the whole body distribution model (data from Bohoslawec et al. [39]) with activated cellular signalling of IFN-α and represents changes in the signalling behaviour while considering the *in vivo* context. Thereby, it captures the non-linear pharmacokinetic behaviour (absorption, distribution, metabolism and elimination) of IFN-α and is schematically described in Figure

4.13. The details of the kinetic rate laws for the PBPK/PD model are described in Table 3.2 with the reference of *multiscale compartment*.

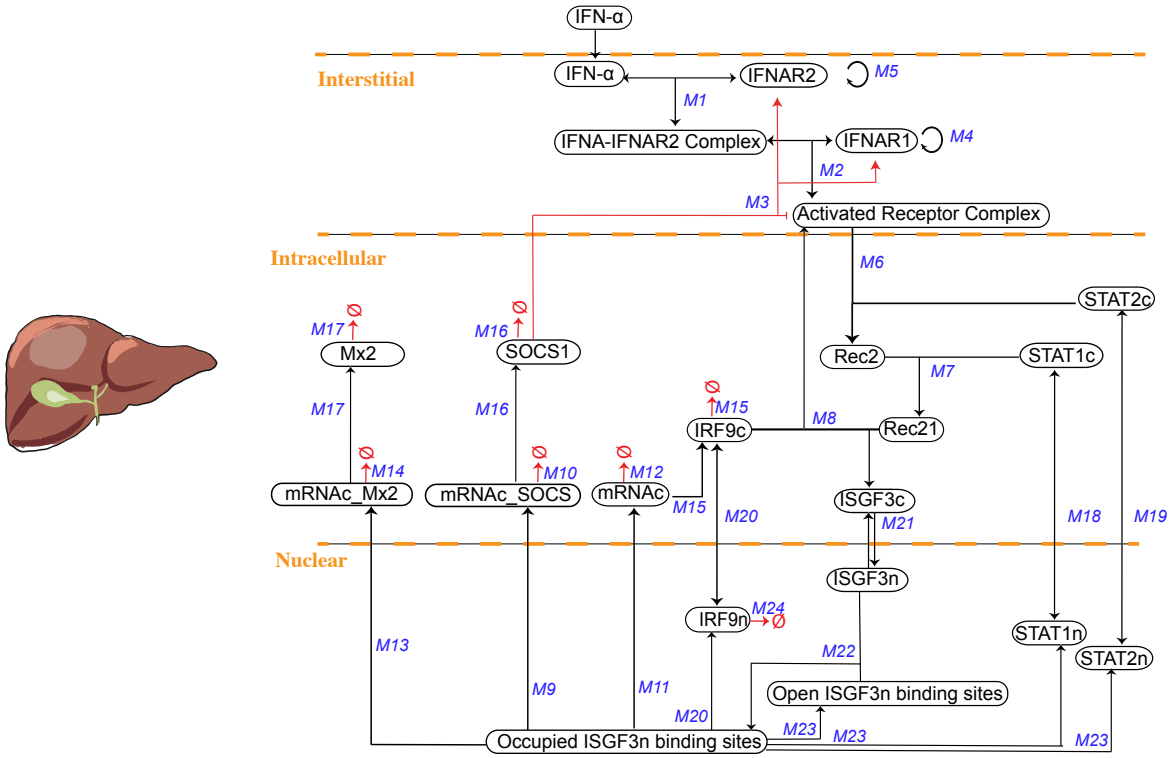

FIGURE 4.13: The diagram is a schematic representation of the structure of the mmouse PBPK/PD model. The murine IFN-α drug dose from the mouse PBPK model arrives in the liver where, it interacts with the receptors in the interstitium of the PBPK model (reactions M1-M5). The downstream mouse JAK/STAT cascade was introduced at the *Activated receptor complex* and the signalling pathway was compartmentalised in the intracellular and the nuclear compartment in the liver (reactions M6-M17).

TABLE 4.1: Collective reaction list: The individual reactions for both mouse models: the *in vitro* hepatocyte and the *in vivo* PBPK/PD model. The column with R# and Cell Compartment depict the reactions that are present in the *in vitro* hepatocyte model. The columns with M# and multi-scale compartment do the same for the *in vivo* PBPK/PD model. The column reactions describe the modelled pathway along with the column kinetic rate law which gives insight on the kinetics used to model each step.

#		Cell Compartment	Multiscale Compartment	Reaction	Kinetic rate law
R1	-	Cell Intracellular	-	IFN $\rightarrow \varnothing$	$k1 \cdot S$
R2	M1	Cell Intracellular	Liver Interstitial	IFNA + IFNAR2 $\rightleftharpoons$ IFNA-IFNAR 2 Complex	$k1 \cdot S1 \cdot S2 - P/keq$
R3	M2	Cell Intracellular	Liver Interstitial	IFNA_R2_Complex + IFNAR1 $\rightleftharpoons$ Activated Receptor Complex	$k1 \cdot S1 \cdot S2 - P/keq$
R4	M3	Cell Intracellular	Liver Interstitial	Activated Receptor Complex $\rightleftharpoons$ [SOCS1] IFNAR1 + IFNAR2	$\frac{V \cdot S \cdot A}{(\mathrm{Kms}+S)(\mathrm{Ka}+A)}$
-	M4	-	Liver Interstitial	$\varnothing \longrightarrow$ IFNAR1	$rel\_exp\_out \times AF \times f\_o \times k\_t - S \times k\_t$
-	M5	-	Liver Interstitial	$\varnothing \longrightarrow$ IFNAR2	$rel\_exp\_out \times AF \times f\_o \times k\_t - S \times k\_t$
R5	M6	Cell Intracellular	Liver Intracellular	Activated Receptor Complex + STAT2c $\rightarrow$ Rec2	$k1 \cdot S$
R6	M7	Cell Intracellular	Liver Intracellular	Rec2 + STAT1c $\longrightarrow$ Rec21	$k1 \cdot S$
R7	M8	Cell Intracellular	Liver Intracellular	Rec21 + IRF9c $\longrightarrow$ ISGF−3c + Activated Receptor Complex	$k1 \cdot S$
R8	M9	Cell Intracellular	Liver Intracellular	$\varnothing \underset{\text{binding sites}}{\overset{\text{Occupied ISGF}-3n}{\rightleftharpoons}}$ mRNAc_SOCS	$k1 \cdot M$
R9	M10	Cell Intracellular	Liver Intracellular	mRNAc_SOCS $\longrightarrow \varnothing$	$k1 \cdot S$
R10	M11	Cell Intracellular	Liver Intracellular	$\varnothing \underset{\text{binding sites}}{\overset{\text{Occupied ISGF}-3n}{\rightleftharpoons}}$ mRNAc	$k1 \cdot M$
R11	M12	Cell Intracellular	Liver Intracellular	mRNAc $\longrightarrow \varnothing$	$k1 \cdot S$
R12	M13	Cell Intracellular	Liver Intracellular	$\varnothing \underset{\text{binding sites}}{\overset{\text{Occupied ISGF}-3n}{\rightleftharpoons}}$ mRNAc_Mx2	$k1 \cdot M$
R13	M14	Cell Intracellular	Liver Intracellular	mRNAc_Mx2 $\longrightarrow \varnothing$	$k1 \cdot S$
R14	M15	Cell Intracellular	Liver Intracellular	$\varnothing \overset{\text{mRNAc}}{\rightleftharpoons}$ IRF9c	$(k_{\text{const}} + k_{\text{act}})M - P \cdot IRF9_{\text{deg}}$
R15	M16	Cell Intracellular	Liver Intracellular	$\varnothing \overset{mRNAc\_SOCS}{\rightleftharpoons}$ SOCS 1	$k\_act \cdot M - K\_deg \cdot P$
R16	M17	Cell Intracellular	Liver Intracellular	$\varnothing \overset{mRNAc\_Mx2}{\rightleftharpoons}$ Mx2	$k\_act \cdot M - K\_deg \cdot P$
R17	M18	Exchange	Exchange	STAT1n $\rightleftharpoons$ STAT1c	$k1 \cdot S - P/keq$
R18	M19	Exchange	Exchange	STAT2n $\rightleftharpoons$ STAT2c	$k1 \cdot S - P/keq$
R19	M20	Exchange	Exchange	IRF9n $\rightleftharpoons$ IRF9c	$k1 \cdot S - P/keq$
R20	M21	Exchange	Exchange	ISGF-3c $\rightleftharpoons$ ISGF-3n	$k1 \cdot S$
R21	M22	Cell Nucleus	Liver Nucleus	Open ISGF-3n binding sites + ISGF-3n $\rightleftharpoons$ Occupied ISGF-3n binding sites	$k1 \cdot S1 \cdot S2 - P/keq$
R22	M23	Cell Nucleus	Liver Nucleus	Occupied ISGF-3n binding sites $\rightarrow$ STAT 1n + STAT 2n + IRF 9n + Open ISGF-3n binding sites	$k1 \cdot S$
R23	M24	Cell Nucleus	Liver Nucleus	IRF9n $\longrightarrow \varnothing$	$k1 \cdot S$

4.7 Discussion

In this chapter, a whole-body mouse PBPK/PD model for murine IFN-α injection is presented. By integrating a mouse hepatocyte model into a whole-body PBPK model, this would improve the understanding of risks and toxicity profile of potential drug candidates and compounds, as well as help reduce costs and animal experimentation. Such QSP model would enable more comprehensive simulations on dose-effect relationship between IFN-α injection and the response of the biomarker Mx2 protein in the future. Ultimately, the PBPK/PD model can quantitatively show the differences between preclinical knowledge of murine and human IFN-α subtypes. This would, in turn, support an in depth understanding of cross-species extrapolation and enable a quantitative understanding of the discrepancy between *in vitro* *in vivo* IFN-α doses.

In general, the lack of quantitative data is a problem in systems pharmacology. For many drugs, such as IFN-α, such data gets scantier as the dosage is commonly quantified in international units resulting to difficulties in quantification. However, the molar concentrations are crucial for mathematical modelling. As there is high variability in the different batches of IFN-α preparations, the conversion factors tend to differ in orders of magnitude. Moreover, the specific activity is not commonly reported in the literature, thus leading to strong uncertainty about the injected dose.

The rapid initial drop (monoexponential decay) of the *in vivo* murine IFN-α plasma concentration was explained by the current PBPK model. However, the model could not explain the data of injected murine IFN-α by Pulverer et al. [157]. This is potentially due to the short-time scale of the dataset (20 mins.) where it exhibits potential distribution phase. Thus, no conclusion could be drawn from this dataset. Type I interferons are reported to have species-selectivity, making it harder to interpret cross-species experiments. The PBPK model was able to shed some light on the differences between the pharmacokinetics of murine IFN-α 4 vs. human IFN-α 2 types, although the simulation could not distinclty describe the termination phase in the pharmacokinetics of human IFN-α 2. The model suggests that the inter-species variability seen in the differences in pharmacokinetics of the subtypes could be due to either unspecific binding of IFN-α to cell-surface receptors or plasma proteins. The measurements of unbound fraction of IFN-α (fu) could help to clarify this. Furthermore, there are various mouse and human IFN-α subtypes and further experiments on them could help in the understanding of which subtype could be used in cross-species experiments.

The mouse PBPK model is an effective tool to quantify and validate the tissue distribution of murine and human IFN-α in mouse as an organism. Using this validation analysis method, the pharmacokinetics and tissue distribution of IFN-α can be well studied in preclinical stage and can therefore effectively reduce the failure of IFN-α in the drug development process. Mouse is a very suitable organism to do tissue or organ distribution analysis of IFN-α and would also contribute to understanding the influence of the distribution on the observed dose-effect relationship.

In literature, the murine Mx2 promoter site is reported to have two putative ISRE binding sites and one IRF-E site, thus allowing for cooperativity [240]. In this work, constitutive luciferase activity has been used as an *in vitro* assays on primary mouse

hepatocytes for Mx2 expression. The mouse hepatocyte model was evaluated for cooperativity in the transcription kinetics and it has been noted that the mass action kinetics was able to describe the experimental data. Until now, the mouse hepatocyte model does not account for the constitutive activity of Mx2 baseline expression hence the initial Mx2 mRNA and protein concentrations were fixed to zero. However, baseline expression of Mx2 have been reported in the literature [241]. Kariko et al. [242] observed that the Mx2 endogenous expression can be caused by cellular stress response which triggers the IFN expression via the activation of the Toll like receptor 3. High expression of Mx protein is the key marker of antiviral resistance by the JAK/STAT pathway. Hence, the incorporation of the basal expression of the ISG would help improve insights into the endogenous activity of the signalling pathway. Most importantly, the model parameters are probable parameters as the compartments are assumed to be well stirred and diffusion processes are not considered in the model, as the diffusion processes are not the focus of this work.

From the experiments, the Mx2 dynamics over time for IFN stimulation is not well determined and hence would need to be repeated with more condensed measurements during the time course. The information on the time at which Mx2 achieves maximum response is missing and the current experiments do not explain whether the maximum response attained by Mx2 is sustained or whether it decreases with the later time-points. Lastly, the experiments on mouse cells for the molecules of the JAK/STAT pathway would be beneficial to add value to the current mouse hepatocyte model.

Commonly, in the *in vitro* assays, the volume of the medium is considerably larger than the volume of the seeded cells. Thus, the absolute amount of IFN-α is commonly higher than the number of receptors present at the cell surface. In such cases, where clearance is absent in *in vitro* assays, time resolved measurements of IFN-α concentration in the medium, in order to analyse if the concentration of IFN-α drops or stays constant over-time, would be most beneficial.

The current PBPK/PD models of human and mouse intentionally neglects the direct binding of IFN-α to IFNAR1 (Interferon alpha receptor 1). This choice was made based on the observation that only a small fraction of IFN-α binds to IFNAR1 due to its weaker binding constant for that receptor [185], [243]. Furthermore, the affinities of IFN-α to the individual receptor subunits have been reported but there is no information on the rate constants for the formation of the ternary complex.

Furthermore, the model could give insights on the influence of target mediated disposition of murine IFN-α concentrations in tissue and blood. Lastly, such a model could be employed in the future to analyse the impact of other biological effect of the trigger of murine IFN-α on the induction of immune response and inflammation hence understanding the tissue distribution of the drug in the light of other biological implications.

Chapter 5

Stochastic effects trigger intracellular responses in IFN-α signalling

5.1 Chapter summary

The work in this chapter is motivated by the response variability of the various induced ISGs by IFN-α stimulation on human hepatocytes. Here we examine the causes for variability between responding and non-responding cells in terms of IFN-α stimulation. We analyse the intra-cellular biochemical noise that leads to the decision of the responding / non-responding cells in an isogenic cell population. In this work, for the first time, we analyse this aspect by using a mechanistically detailed stochastic JAK/STAT pathway model. The model is calibrated to the single-cell time-lapse responses of ISGs, Mx2 and ISG56 to IFN-α stimulation using flow cytometry for Huh7.5 cells. Solving such detailed stochastic models can be time consuming and intensive, thus in order to identify the model parameters we used the recently developed algorithm by Dr. Luis Aguilera [1] [123] that fits the stochastic model to single-cell data. Luis and myself established the project aim, the collaboration and the model for this work.

In this chapter, I detail on establishment of the stochastic model of JAK/STAT pathway which is based on the knowledge of previously developed deterministic JAK/STAT models [114], [116]. I synopsize on the methodology of parameter estimation where the model was calibrated to quantitatively immunoblotted population data and single cell data produced by flow cytometry for various molecules in the pathway in response to IFN-α dose stimulation. The results of this work have been solely generated by Dr. Luis Aguilera and the basis of the text of the results and figures of this chapter has been mostly taken from Aguilera et al. 2018 (in preparation)[244]. Parts of the text of this chapter were originally written by Dr. Luis Aguilera, Prof. Dr. Ursula Kummer and myself. Figures used in this chapter are adapted from Aguilera et al. [244] and were originally produced by Dr. Luis Aguilera. The experimental data used in this chapter is detailed in chapter 2, subsection 2.2.5.

[1] Research group of Brian Munsky, Department of Chemical and Biological Engineering, Colorado State University, Fort Collins

5.2 Motivation and open questions

IFN-α signalling activates the first line of defence against viral infections. On the level of individual cells, the main function of this immune defence is to induce the cell-intrinsic anti-pathogenic response in infected and neighbouring cells so as to limit the spread of the infectious agents, specifically of viruses. Previous studies demonstrated that only a fraction of cells in a cell population produce IFN-α [81], [87], [121]. Both intrinsic and extrinsic noise were reasoned to be the source of this stochastic variability in the inter-cellular response [81], [124], [245], [246]. It was proposed that many functions are driven by biochemical noise within individual cells, e.g., cell fate decision or mRNA and protein abundances [247]. In case of IFN-α, neither the biochemical noise mechanism nor the function are understood. Furthermore, IFIT1 (sometimes also referred to as ISG56) and MxA have been gold standard mRNA/proteins which are expressed as part of the anti-viral response to interferon induction [66], [69], [248]. MxA is one of the most well-studied ISGs. It is the key anti-viral element induced by IFN-α and exerts its antiviral response during the replication cycle of diverse viral families that include *Orthomyxoviridae*, *Rhabdoviridae*, *Paramyxoviridae* among others [69]–[72]. On the other hand, IFIT1 was one of the first ISGs to be discovered and is the most prominent member of human response genes to viral stress. Both, MxA and ISG56 are strongly induced in response to IFN and various viruses [66]–[68]. However, the stochastic behaviour of MxA and IFIT1 gene induction remains a challenge as neither the mechanisms nor the function of intrinsic variability along the IFN-α activated JAK/STAT pathway are well understood.

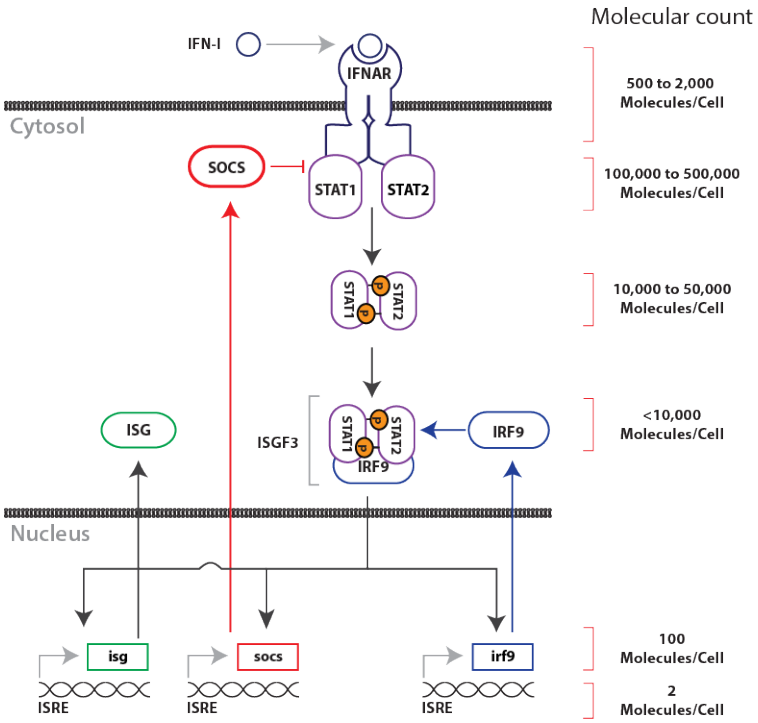

FIGURE 5.1: Molecular count of the JAK-STAT signalling pathway. The molecular count of some of the most relevant elements in the pathway is given at the right. A detailed list of the molecular count used in the model is given in Appendix D, Table D.1

Therefore, this work is motivated by the little explored impact of biochemical noise on the transduced JAK/STAT pathway responses of the induced antiviral ISGs: MxA and IFIT1. In order to have a detailed understanding on the stochastics of the JAK/STAT pathway induced responses, our collaborators from the groups of Marco Binder[2] and Ralf Bartenschlager[3] performed single-cell measurements of IFIT1 and MxA. The Huh7.5 cells expressing bacterial artificial chromosome (BACs) based fluorescent reporters for MxA and ISG56 were stimulated by IFN-α. Single cell data displaying IFIT1 and MxA expression differences in responding or non-responding cells was collected by FACS in a time-lapse experiment. Complementary to the noise assays conducted by our collaborators, we constructed a mechanistic stochastic model and calibrated it to the data for MxA and IFIT1. This allowed us to investigate the influence of intrinsic and extrinsic noise in the JAK/STAT pathway at single cell resolution. The results of this work show that the effects of noise are particularly strong at the receptor level, during the transcription of ISGs and during the formation of the transcription factor ISGF3. Additionally, we concluded that the JAK-STAT signalling pathway is a robust system that can filter extrinsic fluctuations.

5.3 Stochastic model of JAK/STAT signalling upon IFN-α stimulation

To investigate the single-cell dynamic properties of IFN-α signalling, we developed a mathematical model of the known key components, feedback responses and constitutive regulatory mechanism. The model was developed from scratch to describe the single-cell dynamics but was based on previously published deterministic models [114]–[117]. Since stochastic models are computationally expensive to solve, there are constant endeavours on the implementation of new methods to fit single cell data [123], [249], [250].

For the development of this model, the following assumptions were made:

1. The model comprises one compartment representing the cytosol and the nucleus together.
2. The receptor mechanism is irreversible. At this point, the model can only describe a single stimulation without any reactivation of unbound receptors.
3. The variables representing gene activity, (e.g., *socs* / *I_socs*) start fully activated. The promoters can be simulated assuming a two state model.
4. The model does not start in steady state.

In the following sub-section I will describe the model structure and establishment in details.

5.3.1 Mathematical model overview

The following conventions are used for the names of the species in the model:

1. Variables referring to mRNA are denoted by *m* prefix.

[2]Research Group "Dynamics of early viral infection and the innate antiviral response", Division Virus-associated carcinogenesis, German Cancer Research Center (DKFZ), Heidelberg, Germany.

[3]Department of Infectious Diseases, Molecular Virology, University of Heidelberg, Heidelberg, Germany.

2. Variables addressing the phosphorylated state use *p* prefix.

3. Gene promoters are represented by the gene's name in lowercase.

The developed model consists of 28 species and 40 reactions (reactions (**M1**) to (**M40**)). It comprises known key components and feedback mechanisms. The binding between free IFN-*α* and the IFNAR sub-unit 2 (*R2*) to form a pre-active complex (*RC*) (**M1**) was modelled. The pre-active complex bound to the IFNAR sub-unit 1 (*R1*) to form the active complex (*AR*) (**M2**). The activated IFNARs relay the signal inside the cytoplasm by phosphorylating *STAT*1 (**M3**) and *STAT*2 (**M4**). The phosphorylated STATs form the activated heterodimer *STAT1-STAT2* (**M6**). The binding of the hetero-dimer to IRF9 to form ISGF3 (**M7**) was modelled. Subsequently, ISGF3 binding to free DNA binding sites (ISRE) to induce transcriptional activity (**M10-M17**) was modelled in the same compartment. The ISGF3-DNA complex leads to the transcription of the mRNA for IRF9, MxA, ISG56 and SOCS (**M18-M21**). The transcribed mRNAs are translated to: IRF9 as a positive feedback (**M22**), SOCS (**M23**) as a negative feedback given by the SOCS1 degradation of active receptors (**M5**), MxA and ISG56 (**M24 & M25**). Degradation of intermediary elements, such as cytoplasmic mRNAs and cytoplasmic proteins was considered (**M26-M40**). A graphical representation of the interaction between species in the model is given in Fig 5.2 and the model reactions are described in table 5.1.

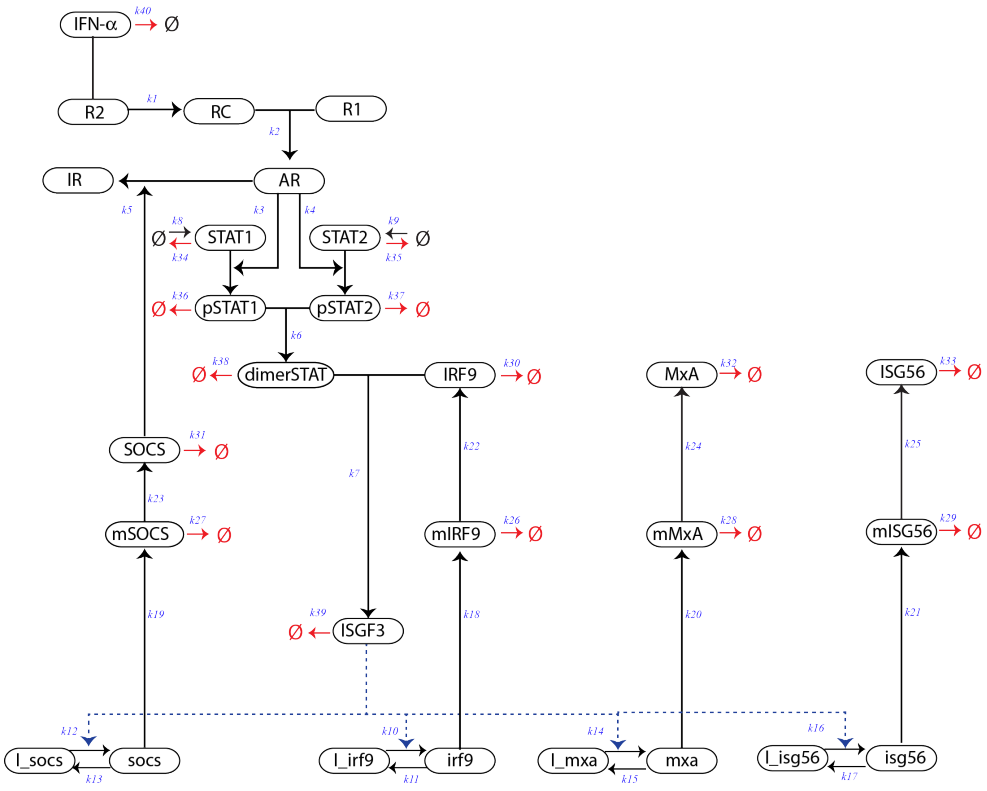

FIGURE 5.2: Figure adapted from Aguilera et al. [244]: Schematic representation of the mechanistically detailed JAK/STAT pathway. The model reactions are denoted by the variables in blue. The model describes the activation of the JAK-STAT signalling pathway by IFN-α. Consequently, phosphorylation of STAT proteins cause a dimerisation of the same along with the formation of the ISGF3 complex by binding to IRF9. Finally, the promoters of the ISGs are activated by ISGF3. A positive feedback loop is exerted by IRF9. SOCS inactivates the receptors, thus exerting a negative feedback on the pathway. In the figure, arrows represent the reactions described in table 5.1.

TABLE 5.1: The reactions following an IFN-α stimulation in the intracellular JAK/STAT pathway for the stochastic model is detailed in this table. The column # describes the reaction number followed by the column describing the reaction and the kinetic rate law used to describe the kinetics of the model reactions.

#	Reaction	Kinetic rate law
M1	$IFN + R2 \rightarrow RC$	$k_1 \cdot S1 \cdot S2$
M2	$RC + R1 \rightarrow AR$	$k_2 \cdot S1 \cdot S2$
M3	$AR + STAT1 \rightarrow pSTAT1 + AR$	$k_3 \cdot S1 \cdot S2$
M4	$AR + STAT2 \rightarrow pSTAT2 + AR$	$k_4 \cdot S1 \cdot S2$
M5	$AR + SOCS \rightarrow IR + SOCS$	$k_5 \cdot S1 \cdot S2$
M6	$pSTAT1 + pSTAT2 \rightarrow dimerSTAT$	$k_6 \cdot S1 \cdot S2$
M7	$dimerSTAT + IRF9 \rightarrow ISGF3$	$k_7 \cdot S1 \cdot S2$
M8	$\varnothing \rightarrow STAT1$	k_8
M9	$\varnothing \rightarrow STAT2$	k_9
M10	$I\_irf9 + ISGF3 \rightarrow irf9 + ISGF3$	$k_{10} \cdot S1 \cdot S2$
M11	$irf9 \rightarrow I\_irf9$	$k_{11} \cdot S1$
M12	$I\_socs + ISGF3 \rightarrow socs + ISGF3$	$k_{12} \cdot S1 \cdot S2$
M13	$socs \rightarrow I\_socs$	$k_{13} \cdot S1$
M14	$I\_mxa + ISGF3 \rightarrow mxa + ISGF3$	$k_{14} \cdot S1 \cdot S2$
M15	$mxa \rightarrow I\_mxa$	$k_{15} \cdot S1$
M16	$I\_isg56 + ISGF3 \rightarrow isg56 + ISGF3$	$k_{16} \cdot S1 \cdot S2$
M17	$isg56 \rightarrow I\_isg56$	$k_{17} \cdot S1$
M18	$irf9 \rightarrow irf9 + mIRF9$	$k_{18} \cdot S1$
M19	$socs \rightarrow socs + mSOCS$	$k_{19} \cdot S1$
M20	$mxa \rightarrow mxa + mMXA$	$k_{20} \cdot S1$
M21	$isg56 \rightarrow isg56 + mISG56$	$k_{21} \cdot S1$
M22	$mIRF9 \rightarrow mIRF9 + IRF9$	$k_{22} \cdot S1$
M23	$mSOCS \rightarrow mSOCS + SOCS$	$k_{23} \cdot S1$
M24	$mMXA \rightarrow mMXA + MXA$	$k_{24} \cdot S1$
M25	$mISG56 \rightarrow mISG56 + ISG56$	$k_{25} \cdot S1$
M26	$mIRF9 \rightarrow \varnothing$	$k_{26} \cdot S1$
M27	$mSOCS \rightarrow \varnothing$	$k_{27} \cdot S1$
M28	$mMXA \rightarrow \varnothing$	$k_{28} \cdot S1$
M29	$mISG56 \rightarrow \varnothing$	$k_{29} \cdot S1$
M30	$IRF9 \rightarrow \varnothing$	$k_{30} \cdot S1$
M31	$SOCS \rightarrow \varnothing$	$k_{31} \cdot S1$
M32	$MXA \rightarrow \varnothing$	$k_{32} \cdot S1$
M33	$ISG56 \rightarrow \varnothing$	$k_{33} \cdot S1$
M34	$STAT1 \rightarrow \varnothing$	$k_{34} \cdot S1$
M35	$STAT2 \rightarrow \varnothing$	$k_{35} \cdot S1$
M36	$pSTAT1 \rightarrow \varnothing$	$k_{36} \cdot S1$
M37	$pSTAT2 \rightarrow \varnothing$	$k_{37} \cdot S1$
M38	$dimerSTAT \rightarrow \varnothing$	$k_{38} \cdot S1$
M39	$ISGF3 \rightarrow \varnothing$	$k_{39} \cdot S1$
M40	$IFN \rightarrow \varnothing$	$k_{40} \cdot S1$

Reactions and rate laws All reactions in the model are described by mass action kinetics 5.1.

$$v_i = k_i * [Substrate1] * [Substrate2] \tag{5.1}$$

Here the velocity of the reaction is determined by k_i and the transitional concentrations of the Substrates are represented by *[Substrate1]* and *[Substrate2]*.

5.3.2 Calculations for the model

Converting IFN-α units: From IU/m to molecules/cell Similar to Chapter 3, subsection 3.4.2, the molecules/ cell were calculated for the stochastic model.

The model parameters were estimated based on data from the experiments of Bolen et al., Maiwald et al. and Bauhofer et al. [82], [116], [161]. In the experimental data, IFN-α stimulus (IFN_{exp}) activated the signalling pathway. Doses of IFN_{exp} ranged from 10 IU/ml to 500 IU/ml (1×10^4 IU/L to 5×10^5 IU/L). To map the model's variable IFN to IFN_{exp}, I transformed the IFN doses (IU/L) to an effective molecular count (molecules/cell).

IFN-α doses (IU/L) were converted to molar concentration (M):

$$IFN_{exp}(M) = \Big(IFN_{exp}(IU/L)/IFN_{sa}(IU/g)\Big)/IFN_w(g/mol), \tag{5.2}$$

where, IFN_{sa} is the IFN-α specific activity. $IFN_{sa} = 1 \times 10^9$ IU/g (R&D Systems, Minneapolis, MN, USA). IFN_w is the IFN molecular weight. $IFN_w = 1924.0$ (g/mol).

Subsequently, I converted IFN_{exp}(M) to total number of IFN-α molecules in the medium (molecules/l), that is:

$$IFN_{exp}(molecules/l) = \Big(IFN_{exp}(mol/l)/V_M(l)\Big) \cdot N_A(molecules/mol), \tag{5.3}$$

where N_A is the Avogrado's constant, $N_A = 6.022 \times 10^{23}(Molecules/mol)$. V_M is the total volume in the medium, $V_M = 2 \times 10^{-3}$ L.

Finally, from the IFN-α molecules in the medium I calculated the effective number of molecules that interact with each cell in the culture. To achieve this unit conversion I assumed that the IFN_{exp} is homogeneously distributed in the cell culture and every cell receives a small percentage of the total IFN-α molecules. This assumption is based on the dilution of the IFN_{exp} in the medium and their low probability of encounter with the cell receptors. This was accounted by the parameter: IFN-α availability A_v = 1%. The molecules of IFN-α available per cell is:

$$IFN_{exp}(molecules/cell) = \Big(IFN_{exp}(molecules/l)/N_C(cells/l)\Big) \times A_v, \tag{5.4}$$

where N_C is the number of cells in the culture volume (N_C = 1.2×10^5 cells/l).

TABLE 5.2: From IFN-α (IU/ml) to molecules/cell

IFN (IU/ml)	M	molecules/cell
500	2.6×10^{-7}	6.52×10^{12}
100	5.19×10^{-8}	1.3×10^{12}
10	5.19×10^{-9}	1.3×10^{11}

As mentioned previously in Chapter 3, subsection 3.4.2 can be affected by different factors including: the IFN-α specific activity that can vary not only depend on the reagent supplier, but also on storage and manipulation.

Promoter analysis for MxA and IFIT1 MxA promoter is reported to contain two functional ISRE leading to cooperative binding of ISGF3 to the DNA sites [239]. Having a cooperative promoter activation is commonly associated with differential gene regulation which determines the systems decision making [247].

Most cell types do not express detectable levels of IFIT1 transcripts in the absence of IFN-α stimuli. IRF3 is known to transactivate IFIT1 [251]. Two ISRE consensus sites are present in the promoter of IFIT1, at positions -92 to -104 (ISRE I) and positions -105 to -117 (ISRE II) [252].

The MxA and IFIT1 promoter sequence was analysed using ENCODE and Jasper and is found in Appendix D, subsection D.1.1.

The half life of the proteins and mRNAc for the model were fitted in the range of the biological values found in the literature as shown in Appendix D, Table D.1.

5.3.3 Parameter estimation

Mapping model variables to experimental data The data implemented for the fitting of the model was not in absolute concentrations. Scaling factors were added to the model to represent the quantitative immunoblotting data and the flow cytometry data.

Time course data The quantitative immunoblotting data was published in Maiwald et al. [116]. The data described the temporal dynamics of different elements of the JAK-STAT signalling pathway. The dynamics of phosphorylated JAK1, pSTAT1 and nuclear IRF9 were measured in Huh7.5 cells after stimulation with 500 UI/ml of IFN-α for a total time of 180 min (total 8 measurements, an average of two replicates). The experimental measurements of phosphorylated JAK1 ($pJAK1^{\dagger}$) were mapped with active receptor (AR) in the model as follows:

$$pJAK1^{\dagger}(t_i) = \varphi_1 * AR(t_i), \tag{5.5}$$

where φ_1 is a scaling factor.

The experiment used the phosphorylation-state specific anitbodies to measure the dynamics of phosphorylation of STAT1 in time. The experimental measurements of cytoplasmic phosphorylated STAT1 ($pSTAT1^{\dagger}$) were mapped to pSTAT1, dimerSTAT and ISGF3 molecules because they collectively contain phosphorylated version of the STAT1 and were not differentiated experimentally. The assignment in the model is as follows:

$$pSTAT1^{\dagger}(t_i) = \varphi_2 * \Big(pSTAT1(t_i) + dimerSTAT(t_i) + IRF3(t_i)\Big), \tag{5.6}$$

where φ_2 is a scaling factor.

The experimental measurements of nuclear IRF9 ($IRF9^{\dagger}$) were mapped to ISGF3 and nuclear IRF9 molecule because the experiment did not differentiate between individual IRF9 molecule or the IRF9 bound to ISGF3. This was described in the model as follows:

$$IRF9^{\dagger}(t_i) = \varphi_3 * \Big(ISGF3(t_i) + IRF9(t_i)\Big), \tag{5.7}$$

where φ_3 is a scaling factor.

Flow cytometry data The data described expression of MxA and ISG56 after IFN-α stimulation in a population of Huh7.5 cells. Huh7.5 cell culture was treated with various concentrations of IFN-α (in the range of 10 to 1250 UI/ml) and single cell FACS measurements of MxA and IFIT1 were performed (see data in Appendix D, section D.2). For the purpose of explaination, I selected the treatment with 250 UI/ml of IFN-α on the Huh7.5 cells. The measurements of MxA and IFIT1 were reported as fluorescence intensity and does not give information on the absolute concentrations, the scaling factor of the two proteins were implemented in the model: The experimental measurements of MxA ($MXA^{\dagger}$) were mapped to MXA in the model as follows:

$$MXA^{\dagger}(t_i) = \varphi_4 * MXA(t_i), \tag{5.8}$$

where φ_4 is a scaling factor.

The experimental measurements of IFIT1 ($ISG56^{\dagger}$) were mapped to $ISG56$ in the model as follows:

$$ISG56^{\dagger}(t_i) = \varphi_5 * ISG56(t_i), \tag{5.9}$$

where φ_5 is a scaling factor.

Fitting the model *The work in the following sections were devised and executed by Dr. Luis Aguilera.*

The model was fitted to two different datasets obtained from different experimental procedures and on different time-scales. The quantitative immunoblotting data was implemented from the publication Maiwald et al. [116]. The flow cytometry dataset was analysed in MATLAB using the function *FCS datareader* (Appendix D, Figures D.1, D.2 and Figure D.3). The stochastic model was calibrated to datasets by implementing the parameter estimation methodology developed by Dr. Luis Aguilera consisted in the fitting of the stochastic version of the model with experimental distributions [123]. In a nutshell, given the distinct resolutions and time-scales of the datasets, the fitting strategy was divided into two steps:

1. A deterministic model was parameterised to the cell population data (time courses and dose-response data) obtained by quantitative immunoblotting. The Genetic algorithm was executed to obtain the parameter-set.

2. Once the parameterisation fulfilling the deterministic regime was found, the method fitted the stochastic version of the model to experimental FACS distributions of MxA and IFIT1. The Kolmogorov-Smirnov (KS) distances of the cumulative density function (CDF) were calculated with respect to the experimental data distributions. This was based on the Monte Carlo simulations of the single cell experimental data. Hence, the final parameter-set of the stochastic model was obtained.

A diagram of the parameter estimation strategy is given in Figure 5.3 A.

Furthermore, the parameter space was narrowed down by parameter values determined in the literature (Appendix D, Table D.1). Notice that in Figure 5.3 B, with this algorithm Luis was able to fit the temporal response of the IFN system and the stochastic dynamics in the final ISG expression of MxA and IFIT1.

5.4 Results

In this section I recap the results that were generated by Dr. Luis Aguilera to lay insight into the findings of this work.

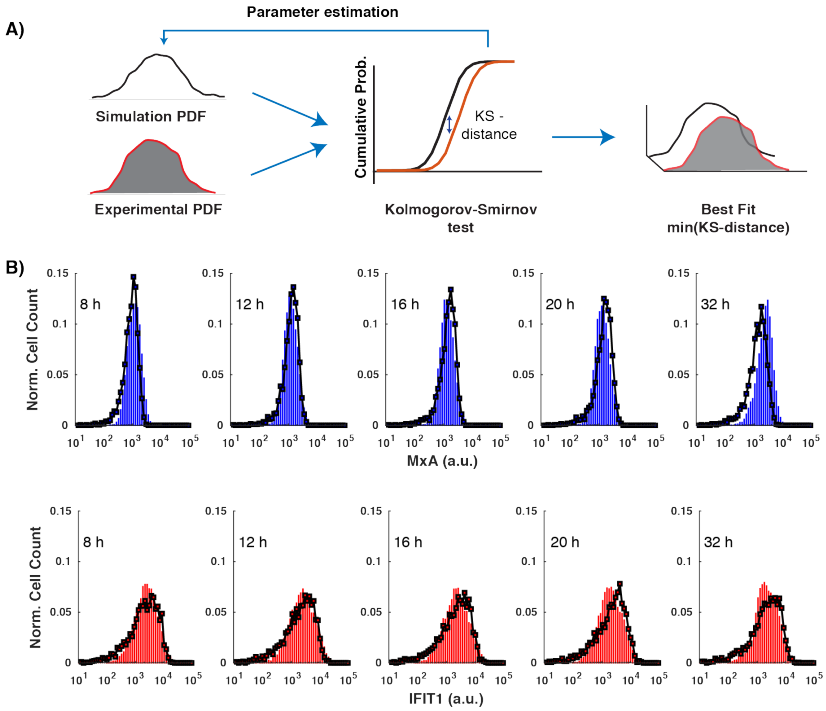

FIGURE 5.3: In the above figure the parameter estimation methodology as published by Aguilera et al. [123] is illustrated. The parameter estimation strategy involved A) First, solving the system for a parameterisation in the deterministic regime. The genetic algorithm was executed to caliberate the model against the time course data dose-response data produced by quantitative immunoblotting as published in Maiwald et al. [116]. Once the deterministic solution was achieved, the obtained parameter-set was implemented to calibrate the stochastic model against flow cytometry data. B) Temporal distributions fitted to the FACS dataset (solid colour distributions, blue for MxA and red for IFIT1). 1000 stochastic simulations of the temporal distribution are plotted as black lines. The y-axis displays the normalised cell-count and the x-axis displays the fluorescence intensities in arbitrary units (a.u.) for the expression of MxA and IFIT1 proteins. Figure adapted from Aguilera et al. [244].

The model was simulated [4] using the Gillespie algorithm which is one of the stochastic simulation algorithm (SSA). To account for the intrinsic noise, the model was solved using Gillespie algorithm as implemented COPASI 4.21. The extrinsic noise was simulated as suggested by Shahrezaei et al. [173] where the extrinsic noise is introduced on the SSA as a time varying parameter and can simultaneously execute on many parameters of the model. This work focuses on introduction of extrinsic noise only on the molecular count of the molecules in the pathway where the noise is normally distributed over the following three values of σ: 0, 0.3, 0.6.

5.4.1 Heterogeneity in the response of MxA and IFIT1 to IFN-α

Previous studies [66], [253], [254] established the interference of MxA and IFIT1 proteins in the viral infection, specifically *Parainfluenza* virus type 5. The single cell experiments executed by our collaborators (see chapter 2) successfully measured the distribution of the response of

[4]The mathematical calculation of the system dynamics over time

MxA and IFIT1 in the Huh7.5 cell population, thereby capturing the cell-to-cell variability (Appendix D, Figures D.1 & D.2). The experiments exhibit unimodal distributions[5] and sustained responses of MxA and IFIT1. The shift in the unimodal distributions over time accounted for the heterogeneity in the response (Figure 5.4). Here, the responding cells are in the **ON** section of the curves in Figures 5.4 B & C while the non-responding cells are in the **OFF** section. As the time elapses after the IFN-α stimulation, the fluorescence intensities of the response biomarkers, MxA and IFIT1 increases, exhibiting the increase in responding cell population. This observation is in contrast to the previous publication based on IRF7 as the reporter ISG [81], where an all-or-none response (bimodal behaviour[6]) was observed, thus separating the population into responding and non-responding cells. However, in our study we did not only use different reporter ISGs (IFIT1 and MxA), but we also we also used data from a different cell line (human hepatic cells instead of mouse fibroblastoid cells). This suggests that induction of the ISGs is cell-type specific [255], [256].

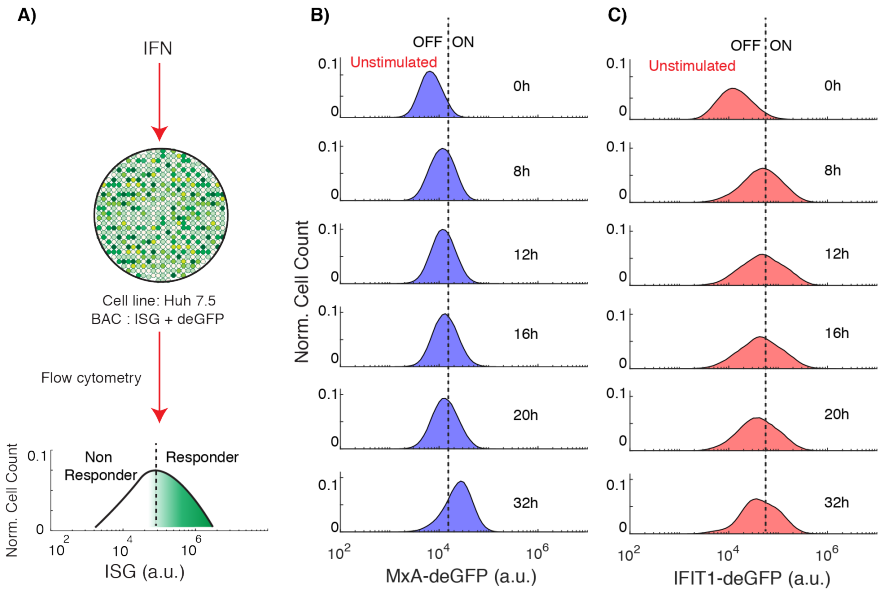

FIGURE 5.4: Induction of response ISGs (MxA and IFIT1) after stimulation of Huh7.5 cells with different dosages of IFN-α. A) schematic representation of the experimental set-up, a threshold is defined on the basis of fluorescence intensities to differentiate the cells as responding or non-responding in a population. B) Distributions of MxA expression at different time points after IFN-α stimulation in the Huh7.5 cells. C) Distributions of IFIT1 expression at different time points after IFN-α stimulation in the Huh7.5 cells. Data collected via FACS. Figure adapted from Aguilera et al. [244].

Furthermore, our experiments tested for temporal dose-response of MxA and IFIT1 to different doses of IFN-α (10, 50, 250, 1250 UI/mL) at time points 8, 12, 16, 20 and 32 hours after respective dose induction. The measurements exhibited that 16 hrs post-induction, the cells shift to higher intensities of signal response for MxA (see Appendix D, Figure D.1) and 12 hrs post induction for IFIT1 (see Appendix D, Figure D.2). Moreover, the cells maintained the graded increase in response of MxA and IFIT1 as the time elapsed for all IFN-α doses. The

[5]Continuum of expression of proteins within a population.

[6]Two distinct populations exhibiting expression of proteins as well as no expression of proteins within a population.

time dependence of the MxA and IFIT1 response were further observed by plotting the average fluorescence intensities (a.k.a mean fluorescence intensities (MFI). (See Appendix D, Figure D.3). In conclusion, the experiments indicate dose-dependent responses of the reporting ISGs which shifts the cell population towards an increased response as the time elapses, after IFN-α stimuli.

5.4.2 Effect of noise on the induced MxA and IFIT1 responses

Effect of intrinsic noise on the pathway 1,000 repetitions of the simulations were run for 32 hours to gain a deeper understanding on the response heterogeneity landscape (of MxA and IFIT1 respectively) in the population of trajectories (representing 1000 cells in a cell population of 1000). The resulting simulation indicated differences in induced temporal responses. For example, proteins activated after the association of IFN-α to the receptors showed fast and transient dynamics, whereas the feedback proteins (positive feedback via IRF9 and negative via SOCS) displayed slower and sustained dynamics. The simulation result indicated that the pathway is sensitive to the IFN-α trigger but the feedback loops help to sustain the pathway response for longer periods of time. Hence, keeping the pathway robust to the intrinsic noise as seen in Figure 5.5 B. We observed that low concentrations of specific species in the signalling pathway, especially, the number of phosphorylated STAT dimers and IRF9 proteins introduce strong variability in the transient dynamics of ISGF3. This suggests that the fate of the response may be determined by bottlenecks in the pathway when the receptors are not recycled.

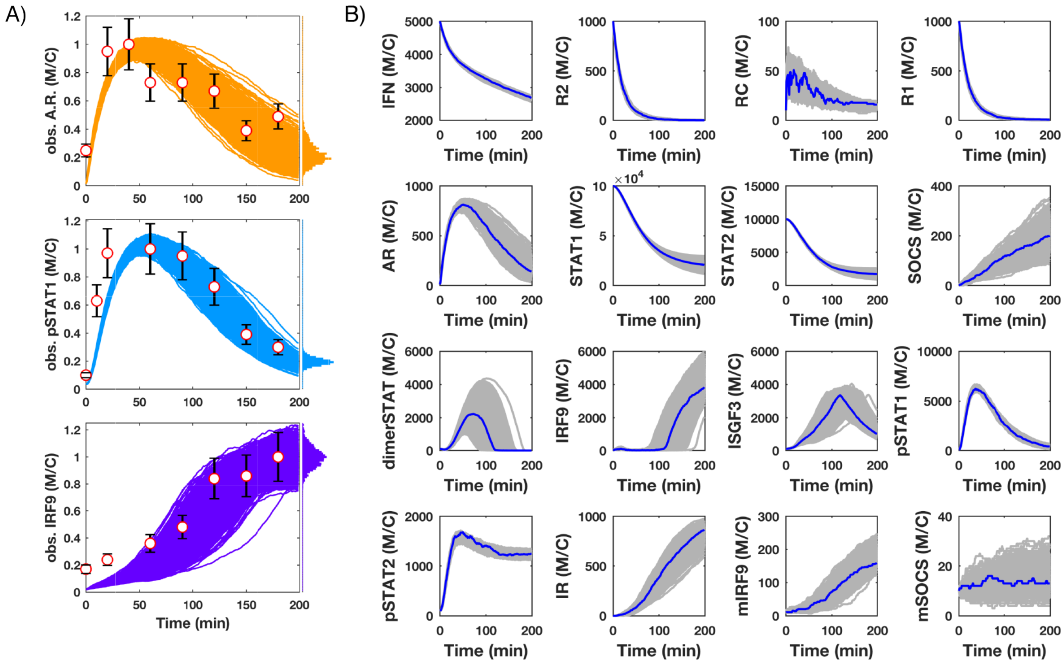

FIGURE 5.5: The temporal dynamics of the model and the cell population distribution are represented in plot. A) Cell population data (obtained by quantitative immunoblotting) describing the temporal dynamics of JAK1, pSTAT1 and nuclear IRF9 as published in Maiwald et al. [116]. Measurement error of 18 % is represented in the figure as error bars. The measurements were done on Huh 7 cells after stimulating them with a dose of 500 U/ml of IFN-α. The induced temporal response was measured using quantitative immunoblotting for 180 mins. Each solid line represents the model trajectory, a total of 1,000 stochastic simulations representing single cells. The histogram on the right side of plot represents the final trajectory distribution of the population. B) The plots represent single stochastic trajectory plotted in grey and the single blue line is the mean of the stochastic trajectory. The plots describe the temporal dynamics of all the simulated species in the induced JAK/STAT signalling pathway. The unit of the y-axis is molecules per cell (M/C). Figure adapted from Aguilera et al. [244].

Effect of extrinsic noise on the pathway Extrinsic fluctuations can originate from different external environmental sources. For example, during cell cycle or inheritance of variable copy numbers of the proteins in different cells during cell division [257]. In this work, we explored the effect of extrinsic variability on the pathway by introducing the noise as the variability in the copy number. Hence, the initial molecular number of the species was varied by introducing random sampling using normal distributions $\mathcal{N}(\mu, \sigma^2)$ with values for μ (Appendix D, Table D.2 and one of three values of σ: 0, 0.3, 0.6. By introducing the σ as noise, we explored the consequence of increased extrinsic noise on the molecule number of the system (Figure 5.6

A). Thus we were able to quantify the variability in the JAK/STAT signalling pathway by performing a variability analysis over initial molecule numbers. This was achieved by calculating the coefficient of variation (ratio of the standard deviation, σ_s to the mean molecule number, where the subindex s represents the species in the pathway). Considering the model can only describe a single stimulation without any reactivation of unbound receptors, this analysis suggests that the pathway shows minimal variability in the cytoplasmic components except for ISGF3 complex. Contrasting that, the model results depict strong effect of noise in the nucleus and on the cell membrane (Figure 5.6 B right column). This is an obvious observation, as the ligand-receptor activation step is governed by complete activation of the receptors thus resulting to saturated activation and no further signal transfer. This shows that the extrinsic noise governs the local dynamics of the cellular response (on molecules present in certain sections of the pathway) but the global response (the induced response to IFN-α trigger) is rather robust to extrinsic noise. A quantification of this is observed in Figures 5.6 C and D where the KS-distance was measured between distributions for MxA and IFIT1 under multiple values of extrinsic variability at different time points. The model results depicts the JAK/STAT pathway is affected by extrinsic noise at early time points (1 and 16 hours) however, the control of extrinsic noise is lost on the pathway at later time point (32 hours).

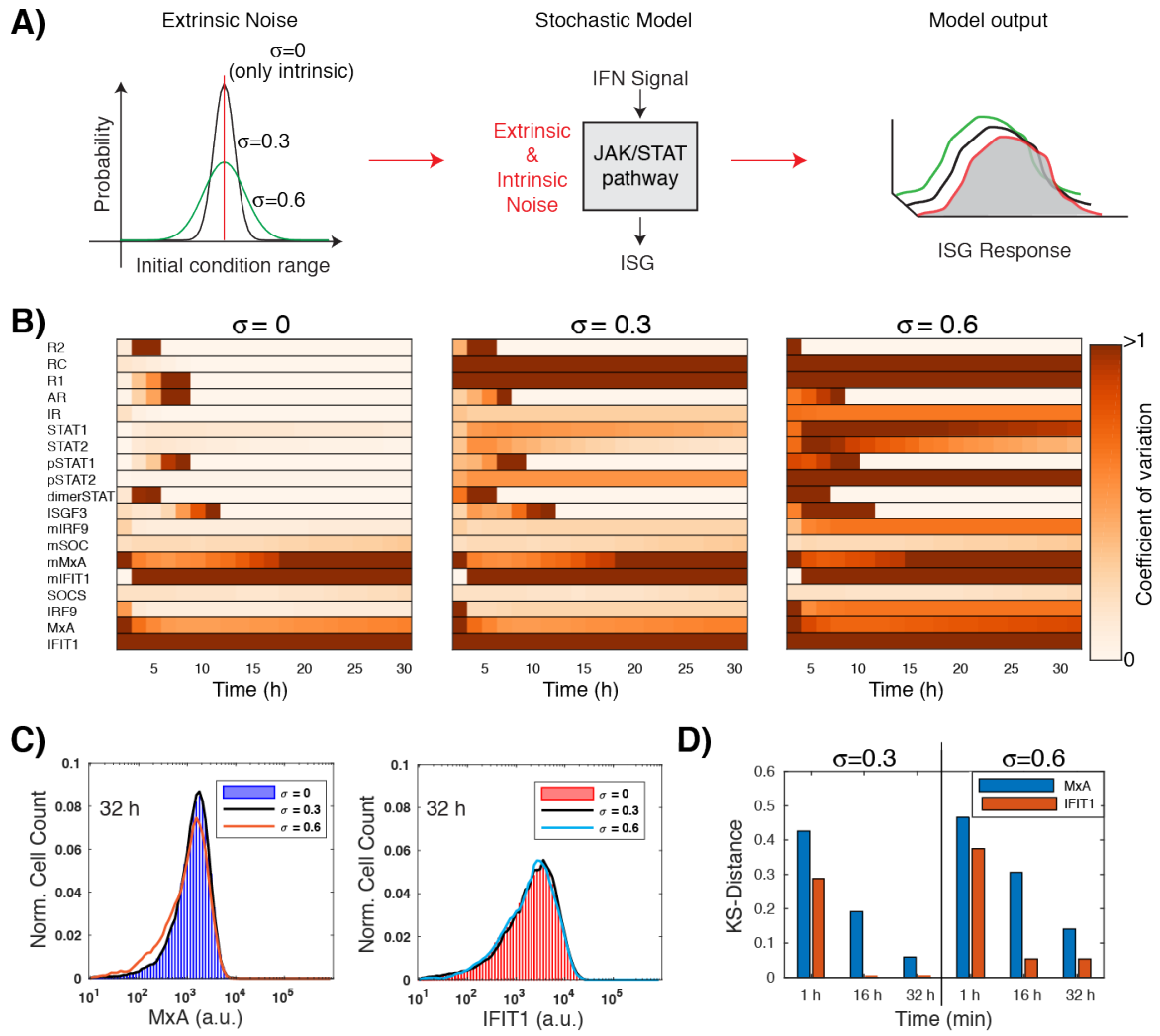

FIGURE 5.6: This figure recaps the introduction of biochemical noise in the JAK/-STAT pathway. A) Introduction of extrinisc noise in the system as the variability in the initial copy number of the molecules of the pathway. Wider distribution or larger σ_s: 0, 0.3 and 0.6 were implemented to increase noise in the system. The control, with $\sigma_s = 0$, only intrinsic noise accounts for variability. B) The variability of the JAK/STAT pathway was measured at different time points and under different conditions of extrinsic noise (σ_s at the top of the panel) on the initial copy number of the species in the pathway. The colour bar represents the coefficient of variation between 0 to 1, the darker the colour, the higher the variability. C) Stochastic simulation of MxA and IFIT1 expression after 32 hours of induction with IFN-α. Note that the perturbations with extrinsic noise are also simulated in the distribution. D) The distribution of MxA and IFIT1 expression at different time points of the simulation to compare the strengths of intrinsic vs. the extrinsic noise using Kolmogorov-Smirnov distance. Figure adapted from Aguilera et al. [244].

5.5 Discussion

In the last two decades, many efforts have been made to increase the understanding of the JAK/STAT signalling pathway that is triggered by IFN-α induction. With regards to biochemical models, models describing the deterministic dynamics in cell populations already exist [114]–[117]. On the single-cell side, stochastic models are slowly being explored to understand how the analogue signal of IFN-α leads to cell specific decisions and variability in the molecule reaction processes [121], [125]. Such variability in decision making arises from noise[7] (intrinsic and extrinsic). Noise is a governing factor in cellular processes - almost all pathways are impacted by noise. Such pathways have often evolved with a strong robustness against the effect of noise in order to react to stress or infection. The lack of stochastic models describing the IFN-α system can be attributed to the scarcity of single cell data and efficient methods to analyse and make use of this data. Promising high-throughput techniques to investigate those mechanisms are flow cytometry [258], microarray analysis[259] and single molecule microscopy [260], which are increasingly being used in biomedical research to characterise infectious diseases and to set therapeutic regimes. These techniques successfully capture the intrinsic variability in the IFN-α responses by measuring the RNA or protein abundance in single cells and the distribution of those molecules in cell populations. On the other hand, incorporating single cell data and stochastic modelling is still a challenging task.

In the presented work, we used the high-throughput technique of FACS to examine the temporal (for 32 hours) stochasticity of MxA and IFIT1 as the response biomarker after stimulation of Huh7.5 cell-line by IFN-α. Simultaneously, we developed a detailed mathematical model and calibrated it to the deterministic time course data of pJAK, pSTAT and SOCS as well as single cell FACS data for MxA and IFIT1 in order to analyse the effect of noise on this system. The novelty of this work is that the model is stochastic, mechanistic and incorporates the major feedback system for a graded response that evolves over a long time span. Our model differs from the other efforts which are made for the mechanistic stochastic model [125] by not following the ISGs that induce an *all-or-nothing* response to the antiviral state. MxA and IFIT1 do not have any enzymatic control on the JAK/STAT pathway itself (unlike IRF1, IRF3, IRF7 and IRF9 which also act as transcriptional factors for the trigger of antiviral response). Thus, we were able to establish graded (unimodal) temporal dynamics of MxA and IFIT1. Therefore, this work shows a clear contrast to the reports based on single cell data for various IRFs, where *all-or-none* response is commonly observed in the cell population [81], [125]. In our understanding, this difference in response arises from two aspects:

1. The architecture of the ISG promoters. For example, the IRF7 promoter contains two different transcriptional binding sites (ISRE and IRF-E), which can be activated not only by ISGF3 but also by IRF7 dimer itself (thus applying a positive feedback to its own production and hence the bimodality) [81]. Both MxA and IFIT1 do not possess any enzymatic activity [67]. The lack of the co-operative behaviour explains the observed graded response [202].

2. Cell-type specific and dose-dependent induction patterns of the MxA and IFIT1. Given the simple architecture of their transcriptional sites (only ISREs), examples of their dose-response expression being very similar in different individuals have been observed [261], [262]. This suggests that the response to IFN-α, especially of MxA and IFIT1, is robust. This explains the graded response that were consistently obtained for all IFN-α doses at different time points.

[7] Random variability that arises in the molecule numbers per cell.

This result is consistent with previous reports for MxA [83]. Higher organisms with intracellular signalling may benefit from such a robustness to be able to sustain signal propagation and shape the anti-viral response in the cell populations.

Model limitations and future work Developing mathematical models to represent a biological system is a subjective task and often depends on the question one needs to ask [263]. In this work, we have focused on implementing the physiological molecule numbers and the well-known mechanistic details which were described in previous works. However, important aspects and intricacies of the signalling network were not considered in the evaluation of the model. The promoters in this model were simulated assuming a two state model. More importantly, the overall idea in the model is that the activation of the pathway (dynamically) not only increases the switching between states, but also the time the variable is in the ON state. The same holds true for some activated compounds like pSTATs, STAT dimer and the transcription factor where the concentrations of the phosphorylated forms are non-zero even without IFN-α stimulation [116], [264], hence the model implements some "basal level" of protein activity. One important mechanistic detail that our model does not describe is receptor recycling, which means the model can only describe a single stimulation without any reactivation of unbound receptors as the receptor activation is irreversible.

Chapter 6

General discussion and concluding remarks

6.1 Chapter summary

Throughout this dissertation, both *in vitro* hepatocyte data and *in vivo* data for mice and humans have been extensively integrated, modelled and analysed, including the response data of the ISGs of the activated JAK/STAT pathway.

In this chapter, I would like to briefly bring together some of the key observations drawn from the work described in the different chapters of my dissertation, modelling the response of the JAK/STAT pathway to IFN-α. I will focus on the effects of dosage at the whole-body level, including insights into the datasets as well as the implications of the use of *in vitro* assays to help develop PBPK/PD models. The coupled PBPK/PD models will then provide insight into the iterative experimental design of the *in vitro* assays and animal experiments. Finally, I conclude with possible avenues and outlook for future work in investigating these important points.

Interferons are important components of the natural defence system found in mammals. IFN-α was reported as an antiviral agent 40 years ago [1] but more than 25 years, since its first clinical use, its potential as a drug for different ailments is still largely unexplored. In the past 20 years, IFN-α has been routinely used in treatment against HCV. In chronic HCV cases, the treatment has been shown to be effective in eradicating viral markers in approximately 20% of the patients. Currently, the FDA recommends a dose of 3 million international units (MIU) IFN-α, 3 times a week for a period of 12 months for patients diagnosed with chronic HCV and responding to the aforementioned therapy after 3 months [265]. After its first success as an antiviral agent against HCV, many pharmacokinetic studies of IFN-α were undertaken in volunteers and patients between 1986 to 1996 [266]. Currently, there is little knowledge on the relationship between the drug dose and its mechanistic effect on the target organ, i.e., the induced intracellular responses within the liver. In the past decade, basic research has provided mechanistic and dynamic understanding of the molecular and cellular responses to IFN-α, reporting it as a double edged sword [267]–[269], as it mediates multifarious response activities by induction or repression of thousands of interferon-stimulated genes (ISGs) [270], [271]. Considering its efficacy in immunomodulation and angiogenesis in different cell-types [9], [10], IFN-α therapy seems to have the potential to contribute as a remedy against many diseases. Thus, it is important to have a quantitative systems understanding of the action of IFN-α as a drug and the complex web of responses it activates at the target site.

In the past years, computational approaches have supported the experimental observations to achieve an understanding of the IFN-α dose-effect relationships on different time-scales and in different experimental set-ups [111]–[114], [116]–[120], as well as in different model organisms (animal studies) [39], [40], [42]. The focus of the modelling approaches in the past years was either on the kinetics of the intracellular reponse to explain *in vitro* cell studies (pharmacodynamics) or on computing the distribution of the drug in the body (the pharmacokinetics). An effort to combine the two different modelling aspects (kinetic models (PD) with pharmacokinetic models (PK)) is needed to establish a systems level understanding of the PK/PD relationship- the quantitative systems pharmacology (QSP) approach [207], [216]–[218], [272], [273]. In a publication in 2011, Van Der Graaf and Benson defined QSP as *"the quantitative analysis of the dynamic interactions between drug(s) and a biological system that aims to understand the behaviour of the system as a whole..."* [274]. In other words, QSP aims to simultaneously detail the description of pharmacokinetics (drug absorption, distribution, metabolism and excretion (ADME)) and the pharmacodynamics (intracellular response) of the drug action from a whole-body perspective. In the area of *biologicals*, [1] PK/PD modelling has been more recently applied for monoclonal antibodies [275], [276], where the use of the QSP approach is still in its nascency. The implementation of PBPK/PD modelling is gaining recognition as an essential step to allow for compliant translation from the pre-clinical to clinical stage while taking into account the principles of the 3Rs (Replacement, Refinement and Reduction) for more humane animal research.

The work in this thesis describes the workflow when applying the state-of-art QSP approach to establish an organism-level understanding of the therapeutic action of the *biologic* IFN-α and its coupled response in the liver. The work in chapter 3 and chapter 4 uses the QSP approach to establish mechanistically detailed the PBPK/PD model of two species: Mouse and human. Most pre-clinical studies are conducted in mice, which are then translated to humans by cross-species extrapolation. The development of mouse PBPK/PD model was undertaken to aid for establishment of quantitative cross-species extrapolation in the future. A human

[1] are therapeutics originating from natural sources- humans, animal or microorganisms and are produced using biological organisms.

PBPK/PD model was developed because by implementing human cohort data and human cell-line data, better estimations of the translational results from animals to humans can be made. Furthermore, such models can be implemented in health-risk assessment of individuals. Thereby, contributing to personalised medicine. Ultimately, the differences between the models of the two organisms would offer an in-depth understanding by providing insights into inter-species differences. This would contribute to improved experimental designs for humane animal research. The work in these chapters integrates the pharmacokinetic and pharmacodynamic knowledge for humans and mice respectively. It describes a dose-response relationship for IFN-α as well as concentration-effect relationships of the biomarkers IRF9 mRNAc and Mx2. The presented PBPK/PD models and the knowledge generated from their analysis lay the foundation for a rational design of experimental *in vitro* assays, dosing regimens and the preclinical to clinical translation. In summary, the presented PBPK/PD approach allows for the quantitative description of IFN-α-induced response modulations in the JAK/STAT signalling pathway associated with the pharmacological action following the intravenous dose of IFN-α in humans (chapter 3) and mice (chapter 4). The presented workflow in this dissertation provides the opportunity to link the JAK/STAT signalling pathway with IFN-α concentration-time profiles, in order to gain more insights into the dynamics induced by target-mediated drug disposition (TMDD) as analysed in chapter 3, subsection 3.5.3.

To calibrate the PBPK/PD models for humans and mice, a high number of *in vitro* assays were integrated from the literature [116], [157], [161], [162] and from collaborations that arose during the course of this work (with Dr. Mario Koester[2]). These datasets sought to capture the time course dynamics of the molecules in the JAK/STAT pathway in order to calibrate the individual hepatocyte models for the human and mouse primary hepatocytes.

First, the presented PBPK models for humans and mice were developed based on results digitised from the literature [39], [48]–[50], [159] in chapter 3 & 4. Although most parameter values of these models lie within the range of reported literature values, there are some limitations due to lack of information of the specific activity of IFN-α in the data sources. We do realise this leads to uncertainty in the calculation of the injected dose.

The pharmacodynamic (kinetic) models presented in chapters 3 & 4 use the approach of model ensembles [203]. In both the cases, the model parameters were not fully identifiable. These model ensembles had different parameterisations for same model structure describing the same behaviour of the cell-population quantitatively. This was done to counteract the problem of non-identifiability of the parameters of the models. Robust predictions that do not depend on the exact parametrisation of the model, but only on the fact that the model can reproduce all known experimental data, still allow a meaningful interpretation. A difficulty for parameter fitting was the complexity of the experimentally observed behaviour of the JAK/-STAT pathway at multiple length and time scales. The amount of data available was limited and comprised of multiple dimensions (some in arbitrary units, while others in relative measurements). Moreover, the quantification of IFN-α is reported in international units (IU) which introduces high variability in the calculation of the pipetted dose due to the high magnitude of differences in the specific activity of batches of IFN-α in each experiment.

The PBPK model and the pharmacodynamic (kinetic) model were coupled to establish the PBPK/PD QSP model. The results from chapter 3, subsection 3.5.3 depict relative differences in *in vitro* vs. *in vivo* response of IRF9 mRNAc to IFN-α. Furthermore, the analysis reflects

[2]Department of Gene Regulation and Differentiation, HZI – Helmholtz Centre for Infection Research, Inhoffenstr. 7, 38124, Braunschweig, Germany.

an important point of the non-linearity in the signal propagation, where an 18-fold difference in dose commonly used in *in vitro* assays relative to the i.v. injected IFN-α only induced a 4-fold difference in response. This is of relevance, as *in vitro* cell cultures are subjected to a significantly different environment compared to that of the organ in the organism. Hence, the implemented PBPK/PD QSP workflow is an important step to translate such *in vitro* calibrated hepatocyte models by the approach of *in vitro* to *in vivo* extrapolation (IVIVE), into a clinically relevant model. Finally, the clearance of IFN-α in the liver of the PBPK/PD model was strongly governed by the variability in the expression of the receptors in the liver.

Mice are often used as animal models of various diseases which are treated with IFN-α. However, performing these experiments is time consuming, expensive and a matter of ethical concerns. In addition, potential differences in the physiological reaction to the drugs and side effects can be missed due to differences between humans and mice. Thus, virtual computational models of the animal contribute to establishment of 3R approaches such as model-based experimental planning as well as targeted and comprehensive analyses of experimental data. In chapter 4, the computational model was expanded by using the PBPK/PD QSP approach to establish and predict murine and human IFN-α concentrations in mouse for the preclinical phase of the drug. The intention was to be able to establish such a complementary mouse model for future in-silico-based predictions of IFN-α efficacy and to be able to extrapolate cross-species differences in the JAK/STAT signalling response to IFN-α. Such a model might help reduce animal testing by implementing the analysis of the same for proper designing, conducting and reporting of experiments. In this chapter, the development of a mouse PBPK model was based on *in vitro* data (e.g., plasma protein binding, signalling pathway experiments) and physio-chemical properties of IFN-α reported in the literature [39], [157]–[160]. All of human IFN-α subtypes and several mouse IFN-α subtypes are commercially available, but there is little knowledge as to which one works best for cross-species extrapolation. Thus, the established model supports quantification of those differences, preliminary work of which is found in chapter 4, subsection 4.4.4.

Lastly, one of the major benefits of using the PBPK/PD approach is that the underlying structure of PBPK/PD models applied in this thesis allows the simulation of reliable PK profiles in several compartments (organs) within the human and mouse body (e.g., the intracellular space of the liver). In particular, PBPK modelling allows us to predict *in vivo* tissue concentrations from easily accessible samples in venous blood through the calculation of organ-plasma partitioning. This feature of the model contributes to the understanding of tissue distribution by using a virtual whole-body model of the organisms which was achieved in the chapters 3 & 4. The presented PBPK/PD QSP approach that utilises PBPK modelling is, thus, applicable for extrapolating IFN-α concentrations at diverse sites of action besides the liver, such as the heart or the kidney, assuming though, an inclusion of adequate signalling model is mostly responsible for the respective mode of action. Furthermore, the analysis of tissue distribution is also useful in developing optimal strategies for the injection of therapeutic agents, such that adequate concentrations would reach the site of action.

While establishing the pharmacodynamic (kinetic) models for chapters 3 & 4, variability in the intracellular response was observed when simulating varying amounts of receptors. This is certainly partially due to the small numbers of receptors reported to be present in both human and mouse hepatoma cell lines (only around 1000 receptors/cell) [90], [277], [278]. Furthermore, important aspects of the response generated by the signal transduction are governed by the stochasticity of the small numbers of signalling molecules present in a cell. This stochasticity adds to the intrinsic noise of the system. Therefore, to explore the intra- and inter-cell variability in the response of the JAK/STAT signalling pathway to IFN-α stimuli, a stochastic

model was established. In the *in vitro* experiments done on mouse primary hepatocytes, the observed dose response of Mx2 to the IFN-α does not necessarily account for individual cell dynamics of high expression of Mx2. There could also be a possibility of all-or-none response and only a fraction of cells could respond to IFN-α stimuli at different doses. These observations initiated the final chapter of this thesis- chapter 5. This work commenced a collaboration with the group of Dr. Marco Binder at DKFZ, Heidelberg during which high-throughput temporal (32 hours) data of MxA and IFIT1 after IFN-α induction in Huh 7.5 cells was obtained at single-cell resolution. The mechanistically detailed stochastic model which followed was calibrated to the deterministic time course data from Maiwald et al. [116] and the single cell FACS data of MxA and IFIT1 from the experiments. Thus, the developed stochastic model differed from previous efforts of other mechanistic stochastic models [125] by not following ISGs which have enzymatic control on the JAK/STAT pathway itself (like IRF1, IRF3, IRF7 and IRF9, which also act as transcriptional factors for the trigger of antiviral response), which would lead to an all-or-none response, but by following ISGs which show a graded response. In addition, extrinsic noise was added to the model to account for the variability in the initial copy numbers of the molecules in the pathway. The established model helped to explain the robustness of the JAK/STAT signalling pathway in allowing a heterogeneous population of cells to be able to have long and stable temporal responses of certain antiviral genes. Higher organisms with intracellular signalling may benefit from such a endurance in order to sustain signal propagation and shape the antiviral response in cell populations. The results obtained in this chapter are also consistent with previous reports for MxA [83]. In this preliminary version, however, one important mechanistic detail that is not yet covered in the stochastic model is the receptor recycling, which implies that the model can only describe a single stimulation without reactivation of unbound receptors. This will be included in the model in order to address the impact of noise and the control of receptor variability on the non-linear propagation of the JAK/STAT pathway. One final point is that in this work we have implemented discrete stochastic methods [123] and have not taken the spatial processes in account.

Despite the improvement in computing time that our new fitting algorithms offer, there is still room for improvements in this field. The stochastic simulation algorithms (SSA) and methods are subjects of ongoing work as they are computationally demanding. One way to make significant improvements would be to implement parallel computing to reduce the time in solving models implementing SSA. There are many multi-scale models in the deterministic domain of systems biology. However, as important such models are for real applications, there is a high potential for the application of SSA in solving multi-scale biological problems which include processes on different time-scales.

Apart from scientific challenges, a significant operational barrier in this work was the lack of well-established model exchange standards for the models between the mark up language SBML (systems biology mark up language) and PKML (pharmacokinetic mark up language). However, the work-flow implemented in this thesis is universal for any protein molecule, making this approach applicable for other drugs beyond IFN-α.

6.2 Concluding remarks

The motivation to integrate systems biology models and principles and the field of pharmacology is to not only to achieve a holistic understanding across different levels of biological organisation. This would help to not only quantitatively understand the biological phenomena in question, but also to establish a high success rate in bench to bedside translations of drug development programs. In conclusion, the quantitative systems pharmacology approach

aims to bridge the above-mentioned gaps such that it can support the prediction of the *in vivo* drug-effects in humans in a quantitative manner by recycling the data produced from *in vivo* animal studies and high-throughput *in vitro* assays. Also, there is a need of trained individuals in both biological and quantitative sciences who can effectively bring this knowledge together in order to develop such models, as well as the lack of computational tools that can integrate diverse sets of data required to establish the QSP models. In spite of these hurdles, the work described in this thesis is a sincere attempt to show the benefits of PBPK/PD QSP approaches that can help to characterise dose-response relationships of translatable biomarkers in order to determine the efficacy of the therapeutic compound.

Despite the increasing use of modelling approaches to support quantitative research in biology, there is still a long way to go until the QSP approach would finally be able to significantly increase the therapeutic succces rates, as such an approach is only as good as the data which has been used for its establishment. In this regard, I hope this work describes some of the challenges and the analyses one can do by implementing the sparse data available on IFN-α to establish meaningful insights using the PBPK/PD QSP approach. I hope that in the near future such an approach emerges as a corner-stone of quantitative drug discovery and development.

Appendix A

Appendix Chapter 2

A.1 Experimental data and conversions

A.1.1 Plasma pharmacokinetic data

Unit conversion IFN-α or mu-IFN-α 4 doses were calculated by using the molecular weight of IFN-α as 19500 g/mol [165]. The doses were calculated as described in Chapter 2, 2.1 and 2.2. The specific activity was provided for human dataset from Wills et al. (1984) [50] as 1.7 X 10^{8} U/mg. The resulting dose was 0.22 mg. For the validation human IFN-α datasets from Shah et al. (1984) [48] and Radwanski et al. (1987) [49] the specific activity was used from Radwanski et al. (1987) as 2.2 X 10^{8} U/mg. The doses from Shah et al. (1984) [48] were: 30U as a dose of 0.136 mg and 60U as a dose of 0.27 mg. The dose in mg for Radwanski et al. (1987) [49] was 0.045 mg. The plasma concentration time profile of IFN-α PK used for fitting is further described in Table A.1.1.

For the mu-IFN-α 4 no specific activity was provided in Bohoslawec et al. [39], hence the assumption of the specific activity of 1.9 X 10^{7} U/mg was made using the average of the specific activity she came across during the work. Hence, the total dose was 0.045 mg or 2.35 nmol per animal. In the case of dataset from Dr. Mario Köster; the dose was 5000U with a specific activity of 1.4 X 10^{8} U/mg; hence to total dose/mouse was calculated to be 3.57 X 10^{-5} mg or 1.83 pmol. The details of the parameters and the doses are recapped in Table C.1. The final values of the concentration/time in plasma for each daaset are further described in

TABLE A.1: This table contains the pharmacokinetic data of IFN-α published by Wills et al. [50] that has been digitised and used for setting up the pharmacokinetic model.

Time [hours]	**Conc. [μmol/ml]**
0.166	0.000194
0.33	0.000368
0.66	0.000686
0.83	0.0005
1	0.000379
1.5	0.000213
2	0.000133
3	6.9494E-05
4	1.7361E-05
5	1.2515E-05
6	8.7453E-06
7	6.6061E-06
8	5.7416E-06
12	3.487E-06
24	1.0668E-06

TABLE A.2: This table contains the calculation for the pharmacokinetic data of mu-IFN-α published by Pulverer et al [157], kindly provided by Mario Koester , from Bohoslawec et al.[39],from Rosztoeczy et al.[158] and from Kiuchi et al.[159]. The data from [39] and Rosztoeczy et al.[158] was used to fit the pharmacokinetic model using PK-Sim. The data from Kiuchi et al.[159] was used to validate the model.

	Koester et al.	
Time[hours]	**Cplasma IFN-α [pg/ml]**	**Cplasma IFN-α[nmol/ml]**
0.016	3047.152	0.000141
0.083	2258.690	0.0001049
0.166	1967.665	9.14173E-05
0.333	2042.735	9.4905E-05
	Bohoslawec et al. (1986)	
Time[hours]	**Serum Dose [%]**	**Cplasma IFN-α[nmol/ml]**
0.033	6.63	0.027436
0.083	3.97	0.016429
0.25	2.35	0.009725
0.5	1.2	0.004965
1	0.1	0.000413
3	0.01	4.13831E-05
	Rosztoeczy et al. (1986)	
Time [hours]	**Activity in plasma [U/ml]**	**Cplasma IFN-α[nmol/ml]**
0.19	13146.07	0.050896
1.44	65.40	0.000253
2.94	31.64	0.000122
5.82	20.34	7.87537E-05
11.36	6.10	2.3635E-05
	Kiuchi et al. (1983)	
Time[hours]	**Serum dose [%] Dataset 1**	**Cplasma IFN-α [nmol/ml] Dataset 1**
0.25	2.37	0.003685
0.5	0.71	0.001107
1	0.26	0.000405
2	0.10	0.000155
3	0.10	0.000168
	Kiuchi et al. (1983)	
Time[hours]	**Serum dose [%] Dataset 2**	**Cplasma IFN-α [nmol/ml] Dataset 2**
0.25	0.90	0.001397
0.5	0.57	0.000887
1	0.20	0.000313
2	0.03	6.01E-05

A.1.2 Human hepatocyte dose response data

In the tables below, the experimental data provided by Bolen et al.[161] and digitised from Jilg et al.

TABLE A.3: This table contains the dataset kindly provided by Steven H. Kleinstein from Yale University. The data was normalised across different doses to be comparable as it was fold change data.

hours	10U	100U	500U	2500U
0	0.016126431	0.016126431	0.016126431	0.016126431
1	0.016126431	0.025479761	0.016126431	0.043218836
4	0.107885825	0.524592808	0.220125786	0.816965006
6	0.149814546	0.592646347	0.278019674	1
12	0.197226254	0.421706176	0.232381874	0.466537655
24	0.130462829	0.277697146	0.173197871	0.36236091

A.1.3 Literature search

In the tables below, the information gathered from the literature and various databases for the purpose of setting up the parameter or the parameter identification limits of the models for each species.

A.2 PBPK model parameterisation

TABLE A.4: This table contains the literature values of the pharmacokinetic parameters used in the PBPK human and mouse model. Wherever stated clearly hu-IFN-α or mu-IFN-α the values were used for the respective model. The parameters which are not included under the respective species header were used as values for both the models. The parameters were varied 50% for the parameter estimation.

Parameter	Literature Value	Reference	Unit
Lipophilicity (Log P)	-0.366	[165]	`Log units`
Fraction unbound (fu)	1	-	
Solubility	100	[165]	`mg/ml` (ref. pH is 7)
		hu-IFN-α	
Molecular Weight	19500	[165], Drugbank (18.03.2014) Accession number: DB00034	`g/mol`
CLplasma (kidney)	2.7	[50][176][279][280]	`ml/min/kg`
IFNAR1 concentration	-	-	μ`mol/l`
IFNAR2 concentration	-	-	μ`mol/l`
K_{off} IFNAR1	0.22	-	`1/s`
K_{off} IFNAR2	0.0077	[187][281]	`1/s`
K_D IFNAR1	3.5	[282]	`nmol/l`
K_D IFNAR2	0.0077	[187][281]	`nmol/l`
$K_{endocytosis}$	-	-	`1/min`
K_t_IFNAR1	-	-	`1/min`
K_t_IFNAR2	-	-	`1/min`
		mu-IFN-α	
Molecular Weight	21922	Uniprot (20.4.2017) P01573	`g/mol`
IFNAR1 Concentration	-	-	μ`mol/l`
IFNAR2 Concentration	-	-	μ`mol/l`
CLplasma (Kidney)	10 -15.65	[39]	`ml/min/kg`
K_{off} IFNAR1	1	[91]	`1/s`
K_{off} IFNAR2	0.015	[91][281]	`1/s`
K_D IFNAR1	5	[91]	μ`mol/l`
K_D IFNAR2	5	[91][281]	`nmol/l`
$K_{endocytosis}$	-	-	`1/min`
K_t_IFNAR1	-	-	`1/min`
K_t_IFNAR2	-	-	`1/min`

Appendix B

Appendix Chapter 3

B.1 PBPK model parameterisation

TABLE B.1: This table contains the information about parameters used for initialising the individuals for PBPK model.

Biometrics	
Species	Human
Population	European $(ICPR, 2002)$
Gender	Male
Age	30 `years`
Weight	73 `kg`
Height	176 `cm`
BMI	23.57 $\texttt{kg}/m^2$

TABLE B.2: This table contains the literature values and the fitted values of the pharmacokinetic parameters used in the PBPK human. The parameters were varied 20% from the values reported in the literature for the parameter estimation.

Parameter	Fitted Value	Literature Value	Reference	Unit
Lipophilicity (Log P)		-0.366	[165]	Log units
Fraction unbound (fu)		1		
Solubility		100	[165]	mg/ml (ref. pH is 7)
		hu-IFN-α		
Molecular weight		19500	[165], Drugbank (18.03.2014) Accession number: DB00034	g/mol
CLplasma (kidney)	3	2.7	[50][176][279][280]	ml/min/kg
IFNAR1 concentration	0.26	-		μmol/l
IFNAR2 concentration	0.5	-		μmol/l
K_{off} IFNAR1	0.1	0.22	-	1/s
K_{off} IFNAR2	0.00022	0.0077	[187][281]	1/s
K_{eq} IFNAR1 0.00077	0.0001-0.01	[187], [281], [282]	l/nmol	
K_{eq} IFNAR2	1.5	0.002-0.1	[187][281]	l/nmol
$K_{endocytosis}$	8.93226	-		1/min
K_t_IFNAR1	0.02298	-	-	1/min
K_t_IFNAR2	0.074999	-	-	1/min

TABLE B.3: The liver compartment is divided into the interstitial, cytoplasmic and nuclear compartment. The volume of the interstitial and the cytoplasm is borrowed from PK-sim organ values while the nuclear compartment was assigned the value 1:4 ratio of the cytoplasm as calculated from the experiments done for Maiwald et al. [116] where the ratio of the nucleus to cytoplasm was measured.

Volume in Litres	
Compartment	l
Interstitial	0.39
Cytoplasm	1.59
Nucleus	0.35

TABLE B.4: The parameter values of the top 5 fits for the PBPK model of IFN-α are listed. The values were well defined for many parameters and hence the first top fit was evaluated further.

Parameter Name	Unit	Fit 1	Fit2	Fit3	Fit4	Fit5
K_t IFNAR2	1/min	1.25E-03	1.25E-03	1.25E-03	1.25E-03	1.25E-03
K_t IFNAR1	1/min	3.83E-04	7.71E-04	5.04E-04	9.99E-04	4.11E-04
R1 concentration	μ mol/l	0.26	0.21	0.19	0.28	0.29
R2 concentration	μ mol/l	0.5	0.5	0.5	0.5	0.5
Complex K_{off}	1/min	2.21E-04	1.04E-06	3.82E-05	1.00E-03	1.14E-04
IFNAR2 binding K_{eq}	l/nmol	1.00E-01	1.00E-01	1.00E-01	1.00E-01	9.81E-03
k endocytosis	1/min	8.93E-06	1.49E-06	2.41E-06	3.27E-05	4.62E-05
Complex K_{eq}	l/nmol	7.76E-04	3.72E-04	5.55E-04	2.56E-05	6.59E-04
IFNAR2 binding K_{off}	1/min	1.50E+00	1.50E+00	1.50E+00	1.50E+00	1.50E+00
Plasma Clearance	ml/ min/mg	3.00E-03	3.00E-03	3.00E-03	3.00E-03	3.00E-03

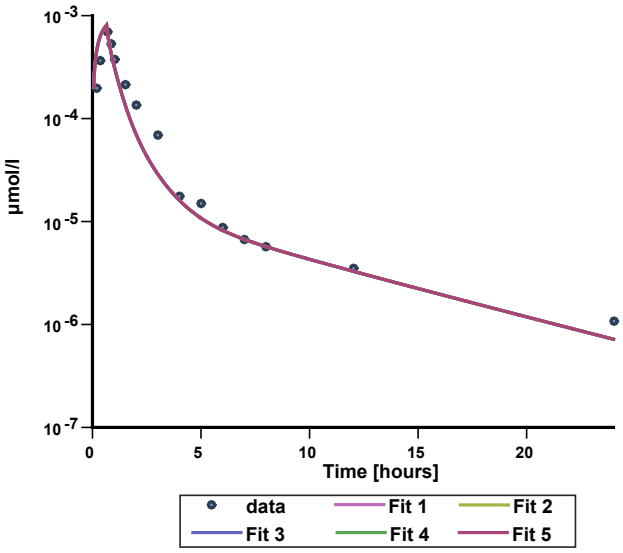

FIGURE B.1: The top 5 models have the RMSE of 0.7 and all the fits were equally good. The plot represents the top 5 models simulating the IFN-α distribution in the venous blood plasma (lines) vs the dataset of Wills et al. [50] (dots).

B.2 Human hepatocyte model parameterisation

B.2.1 Literature search for the hepatocyte model

TABLE B.5: Values of kinetic parameters found in literature

Molecule	Param	Value	References
ISGF3c	k_D	$[10nM(STAT2), 5\mu M(STAT1)]$	[283]
IFN-IFNR2	k_D	$[2.2nM]$*	[284][285]
IFN-IFNR1	k_D	$[2000nM]$	[284] [285]
STAT1-STAT2	k_D	$[< 10nM, 5.5mM(STAT2mutant)]$	[286]
SOCS **	k_i	$[1.5 \pm 0.7\mu M(ForJAK2), 1.2 \pm 0.3\mu M(ForATP)]$	[196]

*IFNAR2 binds IFN-α2 with an equilibrium dissociation constant of around 5 nM and a complex lifetime of around 100 s, whereas the affinity toward IFNAR1 is three orders of magnitude lower, and the complex dissociates about 100-fold faster.
** Non-competitive Inhibition
For COPASI please calculate $k_{eq} = 1/k_D$

Publication	Cells	Dose (U/ml)				Response	Control	Time of stimulus	Unit conversion
Schlaak et al. (2002)	Fibrosarcoma cells	10	100	1000		IRF9	GAPDH	Treated for 8 hours	Roche Molecular Biochemicals
Wolber et al. (2002)	HepG2	5	50	500	5000	IRF1	GAPDH	Treated for 24 hours	Sigma.
Jilg et al. (2014)	Huh7.5	30				mRNA STAT1, Mx1, IRF9	GAPDH	Treated for 0, 4, 8 and 24 hours	Peginterferon alpha 2b from Schering.
	PHH	15							
Maiwald et al. (2010)	Huh 7.5	500		1000		pSTATand pJAK	Cells left untreated	Treated for 0, 1, 2, 3, 4, 8, 12 or 24 hours	PBL Labs human leukocyte interferon.
Bolen et al. (2014)	PHH	500				IRF9 and pSTAT1	Cells left untreated	Treated for 0.5, 1, 2, 4, 6, 12 and 24 hours	Recombinant human interferon alpha 2a.
	Huh 7	10	100	500	2500				

FIGURE B.2: The dose-response of IRF9 in human hepatoma cell lines or PHH or Fibrosarcoma cells treatmented with IFN-α2 upto 24 hours found in various publications [20], [22], [116], [161], [162].

FIGURE B.3: This information is the evidence for TFBS marks. The TFBS for IRF2, IRF1 and ISRE are found at the same position in the DNA of IRF9 gene in HeLa and HepG2 cell-line. Hence this shows that IRF1/IRF2 or IRF7 (evidence that this binds to ISRE) and ISGF3 complex (STAT1-STAT2-IRF9 and evidence that this binds to ISRE) and STAT1/IRF9 (evidence that this binds to ISRE) can all bind at these sites and induce transcription of IRF9.

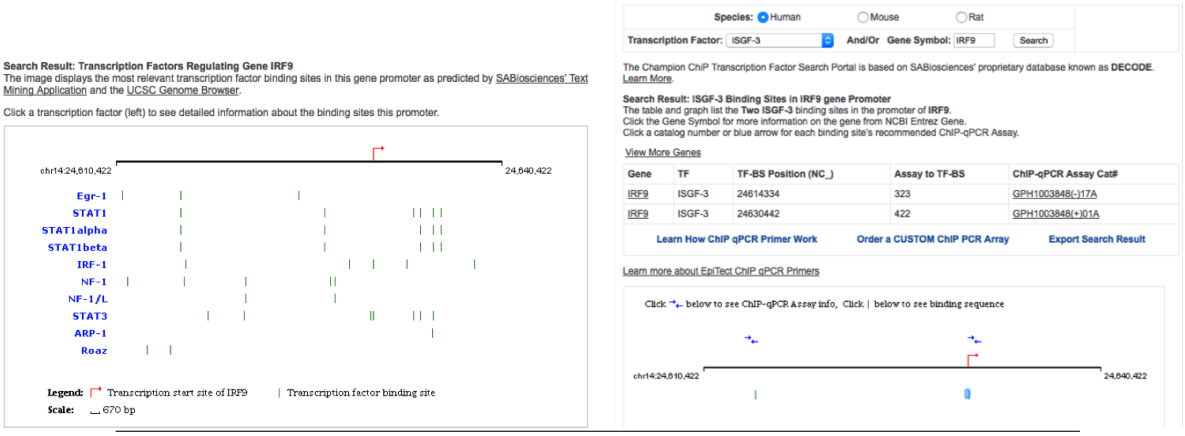

FIGURE B.4: The sabioscience database reported chip experiments of IRF9 gene showing the binding of ISGF3 at two sites- one on positive strand and one on negative strand. Also, note that the most relevant transcription factor of IRF9 regulation is marked in blue. Various promoters of IRF1 are seen; one of which overlaps with ISRE element.

B.2.2 Hepatocyte model overview and parameterisation

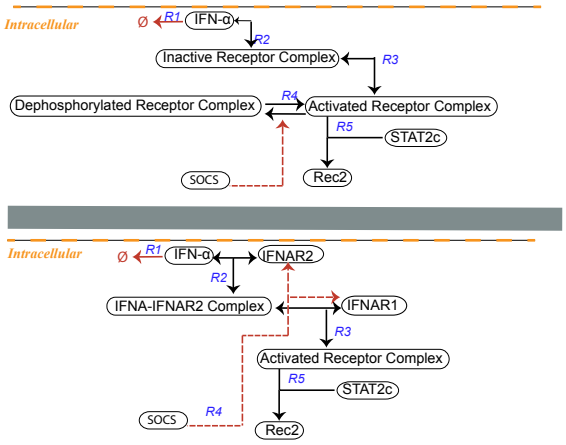

FIGURE B.5: The architectural difference of adapted hepatocyte model to the Maiwald et al. model [116] is described here. In the adapted hepatocyte model the receptor concentrations and the kinetics are implemented from the PK model. All parameters, except the receptor kinetics were fitted in the adapted hepatocyte model.

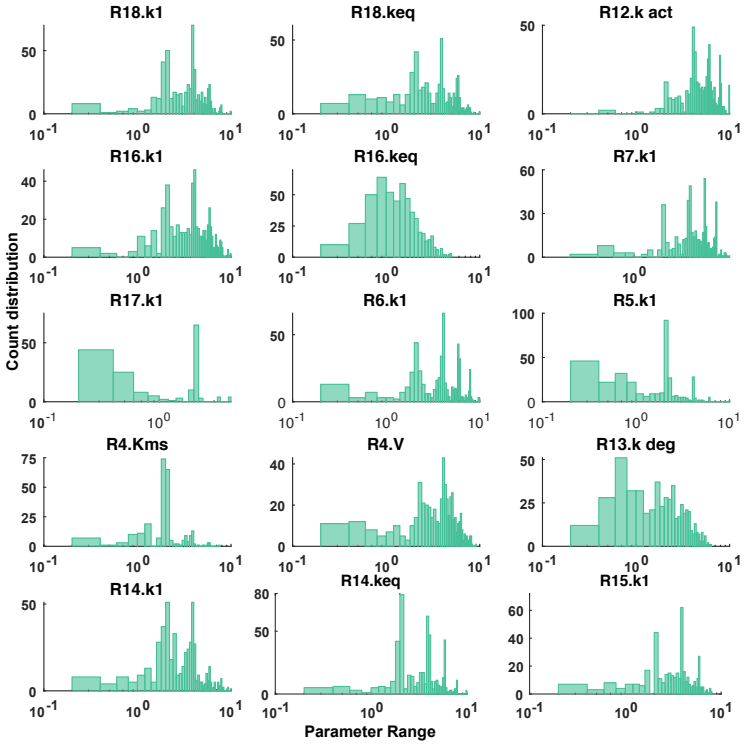

FIGURE B.6: The detailed count distribution of each parameter is plotted as a histogram. The x-axis is the distribution of the parameter value from its lowest to largest value. On the y-axis is the count distribution of that parameter found in 1000 models.

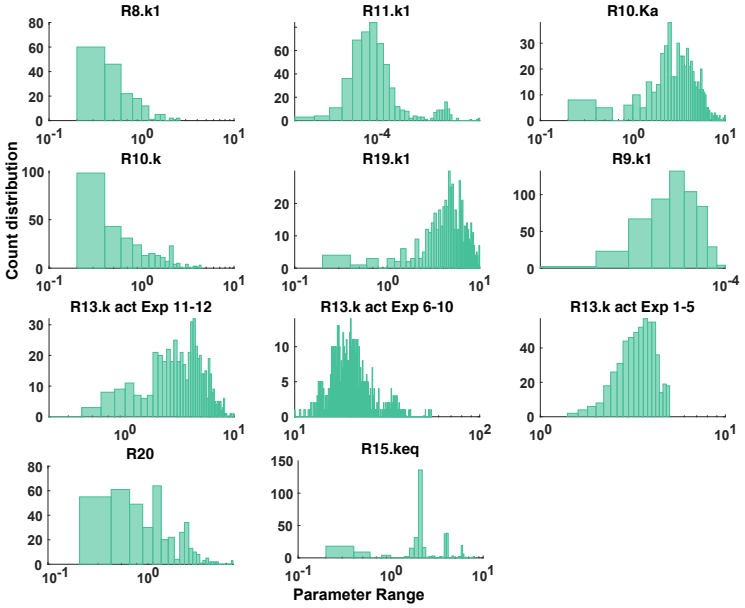

FIGURE B.7: The detailed count distribution of each parameter is plotted as a histogram. The x-axis is the distribution of the parameter value from its least to largest value. On the y-axis is the count distribution of that parameter found in 1000 models.

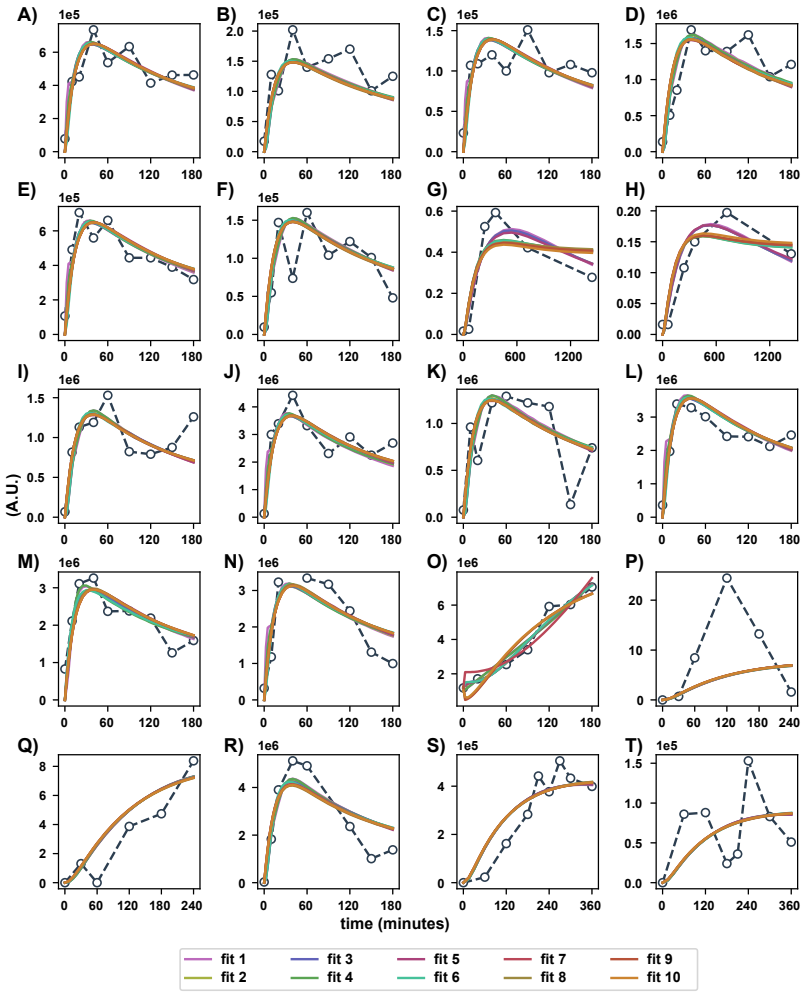

FIGURE B.8: The top ten fits obtained from the fitting process for 20 datasets is depicted. In the figure the time course profile for A) pStat cytoplasm in response to 500 U B) pSTAT nucleus in response to 500 U C) pSTAT cytoplasm with overexpression of IRF9 protein D) pSTAT nucleus with overexpression of IRF9 protein E) pStat cytoplasm in response to 500 U (second replicate) F) pSTAT nucleus in response to 500U (second replicate) G) IRF9 mRNAc in response to 10U from Bolen et al. [161] H) IRF9 mRNAc in response to 100U from Bolen et al. [161] I) pSTAT total in nucleus in response to 500 U J) pSTAT total in cytoplasm in response to 500U K) pSTAT total in nucleus in response to 1000 U L) pSTAT total in cytoplasm in response to 1000U M) pJak in response to 500U (Activated receptor complex)) N) pSTAT total in nucleus O) IRF9 protein total in nucleus P) mrna socs in response to 500U Q) mrna socs with overexpression of IRF9 protein R) pSTAT total in nucleus in response to 500U S) SOCS protein with overexpression of IRF9 protein T) SOCS protein in response to 500U.

TABLE B.6: The below table represents all the kinetic parameters obtained for the model ensemble. The receptor values were preserved from the PBPK model and the value of IFN efflux was also fitted and kept constant. These values can be found in B.7. Most of the values are varied +- 50% or 75% as those used in Maiwald et al [116] or the literature values found for some parameters as stated in D.1 and B.5.

Nr.	Parameter	fit 1	fit 2	fit 3	fit 4	fit 5	fit 6	fit 7	fit 8	fit 9	fit 10	Units
R4 & M3	Kms	6.13131	0.00180	1.48411e-05	0.00362991	0.0530483	9.56746e-07	0.122204	0.000124324	0.00012947	0.0026974	nmol/l
	V	2.61285	1.90736	0.0424023	3.4103	8.79938	0.00792312	6.80457	0.227457	2.98461	9.97814	nmol/(l*s)
	Ka	200	410.13	219.203	487.793	219.325	1383.79	291.406	200.873	879.986	3536.95	nmol/l
R5 & M6	k1	0.0035	0.0038	0.00212197	0.0020049	0.0440604	0.00118631	0.110752	0.112401	0.0683156	0.295528	l/(nmol*s)
R6 & M7	k1	0.000393	0.011137	0.00614481	0.000118306	0.116272	0.00733387	0.297544	0.301031	0.00480034	0.000385657	l/(nmol*s)
R7 & M8	k1	10	14.93	15	10	2.81244	2.90985	9.99396	9.91478	10	10	l/(nmol*s)
R8 & M9	k1	0.00697	0.00010	0.000214199	0.000100974	0.000248786	0.000248112	0.00095402	1e-06	1e-06	1.02804e-05	1/s
R9 & M10	k1	3.54e-05	3.66e-05	3.72397e-05	4.29623e-05	3.42033e-05	4.20262e-05	4.09684e-05	4.14782e-05	4.34948e-05	4.29233e-05	1/s
R10 & M11	k	5.879e-06	0.00656	0.145302	3.02119e-05	0.00329146	0.0826057	0.000524502	9.97918	4.77106	0.162675	nmol/(l*s)
	Ka	0.333955	0.379743	0.150564	5.56749	9.75684	0.488633	7.22666	0.504096	0.3157	7.11777	nmol/l
R11 & M12	k1	1.17183e-05	1.47614e-05	1.48847e-05	4.4256e-05	1.41109e-05	4.45479e-05	4.3915e-05	4.29066e-05	4.3282e-05	4.35455e-05	1/s
R12 & M13	irf9deg	1e-07	0.0007188	0.000577945	1e-07	0.000511354	0.000399455	1e-06	0.10909	0.297425	0.00792213	1/s
	k_const	4.5e-06	0.032350	0.02600752002	4.5e-06	0.02301094365	0.01797546619	4.5e-05	4.90904	13.384125	0.35649	nmol/(l*s)
	k_act	10	2.113	0.356829	6.20201	8.15692	0.0548374	9.99988	0.125117	0.445746	10	1/s
R13 & M14	k_act	5.70548	1.02536	4.60042	0.980916	1.81244	0.98304	1.00833	3.83025	4.68123	4.25086	1/s
	k_deg	0.16196	0.112138	0.150743	2.49471	2.17238	0.0466958	0.905009	0.0981067	0.495813	0.165271	1/s
R14 & M15	k1	0.0001	1.03093	4.33098	0.000169673	0.0109568	3.9328	0.000190079	9.99976	0.0697624	0.172737	1/s
	keq	0.00697504	0.000145781	0.000174285	0.0182716	0.000110169	0.0001	0.0001	0.0001	0.00394036	3.91431	-
R15 & M16	k1	2.20533e-07	1e-06	1e-06	1e-05	1e-06	1e-05	1e-05	1e-05	1e-05	1e-05	1/s
	keq	0.00197389	0.00875874	0.00887611	0.0726266	0.0085101	0.0747027	0.070818	0.0711071	0.0701783	0.0797429	-
R16 & M17	k1	9.92815e-07	0.000266464	0.00135527	9.75714e-07	0.00141323	0.006401	9.96322	0.231379	0.123091	0.000516299	1/s
	keq	0.0297375	2.06451	3.71093	0.0289452	4.04655	4.24893	3.09838	9.41435	8.06671	1.8218	-
R17 & M18	k1	0.00774342	0.0355024	0.0174468	0.0041382	0.166535	0.00964032	0.813382	0.82559	0.505973	2.14223	1/s
R18 & M19	k1	0.123072	9.7025	6.42557e-06	1e-05	0.545132	0.0458358	9.98028	0.0089197	0.22289	0.0180208	l/(nmol*s)
	keq	2.91162e-05	7.949e-06	5.86288	0.00141925	9.67627	0.000239805	9.9993	0.0163734	0.0437206	1.20463	l/nmol
R19 & M20	k1	0.10365	0.659215	4.04029	0.00978293	0.647071	0.0702393	1.98259	2.76704	1.27384	7.71511	1/s
R20 & M21	k1	1e-07	0.000718893	0.000577945	1e-07	0.000511354	0.000399455	1e-06	0.10909	0.297425	0.00792213	1/s

TABLE B.7: The kinetic parameters whose values were fixed for the model ensemble and were borrowed from the PBPK model.

Nr.	Parameter	Value	Unit
R1	k1	0.0213795	1/s
R2	k1	0.1	l/(nmol*s)
	keq	1.5	l/nmol
R3	k1	0.00022	l/(nmol*s)
	keq	0.00077	l/nmol

B.3 Human PBPK/PD model establishment

B.3.1 Establishment of the PBPK/PD model in MoBi

To merge the models, the PK model was saved in pkml format and the cellular model the base project file to work with. The integration of the models was executed manually in MoBi. The heptocyte model was inserted in the liver compartment of the PBPK model and the coupling was established for the intravenous dose of IFN-α simulated from the *event* of application in MoBi building block. The cellular containers were structured in a way to match the PK-Sim format in the way:

- Organism (logical)
- Liver (logical)
- Pericentral (logical) (New PK-Sim Model with zones needed to be taken into account)
- Intracellular (physical, tagged with cytoplasm)
- Nucleus (physical, tagged with nucleus)

After that the existing *Molecules Start Values* and the *Parameter Start Values* were updated by adding liver and pericentral for all paths. Once the cellular model is following the structure of PK-Sim. The spatial structure from PK model was imported and the nuclear compartment was added (using add container and a saved cellular model spatial structure) and connection to the existing Intracellular compartment. Next, the cellular model parameters were added from cytoplasm to Intracellular compartment of PK model (using add Parameter and a saved cellular model spatial structure). The molecules were merged from PK model to cellular model molecules and whenever there was a conflict, new molecules were created for the same. The molecules that were a part of the passive diffusion (like IRF9c, ISGF-3c, STAT1c and STAT2c) were added to PK model molecules by loading from template provided by Mobi as cellular model. The values for fraction unbound, molecular weight, lipophilicity and solubility were set at Reference point. The *Simulation settings* were set to similar start time, end time and resolution as that from COPASI. The transport reactions were merged in the *Passive transports* building block from PK model to cellular model. Whenever they had conflict, they were implemented manually. For the molecules like STAT1, IRF9, ISGF-3c, STAT1c and STAT2c the PassiveDiffusion Pl2Int & PassiveDiffusion Int2Cell were added as they were excluded molecules. Next, the reactions building block of PK model was merged with cellular model. A new *Molecule Start Value (MSV)* block was created using the updated spatial structure and the merged molecules and all the molecules were set to *not present*. This MSV was saved as pkml and then merged with cellular model MSV. For this building block, on conflict the existing objects were chosen to be kept. This combined MSV was merged with an empty MSV.

The merged MSV was opened and the following was taken care of for the molecules IRF9c, ISGF-3c, STAT1 and STAT2 ; set up of *is present = true* in:

- Liver—Pericentral—Interstitial
- Liver—Pericentral—Plasma
- Liver—Periportal—Interstitial
- Liver—Periportal—Plasma
- Liver—Periportal—Intracellular

Finally, the *Parameter Start Values (PSV)* of PK model were merged with cellular model. The final PBPK/PD model was ready and could be created by *Create simulation* in MoBi.

B.4 Human PBPK/PD model analysis

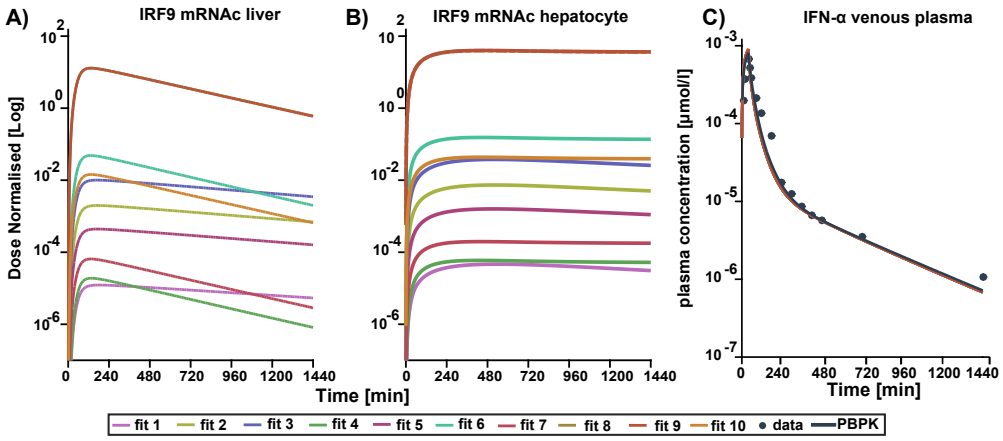

FIGURE B.9: The model ensemble results w.r.t. to the readout, IRF9 mRNAc and the effect of the PD on the IFN-α PK in venous blood is plotted here. It has to be noted that the absolute differences for IRF9 mRNAc are huge. This is because we do not have calibrated absolute measurements for IRF9 mRNAc, therefore, the model ensemble is not able to predict and estimate the same. However, we can work with the relative changes here and hence in the work, everything is dealt with relative changes and normalised for the same. The dose normalised time course of IRF9 mRNAc in A) *in vivo* PBPK/PD model and B) *in vitro* Hepatocyte model is plotted. In C) the result of the model ensemble PD integration (with the feedback SOCS to the receptors) on the IFN-α PK in venous blood for the *in vivo* PBPK/PD model is plotted.

IRF9 mRNAc Tmax		
fit no.	PBPK/PD Liver	Hepatocyte
1	3.034	8.93
2	2.85	8.68
3	2.83	8.71
4	2.26	7.21
5	2.84	8.58
6	2.2	7.41
7	2.21	7.34
8	2.23	7.61
9	2.22	7.62
10	2.23	7.43

FIGURE B.10: IRF9 mRNAc Tmax: In this table one sees the difference in time scale of achieving the maximum concentrations in the top ten models for PBPK/PD model in the liver and in the hepatocyte (*in vitro*) conditions.

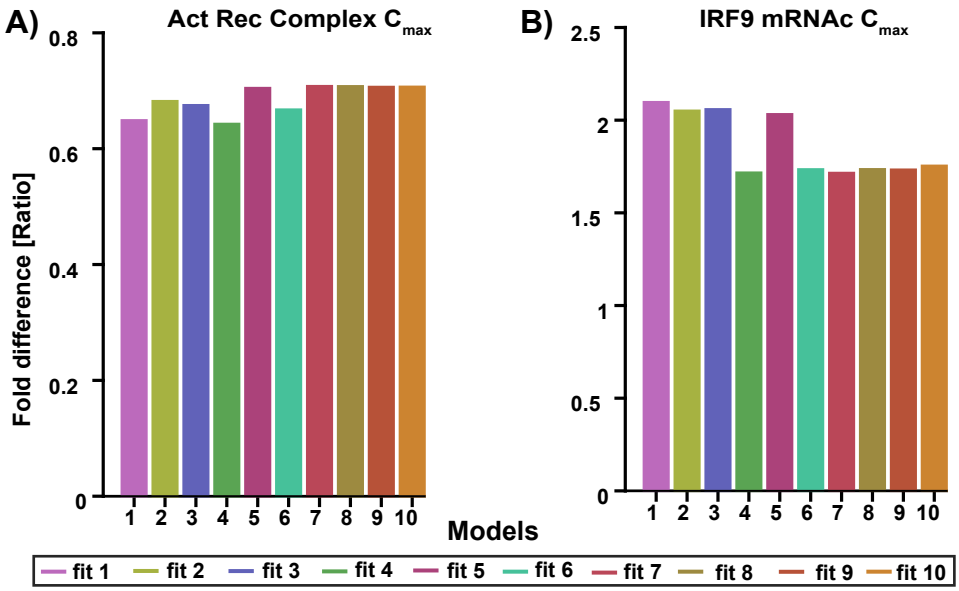

FIGURE B.11: C_{max} of response for the model ensemble for identical doses in PBPK/PD model vs. hepatocyte model: Relative fold difference calculated by simulating the *in vivo* dose (0.7 nmol/l) at the liver from the dose of 36 U injected) of IFN-α for PBPK/PD and *in vitro* model. The model ensemble relative fold difference (bar for each model) in the C_{max} for A) Activated receptor complex and B) IRF9 mRNAc.

Appendix C

Appendix Chapter 4

C.1 PBPK model parameterisation

C.1.1 Literature values for the mouse PBPK model

TABLE C.1: Pharmacokinetic data of mu-IFN-α published by different groups.
The data was used to fit and validate the pharmacokinetic model using PK-Sim.

Parameter	M. Köster data	Bohoslawec et al. (1986)	Rosztoeczy et al. (1986)	Kiuchi et al. (1983)
dose (IU per animal)	5000	870000	42000	100000
dose per body weight (mg/kg)	0.00170068	0.21080	0.1666	0.1587
plasma volume (ml)	0.497	0.497	0.497	0.497
molecular weight (IFN in g/mol)	21524	21524.12	21524.12	21524.12
specific activity (IU/mg)	140000000	196523713.5	120000000	30000000
specific activity (IU/nmol)	-	4230000	258289.44	645723.6
body weight (kg)	0.021	0.021	0.021	0.021

TABLE C.2: Molecular weight of mu-IFN-α found in UniProt of Drugbank.

Molecular weight of mu-IFN-α		
mu-IFN-α subtype	UniProt identifier Drugbank identifier	MW (g/mol) some calculated from protein sequence
IFN-α2 (mouse)	P01573	21921.55
IFN-α4 (mouse)	P07351	21524.12
IFN-αb (mouse)	P01575	22126.77
Roferon IFN-α2 (recombinant, human)		19241.1
IFN-αb (human) variant	P01574	22293.88
Natural IFN-α	DB05258	20700 (range 19300-22100)
peg IFN-α-2a	DB00008	60000

C.1.2 Simulation values for the mouse PBPK model

TABLE C.3: This table contains the information about parameters used for initialising the mouse individuals for PBPK model.

Biometrics	
Species	Mouse
Population	Mouse
Gender	Unknown
Weight	0.021 kg

TABLE C.4: The mouse liver compartment is divided into the interstitial, cytoplasmic and nuclear compartment. The volume of the interstitial and the cytoplasm is borrowed from PK-sim organ values while the nuclear compartment was assigned the value 1:4 ratio of the cytoplasm as calculated from the experiments done for Maiwald et al. [116] where the ratio of the nucleus to cytoplasm was measured.

Volume in Litres	
Compartment	l
Interstitial	0.0002119
Cytoplasm	0.000768
Nucleus	0.000171

TABLE C.5: This table contains the literature values and the fitted values of the pharmacokinetic parameters used in the PBPK human. The parameters were varied 20% for the parameter estimation.

Parameter	Fitted Value	Literature Value	Reference	Unit
Lipophilicity (Log P)		-0.366	[165]	Log units
Fraction unbound (fu)		1		
Solubility		100	[165]	mg/ml (ref. pH is 7)
		mu-IFN-α		
Molecular weight	19500	21922	Uniprot (20.4.2017) P01573	g/mol
IFNAR1 concentration	0.26	-		μmol/l
IFNAR2 concentration	0.5	-		μmol/l
CLplasma (kidney)	9.26	10 -15.65	[39]	ml/min/kg
K_{off} IFNAR1	1E-03	1	[91]	1/s
K_{off} IFNAR2	0.03	0.015	[91], [281]	1/s
K_D IFNAR1	1.01E-05	5	[91]	μmol/l
K_D IFNAR2	3	0.002-0.1	[91], [281]	nmol/l
$K_{endocytosis}$	1.00E-04	-		1/min
K_t_IFNAR1	6.66E-09	-	-	1/min
K_t_IFNAR2	1.72E-06	-	-	1/min

TABLE C.6: The parameter values of the top 5 fits for the PBPK model of mouse IFN-α are listed.

Parameter Name	**Unit**	**Fit 1**	**Fit2**	**Fit3**	**Fit4**	**Fit5**
K_t IFNAR2	1/min	1.72E-06	3.13E-06	2.74E-06	2.10E-07	1.98E-07
K_t IFNAR1	1/min	6.66E-09	1.71E-09	2.36E-08	2.29E-07	8.51E-08
R1 concentration	pmol/ml	0.17	0.02	0.02	0.23	0.04
R2 concentration	pmol/ml	0.46	0.6	0.37	0.59	0.53
Complex K_{off}	1/min	1E-03	1.74E-06	5.74E-06	3.47E-06	1.14E-04
Complex binding K_D	μ mol/l	1.01E-05	8.4E-03	6.1E-03	6.62E-03	2.28E-07
k endocytosis	1/ min	1.00E-04	1.00E-04	1.27	9.3E-03	4.62E-05
IFNAR2 binding K_{off}	1/s	0.03	0.03	0.05	0.05	6.59E-04
IFNAR2 binding K_D	nmol/l	3	3	3	3	4.06
Plasma Clearance	ml/min/kg	9.26	9.34	9.19	9.50	8.76

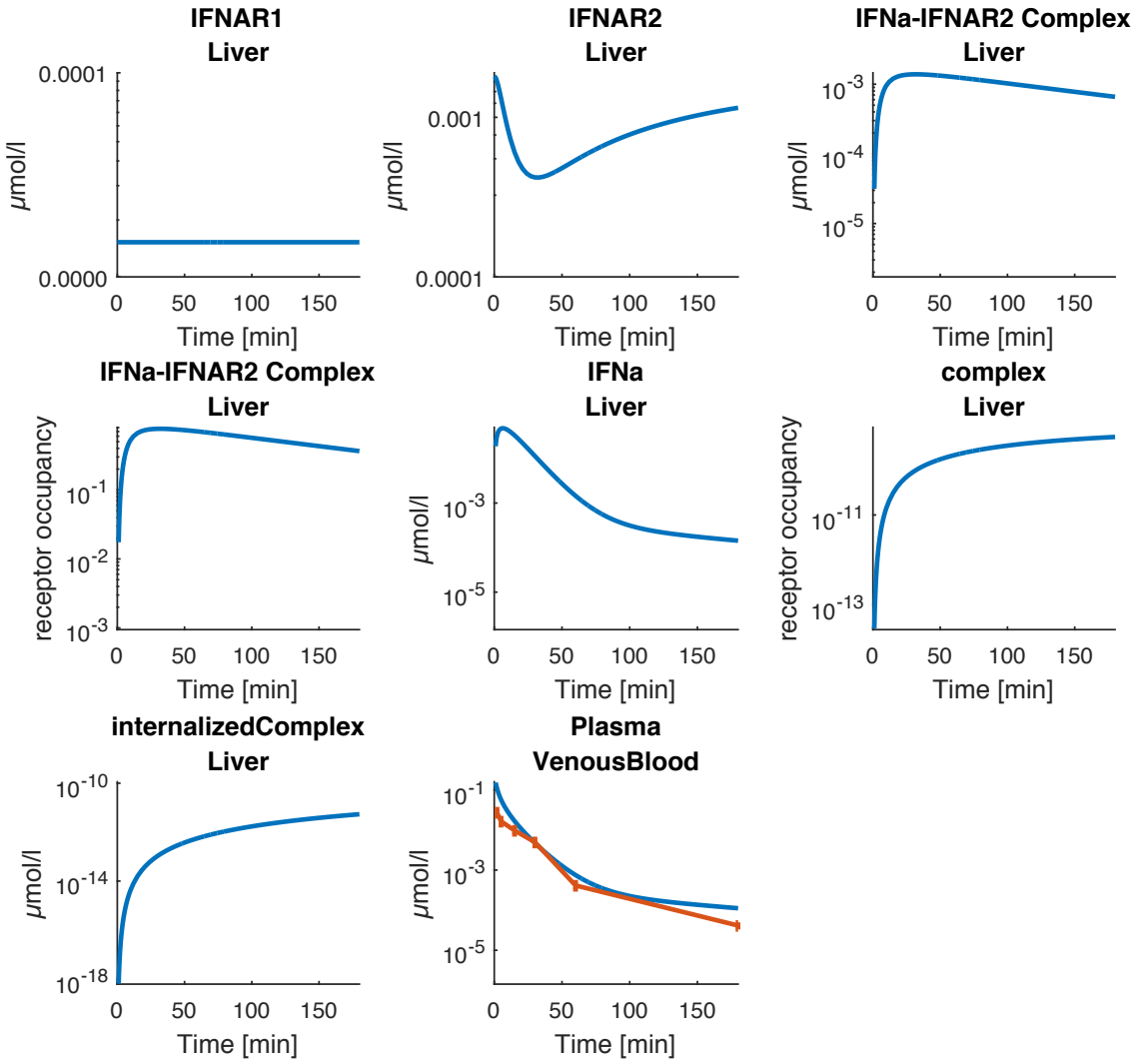

FIGURE C.1: Semi-logarithmic plot of the simulations of *fit 2* where the receptor ratio were not realistic biologically. The model species concentrations in the liver, receptor occupancy of R1 and R2 and murine IFN-α concentration in venous blood are plotted. The ratio of the receptor concentration for this fit was 30 : 1 when the observed ratio in the literature is 2 : 1 [90]. Therefore this fit was not used for further evaluation. The y-axis show the concentration of the species depicted in the title while the x-axis represents the time-course. The dataset in the last plot is the dataset from Bohoslawec et al. [39] and is plotted as the orange solid line.

C.2 Hepatocyte model parameterisation

C.2.1 Literature values for the mouse hepatocyte model

TABLE C.7: This table contains the the sequence identities and the homology of the proteins in the JAK/STAT pathway for the species human and mouse. In BLASTP the Query was human and the subject was mouse.

Name	Species	UniProt ID	Identities (%)	Homology (%)
IFNA	Human IFNA2	P01563	57	75
	Mouse IFNA4	P07351		
IFNAR1	Human	P17181	49	66
	Mouse	P33896		
IFNAR2	Human	P48551	47	63
	Mouse	O35664		
JAK1	Human	P23458	94	96
	Mouse	P52332		
TYK2	Human	P29597	80	86
	Mouse	Q9R117		
STAT1	Human	P42224	92	94
	Mouse	P42225		
STAT2	Human	P52630	73	82
	Mouse	Q9WVL2		
IRF9	Human	Q00978	70	79
	Mouse	Q61179		
SOCS1	Human	O15524	95	96
	Mouse	O35716		

C.2.2 Mouse hepatocyte model parameterisation

TABLE C.8: The below table represents parameterisations of the kinetic values obtained for the model ensemble. The receptor values were preserved from the mouse PBPK model and the IFN efflux values have been maintained from the human hepatocyte model. These values can be found in C.9. Most of the values were taken from the human hepatocyte model under the assumption that the proteins in the cascade exhibit a high homology between mouse and humans.

Nr.	Parameter	fit 1	fit 2	fit 3	fit 4	fit 5	fit 6	fit 7	fit 8	fit 9	fit 10	Units
R4 & M3	Kms	6.13131	6.13131	6.13131	6.13131	6.13131	6.13131	6.13131	1.48411e-05	1.48411e-05	1.48411e-05	nmol/l
	V	2.61285	2.61285	2.61285	2.61285	2.61285	2.61285	2.61285	0.0424023	0.0424023	0.0424023	nmol/(l*s)
	Ka	200	200	200	200	200	200	200	219.203	219.203	219.203	nmol/l
R5 & M6	k1	0.0035	0.0035	0.0035	0.0035	0.0035	0.0035	0.0035	0.00212197	0.00212197	0.00212197	l/(nmol*s)
R6 & M7	k1	0.000393	0.000393	0.000393	0.000393	0.000393	0.000393	0.000393	0.00614481	0.00614481	0.00614481	l/(nmol*s)
R7 & M8	k1	10	10	10	10	10	10	10	15	15	15	l/(nmol*s)
R8 & M9	k1	0.00697	0.00697	0.00697	0.00697	0.00697	0.00697	0.00697	0.000214199	0.000214199	0.000214199	1/s
R9 & M10	k1	3.54e-05	3.54e-05	3.54e-05	3.54e-05	3.54e-05	3.54e-05	3.54e-05	3.72397e-05	3.72397e-05	3.72397e-05	1/s
R10 & M11	k	5.879e-06	5.879e-06	5.879e-06	5.879e-06	5.879e-06	5.879e-06	5.879e-06				nmol/(l*s)
	Ka	0.333955	0.333955	0.150564	0.333955	0.333955	0.333955	0.333955				nmol/l
R11 & M12	k1	1.17183e-05	1.17183e-05	1.17183e-05	1.17183e-05	1.17183e-05	1.17183e-05	1.17183e-05				1/s
R12 & M13	k1	0.000124514	1e-06	2.42899e-05	1e-06	0.00381719	3.35844e-06	4.3915e-05	0.000128617	1.04454e-06	1e-06	1/s
R13 & M14	k1	8.95158e-06	0.000122594	0.000122763	0.000122986	8.67761e-06	8.25502e-06	4.3915e-05	0.000162536	7.10343e-05	7.09477e-05	1/s
R14 & M15	irf9deg	1e-07	1e-07	1e-07	1e-07	1e-07	1e-07	1e-07	0.000577	0.000577	0.000577	1/s
	k_const	4.5e-06	4.5e-06	4.5e-06	4.5e-06	4.5e-06	4.5e-06	4.5e-06	0.026	0.026	0.026	nmol/(l*s)
	k_act	10	10	10	10	10	10	10	0.356829	0.356829	0.356829	1/s
R15 & M16	k_act	5.70548	5.70548	5.70548	5.70548	5.70548	5.70548	5.70548	4.60042	4.60042	4.60042	1/s
	k_deg	0.16196	0.16196	0.16196	0.16196	0.16196	0.16196	0.16196	0.150743	0.150743	0.150743	1/s
R16 & M17	k_act	0.0039677	2.74342	0.00468499	0.0843807	1e-05	0.0145789	0.00767509	0.267533		2.40468	1/s
	k_deg	0.000122591	8.9514e-06	8.94144e-06	8.93296e-06	0.000129823	0.000144197	0.000139028	7.10296e-05	0.000162515	0.000162876	1/s
R17 & M18	k1	0.0001	0.0001	0.0001	0.0001	0.0001	0.0001	0.0001	0.00209186	0.00209186	0.00209186	l/s
	keq	0.00697504	0.00697504	0.00697504	0.00697504	0.00697504	0.00697504	0.00697504	0.000174285	0.000174285	0.000174285	-
R18 & M19	k1	2.20533e-07	2.20533e-07	2.20533e-07	2.20533e-07	2.20533e-07	2.20533e-07	2.20533e-07	4.83e-10	4.83e-10	4.83e-10	l/s
	keq	0.00197389	0.00197389	0.00197389	0.00197389	0.00197389	0.00197389	0.070818	0.00887611	0.00887611	0.00887611	-
R19 & M20	k1	9.92815e-07	9.92815e-07	9.92815e-07	9.92815e-07	9.92815e-07	9.92815e-07	9.92815e-07	6.54595e-07	6.54595e-07	6.54595e-07	l/s
	keq	0.0297375	0.0297375	0.0297375	0.0297375	0.0297375	0.0297375	0.0297375	3.71093	3.71093	3.71093	-
R20 & M21	k1	0.00774342	0.00774342	0.00774342	0.00774342	0.00774342	0.00774342	0.00774342	8.4268e-06	8.4268e-06	8.4268e-06	l/s
R21 & M22	k1	0.123072	0.123072	0.123072	0.123072	0.123072	0.123072	0.123072	6.42557e-06	6.42557e-06	6.42557e-06	l/(nmol*s)
	keq	2.91162e-05	2.91162e-05	2.91162e-05	2.91162e-05	9.67627	2.91162e-05	2.91162e-05	5.86288	5.86288	5.86288	l/nmol
R22 & M23	k1	0.10365	0.10365	0.10365	0.10365	0.10365	0.10365	0.10365	4.04029	4.04029	4.04029	1/s
R23 & M24	k1	1e-07	1e-07	1e-07	1e-07	1e-07	1e-07	1e-07	0.000577	0.000577	0.000577	1/s

TABLE C.9: The kinetic parameters whose values were fixed for the model ensemble and were borrowed from the PBPK model.

Nr.	Parameter	Value	Unit
R2	k_{off}	0.001	1/s
	k_D	0.0100834	nmol/l
R3	k_{off}	0.03	1/s
	k_D	3	nmol/l

Appendix D

Appendix Chapter 5

D.1 Literature search

TABLE D.1: **Half life of the molecules found in literature.**

Molecule	Half-life (h)	k_d (min^{-1})	References
mIRF9	$[1, 10]$*	$[1.16 \times 10^{-3}, 1.16 \times 10^{-2}]$	[287]
mSOCS	$[1, 10]$*	$[1.16 \times 10^{-3}, 1.16 \times 10^{-2}]$	[287]
mMXA	$[1, 10]$*	$[1.16 \times 10^{-3}, 1.16 \times 10^{-2}]$	[287]
IRF9	2	5.78×10^{-3}	[116]
SOCS1	$[1.5, 3]$	$[3.85 \times 10^{-3}, 7.70 \times 10^{-3}]$	[288], [289]
MXA	55*	2.1×10^{-4}	[261]
MXA+dGFP	4*	2.89×10^{-3}	[82]
STAT1	$[16, 24]$	$[3.1 \times 10^{-4}, 4.81 \times 10^{-4}]$	[288], [290]
STAT2	24	$[3.1 \times 10^{-4}, 4.81 \times 10^{-4}]$	[290]
pSTAT1	2	5.78×10^{-3}	[290]
pSTAT2	2	5.78×10^{-3}	[290]
dimerSTAT	24**	4.81×10^{-4}	[290]
ISGF3	24**	4.81×10^{-4}	[290]
IFN	$[4, 10]$	$[1.16 \times 10^{-3}, 2.89 \times 10^{-3}]$	[197], [198]
Inactive Receptor	$[1, 4]$	$[1.25 \times 10^{-3}, 5.02 \times 10^{-3}]$	[291]

* Typical half life of human mRNAs [287].
** dimerSTAT and ISGF3 are reported to have large half-life.
Degradation rates were calculated as $k_d = ln(2)/\tau$, where τ is the species half-life.

D.1.1 Promoter analysis for MxA and IFIT1

MxA promoter sequence

TCATCAGTTAAGGCTGTTTTTACTTCTTTTGTGGATCTTCAGTTACTTTAGGCCATCTGGATGTATACCTGCAAGTCACAGGGGATGCGATGGCCTGGCCTGGGATG
CGATGGCCTGGCCTGACAACTATTACCTATGTTATGTTTATTATTTTAAGCTTTATTATTACTATTTTATTTATTTTATTTTATTTTCCTTCCACACACCCGTTTCCACC
CTGGAGAGGCCAGATGAGCCAGACTCCAGGGAGGCCTAGAAGTGGGCAAGGGGAAAACGGGAAAGGAGGAAGATGGTATGGGTGTGCCTGGTTAGGGGTGGGA
GTGCTGGACGGAGTTCGGGACAAGAGGGGCTCTGCAGCCATTGGCACACAATGCCTGGGAGTCCCTGCTGGTGCTGGGATCATCCCAGTGAGCCCTGGGAGGGA
ACTGAAGACCCCCAATTACCAATGCATCTGTTTTCAAAACCGACGGGGGGAAGGACATGCCTAGGTTCAAGGATACGTGCAGGCTTGGATGACTCCGGGCCATT

AGGGAGCCTCCGGAGCACCTTGATCCTCAGACGGGCCTGATGAAACGAGCATCTGATTCAGCAGGCCTGGGTTCGGGCCCGAGAACCTGCGTCTCCCGCGAGTT
CCCGCGAGGCAAGTGCTGCAGGTGCGGGGCCAGGAGCTAGGTTTCGTTTCTGCGCCCGGAGCCGCCCTCAGCACAGGGTCTGTGAGTTTCATTTCTTCGCGGCGC
GGGGCGGGGCTGGGCGCGGGGTGAAAGAGGCGAAGCGAGAGCGGA

IFIT1 promoter sequence

TTTTAGACGGAGTCTCGCTCTGTCACCAGACTGGAGTACAGTGGTGTGATCTCGGCTCACTGCAACCTCTGCCTCCCAGGTTCAAGCAATTCCCCTGCCTCAGCCT
CTCGAGTAGGTGGGACTACAGGTGCACACCACCACACCCAGCTAATTTTTTGTATTTTAGTAGAGAGGGGGTTTCACCATGTTGGCCACGATGGTCTCCATCTCCT
GACCTTGTCATCCGCCCACCTTGGCCTCCCAAAGTGCTGGGACTACAGGCATGAGCCACCGCACCCAGCCAAGAATCATTATTTTTAACTTGATGACTGAAAATA
ATAATAATAATAGTTACCACTTATTTGCATGCTTCTATGTGCCAGGTAGTTGCTAACTATTTAAACTCAAATTCCATGAACTGTAGTGGAGGTTGTACTGGAATTTG
ATTCAGAATGACAGTGTCCATGATGGAGCAATAGAGGGCTCTCTATTTCAAACCATACCTCCTTGCTTTTACCTCCTGCCTAAGTCATCAGGGGTTAGAAGGCTTT
CTAGGTATTGGTCTCTTTCCTTCATTCCTAAACCAGATTGGTTGCTTATTTCCGTCAAGCTGAAACCAAAAGTAAGCAACCAAAAAGCAACCAGCAACCAAAAGC
CTTGTTACTCAATTAATTAAGAGTAGATTTTTATATTTGATAGTAGGTTCCTTCTAAATATAGAAACTGAAAATAGAGCTATCTCCTTCAATTCTCCTTTTTCTGTGT
ATTCATCCAGAATCCAGCCACCAACTGCCACAATAGGCAGCAATGGACTGATGTTCTTTAGGGAGGACGTGAATCTCGTTCCAAATGCTGGCCAGTCATTGGGTT
TCTGCAGCACTAGAAACATCTATGGTTGCAGGTCTGCAGTTTATCTGTTTTAAAATAGAAACAAAGTTTCATTCCCCACCCCCCCCCGTCAGCAGGAATTCCGCTA
GCTTTAGTTTCACTTTCCCCTTTCGGTTTCCCTAGGTTTCCAACTT

D.2 Experimental data

The experimental data from flow cytometry was analysed using matlab funciton.

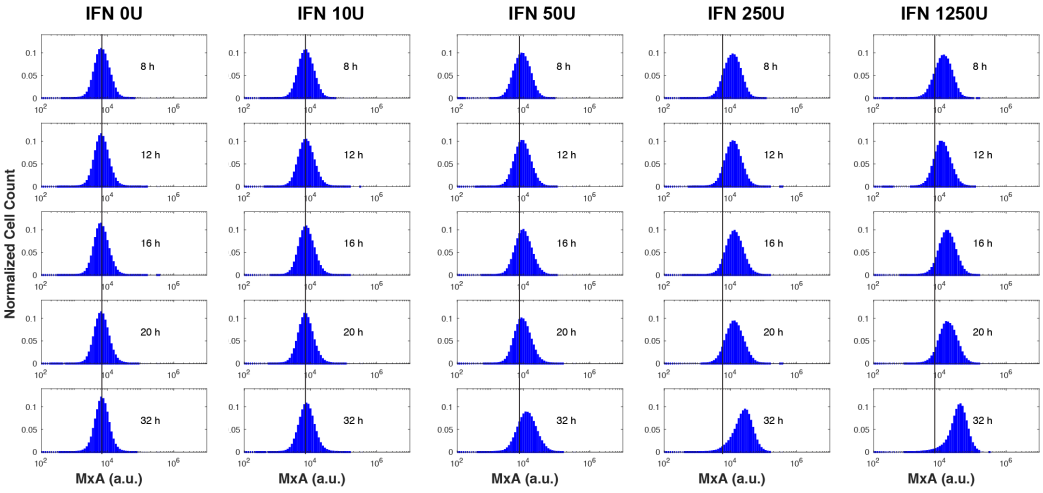

FIGURE D.1: **Figure adapted from Aguilera et al. 2018[244]** Single-cell data in a population of Huh 7.5 cells expressing MxA when stimulated with different doses of IFN-α. This was plotted using matlab function *FCS data reader*. The distribution of the single-cell expression of MxA under different conditions is plotted here(first column, control, without interferon stimulation), subsequent columns represent the MxA expression after multiple IFN doses (from 10 to 1250 UI/mL of IFN-α).

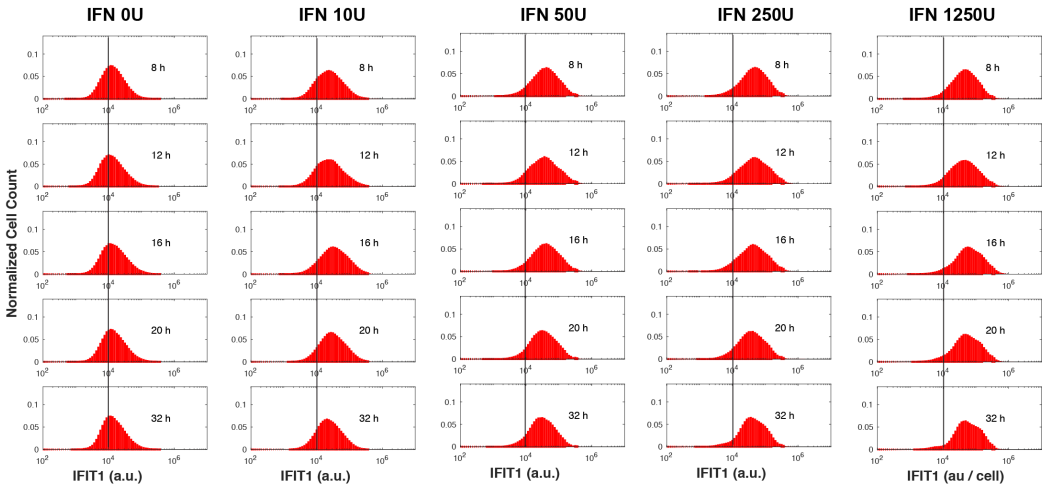

FIGURE D.2: **Figure adapted from Aguilera et al. 2018[244]** Single-cell data in a population of Huh 7.5 cells expressing IFIT1 when stimulated with different doses of IFN-α. This was plotted using matlab function *FCS data reader*. The distribution of the single-cell expression of IFIT1 under different conditions is plotted here(first column, control, without interferon stimulation), subsequent columns represent the MxA expression after multiple IFN doses (from 10 to 1250 UI/mL of IFN-α).

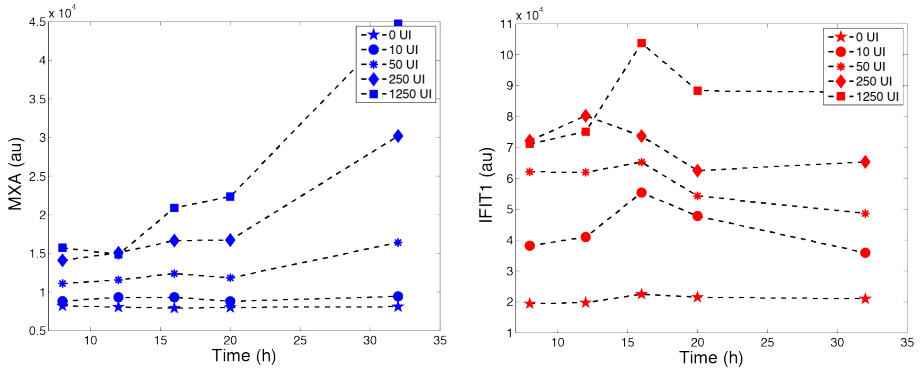

FIGURE D.3: **Figure adapted from Aguilera et al. 2018[244]** The deterministic average of the cell populations was calculated to plot the temporal dynamics of the response of MxA from figure D.1 and IFIT1 from figure D.2 to IFN treatment. The average values indicate that T_{max} of IFIT1 is at 16 hours after IFN stimulation, whereas the T_{max} of MxA were obtained at 32 hours after IFN stimulation.

D.3 Stochastic model parameterisation

TABLE D.2: **System's initial conditions (IC). Table adapted from Aguilera et al. 2018 [244]**

Variable	IC (Molecules/Cell)	References
$^{**}IFN$	$[5 \times 10^3 , 1 \times 10^4]$	Fitted
$R2$	1000	[116], [190], [198], [292]–[294]
RC	10	TS
$R1$	1000	TS
AR	10	TS
$STAT1$	1×10^5	[115], [116], [295], [296]
$STAT2$	1×10^4	[116], [295], [297]
$SOCS$	0	[113]
$^{*}dimerSTAT$	100	[264]
$IRF9$	10	[116]
$^{*}ISGF3$	100	TS
$^{*}pSTAT1$	100	[264]
$^{*}pSTAT2$	100	[264]
IR	0	TS
$irf9$	1	TS
$socs$	1	TS
$isg56$	1	TS
mxa	1	TS
$mIRF9$	10	TS
$mSOCS$	10	TS
$mMXA$	0	TS
$mISG56$	0	TS
MXA	0	TS
$ISG56$	0	TS
I_irf9	0	TS
I_socs	0	TS
I_mxa	0	TS
I_isg56	0	TS

* According to Chatterjee *et al.* [264] there is a very low phosphorylation of STAT proteins, for that reason all forms and complex including phosphorylated STAT proteins are considered to have basal initial concentrations. ** Values for the initial IFN concentration were estimated by fitting the model to the experimental data. Obtaining that 500 U of IFN correspond to 10,000 IFN molecules and 250 U of IFN correspond to 5,000 molecules.

TABLE D.3: **Scaling factors for the stochastic model**

Scaling Factor	Value
φ_1	1.2×10^{-3}
φ_2	1.17×10^{-4}
φ_3	1.79×10^{-4}
φ_4	0.1
φ_5	0.05

TABLE D.4: **Parameter values for the JAK-STAT signalling pathway for the stochastic model. Table adapted from Aguilera et al. 2018 [244]**

Parameter	Nominal	Units	References
k_1	1.146×10^{-5}	Cell/(Molecules·min)	Fitted
k_2	1.136×10^{-3}	Cell/(Molecules·min)	Fitted
k_3	1.56×10^{-5}	Cell/(Molecules·min)	Fitted
k_4	1.96×10^{-5}	Cell/(Molecules·min)	Fitted
k_5	1×10^{-4}	Cell/(Molecules·min)	Fitted
k_6	1×10^{-5}	Cell/(Molecules·min)	Fitted
k_7	1.60×10^{-3}	Molecules/(Cell·min)	Fitted
k_8	3.15	Cell/min	Fitted
k_9	3.15	Cell/min	Fitted
k_{10}	1.12×10^{-3}	Molecules/(Cell·min)	Fitted
k_{11}	3.69	Cell/min	Fitted
k_{12}	1.11	Molecules/(Cell·min)	Fitted
k_{13}	5.06×10^{-5}	1/min	Fitted
k_{14}	1×10^{-3}	Molecules/(Cell·min)	Fitted
k_{15}	0.235	1/min	Fitted
k_{16}	0.0725	Molecules/(Cell·min)	Fitted
k_{17}	1.53×10^{-5}	1/min	Fitted
$^{\ddagger}k_{18}$	3.00	1/min	[298]
$^{\ddagger}k_{19}$	9.653×10^{-2}	1/min	[298]
$^{\ddagger}k_{20}$	2×10^{-2}	1/min	[298]
$^{\ddagger}k_{21}$	1.5×10^{-3}	1/min	[298]
$^{\dagger}k_{22}$	1.61	1/min	[299]
$^{\dagger}k_{23}$	0.1	1/min	[299]
$^{\dagger}k_{24}$	0.911	1/min	[299]
$^{\dagger}k_{25}$	27.09	1/min	[299]
k_{26}	5.02×10^{-4}	1/min	[287]
k_{27}	5.02×10^{-3}	1/min	[287]
k_{28}	1.7×10^{-3}	1/min	[287]
k_{29}	7.4×10^{-3}	1/min	[287]
k_{30}	6.08×10^{-2}	1/min	TS
k_{31}	3.34×10^{-3}	1/min	[290]
k_{32}	3.49×10^{-4}	1/min	[116]
k_{33}	1.6×10^{-3}	1/min	[288], [289]
k_{34}	2.70×10^{-4}	1/min	[288], [290]
k_{35}	2.09×10^{-4}	1/min	[290]
k_{36}	0.125	1/min	[290]
k_{37}	1.65×10^{-5}	1/min	[290]
k_{38}	1.05×10^{-6}	1/min	[261]
k_{39}	2.09×10^{-2}	1/min	[290]
k_{40}	2×10^{-3}	1/min	[197], [198]

† Translations rates assumed to be close to reported averages times ≈ 16 Proteins/mRNA/min [299] . ‡ Transcription rates was assumed to be close to reported averages times to produce a mRNA ≈ 20 min [298]. IFNR dissociation constant of 10^{-9},10^{-11} [292]. RNA half-life was assumed close to the average value reported by [287] This study (TS).

Acknowledgements

Seven years ago I moved to Germany and took a deep dive into my passion for science with a Masters program in systems biology. While I was on my way to complete my masters, I was not sure whether I want to pursue an academic PhD or join the professional world. During those times, Dr. Ursula Kummer, who has been more than a supervisor to me, offered me a PhD position at the university with an industrial collaboration. I cannot thank her enough for providing me with an opportunity that I later realised was worth all my efforts. I would use this opportunity to express my deepest appreciation for her persistent help and guidance, giving me a bunch of people who never made me miss home and to the foremost, for being an outstanding supervisor.

I cannot be more glad to have Dr. Lars Küpfer from Bayer Healthcare as my second supervisor. It is rare that you get to work with someone who establishes a relationship that feels less of a supervisor and more of an inspiring mentor. His politeness, patience and support during the bumpy rides of my work have been immeasurable. In spite of being a long distance supervisor, his doors were always open whenever I ran into a trouble spot. I've never missed his advice or small personal connection and it has been my utmost pleasure to work with him.

Therefore, I am highly glad to have two amazing supervisors who paved my way in these four years of PhD and provided me a strong and positive definition for leadership and team management. They helped me to grow as a person and to learn so much outside science as well.

I wish to express my sincere thanks to the people in the department of Modelling of Biological Processes and friends in Bioquant at Heidelberg University, for making me feel at home during my doctoral studies. The love and support I received from my colleagues is worth mentioning. I thank Dr. Luis Aguilera, my ex office-mate, a mentor and a great friend during this time. His constant presence and support is something I am indebted to. I thank Frank Bergmann for the COPASI versions and for writing special python scripts for my work. Gratitude to Klaus Kapplings for persistent endeavour on my German and great apple fests every year. Thanks to Jocelyn and Nana for handling all the administrative and bureaucratic tasks. Thanks to Nadine, who has been more of a friend and a person to go to for advises, and to my peer, Babak, Lilija, Pascal and Ruth for the amazing times and the chats on small but essential matters. Finally, a thanks to Verena and Rebekka, I got a chance to co-supervise them and in the process, learnt a lot about being a mentor.

I had some great times at Bayer Pharmaceuticals in Leverkuesen and I would like to thank the people there for their immense support towards my work, especially, Thomas Gaub who has been available to help me setup the difficult-to-achieve PBPK/PD model and for being steadily responsive to all my questions. I would like to also thank Dr. Christoph Niederalt for the fruitful discussions on the protein PBPK models.

I would like to take this opportunity to thank my collaborators, without whom I would not have learnt to work in a collaborative, inter-disciplinary environment. I am grateful to Dr. Mario Köster for the effort and discussions on mouse model and mouse cell-line experiments. Dr. Marco Binder for the active involvement in the topic, constant ideas, efforts and support. I thank Prof. Dr. Ralf Bartenschlager for his time and the positive feedback for the topics. I acknowledge the responsiveness and engaging spirit of Pascal Mutz and Christopher Daechert, who not only performed the experiments but were also available for brainstorming discussions.

I place on record, my sincere thanks to the HGS MathComp graduate school for helping me hone my skills, for providing me the financial support to travel for various conferences and for a friendly and positive environment. I want to express my sincere appreciation to the scientific and administrative staff in University Heidelberg for helping me throughout studies.

As quoted by Lewis Carroll *One of the secrets of life is that all that is really worth the doing is what we do for others* - my PhD was worth its time because of my friends and family. Therefore, a big hug, love and thank you to all my friends, far and near. In these years, a fair amount of personal time was spent on making friends like family, having fun and making memories which I cherish immensely when I look back. I have learnt so much in these years, which would not have been possible without you all :). My immense love and gratitude to my childhood friends, Aboli, Akshe, Arjun, Bibhor, Pranjal, Shruti, Swati and Vishal, for sticking with me through all stages of my identity crisis and being a reason of me being super occupied on my phone! My thanks to the friends that have made Germany feel no less than India and have been partner in crime for all my naughtiness, hence never letting the kid inside me die and also for being a part of pushing me to overcome things outside my comfort-zone: Akshat (for the poems, the long drives and being a rock for the friendship), Nick (for the swimming classes motivation, hugs, food wars and love as warm as home), Jan (for being the weird one!), Julia (for the girl time, the chatter, the hugs and the love! Pure poison!), Jannis (for the long-distance friendship and the lovely breads and cakes that you have baked in these years!), Piyu (for being my 'better half' at everything!), Puneet (for disco, disco, party, party!), Thomas (for being the pragmatic voice in my head, the best nerd of my life and one of the first friends I got in my times here), Tim (for the great times we spent together and for Emil!) to name a few. I am glad to have friends from BioQuant who have been a constant source of support, have been the reason of my love for 'Dunkles', great parties and have seen me grow from a naive Priyata to a more balanced one: Arne (for being a good listener), Gustavo (for the fun times of overcooked and for being the plotter!), Jonas (for the R scripting superhero that he is), Jan (for the invites to KIP barbecues and the chatter on video-games), Michael (for forcibly keeping our friendship "distant"), Neha (for the small heart to heart chats), Paola (the most awesome office/girl time), Pete (for the fun conversations on ecological conservation and having his sons presence absolutely break his character), Sam (for lovely British style onion bhaji), Verena (for the french trips, the french wine, the gossips and the girl time) and Vineet (for just being naggy!). Finally, music has been very important to me and I am glad to have friends who supported my childhood dreams to see some of my favourite rock bands: Mauricio, Jari and especially Fabian, who has given me a memory of Meshuggah for life!

Lastly, immense gratitude to my parents Dinesh and Vanita for being the absolute chill parents I could get. Your catching up to technology for your daughters and the amazing whatsapp emoticons never made me feel less loved. I would not be here today if it were not for you, for your vision and the sacrifices that you have done for us. Thank you for the love, support and continuous encouragement. Meeta, thank you for the little princess of joy you have been as a sister. I hope you know that I absolutely dig on the fact that we can discuss anything and that sometimes you have swapped role of an elder sister with me. I have had a childhood filled with love and laughter with you. 15 years ago, when I moved out of home, I could not imagine that the little girl who sat on my suitcase crying and not letting me go would be my best friend now. I am pretty lucky to have the three of you, who are literally- my world.

Thank you.

Bibliography

[1] S. Cohen, P. E. Bigazzi, and T. Yoshida, "Similarities of t cell function in cell-mediated immunity and antibody production", *Cellular Immunology*, vol. 12, no. 1, pp. 150 –159, 1974, ISSN: 0008-8749. DOI: https://doi.org/10.1016/0008-8749(74)90066-5. [Online]. Available: http://www.sciencedirect.com/science/article/pii/0008874974900665.

[2] J. J. O'Shea, M. Gadina, and R. Siegel, "9 - cytokines and cytokine receptors", in *Clinical Immunology (Fourth Edition)*, R. R. Rich, T. A. Fleisher, W. T. Shearer, H. W. Schroeder, A. J. Frew, and C. M. Weyand, Eds., Fourth Edition, London: Content Repository Only!, 2013, pp. 108 –135, ISBN: 978-0-7234-3691-1. DOI: https://doi.org/10.1016/B978-0-7234-3691-1.00033-7. [Online]. Available: https://www.sciencedirect.com/science/article/pii/B9780723436911000337.

[3] M Feldmann and R. N. Maini, "Anti-TNF alpha therapy of rheumatoid arthritis: what have we learned?", *Annual review of immunology*, vol. 19, pp. 163–96, 2001, ISSN: 0732-0582. DOI: 10.1146/annurev.immunol.19.1.163. [Online]. Available: http://www.ncbi.nlm.nih.gov/pubmed/11244034.

[4] P. J. Barnes, "Review series The cytokine network in asthma and chronic obstructive pulmonary disease", *The Journal of clinical investigation*, vol. 118, no. 11, pp. 3546–3556, 2008, ISSN: 0021-9738. DOI: 10.1172/JCI36130.3546.

[5] L. C. Borish, H. S. Nelson, J. Corren, G. Bensch, W. W. Busse, J. B. Whitmore, J. M. Agosti, A. Buchmeier, S. Fell, L. Fuller, C. Gallegos, P. Hall, Y. Kim, P. McHugh, S. Vallery, R. Hanna, and L. A. Bauer, "Efficacy of soluble IL-4 receptor for the treatment of adults with asthma", *Journal of Allergy and Clinical Immunology*, vol. 107, no. 6, pp. 963–970, 2001, ISSN: 00916749. DOI: 10.1067/mai.2001.115624.

[6] E. Vacchelli, F. Aranda, N. Bloy, A. Buqué, I. Cremer, A. Eggermont, W. H. Fridman, J. Fucikova, J. Galon, R. Spisek, L. Zitvogel, G. Kroemer, and L. Galluzzi, "Trial Watch Immunostimulation with cytokines in cancer therapy", *OncoImmunology*, vol. 5, no. 2, 2016, ISSN: 2162402X. DOI: 10.1080/2162402X.2015.1115942.

[7] L. Steinman, *Nuanced roles of cytokines in three major human brain disorders*, 2008. DOI: 10.1172/JCI36532.

[8] A. Isaacs and J. Lindenmann, "Virus Interference. I. The Interferon", *Proceedings of the Royal Society B: Biological Sciences*, vol. 147, no. 927, pp. 258–267, 1957, ISSN: 0962-8452. DOI: 10.1098/rspb.1957.0048. [Online]. Available: http://rspb.royalsocietypublishing.org/cgi/doi/10.1098/rspb.1957.0048.

[9] S. Goodbourn, L. Didcock, and R. E. Randall, *Interferons: Cell signalling, immune modulation, antiviral responses and virus countermeasures*, 2000. DOI: 10.1099/0022-1317-81-10-2341.

[10] D. B. Stetson and R. Medzhitov, *Type I Interferons in Host Defense*, 2006. DOI: 10.1016/j.immuni.2006.08.007.

[11] V. van Pesch, H. Lanaya, J.-C. Renauld, and T. Michiels, "Characterization of the murine alpha interferon gene family.", *Journal of virology*, vol. 78, no. 15, pp. 8219–28, 2004, ISSN: 0022-538X. DOI: 10.1128/JVI.78.15.8219-8228.2004. [Online]. Available: http://www.ncbi.nlm.nih.gov/pubmed/15254193{\%}5Cnhttp://www.pubmedcentral.nih.gov/articlerender.fcgi?artid=PMC446145.

[12] M. Aguet, M. Grobke, and P. Dreiding, "Various human interferon a subclasses cross-react with common receptors: Their binding affinities correlate with their specific biological activities", *Virology*, vol. 132, no. 1, pp. 211–216, 1984, ISSN: 10960341. DOI: 10.1016/0042-6822(84)90105-3.

[13] "Characterization of the type I interferon locus and identification of novel genes", *Genomics*, vol. 84, no. 2, pp. 331–345, 2004, ISSN: 0888-7543 (Print) 0888-7543 (Linking). DOI: 10.1016/j.ygeno.2004.03.003.

[14] S Pestka, "The human interferon-alpha species and hybrid proteins", *Seminars in Oncology*, vol. 24, no. 3 Suppl 9, pp. 4–17, 1997, ISSN: 0093-7754.

[15] P. P. Trotta, "Preclinical biology of alpha interferons", *Semin Oncol*, vol. 13, no. 3 Suppl 2, pp. 3–12, 1986, ISSN: 00937754. [Online]. Available: http://www.ncbi.nlm.nih.gov/entrez/query.fcgi?cmd=Retrieve{\&}db=PubMed{\&}dopt=Citation{\&}list{_}uids=3532333.

[16] M. J. Hawkins, E. C. Borden, J. A. Merritt, B. S. Edwards, L. A. Ball, E. Grossbard, and K. J. Simon, "Comparison of the biologic effects of two recombinant human interferons alpha (rA and rD) in humans", *Journal of Clinical Oncology*, vol. 2, no. 3, pp. 221–226, 1984, ISSN: 0732183X. DOI: 10.1200/JCO.1984.2.3.221.

[17] S. Pestka, *The interferons: 50 Years after their discovery, there is much more to learn*, 2007. DOI: 10.1074/jbc.R700004200.

[18] K. Gibbert, J. F. Schlaak, D. Yang, and U. Dittmer, *IFN-α subtypes: Distinct biological activities in anti-viral therapy*, 2013. DOI: 10.1111/bph.12010.

[19] L. Runkel, L. Pfeffer, M. Lewerenz, D. Monneron, C. H. Yang, A. Murti, S. Pellegrini, S. Goelz, G. Uzé, and K. Mogensen, "Differences in activity between α and β type I interferons explored by mutational analysis", *Journal of Biological Chemistry*, vol. 273, no. 14, pp. 8003–8008, 1998, ISSN: 00219258. DOI: 10.1074/jbc.273.14.8003.

[20] J. F. Schlaak, M. Trippler, C. Hoyo-Becerra, Y. Erim, B. Kis, B. Wang, N. Scherbaum, and G. Gerken, "Selective hyper-responsiveness of the interferon system in major depressive disorders and depression induced by interferon therapy", *PLoS ONE*, 2012, ISSN: 19326203. DOI: 10.1371/journal.pone.0038668.

[21] J. F. Schlaak, C. M. U. Hilkens, A. P. Costa-Pereira, B. Strobl, F. Aberger, A. M. Frischauf, and I. M. Kerr, "Cell-type and donor-specific transcriptional responses to interferon-alpha: Use of customized gene arrays", *Journal of Biological Chemistry*, 2002, ISSN: 00219258. DOI: 10.1074/jbc.M205571200.

[22] E.-M. Wolber, B Haase, and W Jelkmann, "Thrombopoietin production in human hepatic cell cultures (HepG2) is resistant to IFN-α, IFN-β, and IFN-γ treatment", *Journal of Interferon and Cytokine Research*, 2002, ISSN: 1079-9907. DOI: 10.1089/10799900260475704.

[23] E. A. Havell, T. G. Hayes, and J. Vilček, "Synthesis of two distinct interferons by human fibroblasts", *Virology*, vol. 89, no. 1, pp. 330–334, 1978, ISSN: 10960341. DOI: 10.1016/0042-6822(78)90068-5.

[24] E. A. Havell and G. L. Spitalny, "Endotoxin-induced interferon synthesis in macrophage cultures.", *Journal of the Reticuloendothelial Society*, vol. 33, no. 5, pp. 369–380, 1983, ISSN: 00336890.

[25] H. Cucak, U. Yrlid, B. Reizis, U. Kalinke, and B. Johansson-Lindbom, "Type I Interferon Signaling in Dendritic Cells Stimulates the Development of Lymph-Node-Resident T Follicular Helper Cells", *Immunity*, vol. 31, no. 3, pp. 491–501, 2009, ISSN: 10747613. DOI: 10.1016/j.immuni.2009.07.005.

[26] M. Kuwana, J. Kaburaki, T. M. Wright, Y. Kawakami, and Y. Ikeda, "Induction of antigen-specific human CD4+T cell anergy by peripheral blood DC2 precursors", *European Journal of Immunology*, vol. 31, no. 9, pp. 2547–2557, 2001, ISSN: 00142980. DOI: 10.1002/1521-4141(200109)31:9<2547::AID-IMMU2547>3.0.CO;2-J.

[27] F. P. Siegal, N. Kadowaki, M. Shodell, P. A. Fitzgerald-Bocarsly, K. Shah, S. Ho, S. Antonenko, and Y. J. Liu, "The nature of the principal Type 1 interferon-producing cells in human blood", *Science*, vol. 284, no. 5421, pp. 1835–1837, 1999, ISSN: 00368075. DOI: 10.1126/science.284.5421.1835.

[28] J. J. Ferbas, J. F. Toso, A. J. Logar, J. S. Navratil, and C. R. Rinaldo Jr., "CD4+ blood dendritic cells are potent producers of IFN-alpha in response to in vitro HIV-1 infection", *J Immunol*, vol. 152, no. 9, pp. 4649–4662, 1994, ISSN: 0022-1767. [Online]. Available: http://www.ncbi.nlm.nih.gov/entrez/query.fcgi?cmd=Retrieve{\&}db=PubMed{\&}dopt=Citation{\&}list{_}uids=7908920.

[29] J Banchereau, F Briere, C Caux, J Davoust, S Lebecque, Y. J. Liu, B Pulendran, and K Palucka, "Immunobiology of dendritic cells.", *Annual review of immunology*, vol. 18, pp. 767–811, 2000, ISSN: 0732-0582. DOI: 10.1146/annurev.immunol.18.1.767. arXiv: arXiv:1011.1669v3. [Online]. Available: http://www.ncbi.nlm.nih.gov/pubmed/10837075.

[30] M. W. BEILHARZ, W. McDONALD, M. W. WATSON, J. HENG, J. McGEACHIE, and C. M. LAWSON, "Low-Dose Oral Type I Interferons Reduce Early Virus Replication of Murine Cytomegalovirus In Vivo", *Journal of Interferon & Cytokine Research*, vol. 17, no. 10, pp. 625–630, 1997, ISSN: 1079-9907. DOI: 10.1089/jir.1997.17.625. [Online]. Available: http://www.liebertonline.com/doi/abs/10.1089/jir.1997.17.625.

[31] X Hu, S. Chakravarty, and L. Ivashkiv, "Regulation of IFN and TLR Signaling During Macrophage Activation by Opposing Feedforward and Feedback Inhibition Mechanisms", *Immunological reviews*, pp. 41–56, 2008, ISSN: 0105-2896. DOI: 10.1111/j.1600-065X.2008.00707.x.Regulation. [Online]. Available: http://onlinelibrary.wiley.com/doi/10.1111/j.1600-065X.2008.00707.x/full.

[32] W. a. Tompkins, "Immunomodulation and therapeutic effects of the oral use of interferon-alpha: mechanism of action.", *Journal of interferon & cytokine research : the official journal of the International Society for Interferon and Cytokine Research*, vol. 19, no. 8, pp. 817–28, 1999, ISSN: 1079-9907. DOI: 10.1089/107999099313325. [Online]. Available: http://www.ncbi.nlm.nih.gov/pubmed/10476925.

[33] S. Sleijfer, M. Bannink, A. R. Van Gool, W. H. J. Kruit, and G. Stoter, "Side effects of interferon-alpha therapy.", *Pharmacy world & science : PWS*, vol. 27, no. 6, pp. 423–31, 2005, ISSN: 0928-1231. DOI: 10.1007/s11096-005-1319-7. [Online]. Available: http://www.ncbi.nlm.nih.gov/pubmed/16341948.

[34] H. Li, L. Yang, G. Cheng, H. Y. Wei, and Q. Zeng, "Encapsulation, pharmacokinetics and tissue distribution of interferon α-2b liposomes after intramuscular injection to rats", *Archives of Pharmacal Research*, vol. 34, no. 6, pp. 941–948, 2011, ISSN: 02536269. DOI: 10.1007/s12272-011-0611-4.

[35] N. H. Greig, T. T. Soncrant, K. M. Wozniak, and S. I. Rapoport, "Plasma and tissue pharmacokinetics of human interferon-alpha in the rat after its intravenous administration", *J Pharmacol Exp Ther.*, vol. 245, no. 2, pp. 574–80. 1988, ISSN: 0022-3565.

[36] Y. Cai, Z. Zhang, K. Fan, J. Zhang, W. Shen, M. Li, D. Si, H. Luo, Y. Zeng, P. Fu, and C. Liu, "Pharmacokinetics, tissue distribution, excretion, and antiviral activity of pegylated recombinant human consensus interferon-α variant in monkeys, rats and guinea pigs", *Regulatory Peptides*, vol. 173, no. 1-3, pp. 74–81, 2012, ISSN: 01670115. DOI: 10.1016/j.regpep.2011.09.008.

[37] A. Billiau, P. De Somer, and V. G. Edy, "Human fibroblast interferon for clinical trials: Pharmacokinetics and tolerability in experimental animals and humans", *Antimicrobial Agents and Chemotherapy*, vol. 16, no. 1, pp. 56–63, 1979, ISSN: 00664804. DOI: 10.1128/AAC.16.1.56.

[38] I Rutenfranz and H Kirchner, "Pharmacokinetics of recombinant murine interferon-gamma in mice.", *Journal of interferon research*, vol. 8, no. 5, pp. 573–80, 1988, ISSN: 0197-8357. DOI: 10.1089/jir.1988.8.573. [Online]. Available: http://www.ncbi.nlm.nih.gov/pubmed/3148668.

[39] O Bohoslawec, P. W. Trown, and R. J. Wills, "Pharmacokinetics and tissue distribution of recombinant human alpha A, D, A/D(Bgl), and I interferons and mouse alpha-interferon in mice.", *Journal of interferon research*, vol. 6, no. 3, pp. 207–213, 1986, ISSN: 0197-8357. DOI: 10.1089/jir.1986.6.207.

[40] T. G. Johns, J. A. Kerry, B. A. Veitch, I. R. Mackay, P. J. Tutton, M. J. Tymms, B. F. Cheetham, P. J. Hertzog, and A. W. Linnane, "Pharmacokinetics, tissue distribution, and cell localization of [35S]methionine-labeled recombinant human and murine alpha interferons in mice.", *Cancer Research*, vol. 50, no. 15, pp. 4718–4723, 1990, ISSN: 0008-5472 (Print). [Online]. Available: http://eutils.ncbi.nlm.nih.gov/entrez/eutils/elink.fcgi?dbfrom=pubmed{\&}id=2369745{\&}retmode=ref{\&}cmd=prlinks{\%}5Cnpapers2://publication/uuid/CF20ED74-6467-4B44-BC08-ED57ED601AC4.

[41] A. Billiau, H. Heremans, D. Ververken, J. van Damme, H. Carton, and P. de Somer, "Tissue distribution of human interferons after exogenous administration in rabbits, monkeys, and mice", *Archives of Virology*, vol. 68, no. 1, pp. 19–25, 1981, ISSN: 03048608. DOI: 10.1007/BF01315163.

[42] V. Bocci, "Metabolism of protein anticancer agents", *Pharmacology and Therapeutics*, vol. 34, no. 1, pp. 1 –49, 1987, ISSN: 0163-7258. DOI: https://doi.org/10.1016/0163-7258(87)90090-8. [Online]. Available: http://www.sciencedirect.com/science/article/pii/0163725887900908.

[43] K Cantell and L Pyhälä, "Pharmacokinetics of human leukocyte interferon.", *The Journal of Infectious Diseases*, vol. 133 Suppl, A6–A12, 1976.

[44] V. Bocci, P. D. Francesco, A. Pacini, G. Pessina, G. Rossi, and V. Sorrentino, "Renal metabolism of homologous serum interferon", *Antiviral Research*, vol. 3, no. 1, pp. 53 –58, 1983, ISSN: 0166-3542. DOI: https://doi.org/10.1016/0166-3542(83)90014-1. [Online]. Available: http://www.sciencedirect.com/science/article/pii/0166354283900141.

[45] B. L. Osborn, H. S. Olsen, B. Nardelli, J. H. Murray, J. O.E.X. H. Zhou, A. Garcia, G. Moody, L. S. Zaritskaya, and C. Sung, "Pharmacokinetic and Pharmacodynamic Studies of a Human Serum Albumin-Interferon-alpha Fusion Protein in Cynomolgus Monkeys", *J Pharmacol Exp Ther*, vol. 303, no. 2, pp. 540–548, 2002, ISSN: 0022-3565. DOI: 10.1124/jpet.102.037002.weekly.

[46] G Emodi, M Just, R Hernandez, and H. R. Hirt, "Circulating interferon in man after administration of exogenous human leukocyte interferon", *Journal of the National Cancer Institute*, vol. 54, no. 5, pp. 1045–1049, 1975, ISSN: 0027-8874. [Online]. Available: http://www.embase.com/search/results?subaction=viewrecord{\&}from=export{\&}id=L6073568{\%}5Cnhttp://lh-bvsp.cineca.it/Ccube/openclink.do?sid=EMBASE{\&}issn=00278874{\&}id=doi:{\&}atitle=Circulating+interferon+in+man+after+administration+of+exogenous+human+leukocyte+interfero.

[47] L. D. Bornemann, H. E. Spiegel, Z. E. Dziewanowska, S. E. Krown, and W. A. Colburn, "Intravenous and intramuscular pharmacokinetics of recombinant leukocyte a interferon", *European Journal of Clinical Pharmacology*, vol. 28, no. 4, pp. 469–471, 1985, ISSN: 1432-1041. DOI: 10.1007/BF00544369. [Online]. Available: https://doi.org/10.1007/BF00544369.

[48] I. Shah, J. Band, H. M. Samon, J. Young, R. Robinson, B. Bailey, A. Lerner, and A. Prasad, "Pharmacokinetics and tolerance of intravenous and intramuscular recombinant alpha 2 interferon in patients with malignancies.", *American journal of hematology*, vol. 17, pp. 363–71, 1984.

[49] E. Radwanski, G. Perentesis, S. Jacobs, E. Oden, M. Affrime, S. Symchowicz, and N. Zampaglione, "Pharmacokinetics of interferon-2b in healthy volunteers", *The Journal of Clinical Pharmacology*, vol. 27, no. 5, pp. 432–435, 1987, ISSN: 1552-4604. DOI: 10.1002/j.1552-4604.1987.tb03044.x. [Online]. Available: http://dx.doi.org/10.1002/j.1552-4604.1987.tb03044.x.

[50] R. J. Wills, S. Dennis, H. E. Spiegel, D. M. Gibson, and P. I. Nadler, "Interferon kinetics and adverse reactions after intravenous, intramuscular, and subcutaneous injection.", *Clinical Pharmacology & Therapeutics*, vol. 35, 722–727, 1984.

[51] R. J. Wells, P. K. Weck, R. L. Baehner, W. Krivit, R. B. Raney, J. A. Ortega, I. O. Bernstein, B. Lampkin, J. K. Whisnant, and H. N. Sather, "Interferon-alpha n1 in children with recurrent acute lymphocytic leukemia: a phase I study of pharmacokinetics and tolerance", *J. Interferon Res.*, vol. 8, no. 3, pp. 309–318, 1988.

[52] F. Witter, F. Barouki, D. Griffin, P. Nadler, A. Woods, D. Wood, and P. Lietman, "Biologic response (antiviral) to recombinant human interferon alpha 2a as a function of dose and route of administration in healthy volunteers", *Clin. Pharmacol. Ther.*, vol. 42, no. 5, pp. 567–575, 1987.

[53] C Billard, F Sigaux, S Castaigne, F Valensi, G Flandrin, L Degos, E Falcoff, and M Aguet, "Treatment of hairy cell leukemia with recombinant alpha interferon: II. In vivo down-regulation of alpha interferon receptors on tumor cells.", *Blood*, vol. 67, no. 3, pp. 821–6, 1986, ISSN: 0006-4971. [Online]. Available: http://www.ncbi.nlm.nih.gov/pubmed/2936410.

[54] A. S. Lau, G. E. Hannigan, M. H. Freedman, and B. R. Williams, "Regulation of interferon receptor expression in human blood lymphocytes in vitro and during interferon therapy.", *The Journal of clinical investigation*, vol. 77, no. 5, pp. 1632–8, 1986, ISSN: 0021-9738. DOI: 10.1172/JCI112480. [Online]. Available: http://www.ncbi.nlm.nih.gov/pubmed/3009549{\%}5Cnhttp://www.pubmedcentral.nih.gov/articlerender.fcgi?artid=PMC424568.

[55] D. E. Mager, B. Neuteboom, C. Efthymiopoulos, A. Munafo, and W. J. Jusko, "Receptor-mediated pharmacokinetics and pharmacodynamics of interferon-beta1a in monkeys.", *The Journal of pharmacology and experimental therapeutics*, vol. 306, no. 1, pp. 262–70, 2003, ISSN: 0022-3565. DOI: 10.1124/jpet.103.049502. [Online]. Available: http://www.ncbi.nlm.nih.gov/pubmed/12660309.

[56] D. E. Mager and W. J. Jusko, "General pharmacokinetic model for drugs exhibiting target-mediated drug disposition", *Journal of Pharmacokinetics and Pharmacodynamics*, vol. 28, no. 6, pp. 507–532, 2001, ISSN: 1573-8744. DOI: 10.1023/A:1014414520282. [Online]. Available: https://doi.org/10.1023/A:1014414520282.

[57] D. E. Mager and W. J. Jusko, "Receptor-Mediated Pharmacokinetic/ Pharmacodynamic Model of Interferon-beta 1a in Humans", *Pharmaceutical Research*, vol. 19, no. 10, pp. 1537–1543, 2002.

[58] K. Shuai and B. Liu, "Regulation of JAKSTAT signalling in the immune system", *Nature Reviews Immunology*, vol. 3, no. 11, pp. 900–911, 2003, ISSN: 1474-1733. DOI: 10.1038/nri1226. [Online]. Available: http://www.nature.com/doifinder/10.1038/nri1226.

[59] L. B. Ivashkiv and L. T. Donlin, *Regulation of type i interferon responses*, 2014. DOI: 10.1038/nri3581. arXiv: NIHMS150003.

[60] K. Honda and T. Taniguchi, *IRFs: Master regulators of signalling by Toll-like receptors and cytosolic pattern-recognition receptors*, 2006. DOI: 10.1038/nri1900.

[61] W. Yang, J. Soares, P. Greninger, E. J. Edelman, H. Lightfoot, S. Forbes, N. Bindal, D. Beare, J. A. Smith, I. R. Thompson, S. Ramaswamy, P. A. Futreal, D. A. Haber, M. R. Stratton, C. Benes, U. McDermott, and M. J. Garnett, "Genomics of Drug Sensitivity in Cancer (GDSC): A resource for therapeutic biomarker discovery in cancer cells", *Nucleic Acids Research*, vol. 41, no. D1, 2013, ISSN: 03051048. DOI: 10.1093/nar/gks1111. arXiv: NIHMS150003.

[62] S. D. Desai, L. M. Wood, Y.-C. Tsai, T.-S. Hsieh, J. R. Marks, G. L. Scott, B. C. Giovanella, and L. F. Liu, "ISG15 as a novel tumor biomarker for drug sensitivity", *Molecular Cancer Therapeutics*, vol. 7, no. 6, pp. 1430–1439, 2008, ISSN: 1535-7163. DOI: 10.1158/1535-7163.MCT-07-2345. [Online]. Available: http://mct.aacrjournals.org/cgi/doi/10.1158/1535-7163.MCT-07-2345.

[63] R. P. Laljee, S. Muddaiah, B. Salagundi, P. M. Cariappa, A. S. Indra, V. Sanjay, and A. Ramanathan, "Interferon stimulated gene-ISG15 is a potential diagnostic biomarker in oral squamous cell carcinomas.", *Asian Pacific journal of cancer prevention : APJCP*, vol. 14, no. 2, pp. 1147–50, 2013, ISSN: 1513-7368. DOI: 10.7314/APJCP.2013.14.2.1147. [Online]. Available: http://www.ncbi.nlm.nih.gov/pubmed/23621203.

[64] G. I. Rice, G. M. Forte, M. Szynkiewicz, D. S. Chase, A. Aeby, M. S. Abdel-Hamid, S. Ackroyd, R. Allcock, K. M. Bailey, U. Balottin, C. Barnerias, G. Bernard, C. Bodemer, M. P. Botella, C. Cereda, K. E. Chandler, L. Dabydeen, R. C. Dale, C. De Laet, C. G. De Goede, M. del Toro, L. Effat, N. N. Enamorado, E. Fazzi, B. Gener, M. Haldre, J. P. S. Lin, J. H. Livingston, C. M. Lourenco, W. Marques, P. Oades, P. Peterson, M. Rasmussen, A. Roubertie, J. L. Schmidt, S. A. Shalev, R. Simon, R. Spiegel, K. J. Swoboda, S. A. Temtamy, G. Vassallo, C. N. Vilain, J. Vogt, V. Wermenbol, W. P. Whitehouse, D. Soler, I. Olivieri, S. Orcesi, M. S. Aglan, M. S. Zaki, G. M. Abdel-Salam, A. Vanderver, K. Kisand, F. Rozenberg, P. Lebon, and Y. J. Crow, "Assessment of interferon-related biomarkers in Aicardi-Goutières syndrome associated with mutations in TREX1, RNASEH2A, RNASEH2B, RNASEH2C, SAMHD1, and ADAR: A case-control study", *The Lancet Neurology*, vol. 12, no. 12, pp. 1159–1169, 2013, ISSN: 14744422. DOI: 10.1016/S1474-4422(13)70258-8. arXiv: 15334406.

[65] B. X. Wang, S. A. Grover, P. Kannu, G. Yoon, R. M. Laxer, E. A. Yeh, and E. N. Fish, "Interferon-Stimulated Gene Expression as a Preferred Biomarker for Disease Activity in Aicardia Goutieres Syndrome", *Journal of Interferon & Cytokine Research*, vol. 37, no. 4, pp. 147–152, 2017, ISSN: 1079-9907. DOI: 10.1089/jir.2016.0117. [Online]. Available: http://online.liebertpub.com/doi/10.1089/jir.2016.0117.

[66] J Guo, K. L. Peters, and G. C. Sen, "Induction of the human protein P56 by interferon, double-stranded RNA, or virus infection.", *Virology*, vol. 267, no. 2, pp. 209–19, 2000, ISSN: 0042-6822. DOI: 10.1006/viro.1999.0135. [Online]. Available: http://www.ncbi.nlm.nih.gov/pubmed/10662616.

[67] V. Fensterl and G. C. Sen, "The ISG56/IFIT1 gene family.", *Journal of interferon & cytokine research : the official journal of the International Society for Interferon and Cytokine Research*, vol. 31, no. 1, pp. 71–78, 2011, ISSN: 1557-7465. DOI: 10.1089/jir.2010.0101.

[68] M. G. Wathelet, I. M. Clauss, J. Content, and G. A. Huez, "Regulation of two interferon-inducible human genes by interferon, poly (ri)· poly (rc) and viruses", *The FEBS Journal*, vol. 174, no. 2, pp. 323–329, 1988.

[69] O. Haller and G. Kochs, "Human mxa protein: An interferon-induced dynamin-like gtpase with broad antiviral activity", *Journal of Interferon & Cytokine Research*, vol. 31, no. 1, pp. 79–87, 2011.

[70] O. Haller, S. Gao, A. Von Der Malsburg, O. Daumke, and G. Kochs, *Dynamin-like MxA GTPase: Structural insights into oligomerization and implications for antiviral activity*, 2010. DOI: 10.1074/jbc.R110.145839.

[71] A. Roers, H. K. Hochkeppel, M. A. Horisberger, A. Hovanessian, and O. Haller, "MxA gene expression after live virus vaccination: A sensitive marker for endogenous type i interferon", *Journal of Infectious Diseases*, vol. 169, no. 4, pp. 807–813, 1994, ISSN: 15376613. DOI: 10.1093/infdis/169.4.807.

[72] F Gilli, F Marnetto, M Caldano, A Sala, S Malucchi, M Capobianco, and A Bertolotto, "Biological markers of interferon-beta therapy: comparison among interferon-stimulated genes MxA, TRAIL and XAF-1", *Mult Scler*, vol. 12, no. 1, pp. 47–57, 2006, ISSN: 1352-4585. DOI: 10.1191/135248506ms1245oa.

[73] *Regulation of the type I IFN induction: A current view*, 2005. DOI: 10.1093/intimm/dxh318.

[74] V. François-Newton, G. M. de Freitas Almeida, B. Payelle-Brogard, D. Monneron, L. Pichard-Garcia, J. Piehler, S. Pellegrini, and G. Uzé, "USP18-based negative feedback control is induced by type I and type III interferons and specifically inactivates interferon α response", *PLoS ONE*, vol. 6, no. 7, 2011, ISSN: 19326203. DOI: 10.1371/journal.pone.0022200.

[75] D. L. Krebs and D. J. Hilton, "SOCS: physiological suppressors of cytokine signaling.", *Journal of cell science*, vol. 113 (Pt 1, pp. 2813–2819, 2000, ISSN: 0021-9533.

[76] S. S. Andrews, T. Dinh, and A. P. Arkin, *Stochastic models of biological processes*. Springer, 2009, pp. 8730–8749.

[77] D. T. Gillespie, "A general method for numerically simulating the stochastic time evolution of coupled chemical reactions", *Journal of Computational Physics*, vol. 22, no. 4, pp. 403–434, Dec. 1976. DOI: 10.1016/0021-9991(76)90041-3.

[78] M. B. Elowitz, A. J. Levine, E. D. Siggia, and P. S. Swain, "Stochastic gene expression in a single cell", *Science*, vol. 297, no. 5584, pp. 1183–1186, 2002.

[79] R. Cheong, A. Rhee, C. J. Wang, I. Nemenman, and A. Levchenko, "Information transduction capacity of noisy biochemical signaling networks", *science*, vol. 334, no. 6054, pp. 354–358, 2011.

[80] J. E. Ladbury and S. T. Arold, "Noise in cellular signaling pathways: Causes and effects", *Trends in biochemical sciences*, vol. 37, no. 5, pp. 173–178, 2012.

[81] U. Rand, M. Rinas, J. Schwerk, G. Nöhren, M. Linnes, A. Kröger, M. Flossdorf, K. Kály-Kullai, H. Hauser, T. Höfer, *et al.*, "Multi-layered stochasticity and paracrine signal propagation shape the type-i interferon response", *Molecular systems biology*, vol. 8, no. 1, p. 584, 2012.

[82] O. Bauhofer, A. Ruggieri, B. Schmid, P. Schirmacher, and R. Bartenschlager, "Persistence of hcv in quiescent hepatic cells under conditions of an interferon-induced antiviral response", *Gastroenterology*, vol. 143, no. 2, pp. 429–438, 2012.

[83] J. von Recum-Knepper, A. Sadewasser, V. K. Weinheimer, and T. Wolff, "Fluorescence-activated cell sorting-based analysis reveals an asymmetric induction of interferon-stimulated genes in response to seasonal influenza a virus", *Journal of virology*, vol. 89, no. 14, pp. 6982–6993, 2015.

[84] B. Schmid, M. Rinas, A. Ruggieri, E. G. Acosta, M. Bartenschlager, A. Reuter, W. Fischl, N. Harder, J.-P. Bergeest, M. Flossdorf, *et al.*, "Live cell analysis and mathematical modeling identify determinants of attenuation of dengue virus 2'-o-methylation mutant", *PLoS Pathog*, vol. 11, no. 12, e1005345, 2015.

[85] O. P. Tabbaa, G. Nudelman, S. C. Sealfon, and C. Jayaprakash, "Noise propagation through cytokine signaling leads to fluctuations in interferon-induced genes", *Biophysical Journal*, vol. 104, no. 2, Supplement 1, 493a, 2013, ISSN: 0006-3495. DOI: https://doi.org/10.1016/j.bpj.2012.11.2719. [Online]. Available: http://www.sciencedirect.com/science/article/pii/S0006349512039653.

[86] E. Kalie, D. A. Jaitin, Y. Podoplelova, J. Piehler, and G. Schreiber, "The stability of the ternary interferon-receptor complex rather than the affinity to the individual subunits dictates differential biological activities", *Journal of Biological Chemistry*, vol. 283, no. 47, pp. 32 925–32 936, 2008, ISSN: 00219258. DOI: 10.1074/jbc.M806019200.

[87] D. Levin, D. Harari, and G. Schreiber, "Stochastic Receptor Expression Determines Cell Fate upon Interferon Treatment", *Molecular and Cellular Biology*, vol. 31, no. 16, pp. 3252–3266, 2011, ISSN: 0270-7306. DOI: 10.1128/MCB.05251-11. [Online]. Available: http://mcb.asm.org/cgi/doi/10.1128/MCB.05251-11.

[88] C. Thomas, I. Moraga, D. Levin, P. O. Krutzik, Y. Podoplelova, A. Trejo, C. Lee, G. Yarden, S. E. Vleck, J. S. Glenn, G. P. Nolan, J. Piehler, G. Schreiber, and K. C. Garcia, "Structural linkage between ligand discrimination and receptor activation by Type i interferons", *Cell*, vol. 146, no. 4, pp. 621–632, 2011, ISSN: 00928674. DOI: 10.1016/j.cell.2011.06.048. arXiv: NIHMS150003.

[89] G. R. Stark, I. M. Kerr, B. R. Williams, R. H. Silverman, and R. D. Schreiber, "How cells respond to interferons.", *Annual review of biochemistry*, vol. 67, pp. 227–64, 1998, ISSN: 0066-4154. DOI: 10.1146/annurev.biochem.67.1.227. [Online]. Available: http://www.ncbi.nlm.nih.gov/pubmed/9759489.

[90] J. Piehler, C. Thomas, K. Christopher Garcia, and G. Schreiber, "Structural and dynamic determinants of type I interferon receptor assembly and their functional interpretation", *Immunological Reviews*, vol. 250, no. 1, pp. 317–334, 2012, ISSN: 01052896. DOI: 10.1111/imr.12001. arXiv: NIHMS150003.

[91] E. Jaks, M. Gavutis, G. UzÃ©, J. Martal, and J. Piehler, "Differential receptor subunit affinities of type i interferons govern differential signal activation", *Journal of Molecular Biology*, vol. 366, no. 2, pp. 525 –539, 2007, ISSN: 0022-2836. DOI: https://doi.org/10.1016/j.jmb.2006.11.053. [Online]. Available: http://www.sciencedirect.com/science/article/pii/S0022283606015932.

[92] R Hu, Y Gan, J Liu, D Miller, and K. C. Zoon, "Evidence for multiple binding sites for several components of human lymphoblastoid interferon-alpha.", *The Journal of biological chemistry*, vol. 268, no. 17, pp. 12 591–5, 1993, ISSN: 0021-9258. [Online]. Available: http://www.ncbi.nlm.nih.gov/pubmed/8509399.

[93] T. Ariyasu, N. Fujioka, S. Yamamoto, Y. Yanai, H. Yamauchi, H. Ikegami, M. Ikeda, M. Kurimoto, S. Horie, and T. Kitamura, "Correlation between interferon alpha receptor protein expression and sensitivity to interferon alpha subtypes in human renal carcinoma cell lines", *Cancer Genomics and Proteomics*, vol. 1, no. 1, 2004, ISSN: 11096535 17906245.

[94] C. N. Jenne and P. Kubes, *Immune surveillance by the liver*, 2013. DOI: 10.1038/ni.2691.

[95] G. A. Parker and C. A. Picut, "Liver Immunobiology", *Toxicologic Pathology*, vol. 33, no. 1, pp. 52–62, 2005, ISSN: 01926233. DOI: 10.1080/01926230590522365.

[96] B. Gao, W. I. Jeong, and Z. Tian, *Liver: An organ with predominant innate immunity*, 2008. DOI: 10.1002/hep.22034.

[97] Z. Y. Zheng, S. Y. Weng, and Y. Yu, *Signal molecule-mediated hepatic cell communication during liver regeneration*, 2009. DOI: 10.3748/wjg.15.5776.

[98] Z. Zhou, M. J. Xu, and B. Gao, *Hepatocytes: A key cell type for innate immunity*, 2016. DOI: 10.1038/cmi.2015.97.

[99] A. Warren, D. G. Le Couteur, R. Fraser, D. G. Bowen, G. W. McCaughan, and P. Bertolino, "T lymphocytes interact with hepatocytes through fenestrations in murine liver sinusoidal endothelial cells.", *Hepatology (Baltimore, Md.)*, vol. 44, no. 5, pp. 1182–90, 2006, ISSN: 0270-9139. DOI: 10.1002/hep.21378. [Online]. Available: http://www.ncbi.nlm.nih.gov/pubmed/17058232.

[100] I. N. Crispe, "Hepatocytes as Immunological Agents", *The Journal of Immunology*, vol. 196, no. 1, pp. 17–21, 2016, ISSN: 0022-1767. DOI: 10.4049/jimmunol.1501668. [Online]. Available: http://www.jimmunol.org/lookup/doi/10.4049/jimmunol.1501668.

[101] J. Twycross, L. R. Band, M. J. Bennett, J. R. King, and N. Krasnogor, "Stochastic and deterministic multiscale models for systems biology: An auxin-transport case study", *BMC Systems Biology*, 2010, ISSN: 17520509. DOI: 10.1186/1752-0509-4-34.

[102] J. Murray, *Mathematical Biology: I. An Introduction, Third Edition, Models*. Springer-Verlag, 1973.

[103] J. W. Haefner, *Modeling Biological Systems: Principles and Applications*. Springer-Verlag, 2005.

[104] V. Helms, *Principles of Computational Cell Biology, Models*. Springer-Verlag, 2008.

[105] E. Bullinger, "Wilkinson darren: Stochastic modelling for systems biology", *BioMedical Engineering OnLine*, vol. 5, no. 1, p. 64, 2006, ISSN: 1475-925X. DOI: 10.1186/1475-925X-5-64. [Online]. Available: https://doi.org/10.1186/1475-925X-5-64.

[106] P. T. Marius Iosifescu, *Stochastic processes and applications in biology and medicine II, Models*. Springer-Verlag, 1973.

[107] K. A. Janes and D. A. Lauffenburger, "Models of signalling networks - what cell biologists can gain from them and give to them", *Journal of Cell Science*, 2013, ISSN: 0021-9533. DOI: 10.1242/jcs.112045.

[108] D. Hwang and W. U. Kim, *Rheumatoid arthritis: Modelling cytokine signalling networks*, 2017. DOI: 10.1038/nrrheum.2016.194.

[109] M. D. B. Xuedong Liu, *Computational Modeling of Signaling Networks, Methods and protocols*. Springer Protocol, 2012.

[110] I Swameye, T. G. Muller, J Timmer, O Sandra, and U Klingmuller, "Identification of nucleocytoplasmic cycling as a remote sensor in cellular signaling by databased modeling.", *Proceedings of the National Academy of Sciences of the United States of America*, vol. 100, no. 3, pp. 1028–1033, 2003, ISSN: 00278424. DOI: 10.1073/pnas.0237333100.

[111] J. Vera, J. Bachmann, A. C. Pfeifer, V. Becker, J. A. Hormiga, N. V. Darias, J. Timmer, U. Klingmüller, and O. Wolkenhauer, "A systems biology approach to analyse amplification in the JAK2-STAT5 signalling pathway", *BMC Systems Biology*, vol. 2, 2008, ISSN: 17520509. DOI: 10.1186/1752-0509-2-38.

[112] V. Becker, M. Schilling, J. Bachmann, U. Baumann, A. Raue, T. Maiwald, J. Timmer, and U. Klingmüller, "Covering a broad dynamic range: Information processing at the erythropoietin receptor", *Science*, vol. 328, no. 5984, pp. 1404–1408, 2010, ISSN: 00368075. DOI: 10.1126/science.1184913.

[113] J. Bachmann, A. Raue, M. Schilling, M. E. Böhm, C. Kreutz, D. Kaschek, H. Busch, N. Gretz, W. D. Lehmann, J. Timmer, and U. Klingmüller, "Division of labor by dual feedback regulators controls JAK2/STAT5 signaling over broad ligand range", *Molecular Systems Biology*, vol. 7, 2011, ISSN: 17444292. DOI: 10.1038/msb.2011.50.

[114] S. Yamada, S. Shiono, A. Joo, and A. Yoshimura, "Control mechanism of JAK/STAT signal transduction pathway", *FEBS Letters*, vol. 534, no. 1-3, pp. 190–196, 2003, ISSN: 00145793. DOI: 10.1016/S0014-5793(02)03842-5.

[115] J. Smieja, M. Jamaluddin, A. R. Brasier, and M. Kimmel, "Model-based analysis of interferon-beta induced signaling pathway.", *Bioinformatics*, vol. 24, no. 20, pp. 2363–2369, 2008, ISSN: 1367-4811. DOI: 10.1093/bioinformatics/btn400. [Online]. Available: http://eutils.ncbi.nlm.nih.gov/entrez/eutils/elink.fcgi?dbfrom=pubmed{\&}id=18713791{\&}retmode=ref{\&}cmd=prlinks{\%}5Cnpapers3://publication/doi/10.1093/bioinformatics/btn400.

[116] T. Maiwald, A. Schneider, H. Busch, S. Sahle, N. Gretz, T. S. Weiss, U. Kummer, and U. Klingmüller, "Combining theoretical analysis and experimental data generation reveals IRF9 as a crucial factor for accelerating interferon-α induced early antiviral signalling", *FEBS Journal*, vol. 277, no. 22, pp. 4741–4754, 2010, ISSN: 1742464X. DOI: 10.1111/j.1742-4658.2010.07880.x.

[117] M. Rybiński and A. Gambin, "Model-based selection of the robust jak-stat activation mechanism", *Journal of theoretical biology*, vol. 309, pp. 34–46, 2012.

[118] V. Sharma and A. B. Compagnoni, "Computational and mathematical models of the jak-stat signal transduction pathway", in *SummerSim*, 2013.

[119] J. A. Papin and B. O. Palsson, "The JAK-STAT signaling network in the human B-cell: An extreme signaling pathway analysis", *Biophysical Journal*, 2004, ISSN: 00063495. DOI: 10.1529/biophysj.103.029884.

[120] R. Heinrich, B. G. Neel, and T. A. Rapoport, "Mathematical models of protein kinase signal transduction", *Molecular Cell*, 2002, ISSN: 10972765. DOI: 10.1016/S1097-2765(02)00528-2.

[121] F. Wimmers, N. Subedi, N. van Buuringen, D. Heister, J. Vivie, I. Beeren-Reinieren, R. Woestenenk, H. Dolstra, A. Piruska, J. F. M. Jacobs, A. van Oudenaarden, C. G. Figdor, W. T. S. Huck, I. J. M. de Vries, and J. Tel, "Single-cell analysis reveals that stochasticity and paracrine signaling control interferon-alpha production by plasmacytoid dendritic cells", *Nat Commun*, vol. 9, no. 1, p. 3317, 2018.

[122] A. Gambin, A. Charzyska, A. Ellert-Miklaszewska, and M. Rybiski, "Computational models of the JAK1/2-STAT1 signaling", *JAKSTAT*, vol. 2, no. 3, e24672, 2013.

[123] L. U. Aguilera, C. Zimmer, and K. Ursula, "A new efficient approach to fit stochastic models on the basis of high-throughput experimental data using a model of irf7 gene expression as case study", *BMC Systems Biology*, vol. 11, no. 26, 2017.

[124] W. Zhang, T. Tian, and X. Zou, "Negative feedback contributes to the stochastic expression of the interferon-beta gene in virus-triggered type i interferon signaling pathways", *Mathematical Biosciences*, vol. 265, pp. 12 –27, 2015, ISSN: 0025-5564. DOI: https://doi.org/10.1016/j.mbs.2015.04.003.

[125] M. Czerkies, Z. Korwek, W. Prus, M. Kochaczyk, J. Jaruszewicz-Boska, K. Tudelska, S. Boski, M. Kimmel, A. R. Brasier, and T. Lipniacki, "Cell fate in antiviral response arises in the crosstalk of IRF, NF-kappaB and JAK/STAT pathways", *Nat Commun*, vol. 9, no. 1, p. 493, 2018.

[126] B Meibohm and H Derendorf, "Basic concepts of pharmacokinetic/pharmacodynamic (PK/PD) modelling.", *International journal of clinical pharmacology and therapeutics*, vol. 35, no. 10, pp. 401–13, 1997, ISSN: 0946-1965. DOI: 10.1155/2014/506287. [Online]. Available: http://www.ncbi.nlm.nih.gov/pubmed/9352388.

[127] M. Danhof, E. C. de Lange, O. E. Della Pasqua, B. A. Ploeger, and R. A. Voskuyl, *Mechanism-based pharmacokinetic-pharmacodynamic (PK-PD) modeling in translational drug research*, 2008. DOI: 10.1016/j.tips.2008.01.007.

[128] B. A. Ploeger, P. H. van der Graaf, and M. Danhof, "Incorporating Receptor Theory in Mechanism-Based Pharmacokinetic-Pharmacodynamic (PK-PD) Modeling", *Drug Metab. Pharmacokinet*, vol. 24, no. 1, pp. 3–15, 2009, ISSN: 1347-4367. DOI: 10.2133/dmpk.24.3. [Online]. Available: http://www.jstage.jst.go.jp/browse/dmpk.

[129] W. P. Hofmann, E. Herrmann, C. Sarrazin, and S. Zeuzem, *Ribavirin mode of action in chronic hepatitis C: From clinical use back to molecular mechanisms*, 2008. DOI: 10.1111/j.1478-3231.2008.01896.x.

[130] M. H. Heim, *Interferons and hepatitis C virus*, 2012. DOI: 10.4414/smw.2012.13586.

[131] J. J. Feld and J. H. Hoofnagle, "Mechanism of action of interferon and ribavirin in treatment of hepatitis C", *Nature.*, 2005, ISSN: 1476-4687 (Electronic) 0028-0836 (Linking). DOI: 10.1038/nature04082.

[132] *Viral determinants of resistance to treatment in patients with hepatitis C*, 2007. DOI: 10.1128/CMR.00010-06.

[133] M. K. Jain, J. G. Pasipanodya, L. Alder, W. M. Lee, and T. Gumbo, "Pegylated interferon fractal pharmacokinetics: Individualized dosing for hepatitis c virus infection", *Antimicrobial Agents and Chemotherapy*, 2013, ISSN: 00664804. DOI: 10.1128/AAC.02208-12.

[134] N. Benson, J. De Jongh, J. D. Duckworth, H. M. Jones, H. E. Pertinez, J. K. Rawal, T. J. Van Steeg, and P. H. Van Der Graaf, "Pharmacokinetic-pharmacodynamic modeling of alpha interferon response induced by a toll-like 7 receptor agonist in mice", *Antimicrobial Agents and Chemotherapy*, vol. 54, no. 3, pp. 1179–1185, 2010, ISSN: 00664804. DOI: 10.1128/AAC.00551-09.

[135] C. Laouénan, P. Marcellin, M. Lapalus, F. Khelifa-Mouri, N. Boyer, F. Zoulim, L. Serfaty, J. P. Bronowicki, M. Martinot-Peignoux, O. Lada, T. Asselah, C. Dorival, C. Hézode, F. Carrat, F. Nicot, G. Peytavin, F. Mentré, and J. Guedj, "Using pharmacokinetic and viral kinetic modeling to estimate the antiviral effectiveness of telaprevir, boceprevir, and pegylated interferon during triple therapy in treatment-experienced hepatitis C virus-infected cirrhotic patients", *Antimicrobial Agents and Chemotherapy*, 2014, ISSN: 10986596. DOI: 10.1128/AAC.02611-14.

[136] E. Chatelut, L. Rostaing, N. Grégoire, J. L. Payen, A. Pujol, J. Izopet, G. Houin, and P. Canal, "A pharmacokinetic model for alpha interferon administered subcutaneously", *British Journal of Clinical Pharmacology*, vol. 47, no. 4, pp. 365–371, 1999, ISSN: 03065251. DOI: 10.1046/j.1365-2125.1999.00912.x.

[137] K. a. Powers, N. M. Dixit, R. M. Ribeiro, P. Golia, A. H. Talal, and A. S. Perelson, "Modeling viral and drug kinetics: hepatitis C virus treatment with pegylated interferon alfa-2b.", *Seminars in liver disease*, vol. 23 Suppl 1, no. 212, pp. 13–18, 2003, ISSN: 0272-8087. DOI: 10.1055/s-2003-41630.

[138] S. Jeon, J. H. Juhn, S. Han, J. Lee, T. Hong, J. Paek, and D. S. Yim, "Saturable human neopterin response to interferon-α assessed by a pharmacokinetic-pharmacodynamic model", *Journal of Translational Medicine*, vol. 11, no. 1, 2013, ISSN: 14795876. DOI: 10.1186/1479-5876-11-240.

[139] M. Zhao, A. J. Lepak, and D. R. Andes, "Animal models in the pharmacokinetic/pharmacodynamic evaluation of antimicrobial agents", *Bioorganic & Medicinal Chemistry*, 2016, ISSN: 09680896. DOI: 10.1016/j.bmc.2016.11.008.

[140] P. McGonigle and B. Ruggeri, *Animal models of human disease: Challenges in enabling translation*, 2014. DOI: 10.1016/j.bcp.2013.08.006.

[141] D. Andes and W. A. Craig, "Animal model pharmacokinetics and pharmacodynamics: A critical review", in *International Journal of Antimicrobial Agents*, 2002. DOI: 10.1016/S0924-8579(02)00022-5.

[142] A. K. Abraham, L. Kagan, S. Kumar, and D. E. Mager, "Type I interferon receptor is a primary regulator of target-mediated drug disposition of interferon-beta in mice", *J Pharmacol Exp Ther*, vol. 334, no. 1, pp. 327–332, 2010, ISSN: 1521-0103 (Electronic). DOI: 10.1124/jpet.110.167650.

[143] L. T. Baxter, H. Zhu, R. K. Jain, H. Zhu, D. G. Mackensen, and W. F. Butler, "Biodistribution of Monoclonal Antibodies: Scale-up from Mouse to Human Using a Physiologically Based Pharmacokinetic Model", *Cancer Research*, 1995, ISSN: 15387445.

[144] *Applied Concepts in PBPK Modeling: How to Build a PBPK/PD Model*, 2016. DOI: 10.1002/psp4.12134.

[145] T. Lave, B. Levet-Trafit, A. H. Schmitt-Hoffmann, B. Morgenroth, W. Richter, and R. C. Chou, "Interspecies scaling of interferon disposition and comparison of allometric scaling with concentration–time transformations", *Journal of Pharmaceutical Sciences*, vol. 84, no. 11, pp. 1285–1290, 1995, ISSN: 15206017. DOI: 10.1002/jps.2600841106.

[146] L. Kagan, A. K. Abraham, J. M. Harrold, and D. E. Mager, "Interspecies scaling of receptor-mediated pharmacokinetics and pharmacodynamics of type I interferons", *Pharmaceutical Research*, vol. 27, no. 5, pp. 920–932, 2010, ISSN: 07248741. DOI: 10.1007/s11095-010-0098-6.

[147] H. Jones and K. Rowland-Yeo, "Basic concepts in physiologically based pharmacokinetic modeling in drug discovery and development", *CPT Pharmacometrics Syst Pharmacol*, vol. 2, e63, 2013.

[148] A. N. Edginton, F.-P. Theil, W. Schmitt, and S. Willmann, "Whole body physiologically-based pharmacokinetic models: their use in clinical drug development", *Expert Opinion on Drug Metabolism & Toxicology*, vol. 4, no. 9, pp. 1143–1152, 2008, ISSN: 1742-5255. DOI: 10.1517/17425255.4.9.1143. [Online]. Available: http://www.tandfonline.com/doi/full/10.1517/17425255.4.9.1143.

[149] I. Nestorov, *Whole body pharmacokinetic models*, 2003. DOI: 10.2165/00003088-200342100-00002.

[150] T. A. Leil and S. Ermakov, "Editorial: The emerging discipline of quantitative systems pharmacology", *Frontiers in Pharmacology*, vol. 6, no. JUN, 2015, ISSN: 16639812. DOI: 10.3389/fphar.2015.00129.

[151] M. Danhof, "Systems pharmacology – Towards the modeling of network interactions", *European Journal of Pharmaceutical Sciences*, vol. 94, pp. 4–14, 2016, ISSN: 18790720. DOI: 10.1016/j.ejps.2016.04.027.

[152] S. A. G. Visser, D. P. De Alwis, T. Kerbusch, J. A. Stone, and S. R. B. Allerheiligen, *Implementation of quantitative and systems pharmacology in large pharma*, 2014. DOI: 10.1038/psp.2014.40.

[153] S. Schaller, J. Lippert, L. Schaupp, T. Pieber, A. Schuppert, and T. Eissing, "Robust PBPK/PD based Model Predictive Control of Blood Glucose.", *IEEE transactions on biomedical engineering*, vol. PP, no. 99, p. 1, 2015, ISSN: 1558-2531. DOI: 10.1109/TBME.2015.2497273. [Online]. Available: http://www.ncbi.nlm.nih.gov/pubmed/26552072.

[154] R. P. Sharma, M. Schuhmacher, and V. Kumar, "Developing integrated PBPK/PD coupled mechanistic pathway model (miRNA-BDNF): An approach towards system toxicology", *Toxicology Letters*, vol. 280, pp. 79–91, 2017, ISSN: 18793169. DOI: 10.1016/j.toxlet.2017.08.003.

[155] R. D. Emes, L. Goodstadt, E. E. Winter, and C. P. Ponting, *Comparison of the genomes of human and mouse lays the foundation of genome zoology*, 2003. DOI: 10.1093/hmg/ddg078.

[156] "Alternatives to animal testing: A review.", *Saudi pharmaceutical journal : SPJ : the official publication of the Saudi Pharmaceutical Society*, 2015, ISSN: 1319-0164. DOI: 10.1016/j.jsps.2013.11.002.

[157] J. E. Pulverer, U. Rand, S. Lienenklaus, D. Kugel, N. Zietara, G. Kochs, R. Naumann, S. Weiss, P. Staeheli, H. Hauser, and M. Köster, "Temporal and spatial resolution of type I and III interferon responses in vivo.", *Journal of virology*, vol. 84, no. 17, pp. 8626–8638, 2010, ISSN: 1098-5514. DOI: 10.1128/JVI.00303-10. [Online]. Available: http://www.pubmedcentral.nih.gov/articlerender.fcgi?artid=2919002{\&}tool=pmcentrez{\&}rendertype=abstract.

[158] I Rosztóczy, "Study of the in vivo priming effect of interferon in mice.", *The Journal of general virology*, vol. 67 (Pt 12, no. 12, pp. 2731–7, 1986, ISSN: 0022-1317. DOI: 10.1099/0022-1317-67-12-2731. [Online]. Available: http://jgv.microbiologyresearch.org/content/view.action?itemId=http{\%}3A{\%}2F{\%}2Fsgm.metastore.ingenta.com{\%}2Fcontent{\%}2Fjournal{\%}2Fjgv{\%}2F10.1099{\%}2F0022-1317-67-12-2731{\&}view={\&}itemType=http{\%}3A{\%}2F{\%}2Fpub2web.metastore.ingenta.com{\%}2Fns{\%}2FArticle.

[159] Y. Kiuchi, M. Yonehara, K. Okada, J. Suzuki, and S. Kobayashi, "The kinetics of interferon clearance in mice: comparison of mouse and human interferon", *Jikken Dobutsu*, vol. 33, no. 1, pp. 85–89, 1984.

[160] S Koyanagi, S Ohdo, E Yukawa, and S Higuchi, "Chronopharmacological study of interferon-α in mice", *Journal of Pharmacology and ...*, vol. 283, no. 1, pp. 259–64, 1997, ISSN: 0022-3565. [Online]. Available: http://www.ncbi.nlm.nih.gov/pubmed/9336331{\%}5Cnhttp://jpet.aspetjournals.org/content/283/1/259.short.

[161] C. R. Bolen, S. Ding, M. D. Robek, and S. H. Kleinstein, "Dynamic expression profiling of type I and type III interferon-stimulated hepatocytes reveals a stable hierarchy of gene expression", *Hepatology*, vol. 59, no. 4, pp. 1262–1272, 2014.

[162] N. Jilg, W. Lin, J. Hong, E. A. Schaefer, D. Wolski, J. Meixong, K. Goto, C. Brisac, P. Chusri, D. N. Fusco, S. Chevaliez, J. Luther, K. Kumthip, T. J. Urban, L. F. Peng, G. M. Lauer, and R. T. Chung, "Kinetic differences in the induction of interferon stimulated genes by interferon-alpha and interleukin 28b are altered by infection with hepatitis c virus", *Hepatology*, vol. 59, no. 4, pp. 1250–1261, 2014, ISSN: 1527-3350. DOI: 10.1002/hep.26653. [Online]. Available: http://dx.doi.org/10.1002/hep.26653.

[163] R. Milo, P. Jorgensen, U. Moran, G. Weber, and M. Springer, "BioNumbers The database of key numbers in molecular and cell biology", *Nucleic Acids Research*, vol. 38, no. SUPPL.1, 2009, ISSN: 03051048. DOI: 10.1093/nar/gkp889.

[164] S. F. Altschul, W. Gish, W. Miller, E. W. Myers, and D. J. Lipman, *Altschul et al.. 1990. Basic Local Alignment Search Tool.pdf*, 1990. DOI: 10.1016/S0022-2836(05)80360-2.

[165] D. S. Wishart, C. Knox, A. C. Guo, S. Shrivastava, M. Hassanali, P. Stothard, Z. Chang, and J. Woolsey, "DrugBank: a comprehensive resource for in silico drug discovery and exploration.", *Nucleic acids research*, vol. 34, no. Database issue, pp. D668–72, 2006, ISSN: 1362-4962. DOI: 10.1093/nar/gkj067. [Online]. Available: http://www.ncbi.nlm.nih.gov/pubmed/16381955$\backslash$nhttp://www.pubmedcentral.nih.gov/articlerender.fcgi?artid=PMC1347430.

[166] E. P. Consortium, I. Dunham, A. Kundaje, S. F. Aldred, P. J. Collins, C. a. Davis, F. Doyle, C. B. Epstein, S. Frietze, J. Harrow, R. Kaul, J. Khatun, B. R. Lajoie, S. G. Landt, B.-K.B.-K. Lee, F. Pauli, K. R. Rosenbloom, P. Sabo, A. Safi, A. Sanyal, N. Shoresh, J. M. Simon, L. Song, N. D. Trinklein, R. C. Altshuler, E. Birney, J. B. Brown, C. Cheng, S. Djebali, X. Dong, J. Ernst, T. S. Furey, M. Gerstein, B. Giardine, M. Greven, R. C. Hardison, R. S. Harris, J. Herrero, M. M. Hoffman, S. Iyer, M. Kelllis, P. Kheradpour, T. Lassman, Q. Li, X. Lin, G. K. Marinov, A. Merkel, A. Mortazavi, S. C.J.S. L. Parker, T. E. Reddy, J. Rozowsky, F. Schlesinger, R. E. Thurman, J. Wang, L. D. Ward, T. W. Whitfield, S. P. Wilder, W. Wu, H. S. Xi, K. Y. Yip, J. Zhuang, B. E. Bernstein, E. D. Green, C. Gunter, M. Snyder, M. J. Pazin, R. F. Lowdon, L. a. L. Dillon, L. B. Adams, C. J. Kelly, J. Zhang, J. R. Wexler, P. J. Good, E. a. Feingold, G. E. Crawford, J. Dekker, L. Elinitski, P. J. Farnham, M. C. Giddings, T. R. Gingeras, R. Guigó, T. J.T. J. Hubbard, M. Kellis, W. J. Kent, J. D. Lieb, E. H. Margulies, R. M. Myers, J. a. Starnatoyannopoulos, S. a. Tennebaum, Z. Weng, K. P. White, B. Wold, Y. Yu, J. Wrobel, B. a. Risk, H. P. Gunawardena, H. C. Kuiper, C. W. Maier, L. Xie, X. Chen, T. S. Mikkelsen, S. Gillespie, A. Goren, O. Ram, X. Zhang, L. Wang, R. Issner, M. J. Coyne, T. Durham, M. Ku, T. Truong, M. L. Eaton, A. Dobin, T. Lassmann, A. Tanzer, J. Lagarde, W. Lin, C. Xue, B. a. Williams, C. Zaleski, M. Röder, F. Kokocinski, R. F. Abdelhamid, T. Alioto, I. Antoshechkin, M. T. Baer, P. Batut, I. Bell, K. Bell, S. Chakrabortty, J. Chrast, J. Curado, T. Derrien, J. Drenkow, E. Dumais, J. Dumais, R. Duttagupta, M. Fastuca, K. Fejes-Toth, P. Ferreira, S. Foissac, M. J. Fullwood, H. Gao, D. Gonzalez, A. Gordon, C. Howald, S. Jha, R. Johnson, P. Kapranov, B. King, C. Kingswood, G. Li, O. J. Luo, E. Park, J. B. Preall, K. Presaud, P. Ribeca, D. Robyr, X. Ruan, M. Sammeth, K. S. Sandu, L. Schaeffer, L.-H. See, A. Shahab, J. Skancke, A. M. Suzuki, H. Takahashi, H. Tilgner, D. Trout, N. Walters, H. H. Wang, Y. Hayashizaki, A. Reymond,

S. E. Antonarakis, G. J. Hannon, Y. Ruan, P. Carninci, C. a. Sloan, K. Learned, V. S. Malladi, M. C. Wong, G. P. Barber, M. S. Cline, T. R. Dreszer, S. G. Heitner, D. Karolchik, V. M. Kirkup, L. R. Meyer, J. C. Long, M. Maddren, B. J. Raney, L. L. Grasfeder, P. G. Giresi, A. Battenhouse, N. C. Sheffield, K. a. Showers, D. London, A. a. Bhinge, C. Shestak, M. R. Schaner, S. K. Kim, Z. Z. Z. Zhang, P. a. Mieczkowski, J. O. Mieczkowska, Z. Liu, R. M. McDaniell, Y. Ni, N. U. Rashid, M. J. Kim, S. Adar, T. Wang, D. Winter, D. Keefe, V. R. Iyer, K. S. Sandhu, M. Zheng, P. Wang, J. Gertz, J. Vielmetter, E. C. Partridge, K. E. Varley, C. Gasper, A. Bansal, S. Pepke, P. Jain, H. Amrhein, K. M. Bowling, M. Anaya, M. K. Cross, M. a. Muratet, K. M. Newberry, K. McCue, A. S. Nesmith, K. I. Fisher-Aylor, B. Pusey, G. DeSalvo, S. S. Balasubramanian, N. S. Davis, S. K. Meadows, T. Eggleston, J. S. Newberry, S. E. Levy, D. M. Absher, W. H. Wong, M. J. Blow, A. Visel, L. a. Pennachio, L. Elnitski, H. M. Petrykowska, A. Abyzov, B. Aken, D. Barrell, G. Barson, A. Berry, A. Bignell, V. Boychenko, G. Bussotti, C. Davidson, G. Despacio-Reyes, M. Diekhans, I. Ezkurdia, A. Frankish, J. Gilbert, J. M. Gonzalez, E. Griffiths, R. Harte, D. a. Hendrix, T. Hunt, I. Jungreis, M. Kay, E. Khurana, J. Leng, M. F. Lin, J. Loveland, Z. Lu, D. Manthravadi, M. Mariotti, J. Mudge, G. Mukherjee, C. Notredame, B. Pei, J. M. Rodriguez, G. Saunders, A. Sboner, S. Searle, C. Sisu, C. Snow, C. Steward, E. Tapanari, M. L. Tress, M. J. van Baren, S. Washieti, L. Wilming, A. Zadissa, Z. Zhengdong, M. Brent, D. Haussler, A. Valencia, A. Raymond, N. Addleman, R. P. Alexander, R. K. Auerbach, K. Bettinger, N. Bhardwaj, A. P. Boyle, A. R. Cao, P. Cayting, A. Charos, Y. Cheng, C. Eastman, G. Euskirchen, J. D. Fleming, F. Grubert, L. Habegger, M. Hariharan, A. Harmanci, S. Iyenger, V. X. Jin, K. J. Karczewski, M. Kasowski, P. Lacroute, H. Lam, N. Larnarre-Vincent, J. Lian, M. Lindahl-Allen, R. Min, B. Miotto, H. Monahan, Z. Moqtaderi, X. J. Mu, H. O'Geen, Z. Ouyang, D. Patacsil, D. Raha, L. Ramirez, B. Reed, M. Shi, T. Slifer, H. Witt, L. Wu, X. Xu, K.-K. Yan, X. Yang, K. Struhl, S. M. Weissman, S. a. Tenebaum, L. O. Penalva, S. Karmakar, R. R. Bhanvadia, A. Choudhury, M. Domanus, L. Ma, J. Moran, A. Victorsen, T. Auer, L. Centarin, M. Eichenlaub, F. Gruhl, S. Heerman, B. Hoeckendorf, D. Inoue, T. Kellner, S. Kirchmaier, C. Mueller, R. Reinhardt, L. Schertel, S. Schneider, R. Sinn, B. Wittbrodt, J. Wittbrodt, G. Jain, G. Balasundaram, D. L. Bates, R. Byron, T. K. Canfield, M. J. Diegel, D. Dunn, A. K. Ebersol, T. Frum, K. Garg, E. Gist, R. S. Hansen, L. Boatman, E. Haugen, R. Humbert, A. K. Johnson, E. M. Johnson, T. M. Kutyavin, K. Lee, D. Lotakis, M. T. Maurano, S. J. Neph, F. V. Neri, E. D. Nguyen, H. Qu, A. P. Reynolds, V. Roach, E. Rynes, M. E. Sanchez, R. S. Sandstrom, A. O. Shafer, A. B. Stergachis, S. Thomas, B. Vernot, J. Vierstra, S. Vong, M. a. Weaver, Y. Yan, M. Zhang, J. a. Akey, M. Bender, M. O. Dorschner, M. Groudine, M. J. MacCoss, P. Navas, G. Stamatoyannopoulos, J. a. Stamatoyannopoulos, K. Beal, A. Brazma, P. Flicek, N. Johnson, M. Lukk, N. M. Luscombe, D. Sobral, J. M. Vaquerizas, S. Batzoglou, A. Sidow, N. Hussami, S. Kyriazopoulou-Panagiotopoulou, M. W. Libbrecht, M. a. Schaub, W. Miller, P. J. Bickel, B. Banfai, N. P. Boley, H. Huang, J. J. Li, W. S. Noble, J. a. Bilmes, O. J. Buske, A. O. Sahu, P. V. Kharchenko, P. J. Park, D. Baker, J. Taylor, and L. Lochovsky, "An integrated encyclopedia of DNA elements in the human genome", *Nature*, 2012, ISSN: 1476-4687. DOI: 10.1038/nature11247. arXiv: 1111.6189v1.

[167] S. Willmann, J. Lippert, M. Sevestre, J. Solodenko, F. Fois, and W. Schmitt, "Pk-sim: A physiologically based pharmacokinetic whole-body model", *BIOSILICO*, vol. 1, no. 4, pp. 121 –124, 2003, ISSN: 1478-5382. DOI: https://doi.org/10.1016/S1478-5382(03)02342-4. [Online]. Available: http://www.sciencedirect.com/science/article/pii/S1478538203023424.

[168] T. Eissing, L. Kuepfer, C. Becker, M. Block, K. Coboeken, T. Gaub, L. Goerlitz, J. Jaeger, R. Loosen, B. Ludewig, M. Meyer, C. Niederalt, M. Sevestre, H. U. Siegmund, J. Solodenko, K. Thelen, U. Telle, W. Weiss, T. Wendl, S. Willmann, and J. Lippert, "A computational systems biology software platform for multiscale modeling and simulation: Integrating whole-body physiology, disease biology, and molecular reaction networks", *Frontiers in Physiology*, vol. FEB, 2011, ISSN: 1664042X. DOI: 10.3389/fphys.2011.00004.

[169] S. Hoops, R. Gauges, C. Lee, J. Pahle, N. Simus, M. Singhal, L. Xu, P. Mendes, and U. Kummer, "COPASI - A COmplex PAthway SImulator", *Bioinformatics*, vol. 22, no. 24, pp. 3067–3074, 2006, ISSN: 13674803. DOI: 10.1093/bioinformatics/btl485.

[170] B. B. Aldridge, J. M. Burke, D. a. Lauffenburger, and P. K. Sorger, "Physicochemical modelling of cell signalling pathways.", *Nature cell biology*, vol. 8, no. 11, pp. 1195–203, 2006, ISSN: 1465-7392. DOI: 10.1038/ncb1497. [Online]. Available: http://www.ncbi.nlm.nih.gov/pubmed/17060902.

[171] E. Klipp and W. Liebermeister, "Mathematical modeling of intracellular signaling pathways.", *BMC neuroscience*, vol. 7 Suppl 1, no. 1, S10, 2006, ISSN: 1471-2202. DOI: 10.1186/1471-2202-7-S1-S10. [Online]. Available: http://bmcneurosci.biomedcentral.com/articles/10.1186/1471-2202-7-S1-S10.

[172] L. Petzold, "Automatic Selection of Methods for Solving Stiff and Nonstiff Systems of Ordinary Differential Equations", *SIAM Journal on Scientific and Statistical Computing*, vol. 4, no. 1, pp. 136–148, 1983, ISSN: 0196-5204. DOI: 10.1137/0904010. [Online]. Available: http://epubs.siam.org/doi/10.1137/0904010.

[173] V. Shahrezaei, J. F. Ollivier, and P. S. Swain, "Colored extrinsic fluctuations and stochastic gene expression", *Molecular systems biology*, vol. 4, no. 1, p. 196, 2008.

[174] P. Kalra, J. Brandl, T. Gaub, C. Niederalt, J. Lippert, S. Sahle, L. Kuepfer, and U. Kummer, "Quantitative Systems Pharmacology of Interferon Alpha Administration: A Multiscale Approach.", In preparation, 2018.

[175] M. L. Rizk, L. Zou, R. M. Savic, and K. E. Dooley, *Importance of Drug Pharmacokinetics at the Site of Action*, 2017. DOI: 10.1111/cts.12448.

[176] V Bocci, A Pacini, M Muscettola, L Paulesu, G. P. Pessina, M Santiano, and I Viano, "Renal filtration, absorption and catabolism of human alpha interferon.", *Journal of interferon research*, vol. 1, pp. 347–352, 1981, ISSN: 0197-8357. DOI: 10.1089/jir.1981.1.347.

[177] D. Rycroft, J. Sosabowski, E. Coulstock, M. Davies, J. Morrey, S. Friel, F. Kelly, R. Hamatake, M. Ovečka, R. Prince, L. Goodall, A. Sepp, and A. Walker, "Pharmacokinetic characteristics, pharmacodynamic effect and in vivo antiviral efficacy of liver-targeted interferon alpha", *PLoS ONE*, vol. 10, no. 2, 2015, ISSN: 19326203. DOI: 10.1371/journal.pone.0117847.

[178] L. Prosperini, M. Capobianco, and C. Gianni, "Identifying responders and nonresponders to interferon therapy in multiple sclerosis", *Degenerative Neurological and Neuromuscular Disease*, p. 75, 2014, ISSN: 1179-9900. DOI: 10.2147/DNND.S42734. [Online]. Available: http://www.dovepress.com/identifying-responders-and-nonresponders-to-interferon-therapy-in-mult-peer-reviewed-article-DNND.

[179] T. K. Motawi, O. G. Shaker, S. A. El-Maraghy, and M. A. Senousy, "Serum Interferon-Related MicroRNAs as Biomarkers to Predict the Response to Interferon Therapy in Chronic Hepatitis C Genotype 4", *PLOS ONE*, vol. 10, no. 3, e0120794, 2015, ISSN: 1932-6203. DOI: 10.1371/journal.pone.0120794. [Online]. Available: http://dx.plos.org/10.1371/journal.pone.0120794.

[180] O. V. Carvalho, G. L. Saraiva, C. G. T. Ferreira, D. M. Felix, J. L. R. Fietto, G. C. Bressan, M. R. Almeida, and A. Silva, "In-vitro antiviral efficacy of ribavirin and interferon-alpha against canine distemper virus", *Canadian Journal of Veterinary Research*, vol. 78, no. 4, pp. 283–289, 2014, ISSN: 08309000.

[181] A. Beniers, W. Peelen, B. Hendriks, J. Schalken, J. Romijn, and F. Debruyne, "In vitro antiproliferative efficacy of Interferon-alpha,-gamma and Tumor Necrosis Factor on two human renal tumor xenografts", *Urological Research*, vol. 16, no. 4, 1988, ISSN: 03005623. DOI: 10.1007/BF00263641.

[182] X. Zhuang and C. Lu, *PBPK modeling and simulation in drug research and development*, 2016. DOI: 10.1016/j.apsb.2016.04.004.

[183] L. Zhao, T. H. Ren, and D. D. Wang, *Clinical pharmacology considerations in biologics development*, 2012. DOI: 10.1038/aps.2012.51.

[184] M. Meyer, S. Schneckener, B. Ludewig, L. Kuepfer, and J. Lippert, "Using expression data for quantification of active processes in physiologically based pharmacokinetic modeling", *Drug Metabolism and Disposition*, 2012, ISSN: 00909556. DOI: 10.1124/dmd.111.043174.

[185] P. Lamken, S. Lata, M. Gavutis, and J. Piehler, "Ligand-induced assembling of the type i interferon receptor on supported lipid bilayers", *Journal of Molecular Biology*, vol. 341, no. 1, pp. 303 –318, 2004, ISSN: 0022-2836. DOI: http://dx.doi.org/10.1016/j.jmb.2004.05.059. [Online]. Available: http://www.sciencedirect.com/science/article/pii/S0022283604006394.

[186] M. Gavutis, S. Lata, P. Lamken, P. Müller, and J. Piehler, "Lateral ligand-receptor interactions on membranes probed by simultaneous fluorescence-interference detection", *Biophysical Journal*, vol. 88, no. 6, pp. 4289 –4302, 2005, ISSN: 0006-3495. DOI: http://dx.doi.org/10.1529/biophysj.104.055855. [Online]. Available: http://www.sciencedirect.com/science/article/pii/S0006349505734780.

[187] M. Gavutis, E. Jaks, P. Lamken, and J. Piehler, "Determination of the two-dimensional interaction rate constants of a cytokine receptor complex", *Biophysical Journal*, vol. 90, no. 9, pp. 3345 –3355, 2006, ISSN: 0006-3495. DOI: http://dx.doi.org/10.1529/biophysj.105.072546. [Online]. Available: http://www.sciencedirect.com/science/article/pii/S0006349506725164.

[188] A.-K. Sohlenius-Sternbeck, "Determination of the hepatocellularity number for human, dog, rabbit, rat and mouse livers from protein concentration measurements", *Toxicology in Vitro*, vol. 20, no. 8, pp. 1582 –1586, 2006, ISSN: 0887-2333. DOI: http://dx.doi.org/10.1016/j.tiv.2006.06.003. [Online]. Available: http://www.sciencedirect.com/science/article/pii/S088723330600124X.

[189] "Determination of microsome and hepatocyte scaling factors for in vitro/in vivo extrapolation in the rat and dog", *Xenobiotica*, 2008, ISSN: 00498254. DOI: 10.1080/00498250802491662.

[190] S. Wilmes, O. Beutel, Z. Li, V. Francois-Newton, C. P. Richter, D. Janning, C. Kroll, P. Hanhart, K. Hötte, C. You, *et al.*, "Receptor dimerization dynamics as a regulatory valve for plasticity of type i interferon signaling", *The Journal of cell biology*, vol. 209, no. 4, pp. 579–593, 2015.

[191] V. Francois-Newton, M. Livingstone, B. Payelle-Brogard, G. Uzé, and S. Pellegrini, "USP18 establishes the transcriptional and anti-proliferative interferon α/β differential", *Biochemical Journal*, vol. 446, no. 3, pp. 509–516, 2012, ISSN: 0264-6021. DOI: 10.1042/BJ20120541. [Online]. Available: http://biochemj.org/lookup/doi/10.1042/BJ20120541.

[192] I. Moraga, D. Harari, G. Schreiber, G. Uzé, and S. Pellegrini, "Receptor density is key to the alpha2/beta interferon differential activities.", *Molecular and cellular biology*, vol. 29, no. 17, pp. 4778–87, 2009, ISSN: 1098-5549. DOI: 10.1128/MCB.01808-08. [Online]. Available: http://mcb.asm.org/content/29/17/4778.full.

[193] G. Schreiber and J. Piehler, "The molecular basis for functional plasticity in type I interferon signaling", *Trends in Immunology*, vol. 36, no. 3, pp. 139–149, 2015, ISSN: 14714981 14714906. DOI: 10.1016/j.it.2015.01.002.

[194] J. F. Coleman, *Robbins and Cotrans Pathologic Basis of Disease*. 2010, ISBN: 1437720153. DOI: 10.1097/PAS.0b013e3181bc5f0f. arXiv: arXiv:1011.1669v3.

[195] N. U. Khan, K. a. Pulford, M. a. Farquharson, a Howatson, C Stewart, R Jackson, a. M. McNicol, and a. K. Foulis, "The distribution of immunoreactive interferon-alpha in normal human tissues.", *Immunology*, 1989, ISSN: 0019-2805.

[196] J. J. Babon, N. J. Kershaw, J. M. Murphy, L. N. Varghese, A. Laktyushin, S. N. Young, I. S. Lucet, R. S. Norton, and N. A. Nicola, "Suppression of Cytokine Signaling by SOCS3: Characterization of the Mode of Inhibition and the Basis of Its Specificity", *Immunity*, vol. 36, no. 2, pp. 239–250, 2012, ISSN: 10747613. DOI: 10.1016/j.immuni.2011.12.015.

[197] A. Branca, C. R. Faltynek, S. B. D'Alessandro, and C. Baglioni, "Interaction of interferon with cellular receptors. internalization and degradation of cell-bound interferon.", *Journal of Biological Chemistry*, vol. 257, no. 22, pp. 13 291–13 296, 1982.

[198] H. Arnheiter, M. Ohno, M. Smith, B. Gutte, and K. C. Zoon, "Orientation of a human leukocyte interferon molecule on its cell surface receptor: Carboxyl terminus remains accessible to a monoclonal antibody made against a synthetic interferon fragment", *Proceedings of the National Academy of Sciences*, vol. 80, no. 9, pp. 2539–2543, 1983.

[199] T. W. Whitfield, J. Wang, P. J. Collins, E. C. Partridge, S. Aldred, N. D. Trinklein, R. M. Myers, and Z. Weng, "Functional analysis of transcription factor binding sites in human promoters", *Genome Biology*, 2012, ISSN: 1465-6906. DOI: 10.1186/gb-2012-13-9-r50.

[200] S. Schmid, M. Mordstein, G. Kochs, A. García-Sastre, and B. R. TenOever, "Transcription factor redundancy ensures induction of the antiviral state", *Journal of Biological Chemistry*, 2010, ISSN: 00219258. DOI: 10.1074/jbc.M110.165936.

[201] S. Rengachari, S. Groiss, J. M. Devos, E. Caron, N. Grandvaux, and D. Panne, "Structural basis of STAT2 recognition by IRF9 reveals molecular insights into ISGF3 function", *Proceedings of the National Academy of Sciences*, 2018, ISSN: 0027-8424. DOI: 10.1073/pnas.1718426115.

[202] A. Begitt, M. Droescher, T. Meyer, C. D. Schmid, M. Baker, F. Antunes, M. R. Owen, R. Naumann, T. Decker, and U. Vinkemeier, "STAT1-cooperative DNA binding distinguishes type 1 from type 2 interferon signaling", *Nature Immunology*, 2014, ISSN: 15292908. DOI: 10.1038/ni.2794.

[203] L. Kuepfer, M. Peter, U. Sauer, and J. Stelling, "Ensemble modeling for analysis of cell signaling dynamics", *Nature Biotechnology*, vol. 25, no. 9, pp. 1001–1006, 2007, ISSN: 10870156. DOI: 10.1038/nbt1330.

[204] R. M. Turner, B. K. Park, and M. Pirmohamed, *Parsing interindividual drug variability: An emerging role for systems pharmacology*, 2015. DOI: 10.1002/wsbm.1302.

[205] H. Cordes, C. Thiel, V. Baier, L. M. Blank, and L. Kuepfer, "Integration of genome-scale metabolic networks into whole-body PBPK models shows phenotype-specific cases of drug-induced metabolic perturbation", *npj Systems Biology and Applications*, vol. 4, no. 1, p. 10, 2018, ISSN: 2056-7189. DOI: 10.1038/s41540-018-0048-1. [Online]. Available: http://www.nature.com/articles/s41540-018-0048-1.

[206] M. Krauss, S. Schaller, S. Borchers, R. Findeisen, J. Lippert, and L. Kuepfer, "Integrating Cellular Metabolism into a Multiscale Whole-Body Model", *PLoS Computational Biology*, vol. 8, no. 10, 2012, ISSN: 1553734X. DOI: 10.1371/journal.pcbi.1002750.

[207] C. Theil, I. Smit, V. Baier, H. Cordes, B Fabry, L. Blank, and L. Kuepfer, "Using quantitative systems pharmacology to evaluate the drug efficacy of cox-2 and 5-lox inhibitors in therapeutic situations", *npj SBA*, 2018.

[208] W. H. Max von Kleist Charlotte Kloft, Ed., *Combining Systems Biology with physiologically-based pharmacokinetics to support the understanding of drug effects*, vol. 231, Proceedings of Foundations of Systems Biology in Engeneering FOSBE, 2007.

[209] A. I. Daud, C. Xu, W. J. Hwu, P. Urbas, S. Andrews, N. E. Papadopoulos, L. C. Floren, A. Yver, R. C. Deconti, and V. K. Sondak, "Pharmacokinetic/pharmacodynamic analysis of adjuvant pegylated interferon α-2b in patients with resected high-risk melanoma", *Cancer Chemotherapy and Pharmacology*, vol. 67, no. 3, pp. 657–666, 2011, ISSN: 03445704. DOI: 10.1007/s00280-010-1326-9.

[210] K. A. Nieforth, R. Nadeau, I. H. Patel, and D. Mould, "Use of an indirect pharmacodynamic stimulation model of MX protein induction to compare in vivo activity of interferon alfa-2a and a polyethylene glycol-modified derivative in healthy subjects", *Clinical Pharmacology and Therapeutics*, vol. 59, no. 6, pp. 636–646, 1996, ISSN: 00099236. DOI: 10.1016/S0009-9236(96)90003-X.

[211] K. R. Reddy, *Development and pharmacokinetics and pharmacodynamics of pegylated interferon alfa-2a (40 kD)*, 2004. DOI: 10.1055/s-2004-832926.

[212] H. B. Greenberg, R. B. Pollard, L. I. Lutwick, P. B. Gregory, W. S. Robinson, and T. C. Merigan, "Effect of human leukocyte interferon on hepatitis B virus infection in patients with chronic active hepatitis.", *The New England journal of medicine*, vol. 295, no. 10, pp. 517–22, 1976, ISSN: 0028-4793. DOI: 10.1056/NEJM197609022951001. [Online]. Available: http://www.ncbi.nlm.nih.gov/pubmed/950957.

[213] M. J. Hawkins, E. C. Borden, J. A. Merritt, B. S. Edwards, L. A. Ball, E Grossbard, and K. J. Simon, "Comparison of the biologic effects of two recombinant human interferons alpha (ra and rd) in humans.", *Journal of Clinical Oncology*, vol. 2, no. 3, pp. 221–226, 1984, PMID: 6321691. DOI: 10.1200/JCO.1984.2.3.221. eprint: http://ascopubs.org/doi/pdf/10.1200/JCO.1984.2.3.221. [Online]. Available: http://ascopubs.org/doi/abs/10.1200/JCO.1984.2.3.221.

[214] M. H. Heim, "Interferon signaling", in *Signaling Pathways in Liver Diseases*, J.-F. Dufour and P.-A. Clavien, Eds. Berlin, Heidelberg: Springer Berlin Heidelberg, 2010, pp. 189–200, ISBN: 978-3-642-00150-5. DOI: 10.1007/978-3-642-00150-5_12. [Online]. Available: http://dx.doi.org/10.1007/978-3-642-00150-5_12.

[215] ——, "25 years of interferon-based treatment of chronic hepatitis c: An epoch coming to an end", *Nat Rev Immunol*, vol. 13, no. 7, pp. 535–542, 2013, ISSN: 1474-1733. DOI: 10.1038/nri3463. [Online]. Available: http://dx.doi.org/10.1038/nri3463http://www.nature.com/nri/journal/v13/n7/pdf/nri3463.pdf.

[216] C. Thiel, H. Cordes, I. Conde, J. V. Castell, L. M. Blank, and L. Kuepfer, "Model-based contextualization of in vitro toxicity data quantitatively predicts in vivo drug response in patients", *Archives of Toxicology*, vol. 91, no. 2, pp. 865–883, 2017, ISSN: 14320738. DOI: 10.1007/s00204-016-1723-x.

[217] C. Thiel, H. Cordes, L. Fabbri, H. E. Aschmann, V. Baier, I. Smit, F. Atkinson, L. M. Blank, and L. Kuepfer, "A Comparative Analysis of Drug-Induced Hepatotoxicity in Clinically Relevant Situations", *PLoS Computational Biology*, vol. 13, no. 2, 2017, ISSN: 15537358. DOI: 10.1371/journal.pcbi.1005280.

[218] C. Thiel, H. Cordes, V. Baier, L. M. Blank, and L. Kuepfer, "Multiscale modeling reveals inhibitory and stimulatory effects of caffeine on acetaminophen-induced toxicity in humans", *CPT: Pharmacometrics and Systems Pharmacology*, vol. 6, no. 2, pp. 136–146, 2017, ISSN: 21638306. DOI: 10.1002/psp4.12153.

[219] L. Kuepfer, O. Clayton, C. Thiel, H. Cordes, R. Nudischer, L. M. Blank, V. Baier, S. Heymans, F. Caiment, A. Roth, D. A. Fluri, J. M. Kelm, J. Castell, N. Selevsek, R. Schlapbach, H. Keun, J. Hynes, U. Sarkans, H. Gmuender, R. Herwig, S. Niederer, J. Schuchhardt, M. Segall, and J. Kleinjans, *A model-based assay design to reproduce in vivo patterns of acute drug-induced toxicity*, 2018. DOI: 10.1007/s00204-017-2041-7.

[220] T. Witthoft, "Review of consensus interferon in the treatment of chronic hepatitis C", *Biologics*, vol. 2, no. 4, pp. 635–643, 2008.

[221] M. Sarasin-Filipowicz, X. Wang, M. Yan, F. H. T. Duong, V. Poli, D. J. Hilton, D.-E. Zhang, and M. H. Heim, "Alpha Interferon Induces Long-Lasting Refractoriness of JAK-STAT Signaling in the Mouse Liver through Induction of USP18/UBP43", *Molecular and Cellular Biology*, 2009, ISSN: 0270-7306. DOI: 10.1128/MCB.00224-09.

[222] W. E. Grizzlea, W. C. Bella, and K. C. Sextonb, "Issues in collecting, processing and storing human tissues and associated information to support biomedical research", in *Translational pathology of early cancer*, 2012, ISBN: 9781614990239. DOI: 10.3233/978-1-61499-024-6-531. arXiv: NIHMS150003.

[223] J. P. A. Ioannidis, *Extrapolating from animals to humans*, 2012. DOI: 10.1126/scitranslmed.3004631.

[224] P. Pound, "Where is the evidence that animal research benefits humans?", *BMJ*, 2004, ISSN: 0959-8138. DOI: 10.1136/bmj.328.7438.514.

[225] D. G. Hackam and D. A. Redelmeier, "Translation of Research Evidence From Animals to Humans", *JAMA*, 2006, ISSN: 0098-7484. DOI: 10.1001/jama.296.14.1731.

[226] H. Bart van der Worp, D. W. Howells, E. S. Sena, M. J. Porritt, S. Rewell, V. O Collins, and M. R. Macleod, "Can animal models of disease reliably inform human studies?", *PLoS Medicine*, 2010, ISSN: 15491277. DOI: 10.1371/journal.pmed.1000245.

[227] "Genomic responses in mouse models poorly mimic human inflammatory diseases", *Proceedings of the National Academy of Sciences*, 2013, ISSN: 0027-8424. DOI: 10.1073/pnas.1222878110.

[228] M. Noureddin and M. G. Ghany, "Pharmacokinetics and pharmacodynamics of peginterferon and ribavirin: Implications for clinical efficacy in the treatment of chronic hepatitis c", *Gastroenterology Clinics of North America*, vol. 39, no. 3, pp. 649 –658, 2010, Clinical Pharmacology of Gastrointestinal and Liver Disease, ISSN: 0889-8553. DOI: https://doi.org/10.1016/j.gtc.2010.08.008. [Online]. Available: http://www.sciencedirect.com/science/article/pii/S0889855310000506.

[229] A. J. Sadler and B. R. Williams, *Interferon-inducible antiviral effectors*, 2008. DOI: 10.1038/nri2314.

[230] J. Verhelst, P. Hulpiau, and X. Saelens, "Mx Proteins: Antiviral Gatekeepers That Restrain the Uninvited", *Microbiology and Molecular Biology Reviews*, 2013, ISSN: 1092-2172. DOI: 10.1128/MMBR.00024-13.

[231] R. Milo and R. Phillips, "Cell Biology By the Numbers", *Current opinion in plant biology*, 2014, ISSN: 1879-0356. DOI: 10.1016/j.pbi.2009.10.009. arXiv: 1406.6401.

[232] D. Harari, R. Abramovich, A. Zozulya, P. Smith, S. Pouly, M. Köster, H. Hauser, and G. Schreiber, "Bridging the species divide: Transgenic mice humanized for type-I interferon response", *PLoS ONE*, 2014, ISSN: 19326203. DOI: 10.1371/journal.pone.0084259.

[233] N. Maehara, M. Ho, and J. A. Armstrong, "Differences in mouse interferons according to cell source and mode of induction", *Infect. Immun.*, vol. 17, no. 3, pp. 572–579, 1977.

[234] 1979. DOI: 10.1007/978-3-7091-3432-0.

[235] Y. I. Satoh, K Kasama, A Kajita, H Shimizu, and N Ida, "Different pharmacokinetics between natural and recombinant human interferon beta in rabbits.", *Journal of interferon research*, 1984, ISSN: 0197-8357. DOI: 10.1089/jir.1984.4.411.

[236] J. Vilcek, I. T. Sulea, I. L. Zerebeckyj, and Y. K. Yip, "Pharmacokinetic properties of human fibroblast and leukocyte interferon in rabbits", *J. Clin. Microbiol.*, vol. 11, no. 1, pp. 102–105, 1980.

[237] H. K. Jin, a Takada, Y Kon, O Haller, and T Watanabe, "Identification of the murine Mx2 gene: interferon-induced expression of the Mx2 protein from the feral mouse gene confers resistance to vesicular stomatitis virus.", *Journal of virology*, 1999, ISSN: 0022-538X.

[238] M Aebi, J Fäh, N Hurt, C. E. Samuel, D Thomis, L Bazzigher, J Pavlovic, O Haller, and P Staeheli, "cDNA structures and regulation of two interferon-induced human Mx proteins.", *Molecular and cellular biology*, 1989, ISSN: 0270-7306. DOI: 10.1128/MCB.9.11.5062.

[239] T Ronni, S Matikainen, A Lehtonen, J Palvimo, J Dellis, F Van Eylen, J. Goetschy, M Horisberger, J Content, and I Julkunen, "The proximal interferon-stimulated response elements are essential for interferon responsiveness: A promoter analysis of the antiviral mxa gene.", *Journal of interferon & cytokine research*, vol. 18, no. 9, pp. 773–781, 1998.

[240] A. Asano, H. K. Jin, and T. Watanabe, "Mouse Mx2 gene: Organization, mRNA expression and the role of the interferon-response promoter in its regulation", *Gene*, 2003, ISSN: 03781119. DOI: 10.1016/S0378-1119(03)00428-1.

[241] P. Staeheli, O. Haller, W. Boll, J. Lindenmann, and C. Weissmann, "Mx protein: Constitutive expression in 3t3 cells transformed with cloned mx cdna confers selective resistance to influenza virus", *Cell*, vol. 44, no. 1, pp. 147 –158, 1986, ISSN: 0092-8674. DOI: https://doi.org/10.1016/0092-8674(86)90493-9. [Online]. Available: http://www.sciencedirect.com/science/article/pii/0092867486904939.

[242] K. Karikó, H. Ni, J. Capodici, M. Lamphier, and D. Weissman, "mRNA is an endogenous ligand for Toll-like receptor 3.", *The Journal of biological chemistry*, 2004, ISSN: 0021-9258. DOI: 10.1074/jbc.M310175200.

[243] G. Schreiber, *The molecular basis for differential type i interferon signaling*, 2017. DOI: 10.1074/jbc.R116.774562.

[244] L. Aguilera, P. Kalra, P. Mutz, S. Sahle, C. Daechert, R. Bartenschlager, M. Binder, and U. Kummer, "Stochastic Dynamics of Type-I Interferon Responses", In preparation, 2018.

[245] C. Cai, J. Zhou, X. Sun, T. Sun, W. Xie, and J. Cui, "Integrated modeling and analysis of intracellular and intercellular mechanisms in shaping the interferon response to viral infection", *PLoS ONE*, 2017, ISSN: 19326203. DOI: 10.1371/journal.pone.0186105.

[246] A. K. Shalek, R. Satija, J. Shuga, J. J. Trombetta, D. Gennert, D. Lu, P. Chen, R. S. Gertner, J. T. Gaublomme, N. Yosef, S. Schwartz, B. Fowler, S. Weaver, J. Wang, X. Wang, R. Ding, R. Raychowdhury, N. Friedman, N. Hacohen, H. Park, A. P. May, and A. Regev, "Single-cell RNA-seq reveals dynamic paracrine control of cellular variation", *Nature*, 2014, ISSN: 14764687. DOI: 10.1038/nature13437. arXiv: NIHMS150003.

[247] G. Balázsi, A. Van Oudenaarden, and J. J. Collins, *Cellular decision making and biological noise: From microbes to mammals*, 2011. DOI: 10.1016/j.cell.2011.01.030.

[248] D Levy, A Larner, A Chaudhuri, L. E. Babiss, and J. E. Darnell Jr., "Interferon-stimulated transcription: isolation of an inducible gene and identification of its regulatory region", *Proc Natl Acad Sci U S A*, vol. 83, no. 23, pp. 8929–8933, 1986. [Online]. Available: http://www.ncbi.nlm.nih.gov/entrez/query.fcgi?cmd=Retrieve{\&}db=PubMed{\&}dopt=Citation{\&}list{_}uids=3466167.

[249] G. Lillacci and M. Khammash, "The signal within the noise: Efficient inference of stochastic gene regulation models using fluorescence histograms and stochastic simulations", *Bioinformatics*, vol. 29, no. 18, pp. 2311–2319, 2013.

[250] B. Munsky, B. Trinh, and M. Khammash, "Listening to the noise: Random fluctuations reveal gene network parameters", *Molecular systems biology*, vol. 5, no. 1, p. 318, 2009.

[251] N. Grandvaux, M. J. Servant, B. TenOever, G. C. Sen, S. Balachandran, G. N. Barber, R. Lin, and J. Hiscott, "Transcriptional Profiling of Interferon Regulatory Factor 3 Target Genes: Direct Involvement in the Regulation of Interferon-Stimulated Genes", *Journal of Virology*, 2002, ISSN: 0022-538X. DOI: 10.1128/JVI.76.11.5532-5539.2002.

[252] M. G. Wathelet, C. H. Lin, J Parekh other authors, and Huez, "Virus Infection Induces the Assembly of Coordinately Activated Transcription Factors on the IFN-β Enhancer In Vivo", *Molecular Cell*, vol. 1, no. 4, pp. 507–518, 1998, ISSN: 10972765. DOI: 10.1016/S1097-2765(00)80051-9.

[253] F. Terenzi, S. Pal, and G. C. Sen, "Induction and mode of action of the viral stress-inducible murine proteins, P56 and P54", *Virology*, 2005, ISSN: 00426822. DOI: 10.1016/j.virol.2005.06.011.

[254] T. S. Carlos, R Fearns, and R. E. Randall, "Interferon-induced alterations in the pattern of parainfluenza virus 5 transcription and protein synthesis and the induction of virus inclusion bodies.", *Journal of virology*, 2005, ISSN: 0022-538X. DOI: 10.1128/JVI.79.22.14112-14121.2005.

[255] W. M. Schneider, M. D. Chevillotte, and C. M. Rice, "Interferon-Stimulated Genes: A Complex Web of Host Defenses", *Annual Review of Immunology*, 2014, ISSN: 0732-0582. DOI: 10.1146/annurev-immunol-032713-120231. arXiv: NIHMS150003.

[256] J. W. Schoggins and C. M. Rice, "Interferon-stimulated genes and their antiviral effector functions", *Current Opinion in Virology*, 2011, ISSN: 18796257. DOI: 10.1016/j.coviro.2011.10.008. arXiv: NIHMS150003.

[257] J. Joo, S. J. Plimpton, and J. L. Faulon, "Statistical ensemble analysis for simulating extrinsic noise-driven response in NF-??B signaling networks", *BMC Systems Biology*, 2013, ISSN: 17520509. DOI: 10.1186/1752-0509-7-45. arXiv: 1010.0904.

[258] Y. Hori, M. H. Khammash, and S. Hara, "Efficient Parameter Identification for Stochastic Biochemical Networks Using a Reduced-Order Realization", *Proceedings of the European Control Conference 2013*, pp. 4154–4159, 2013.

[259] H. H. Chang, M. Hemberg, M. Barahona, D. E. Ingber, and S. Huang, "Transcriptome-wide noise controls lineage choice in mammalian progenitor cells", *Nature*, vol. 453, no. 7194, pp. 544–547, 2008, ISSN: 0028-0836. DOI: 10.1038/nature06965. [Online]. Available: http://www.nature.com/doifinder/10.1038/nature06965.

[260] T. Morisaki, K. Lyon, K. F. DeLuca, J. G. DeLuca, B. P. English, Z. Zhang, L. D. Lavis, J. B. Grimm, S. Viswanathan, L. L. Looger, *et al.*, "Real-time quantification of single rna translation dynamics in living cells", *Science*, vol. 352, no. 6292, pp. 1425–1429, 2016.

[261] T Ronni, K Melen, A Malygin, and I Julkunen, "Control of ifn-inducible mxa gene expression in human cells.", *The Journal of Immunology*, vol. 150, no. 5, pp. 1715–1726, 1993.

[262] "Human and Murine IFIT1 Proteins Do Not Restrict Infection of Negative-Sense RNA Viruses of the Orthomyxoviridae, Bunyaviridae, and Filoviridae Families", *Journal of Virology*, 2015, ISSN: 0022-538X.

[263] E. Klipp, W. Liebermeister, C. Wierling, A. Kowald, and R. Herwig, *Systems biology: a textbook*. John Wiley & Sons, 2016.

[264] M. Chatterjee-Kishore, K. L. Wright, J. P.-Y. Ting, and G. R. Stark, "How stat1 mediates constitutive gene expression: A complex of unphosphorylated stat1 and irf1 supports transcription of the lmp2 gene", *The EMBO journal*, vol. 19, no. 15, pp. 4111–4122, 2000.

[265] National Institutes of Health Consensus Development Conference Panel, "National Institutes of Health Consensus Development Conference Panel Statement: Management of Hepatitis C", *Hepatology*, 1997, ISSN: 0270-9139. DOI: 10.1002/hep.510260701.

[266] M. P. Manns, J. G. McHutchison, S. C. Gordon, V. K. Rustgi, M Shiffman, R Reindollar, Z. D. Goodman, K Koury, M Ling, and J. K. Albrecht, "Peginterferon alfa-2b plus ribavirin compared with interferon alfa-2b plus ribavirin for initial treatment of chronic hepatitis C: a randomised trial.", *Lancet*, 2001, ISSN: 0140-6736. DOI: 10.1016/S0140-6736(01)06102-5.

[267] R. J. Duhé and W. L. Farrar, "Structural and mechanistic aspects of Janus kinases: how the two-faced god wields a double-edged sword", *Journal of Interferon & Cytokine Research: The Official Journal of the International Society for Interferon and Cytokine Research*, 1998, ISSN: 1079-9907. DOI: 10.1089/jir.1998.18.1.

[268] F. McNab, K. Mayer-Barber, A. Sher, A. Wack, and A. O'Garra, "Type I interferons in infectious disease", *Nat Rev Immunol*, 2015, ISSN: 1474-1733. DOI: 10.1038/nri3787.

[269] G. Trinchieri, "Type I interferon: friend or foe?", *The Journal of Experimental Medicine*, 2010, ISSN: 0022-1007. DOI: 10.1084/jem.20101664.

[270] M. J. de Veer, M Holko, M Frevel, E Walker, S Der, J. M. Paranjape, R. H. Silverman, and B. R. Williams, "Functional classification of interferon-stimulated genes identified using microarrays", *Journal of leukocyte biology*, 2001, ISSN: 0741-5400. DOI: 10.1189/jlb.69.6.912.

[271] I. Rusinova, S. Forster, S. Yu, A. Kannan, M. Masse, H. Cumming, R. Chapman, and P. J. Hertzog, "INTERFEROME v2.0: An updated database of annotated interferon-regulated genes", *Nucleic Acids Research*, 2013, ISSN: 03051048. DOI: 10.1093/nar/gks1215.

[272] V. I. Pérez-Nueno, "Using quantitative systems pharmacology for novel drug discovery", *Expert Opinion on Drug Discovery*, 2015, ISSN: 1746-0441. DOI: 10.1517/17460441.2015.1082543.

[273] T. A. Leil and R. Bertz, "Quantitative systems pharmacology can reduce attrition and improve productivity in pharmaceutical research and development", *Frontiers in Pharmacology*, 2014, ISSN: 16639812. DOI: 10.3389/fphar.2014.00247.

[274] P. H. van der Graaf and N. Benson, "Systems Pharmacology: Bridging Systems Biology and Pharmacokinetics-Pharmacodynamics (PKPD) in Drug Discovery and Development", *Pharmaceutical Research*, 2011, ISSN: 0724-8741. DOI: 10.1007/s11095-011-0467-9.

[275] M. Danhof, P. V. der Graaf, D. Jonker, S. Visser, and K. Zuideveld, "5.38 - mechanism-based pharmacokinetic–pharmacodynamic modeling for the prediction of in vivo drug concentration–effect relationships – application in drug candidate selection and lead optimization", in *Comprehensive Medicinal Chemistry II*, J. B. Taylor and D. J. Triggle, Eds., Oxford: Elsevier, 2007, pp. 885 –908, ISBN: 978-0-08-045044-5. DOI: https://doi.org/10.1016/B0-08-045044-X/00154-1. [Online]. Available: http://www.sciencedirect.com/science/article/pii/B008045044X001541.

[276] W. Gao and W. J. Jusko, "Target-mediated pharmacokinetic and pharmacodynamic model of exendin-4 in rats, monkeys, and humans.", *Drug metabolism and disposition: the biological fate of chemicals*, 2012, ISSN: 1521-009X. DOI: 10.1124/dmd.111.042291.

[277] K. E. Thummel and Y. S. Lin, "Sources of interindividual variability", *Methods in Molecular Biology*, 2014, ISSN: 10643745. DOI: 10.1007/978-1-62703-758-7_17.

[278] M. Imai and Y. Kawaoka, "The role of receptor binding specificity in interspecies transmission of influenza viruses", *Current Opinion in Virology*, 2012, ISSN: 18796257. DOI: 10.1016/j.coviro.2012.03.003. arXiv: 15334406.

[279] A. G. TAMAR BINO ZACHARIA MADAR and H. ROSENBERG., "The Kidney is the Main Site of Interferon Degradation", *Journal of Interferon Research.*, vol. 2, pp. 301–308, 1982. DOI: 10.1089/jir.1982.2.301.

[280] G. A. Bino T Edery H and R. H., "Involvement of the kidney in catabolism of human leukocyte interferon", *The Journal of general virology.*, vol. 59(Pt 1), pp. 39–45, Mar 1982. DOI: 10.1099/0022-1317-59-1-39.

[281] T. B. Lavoie, E. Kalie, S. Crisafulli-Cabatu, R. Abramovich, G. DiGioia, K. Moolchan, S. Pestka, and G. Schreiber, "Binding and activity of all human alpha interferon subtypes", *Cytokine*, vol. 56, no. 2, pp. 282–289, 2011, ISSN: 10434666. DOI: 10.1016/j.cyto.2011.07.019.

[282] E. C. Cutrone and J. A. Langer, "Contributions of cloned type I interferon receptor subunits to differential ligand binding", *FEBS Letters*, vol. 404, no. 2-3, pp. 197–202, 1997, ISSN: 00145793. DOI: 10.1016/S0014-5793(97)00129-4.

[283] S. Rengachari, S. Groiss, J. Devos, E. Caron, N. Grandvaux, and D. Panne, "Structural basis of stat2 recognition by irf9 reveals molecular insights into isgf3 function", *bioRxiv*, 2017. DOI: 10.1101/131714. eprint: https://www.biorxiv.org/content/early/2017/04/28/131714.full.pdf. [Online]. Available: https://www.biorxiv.org/content/early/2017/04/28/131714.

[284] D. Levin, D. Harari, and G. Schreiber, "Stochastic receptor expression determines cell fate upon interferon treatment", *Molecular and Cellular Biology*, vol. 31, no. 16, pp. 3252–3266, 2011, 21690295[pmid] 5251-11[PII] Mol Cell Biol, ISSN: 0270-7306 1098-5549. DOI: 10.1128/MCB.05251-11. [Online]. Available: http://www.ncbi.nlm.nih.gov/pmc/articles/PMC3147786/.

[285] C. You, T. T. Marquez-Lago, C. P. Richter, S. Wilmes, I. Moraga, K. C. Garcia, A. Leier, and J. Piehler, "Receptor dimer stabilization by hierarchical plasma membrane microcompartments regulates cytokine signaling", *Science Advances*, vol. 2, no. 12, pp. 1–13, 2016, ISSN: 2375-2548. DOI: 10.1126/sciadv.1600452.

[286] J. Ho, C. Pelzel, A. Begitt, M. Mee, H. M. Elsheikha, D. J. Scott, and U. Vinkemeier, "STAT2 Is a Pervasive Cytokine Regulator due to Its Inhibition of STAT1 in Multiple Signaling Pathways", *PLoS Biology*, vol. 14, no. 10, 2016, ISSN: 15457885. DOI: 10.1371/journal.pbio.2000117.

[287] E. Yang, E. van Nimwegen, M. Zavolan, N. Rajewsky, M. Schroeder, M. Magnasco, and J. E. Darnell, "Decay rates of human mrnas: Correlation with functional characteristics and sequence attributes", *Genome research*, vol. 13, no. 8, pp. 1863–1872, 2003.

[288] E. Siewert, W. Müller-Esterl, R. Starr, P. C. Heinrich, and F. Schaper, "Different protein turnover of interleukin-6-type cytokine signalling components", *European Journal of Biochemistry*, vol. 265, no. 1, pp. 251–257, 1999.

[289] C. Feifei, K. Ogawa, R. P. Nagarajan, M. Zhang, C. Kuang, and c. Yan, "Regulation of tg-interacting factor by transforming growth factor-beta", *Biochemical Journal*, vol. 371, no. 2, pp. 257–263, 2003.

[290] C.-K. Lee, H. A. Bluyssen, and D. E. Levy, "Regulation of interferon alpha responsiveness by the duration of janus kinase activity", *Journal of Biological Chemistry*, vol. 272, no. 35, pp. 21 872–21 877, 1997.

[291] Z. Marijanovic, J. Ragimbeau J Fau van der Heyden, G. van der Heyden J Fau Uze, S. Uze G Fau Pellegrini, and S. Pellegrini, "Comparable potency of ifnalpha2 and ifnbeta on immediate jak/stat activation but differential down-regulation of ifnar2", no. 1470-8728 (Electronic), DOI: D-NLM:PMC2267396EDAT-2007/07/1409:00MHDA-2007/11/0709:00CRDT-2007/07/1409:00AID-BJ20070605[pii]AID-10.1042/BJ20070605[doi]PST-ppublish.

[292] A. N. Theofilopoulos, R. Baccala, B. Beutler, and D. H. Kono, "Type i interferons (alpha or beta) in immunity and autoimmunity", *Annual Review of Immunology*, vol. 23, no. 1, pp. 307–335, 2005, PMID: 15771573. DOI: 10.1146/annurev.immunol.23.021704.115843. eprint: https://doi.org/10.1146/annurev.immunol.23.021704.115843. [Online]. Available: https://doi.org/10.1146/annurev.immunol.23.021704.115843.

[293] E. M. DeMaeyer, D. Maeyer-Guignard, *et al.*, *Interferons and other regulatory cytokines*. Wiley, 1988.

[294] J. A. Langer and S. Pestka, "Interferon receptors", *Immunology today*, vol. 9, no. 12, pp. 393–400, 1988.

[295] B. Precious, T. Carlos, S Goodbourn, and R. Randall, "Catalytic turnover of stat1 allows piv5 to dismantle the interferon-induced anti-viral state of cells", *Virology*, vol. 368, no. 1, pp. 114–121, 2007.

[296] N. Wenta, H. Strauss, S. Meyer, and U. Vinkemeier, "Tyrosine phosphorylation regulates the partitioning of stat1 between different dimer conformations", *Proceedings of the National Academy of Sciences*, vol. 105, no. 27, pp. 9238–9243, 2008.

[297] M. O. Hottiger, L. K. Felzien, and G. J. Nabel, "Modulation of cytokine-induced hiv gene expression by competitive binding of transcription factors to the coactivator p300", *The EMBO Journal*, vol. 17, no. 11, pp. 3124–3134, 1998.

[298] X. Darzacq, Y. Shav-Tal, V. De Turris, Y. Brody, S. M. Shenoy, R. D. Phair, and R. H. Singer, "In vivo dynamics of rna polymerase ii transcription", *Nature structural & molecular biology*, vol. 14, no. 9, pp. 796–806, 2007.

[299] B. Schwanhäusser, D. Busse, N. Li, G. Dittmar, J. Schuchhardt, J. Wolf, W. Chen, and M. Selbach, "Global quantification of mammalian gene expression control.", *Nature*, vol. 473, no. 7347, pp. 337–42, May 2011. DOI: 10.1038/nature10098.